Mechanisms of lipid transport by the ORP/Osh proteins

Joachim Moser von Filseck

Université de Nice Sophia Antipolis – UFR Sciences

Ecole Doctorale SVS (Sciences de la Vie et de la Santé)

THESE

pour obtenir le titre de

Docteur en Sciences

de l'Université de Nice Sophia Antipolis

Mention

Interactions moléculaires et cellulaires

Mechanisms of lipid transport by the ORP/Osh proteins

Mécanismes du transport lipidique par les protéines ORP/Osh

par

Joachim MOSER VON FILSECK

Thèse dirigée par Guillaume DRIN

Soutenance prévue le 16 décembre 2014

Jury:	Pr Laurent COUNILLON	Président
	Dr Catherine JACKSON	Rapporteur
	Dr Guillaume LENOIR	Rapporteur
	Pr Felix WIELAND	Examinateur
	Dr Bruno ANTONNY	Examinateur
	Dr Guillaume DRIN	Directeur de thèse

TABLE OF CONTENTS

LIST OF ILLUSTRATIONS

LIST OF ABBREVIATIONS

25-OH:	25-hydroxycholesterol
aa:	Amino acid
ABC:	ATP-binding cassette
CoA:	Coenzyme A
CERT:	Ceramide transfer protein
DAG:	Diacylglycerol
DHE:	Dehydroergosterol
DOPS:	Dioleoyl-Phosphatidylserine
DTT:	Dithiothreitol
ER:	Endoplasmic reticulum
ERMES:	ER-Mitochondria Encounter Structure
FAPP:	Four Phosphate Adaptor Protein
FFAT:	Two phenylalanines in an acidic tract
GPL:	Glycerophospholipid
IMM:	Inner Mitochondrial Membrane
IPTG:	Isopropyl β-D-1-thiogalactopyranoside
LBPA:	Lysobisphosphatidic acid
LDL:	Low-density lipoprotein
LE:	Late endosome
LY:	Lysosome
LTP:	Lipid transfer protein
MAM:	Mitochondria-associated membrane
MCS:	membrane contact site
NBD:	7-Nitrobenz-2-Oxa-1,3-Diazole
NPC:	Niemann-Pick type C
NVJ:	Nucleus Vacuole Junction
OMM:	Outer mitochondrial membrane
OSBP	Oxysterol-Binding Protein
ORP:	OSBP-related protein
Osh:	OSBP homolog
P4-ATPase:	Class IV P-type ATPase
PA:	Phosphatidic acid
PAM:	PM-associated membrane
PC:	Phosphatidylcholine
PE:	Phoshpatidylethanolamine
PEMT:	PE methyl-transferase
PH:	Pleckstrin homology
PI:	Phosphatidylinositol
PIK:	PI Kinase
PI3K	PI 3-Kinase
PI4K	PI 4-Kinase
PIP:	Phosphoinositide
PI(3)P:	PI 3-phosphate
PI(3,5)P_2:	PI 3,5-bisphosphate
PI(4)P:	PI 4-phosphate
PI(4,5)P_2:	PI 4,5-bisphosphate
PMN:	Piecemeal microautophagy at the nucleus
PS:	Phosphatidyl-*L*-serine
PSD:	PS decarboxylase
PSS:	PS synthase
PM:	Plasma membrane
Sfh:	Sec fourteen homologs
SM:	Sphingomyelin
SMP:	Synaptotagmin-like mitochondrial lipid-binding proteins
SREBP:	Sterol Regulatory Element Binding Protein
StAR:	Steroidogenic Acute Regulatory Protein
START:	StAR-related lipid transfer
TGN:	*trans*-Golgi network
TM:	Transmembrane
VAP:	Vesicle-associated membrane protein (VAMP)-associated protein
WT	Wild type

RESUME

Une distribution hétérogène des lipides est essentielle à l'identité et à la fonction des diverses organelles qui constituent les cellules eucaryotes. Néanmoins, l'échange incessant de matériel entre ces organelles, notamment par les processus de transport vésiculaire, tend à annuler ces différences de composition. Ainsi, il existe des mécanismes de synthèse et de transport de lipides qui assurent à tout instant le maintien de ces compositions lipidiques, autrement dit, qui garantissent l'homéostasie cellulaire des lipides.

Alors que la plupart des lipides est synthétisée au réticulum endoplasmique (RE) et doit être transportée vers sa destination, certains sont métabolisés dans d'autres organelles, établissant un réservoir de lipides spécifiques à celles-ci. Cela est le cas, par exemple, des sphingolipides complexes, des phosphoinositides, ainsi que des lipides mitochondriaux (van Meer, Voelker *et al.* 2008). Les mécanismes de transport actif de lipides entre organelles peuvent être divisés en deux classes:

- Le transport vésiculaire sélectif, permettant l'intégration ou l'exclusion de certains lipides dans les vésicules de transport naissantes afin d'en augmenter ou d'en diminuer le niveau.
- Le transport non-vésiculaire, dépendant de protéines de transfert de lipides (lipid transfer proteins, LTPs), capables d'extraire un lipide d'une membrane pour le protéger du milieu aqueux et ce afin de le transporter vers une deuxième membrane et de l'y insérer.

La participation des LTPs à la formation d'un gradient lipidique, nécessaire pour maintenir l'homéostasie lipidique, est un sujet particulièrement intéressant et méconnu. Forts de ce constat, nous avons cherché à comprendre comment des LTPs appartenant à la famille ORP/Osh peuvent contribuer à cette régulation, en nous attachant plus précisément à étudier comment ces protéines parviennent, par transport de lipides à travers le cytosol, à créer et à maintenir un gradient de concentration de certains lipides entre le RE et les membranes tardives de la voie sécrétoire.

Les Oxysterol-Binding Protein (OSBP)-Related Proteins (ORP) chez les mammifères et les protéines Osh chez la levure à bourgeons *Saccharomyces cerevisiae* sont des transporteurs de lipides. L'accessibilité des protéines Osh ainsi que leur relative simplicité par

rapport à leurs homologues humains nous ont permis d'effectuer des analyses mécanistiques approfondies. Il a été décrit récemment que la protéine Osh4p peut, entre deux membranes, échanger de l'ergostérol (le stérol majoritaire chez la levure) contre un deuxième ligand lipidique, le phosphatidylinositol-4-phosphate (PI(4)P) présent sur la face *trans* de l'appareil de Golgi (de Saint-Jean, Delfosse *et al.* 2011). Le PI(4)P y est synthétisé par une des PI 4-kinases et hydrolysé sur les membranes du RE par la PI(4)P phosphatase Sac1p, assurant ainsi un gradient de concentration du PI(4)P entres ces organelles (Manford, Xia *et al.* 2010).

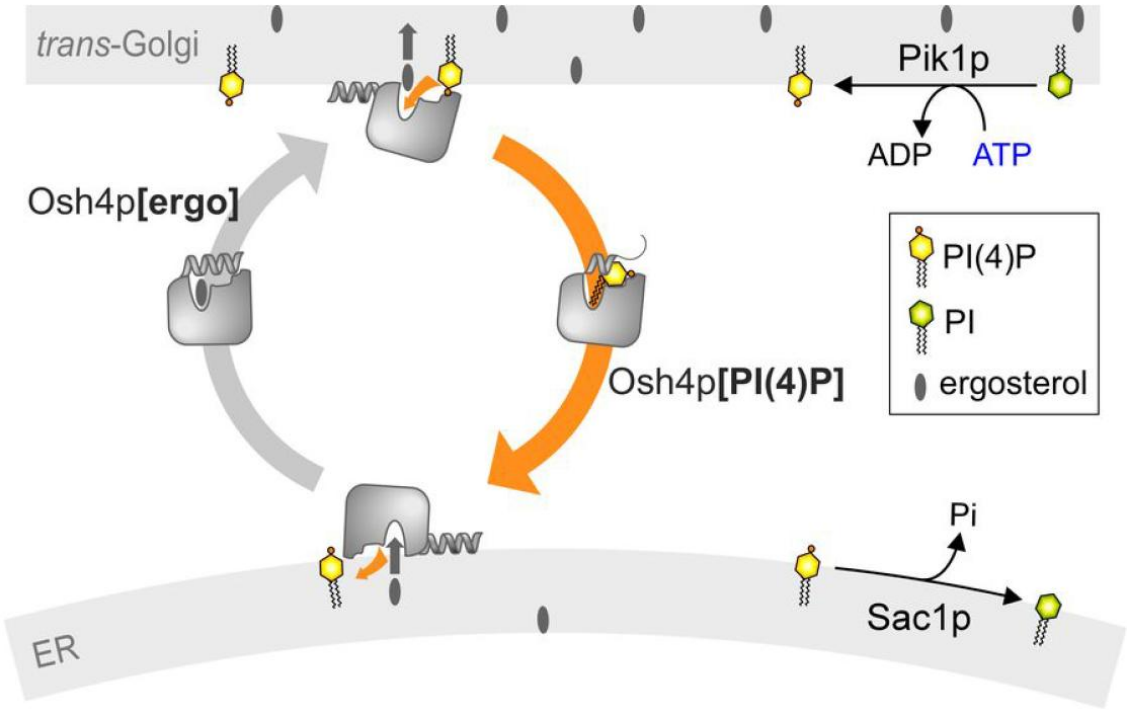

Modèle de travail.
Le contre-échange entre l'ergostérol et du PI(4)P permettrait à Osh4p d'utiliser l'énergie du métabolisme des phosphoinositides pour transporter de l'ergostérol du réticulum endoplasmique (ER) au *trans*-Golgi en créant ainsi un gradient de stérol.

Dans le but d'observer le transport lipidique, nous avons opté pour une approche reconstructive. L'utilisation de membranes artificielles, de protéines recombinantes purifiées à homogénéité ainsi que de lipides naturellement fluorescents et la création de sondes fluorescentes spécifiques à certains lipides, nous ont permis d'effectuer nos recherches dans des conditions de haute résolution temporelle, tout en évitant des influences extérieures.

Pour optimiser l'analyse de l'activité de la protéine Osh4p, nous avons mis au point des outils de fluorescence permettant de mesurer avec une précision inégalée le mouvement du stérol et du PI(4)P entre des membranes lipidiques artificielles. Le domaine d'homologie

pleckstrin (PH) de la protéine humaine FAPP1 reconnaît spécifiquement le PI(4)P et insère une partie du domaine dans la membrane lors de cette reconnaissance. En partant de la structure cristallographique du domaine PH de FAPP1 (Lenoir, Coskun *et al.* 2010) remplacer un résidu par une cystéine (T13C), dans la partie insérée dans la membrane, permet d'attacher une sonde fluorescente NBD sensible à son environnement. Lors de la reconnaissance d'une molécule de PI(4)P par le NBD-PH_{FAPP}, la partie du domaine marquée au NBD est insérée dans la membrane entraînant un décalage du spectre NBD et en une augmentation de sa fluorescence.

A l'aide de cet outil nous démontrons que la protéine Osh4p peut échanger de l'ergostérol et du PI(4)P entre deux membranes par un mécanisme de contre-échange liant intimement le transport d'un des deux ligands au transport de l'autre. La protéine est capable de transporter du stérol contre son gradient de concentration en utilisant l'énergie d'un gradient de PI(4)P. L'intégration de la phosphatase Sac1 dans notre système reconstitué permet un maintien du transport de stérol grâce au maintien du gradient de PI(4)P. Le couplage entre le transport de stérol et le métabolisme des phosphoinositides dans la cellule permettrait à Osh4p d'alimenter la membrane du *trans*-Golgi avec du stérol synthétisé dans le RE. Il a été proposé que le transport de stérols soit maintenu par un gradient d'activité chimique entre les organelles. En utilisant des membranes artificielles à différentes activités chimiques, nous avons pu démontrer que la présence d'un tel gradient favorise le transport mais n'est pas suffisante pour un transport de stérol contre son gradient de concentration à l'échelle de temps cellulaire. Notre conclusion est qu'Osh4p possède la capacité de créer et de maintenir le gradient de stérol observé entre ces organelles grâce au métabolisme du PI(4)P.

En parallèle nous avons prouvé que ce mécanisme de contre-échange est conservé dans la protéine humaine OSBP. Plus complexe que la protéine Osh4p, elle participe à la création de zones de jonction entre deux organelles, *via* sa capacité à connecter la membrane du RE à celle du *trans*-Golgi (Levine and Munro 2002). Nous avons aussi vérifié qu'elle utilise le PI(4)P pour transporter du cholestérol du RE au *trans*-Golgi et que la maintenance du gradient de concentration du PI(4)P par Sac1 favorise ce transport. L'activation d'OSBP par son partenaire d'interaction VAP-A, ancré sur le RE, est néanmoins requise pour cette activité de transport. Ce contre-échange stérol/PI(4)P permet également à OSBP d'autoréguler sa capacité à former des jonctions RE-Golgi grâce à son domaine PH

reconnaissant le PI(4)P. La capacité de certaines protéines ayant une structure globale similaire (type CERT ou FAPP2) à peupler les zones de jonction entre le RE et le Golgi, dépendrait donc également de l'activité d'OSBP et de Sac1.

Enfin, la découverte de la phosphatidylsérine (PS) comme ligand de la protéine Osh6p (Maeda, Anand *et al.* 2013) nous a permis d'analyser la possibilité d'une extrapolation du mécanisme de contre-échange avec le PI(4)P. Osh6p est capable de transporter ce lipide entre membranes artificielles ainsi qu'entre le RE et la MP chez *S. cerevisiae*. En collaboration avec le Centre de Biologie Structurale de Montpellier, nous avons résolu la structure cristallographique de la protéine Osh6p en complexe avec du PI(4)P. La structure montre une géométrie globale conservée entre les protéines Osh, et en particulièrement celle de la liaison au PI(4)P. Utilisant notre outil fluorescent reconnaissant le PI(4)P, nous avons pu déterminer que la liaison du PI(4)P et son transport sont un aspect fonctionnel conservé des protéines Osh. Afin de mesurer le transport de la PS nous avons développé un autre outil fluorescent, selon le même principe que pour le NBD-PH_{FAPP}, mais basé sur un domaine C2 de la Lactadherin bovine (Yeung, Gilbert *et al.* 2008). Cet outil, le NBD-$C2_{Lact}$, permet de suivre le transport de la PS et du PI(4)P entre membranes artificielles, dans les mêmes conditions en temps réel. Ainsi nous avons pu observer que le transport par Osh6p des deux ligands entre deux membranes artificielles est accéléré sous condition de leur contre-échange et qu'il existe une sélectivité de la protéine par rapport au niveau de saturation des chaînes acyl de ses ligands. Ce contre-échange permettrait à Osh6p d'alimenter de PS, synthétisée au RE, la MP en consommant le réservoir de PI(4)P de la MP. Reste à démontrer l'effet du métabolisme du PI(4)P et la conservation de ce mécanisme de contre-échange sur le transport de PS *in vivo*.

En conclusion, cette étude nous permet de suggérer que l'échange de PI(4)P avec divers lipides, *via* certaines protéines ORP/Osh, serait un mécanisme général par lequel les cellules maintiendraient des gradients de lipides entre le RE et les compartiments tardifs de la voie sécrétoire.

PREFACE: STUDYING BIOLOGICAL MEMBRANES – WHY AND HOW?

Life necessitates boundaries.

Where does life begin? Where does it end? One particularly simple yet undoubtedly correct answer to these highly philosophical questions could be: at a membrane. Delimiting themselves from their environment with a membrane is a common feature for every living being. These membranes may vary significantly in their composition between life forms, but they are all based on the same class of molecules, the lipids. Lipid membranes not only allow cells to separate themselves from their environment, but also to accumulate nutrients, energy, ions and other cytosolic factors necessary for their proper function.

Constant change and unchanged constants

Within eukaryotic cells, at a smaller level, the sub-cellular organization into organelles is also defined by their respective membranes, and that separation is likewise mandatory for their functions. These organelles are highly dynamic and in perpetual contact with each other, exchanging material and signals. Notwithstanding these dynamics, they keep their organelles functionally separated and their membrane composition constant. The mechanisms of how this lipid homeostasis between membranes is created and sustained are not yet fully understood. Our scope is to demonstrate the implication of a family of lipid transfer proteins, the Osh proteins that are found in the baker's yeast (or budding yeast) *Saccharomyces cerevisiae*, in lipid homeostasis, and to extrapolate our hypothesis to higher eukaryotes in order to ultimately understand how functional separation is maintained between organelles despite current exchange of membrane material.

Reducing the complexity of a biological system

Trying to understand how cells conserve the properties of their membranes has been a challenge for biologists, as these processes are extremely rapid and it is particularly delicate to follow lipid transfer specifically and in real time. Our approach aims on identifying mechanisms of lipid transport between membranes by reducing the complexity of a cellular system by experimenting *in vitro*. Instead of using real cellular membranes, we use liposomes, artificial bilayers with a defined composition that mimic the cellular membranes. We also reduce the number of proteins implied in transport to a level where we can precisely follow their activity, giving a unique insight into the function of lipid transfer proteins without eventual interference of other cellular factors. We use fluorescence-based assays to measure the motion of various lipids in real-time. In our reduced system, no compensatory mechanisms or regulatory response can interfere with our measurements, even though they might *in vivo*, thus allowing us to do measure with an unprecedented precision the activity of lipid transfer proteins. Despite the advantages of this kind of approach, we are aware of its limitations, since our reconstituted system might lack so far unidentified key factors involved in lipid transfer.

INTRODUCTION

LIPIDS AND BILAYERS:

A PHYSICAL AND CHEMICAL POINT OF VIEW

Definition and self-organization of lipids

Lipids (their name derives from the greek λίπος (lipos), meaning fat) are organic molecules that are insoluble in water due to their long (>10), non-polar carbon chains. Lipids thus cannot be hydrated and form aggregates in an aqueous environment, like oil drops in water, for example. Some lipids dispose of a water insoluble part (often referred to as "tail") as well as of a polar moiety (referred to as "head") that, unlike the tail part, can be hydrated. This particular feature, called **amphipathicity** (or **amphiphilicty**), has an intriguing effect: amphipathic lipids do not aggregate into lipid drops, but rather form micelles or vesicles (**Figure 1**).

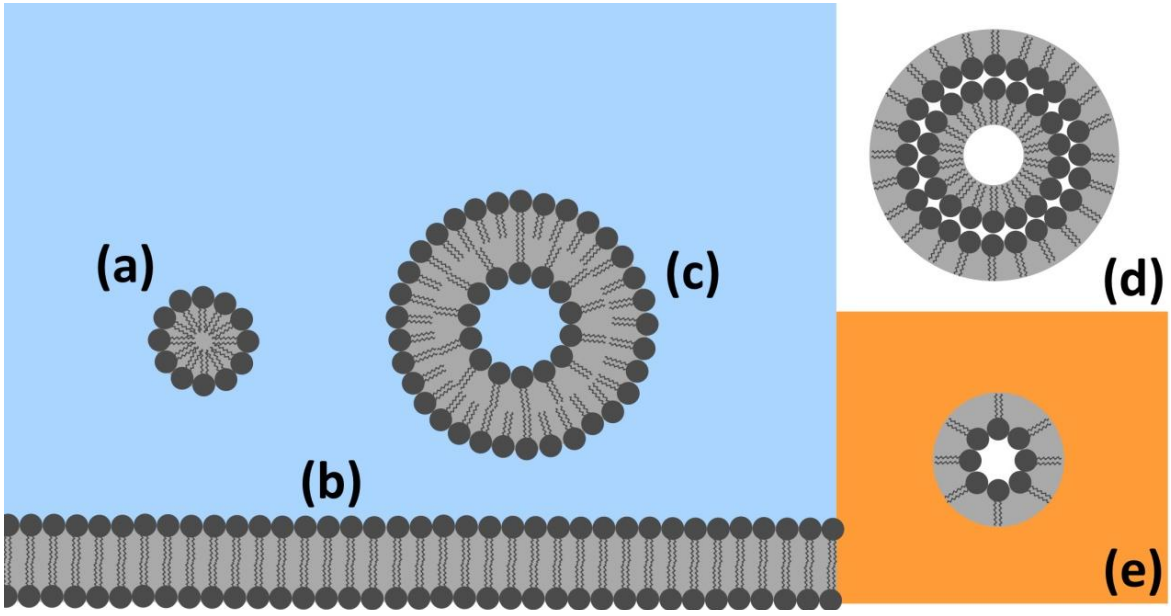

Figure 1. Self-organization of amphipathic lipid molecules in different media.

Amphipathic lipids in water (blue), forming **(a)** a micelle, **(b)** a lipid bilayer or **(c)** a liposome, a vesicle in which an inner aqueous phase is separated from the outer one by a lipid bilayer. **(d)** represents a soap bubble in air (white), an example for an inverted vesicle; **(e)** shows an inverted micelle in a non-polar solvent (orange).

In micelles, the tails of the lipids interact with each other allowing the heads to interact with the aqueous environment, forming spheres of a diameter approximately twice the length of one lipid molecule. In an apolar environment, amphiphilic lipids organize into

inverted micelles with inverted lipid geometry. In vesicles, the internal environment is separated from the external medium by a lipid bilayer i.e. two lipid sheets. In each sheet, the polar headgroups face the aqueous phase whereas the liposoluble tails of two layers face each other. With few exceptions, biological membranes are lipid bilayers. In some cases, inverted bilayers, analogous to inverted micelles, can be formed (**Figure 1**).

Due to the low polarity of the membrane, polar molecules cannot cross such a bilayer. Pores and specialized transporters that are inserted in a membrane can allow or, on the contrary, prohibit exchange between the two compartments delimited by the membrane, and thus create concentration gradients between the inside and the outside.

Thermodynamics in vesicle formation:

The hydrophobic effect

When dissolved in water, lipid molecules are surrounded by a "water cage", in which the water molecules are ordered due to their restricted participation in the formation of a network of interactions between water molecules. The water molecules implied in this "cage" formation are limited in terms of their degrees of freedom. Association of multiple lipid molecules with each other reduces the surface accessible for the surrounding water and more water molecules hence gain their full degrees of freedom. This process is called spontaneous demixing.

The criterion for spontaneity of a chemical reaction is the free enthalpy or Gibb's free energy, defined by the enthalpy of the reaction and an entropic term:

$$G = H - TS$$

defines the free enthalpy for any system, in which G is the free enthalpy, H the enthalpy, T the temperature and S the entropy. The free enthalpy of any isothermal change (where the temperature does not change) of that system is

$$\Delta G = \Delta H - T\Delta S.$$

By definition, chemical reactions are spontaneous for $\Delta G < 0$. In the case of most amphipathic lipids, the enthalpy of association with other lipids is neglectably small

compared to the entropic term, mainly governed by the water “cage”. This makes the demixing a spontaneous process, yet in some cases spontaneous demixing occurs only above a critical temperature. Other physical factors facilitating spontaneous demixing of amphipaths in water such as water surface tension and dielectric constant shall be mentioned here, but not be detailed any further.

CLASSIFICATION OF BIOLOGICALLY RELEVANT LIPID SPECIES

Different functions of lipid molecules in cells

Considering functional biological membranes, the overall physical properties of lipids are no longer sufficient to understand the interactions between them and the functionality of a membrane. We thus have to take a closer look at the lipids existing in cells, particularly highlighting the fact that numerous lipid species serve as building blocks for biological membranes.

In this work only eukaryotic cells are studied, hence the lipids described in the following chapters are those found in Eukaryotes. However, it is noteworthy that the three kingdoms of life (Eukaryotes, Archea and Bacteria) have different lipidomes, i.e. they use different lipid species to form their respective membranes. According to the endosymbiotic theory, (later to be eukaryotic) cells absorbed during evolution protobacteria that became cellular organelles, namely peroxisomes, mitochondria and, in plants, the plastids. These organelles therefore have a lipidome that varies significantly from the lipidome of the surrounding cell, and in order to preserve this difference, these organelles must independently produce their own lipids species. In mitochondria, phophatidylglycerol and cardiolipin are lipids that are very akin to the lipids of bacterial lipidome and indeed necessitate independent synthesis machineries.

The eukaryotic lipids can be subdivided in two major subfamilies: The lipids based on fatty acids and those based on terpenoids (**Figure 2**). Fatty acid-based lipids are the major building blocks of cellular membranes, and their structure and function will be detailed below, but it is nonetheless noteworthy that fatty acids are not only used as membrane building blocks. They can serve as storage for lipids (triacylglycerols), as energy source, as signaling molecules, or as precursors for eicosanoid biosynthesis. The fatty acid-based membrane building blocks are the phospholipids, which can again be subdivided in the glycerophospholipids and the sphingolipids.

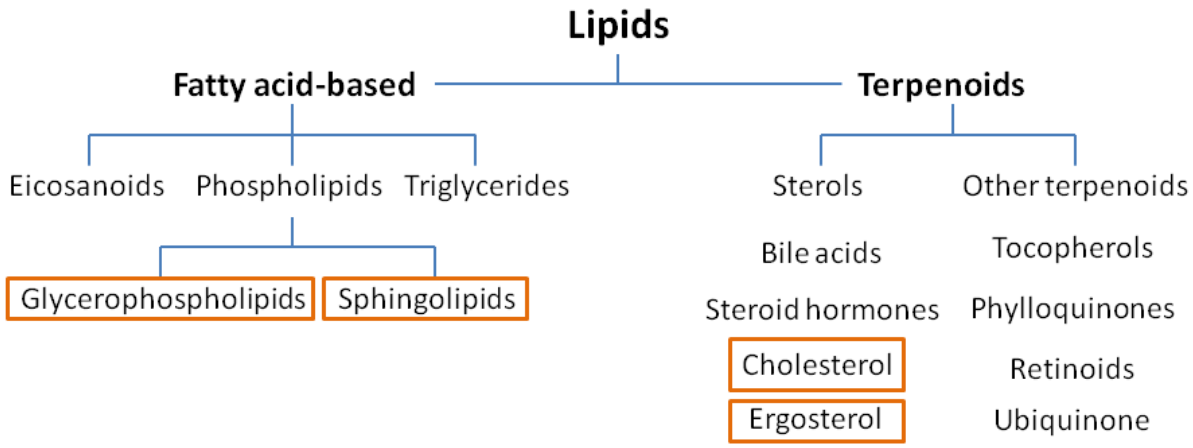

Figure 2. Cellular lipids and membrane building blocks

Lipid classes in eukaryotic cells, the membrane building blocks are highlighted in orange.

The only terpenoid lipids that serve as membrane building blocks are the sterols. Again, it must not be forgotten that other terpenoid molecules play major roles unrelated to their function as building blocks, such as sterol metabolites (bile acids, steroid hormones, vitamine D), retinoids (vitamin A), tocopherols (vitamin E), phylloquinones (vitamin K) and ubiquinone (coenzyme Q).

Major building blocks of cellular membranes

Inside the eukaryotic kingdom, differences in lipidomes exist between species. Our laboratory examines two types of eukaryotic model systems: human (*Homo sapiens*) and the budding yeast *Saccharomyces cerevisiae* (baker's yeast); differences between these two species will be highlighted.

Glycerophospholipids

Glycerophospholipids (GPLs) are the most important building blocks of eukaryotic cellular membranes. The common basis of those GPLs is the hydrophobic moiety diacylglycerol (DAG) in wich two acyl chains are linked in *sn*-1 and *sn*-2 position by an ester bond (or ether bond in the case of plasmalogen) to a glycerol "backbone" that is further modified in order to yield phospholipids (**Figure 3**). Phosphatidic acid (PtdOH or PA) is DAG phosphorylated on its *sn*-3 hydroxyl function. Under physiological conditions, phosphate moieties bear a negative charge; they thus participate in the total charge of GPLs attributing

one negative charge. Esterification of the *sn*-3 phosphate with different headgroups gives the remaining four GPLs: phosphatidylcholine (PtdCho or PC), phosphatidylethanolamine (PtdEtn or PE), phosphatidylinositol (PtdIns or PI) and phosphatidyl-*L*-serine (PtdSer or PS; only the *L*-form is found in eukaryotes). The first two, that are also the most abundant GPLs in higher eukaryotes, have a headgroup formed of choline and ethanolamine, respectively, bearing a positive charge; they are thus zwitterionic (no total net charge). In PI the headgroup is formed by a *myo*-inositol and in PS it is *L*-serine. *Myo*-inositol is neutral and serine zwitterionic, therefore PI and PS bear a total negative charge, just as PA. Phosphoinositides (PIPs) are PI species phosphorylated on one (or more) hydroxyl groups on the inositol ring and therefore bear additional negative charge on their headgroup. They do not serve as major building blocks, but despite their scarceness are key functional lipids for organelle identification and signaling events (van Meer, Voelker *et al.* 2008). In phospholipids, the headgroup can not only vary in terms of overall charge but also in terms of volume; the **headgroup size** is greatest in PI and decreases from PC, PE and PS to PA, with absence of headgroups in DAG.

The tails of lipid molecules are formed by acyl chains, which can be fully **saturated, mono- or polyunsaturated**, that means they carry no, one or several double bonds. These double bonds can be in *cis*- or *trans*-configuration, but in lipid molecules the *cis*-conformation is predominant. In phospholipids generally only one chain is unsaturated. The range of acyl chain lengths in eukaryotic cells is broad, ranging from 12 to 26; however only chain lengths are always even. Most phospholipids have chain lengths between 16 and 22 carbon atoms, with C12 and C14 being minor fatty acids, and have zero to four double bonds (Schneiter, Brugger *et al.* 1999; Ejsing, Sampaio *et al.* 2009). Describing an acyl chain, the number of carbon atoms (20, for example) and double bonds (4, for example) are usually noted as C20:4.

Under normal growth conditions, *S. cerevisiae* produces only saturated and monounsaturated fatty acids, narrowing down the variety of saturation levels. The most abundant acyl chain lengths are C16 and C18, overall palmitoleic acid (C16:1) and oleic acid (C18:1) are the most abundant fatty acids, followed by palmitic acid (C16:0) and stearic acid (C18:0) (Ejsing, Sampaio *et al.* 2009).

It is noteworthy that polycarbon chains are flexible, however a double bond decreases the flexibility and particularly the kink induced by *cis*-double bonds also increases

the volume occupied by the chains. The number, length and saturation level of acyl chains thus define together with the headgroup size, the overall geometry of GPLs. Phospholipids can have a **conical** (bis-unsaturated DAG), **cylindrical** (saturated PC or saturated PS) or **inversed-conical** (lyso-GPLs) **shape.** This has important implication for the membrane properties (**Figure 7**).

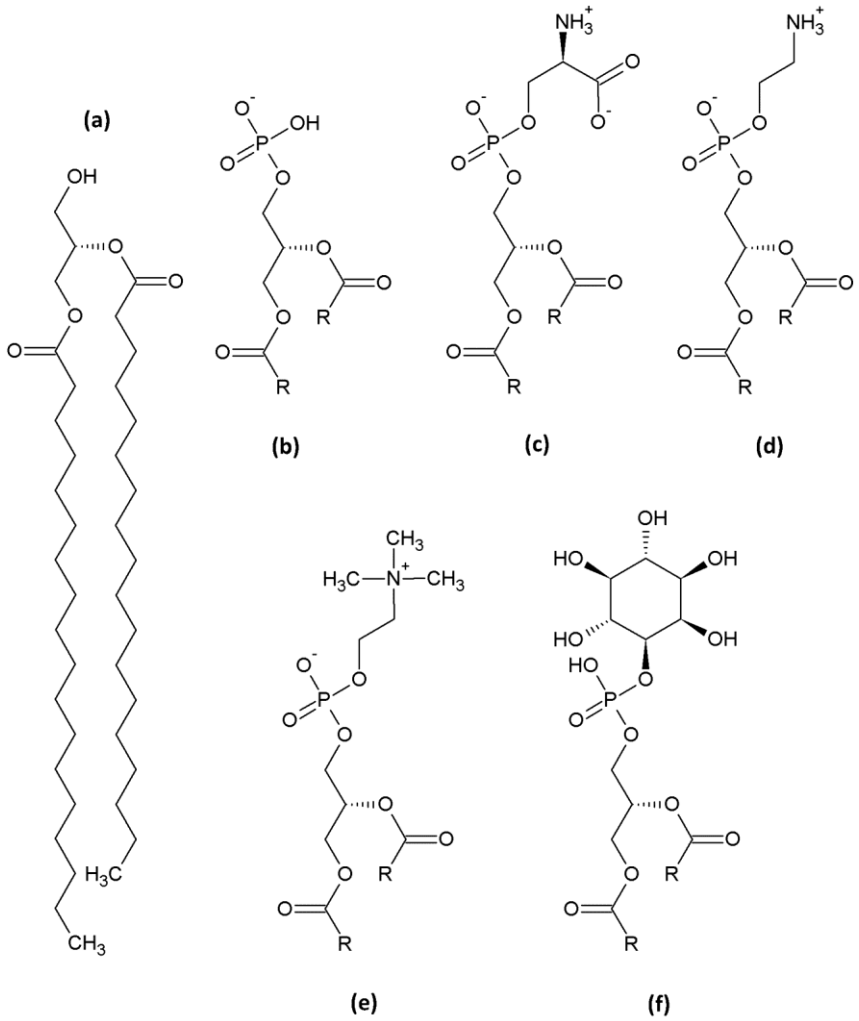

Figure 3. The five members of the GPL membrane building blocks.

(a) Diacylglycerol (DAG), **(b)** Phosphatidic acid (PA), **(c)** Phosphatidyl-*L*-serine (PS), **(d)** Phosphatidylethanolamine (PE), **(e)** Phosphatidylcholine, **(f)** Phosphatidylinositol. In (b)-(f), acyl chains are shown as rest (R).

Sphingolipids

Sphingolipids are phospholipids in which the backbone is not a glycerol but derives from serine and palmitic acid, forming the long-chain base or sphingosine backbone (**Figure 4**). Sphingosines can be N-acetylated with a very long chain fatty acid (VLCFA, C24:0 or C26:0)

to form ceramide. In yeast, the long chain base and acyl chains are saturated and can be hydroxylated in C4 of the long chain base (phytosphingosine) and/or in C2 of the VLCFA, increasing the amphiphilicity of sphingolipids compared to GPLs.

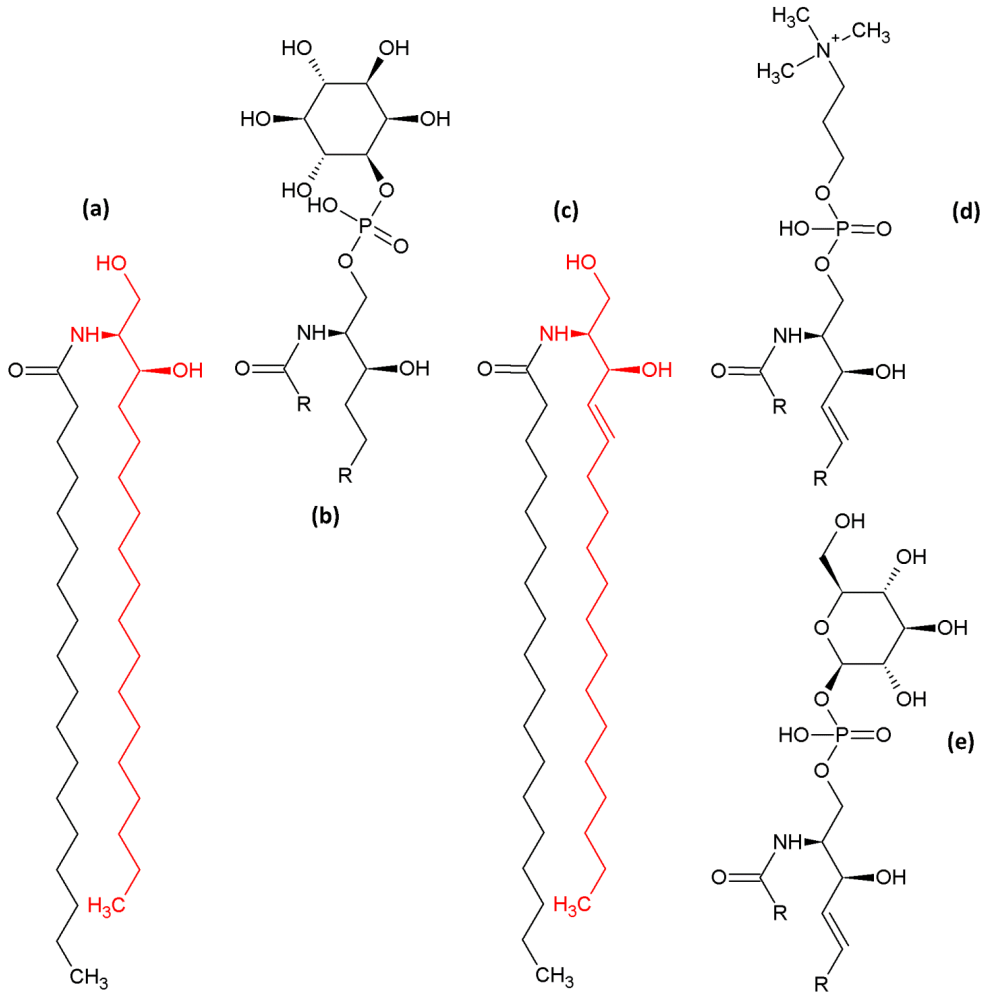

Figure 4. Simple and complex sphingolipids of yeast and mammalian.

Yeast sphingolipids (a)-(b): **(a)** Dihydroceramide, the yeast long-chain base dehydrosphingosine is highlighted in red. **(b)** inositol-phosphorylceramide (IPC). Complex mammalian sphingolipids (c)-(e): **(c)** ceramide, the mammalian long-chain base dehydrosphingosine is highlighted in red, **(d)** a sphingomyelin (SM), **(e)** a simple cerebroside. In (b), (d) and (e) acyl chains of the fatty acid and the sphingoid backbone are shown as rest (R).

Like in GPLs, the ceramide backbone can be phosphorylated on its 1-OH function and headgroups can be added for formation of complex sphingolipids. In mammalian cells, addition of choline or ethanolamine yields sphingomyelins (SMs), whereas one or more glycosylations allow the formation of a variety of glycosphingolipids (cerebrosides and gangliosides). SMs are more abundant that cerebrosides and gangliosides. In yeast only three complex sphingolipids are synthesized, all of them with an inositol headgroup that can be glycosylated: inositol-phosphorylceramide (IPC), mannosyl-inositol-phosphorylceramide

(MIPC) and mannosyl-diinositol-phosphorylceramine ($M(IP)_2C$). Complex sphingolipids have an important role in biological membranes, notably due to their affinity for sterols (Schneiter 1999).

As for GPLs, sphingolipids shape is controlled by acyl chain length and saturation and the headgroup size. Sphingolipids display the longest acyl chains, C24 and C26 (VLCFAs) are only found in sphingolipids, and are generally saturated. Ceramide displays a conical shape like DAG, whereas complex sphingolipids with their bulky headgroups display an inversed-conical shape (Schneiter, Brugger *et al.* 1999; Ejsing, Sampaio *et al.* 2009).

Sterols

Sterols, lipids from the isoprenoid lipid family, are also major building blocks for membranes in eukaryotic cells. Though both are amphiphilic, but their particular shape varies significantly from the aforementioned phospholipid species: Their polar headgroup (3-OH in cholesterol) is tiny and displays no charge; their hydrophobic moiety does not have a flexible and long shape but a planar four-ringed structure (the steroid backbone) with a short aliphatic "tail". Their particular shape allows specific interactions with phospholipids, particularly saturated GPLs and sphingolipids, and these features make sterol an essential, yet unconventional membrane building block. Higher eukaryotes contain mainly cholesterol, whereas in budding yeast ergosterol (bis-unsaturated, methylated cholesterol) is the most abundant sterol (Mesmin, Antonny *et al.* 2013) (**Figure 5**).

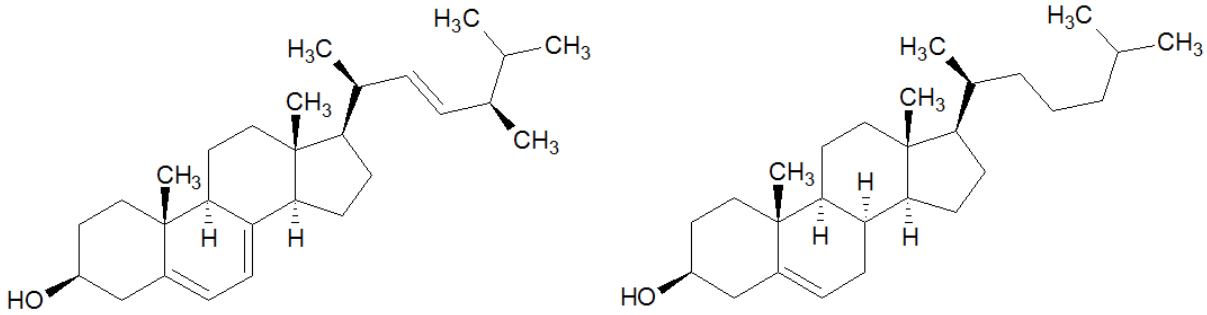

Ergosterol **Cholesterol**

Figure 5. Chemical structure of ergosterol and cholesterol.

Ergosterol and cholesterol are the major sterol species found in budding yeast and mammalian membranes, respectively.

Oxidized metabolites of sterol, oxysterols, are precursors of steroid hormones and bile acids and implied in signaling (Massey 2006). 25-hydroxycholesterol (25-OH), for example, is a potent cholesterol biosynthesis inhibitor in concentrations in the nanomolar range (Olsen, Schlesinger *et al.* 2009). Sterol oxidation significantly alters its behavior towards membranes: Oxidation leads to more hydrophilic properties, and oxysterols in membranes are twisted into an orthogonal orientation compared to phospholipids (Olsen, Schlesinger *et al.* 2009). Cholesterol orientation is mainly governed by interaction between its 3-OH headgroup and surrounding phospholipid headgroups, it is inserted parallel to phospholipids. Due to their increased hydrophilicity, oxysterols diffuse more rapidly (10^2-fold increase compared to cholesterol) between membranes (van Amerongen, Demel *et al.* 1989)

LIPID DISTRIBUTION

BETWEEN AND INSIDE CELL MEMBRANES

Cellular lipidomics and lipid homeostasis

Biological membranes are not at all as homogenous as they are often represented. Their composition varies significantly between species, tissues, cell types and their respective organelles. These variations can concern the protein/lipid ratio, membrane symmetry and overall lipid composition (ratio of charge and neutral GPL species, abundance of sterol and sphingolipids, acyl chain length and saturation), altogether governing membrane properties. The study of differences in lipid distribution and its dynamics has given rise to a new field in membrane biology: **cellular lipidomics**. This chapter will give insight into differences between of organellar membranes and the therefore emerging properties (van Meer, Voelker *et al.* 2008; Bigay and Antonny 2012; Holthuis and Menon 2014).

Some general features are conserved among all eukaryotic cells: The nuclear envelope is continuous with the endoplasmic reticulum (ER) and their lipid compositions are alike: > 40 % PC, 30 % PE, 10 % PI, 5 % PS, 5% sterol (Drin 2014) (**Figure 6**). ER and nuclear envelope are protein-rich membranes, with > 10 mg protein/mg phospholipid (Zinser, Sperka-Gottlieb *et al.* 1991). This ratio is only 3 mg/mg for the plasma membrane (PM), and anionic phospholipids (PS, PI) are enriched there as well as sphingolipids and sterols, and it is thicker (9.2 ± 0.4 nm for the PM and 7.5 ± 0.8 for the ER (Schneiter, Brugger *et al.* 1999)) and denser (Zinser, Sperka-Gottlieb *et al.* 1991; Schneiter, Brugger *et al.* 1999). The Golgi apparatus is at the crossroad between the ER and the PM, its composition changes from *cis*-Golgi (whose membranes are like those of the ER) to more PM-resembling *trans*-Golgi membranes. Endosomal compartments have compositions comparable to those of the PM from which they originate, but are characterized by the presence of an specific endosomal GPL, lyso-bisphosphatidic acid (LBPA, also bis(monoacylglycero)phosphate BMP) (van Meer, Voelker *et al.* 2008). Budding yeast vacuolar membranes are rather loose and deprived of sterols and protein, but contain steryl esters (Schneiter, Brugger *et al.* 1999). Certain

organelles are labeled by minor pools of PIPs that have important functions. Mitochondria are surrounded by two lipid bilayers (Outer mitochondrial membrane OMM and inner mitochondrial membrane IMM) that show important differences in their lipid composition. The OMM is quite alike to the PM, but deprived of ionic phospholipids, whereas the IMM has a high protein/lipid ratio (7 mg protein / mg phospholipid), high amounts of unsaturated acyl chains and is rich in (≈ 10 mol%) a specific mitochondrial lipid, cardiolipin (Comte, Maisterrena *et al.* 1976; Schneiter, Brugger *et al.* 1999). Despite these general features, it is noteworthy that in all yeast membranes PI is more abundant at the expense of PC, particularly in the PM, which also has an elevated PS content compared to higher eukaryotes (McGee, Skinner *et al.* 1994; van Meer, Voelker *et al.* 2008).

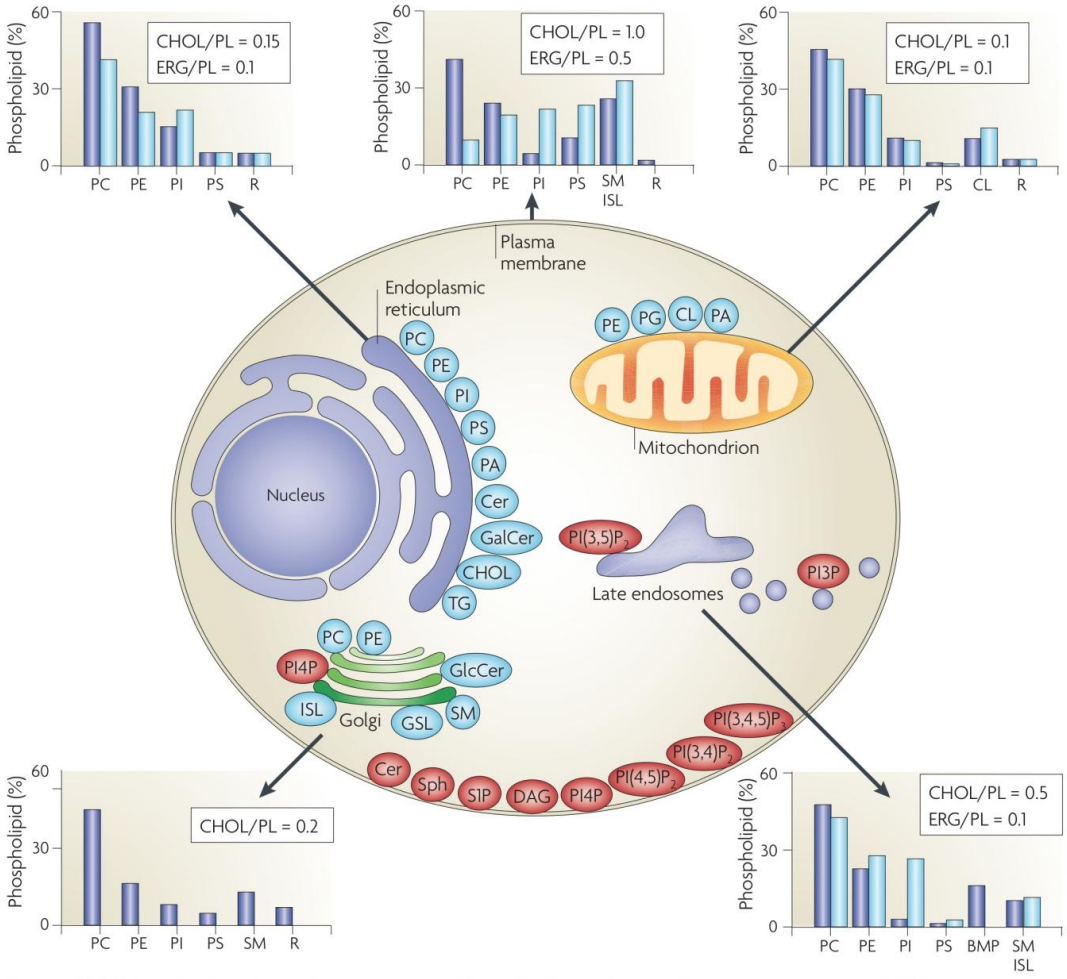

Figure 6. Lipid distribution in eukaryotic cells.

The cellular organelles and their respective lipid composition with phospholipid concentrations expressed in percent of total phospholipid. Sterol abundance is described as ratio over total phospholipid for mammalian cells (CHOL/PL) and budding yeast (ERG/PL). Illustration from (van Meer, Voelker *et al.* 2008).

The uneven lipid distribution between and within organellar membranes allow each of them to optimize its function. Membrane composition, curvature, electrostatics and packing have to be considered as a whole in order to understand the functionalization of subcellular membranes (Bigay and Antonny 2012). It is thus important to describe how overall membrane properties arise from lipid composition.

Biophysical aspects of lipid bilayers

Effects of lipid shape and saturation levels

Lipid shape governs different aspects of membranes. The archetypal cylindrical lipids will take a lamellar organization as shown in (**Figure 1b**). With lipids deviating from the ideal, cylindrical shape, interaction either between headgroups of between acyl chains is decreased, as the accessible volume for the headgroups and the acyl chains, respectively, increases. The volume and charge is thus no longer homogenously distributed on a membrane, but locally displays dynamic higher or lower density. These imperfections in headgroup distribution are called **lipid packing defects** (Vamparys, Gautier *et al.* 2013) (**Figure 7**). Locally, such packing defects can increase membrane fluidity and facilitate protein interaction with lipids, but on a larger scale will deform the membrane: Local accumulation of conical or inversed-conical lipids will bend membranes to optimize the interactions between lipids, and thus induce **membrane curvature** (Bigay and Antonny 2012) (**Figure 7**).

Three **phase states** can be defined for a bilayer: a **liquid-disordered phase** (l_d, low degree of order, fast diffusion), a **solid gel phase** (s_o, high degree of order, slow diffusion) and **liquid-ordered phase** (l_o, high degree of order, fast diffusion). These phases depend on the composition of the membrane and on the temperature. In liquid-ordered membranes the interaction of lipids with each other is stronger; formation of these phases is thus favored by high acyl chain saturation levels: Saturated phospholipids with a cylindrical shape are not subject to steric hindrance as conical, unsaturated phospholipids are due to their kinked acyl chains; cylindrical lipids hence display larger surfaces for lipid-lipid interaction (van Meer, Voelker *et al.* 2008) (**Figure 7**).

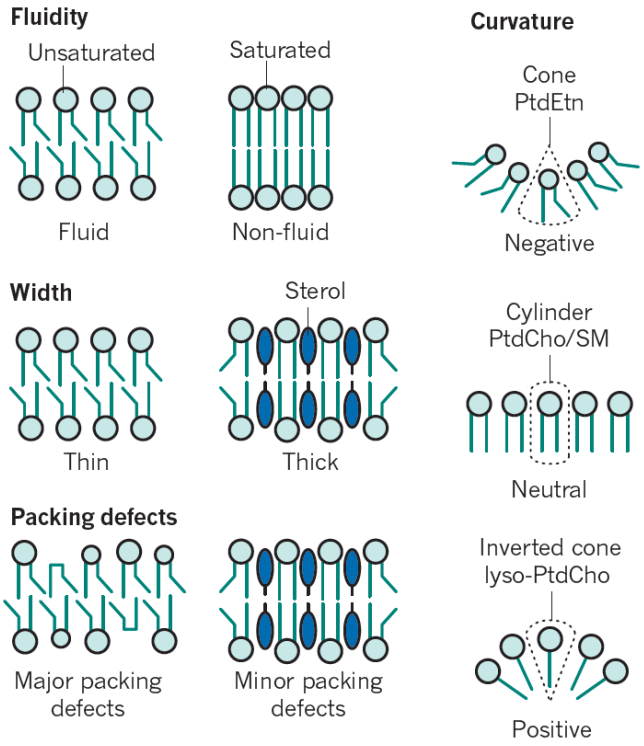

Figure 7. Impact of lipid shape and saturation on membrane organization.

See text for details. Illustration from (Holthuis and Menon 2014).

Sterols play an intriguing role in membranes depending on their phase: Their particular shape allows upon insertion in a lipid bilayer the stabilization of the membrane: It decreases the interaction between phospholipids by interacting with their acyl chains, thus preventing formation of solid gel phases. This interaction is stronger when the acyl chains surrounding the sterol molecule are saturated; lipid saturation can therefore allow segregation of sterol and *vice versa*. On the other hand, fluid membranes are rigidified and thickened by sterol insertion by the "condensing effect". The acyl chain length together with the saturation level also govern **membrane thickness**: longer and saturated acyl chains can interact with sterols in the core of the membrane. Saturated and sterol-rich membranes are thus thicker than unsaturated membranes deprived of sterol (Munro 2003) (**Figure 7**).

Additionally, under certain circumstances one lipid bilayer can separate into two distinct coexisting phases (van Meer, Voelker *et al.* 2008). The **microdomains** formed by phase separation in one membrane, also referred to as **'lipid rafts'**, which are enriched in sterols and sphingolipids, have been analyzed, but whether they can play a physiological role is still discussed (Munro 2003; van Meer, Voelker *et al.* 2008; Toulmay and Prinz 2013). Despite the possibility of phase formation and separation in artificial membranes, the situation in biological membranes might not be so clear cut.

Transbilayer asymmetry and anionic lipids

Biological membranes are lipid bilayers and therefore have one cytosolic and one lumenal (in the case of the PM: extracellular or exoplasmic) leaflet. In some membranes, the two leaflets do not share the same lipid composition, i. e. they display a **transbilayer asymmetry** (van Meer, Voelker *et al.* 2008). In the ER, anionic lipids, particularly PS, are mainly facing the ER lumen. In the PM the extracellular face is devoid of PS and highly enriched in sphingolipids, PC and sterols whereas its cytosolic face displays opposite pattern with an elevated PS concentration thus increasing PM surface charge on its cytoplasmic face (Leventis and Grinstein 2010) (**Figure 15**).

Conservation of transbilayer asymmetry is mostly due to the inability of phospholipids to cross the membrane. Diffusion from one leaflet to another implies for a lipid molecule disruption of headgroup interaction and passage of the polar moiety through the hydrophobic core of the bilayer, which is the reason for the slow transbilayer movement of phospholipids, called **flip-flop**. GPLs and sphingolipids flip with $t_{1/2}$ of hours (Holthuis and Levine 2005). Lipids without polar headgroup (such as DAG and ceramide) and neutral sterol molecules, on the other hand, can flip rapidly ($t_{1/2}$ of seconds to minutes) between leaflets of one membrane (Holthuis and Levine 2005; Leventis and Grinstein 2010). The establishment of transbilayer asymmetry will be discussed below (See The origins of transbilayer asymmetry).

Special lipids: Phosphoinositides

Certain organelles are labeled by minor pools of PIPs that were initially seen as mere precursors for the formation of PI(4,5)P_2 that is cleaved by phospholipase C (PLC) to yield Ins(1,4,5)P_3 and DAG, two signaling molecules associated to G-protein coupled receptors at the PM. Moreover, a variety of functions of PIPs in multiple cellular processes have been unveiled. The PIPs are no major membrane constituents, but act, together with small G-proteins, as specific organellar signposts to facilitate their recognition. For example, PI(4)P marks mainly the *trans*-Golgi region, but it should be noted that functionally distinct pools mark also the PM and endosomal fractions. One of the most common protein domains to interact with PI(4)P are Pleckstrin Homology (PH) domains that will be detailed below (PI(4)P detection by NBD-PHFAPP). Other PI(4)P-interacting protein domains are found in the

clathrin adaptor proteins, such as AP-1 and GGAs, that recognize both cargo protein and PI(4)P to mediate clathrin coat formation. The γ subunit of dimeric human AP-1 (Apl4p in budding yeast) allows PI(4)P recognition by a conserved binding site inferred from homology from the crystal structure of murine AP-2, but the detailed mechanism remains to be elucidated (Collins, McCoy *et al.* 2002). **G**olgi-localized, **γ**-ear-containing, **A**RF (ADP (adenosine diphosphate) ribosylation factor)-binding proteins (GGAs, Gga1p and Gga2p in yeast) are clathrin-adaptors required for Golgi-to-endosome traffic. They all contain a GAT domain that detects both PI(4)P and Arf1-GTP by coincidence detection. The binding site for PI(4)P has been identified in a solvent-exposed three helix bundle of that domain that shows no homology with other PI(4)P-binding domains (Wang, Sun *et al.* 2007; Lenoir and Overduin 2013).

PI(4,5)P_2 in key for PLC signaling at the PM and it plays an important role in the interaction between PM and the cytoskeleton as well as for exocytotic and endocytotic events (Tan and Brill 2014). Intriguingly, in yeast, PI(4,5)P_2 deficiency phenotypes differ depending on the PI(4)P pool used for PI(4,5)P_2 synthesis, indicating that there are distinct pools of PI(4,5)P_2 within the PM (Audhya, Foti *et al.* 2000); nevertheless, both of these pools can be recognized by PH domains.

PI(3)P is mainly found on early endosomal compartments, and PI(3,5)P_2 labels mainly late endosomal compartments (Behnia and Munro 2005; Mayinger 2012). PI(3)P is recognized by zinc finger motifs called FYVE (named after the proteins **F**ab1p, **Y**OTB, **V**ac1p and **E**EA1 where it was first identified) domains and Phox homology (PX) domains that target proteins to the endolysosomal system. PI(3,5)P_2 is synthesized from PI(3)P at the late endosomal/lysosomal system and epsin N-terminal homology (ENTH) domain containing proteins are recruited there by PI(3,5)P_2 recognition (Mayinger 2012).

Certain protein domains thus allow specific recognition of different subcellular membranes highlighted by different PIPs.

Marking territories in eukaryotic cells

Combining the general trends in membrane compositions and their biophysical implications, an overall tendency can be seen in lipid distribution: The ER is rich in unsaturated lipids and sterol is scarce and therefore mainly in a liquid-disordered phase.

Such fluidity is thought to be important for the folding of proteins with transmembrane-spanning domains and the tabulated structure of the ER, implying high curvature. Anionic phospholipids are scarce, thus making the ER and early membranes of the secretory pathway a subcellular region mainly defined by high packing defects (Bigay and Antonny 2012).

Continuing along the secretory pathway these characteristics are reversed, with the Golgi apparatus being and intermediate compartment crucial for this change. At the PM, the lipids there have higher saturation levels and the enrichment of sterol and complex sphingolipids allows a more liquid-ordered phase state, and packing defects are scarce. The cytoplasmic face of the PM additionally is enriched in the anionic phospholipid PS, together with PIPs making late membranes as the *trans*-Golgi and the PM mainly governed by electrostatics (Bigay and Antonny 2012) (**Figure 8**).

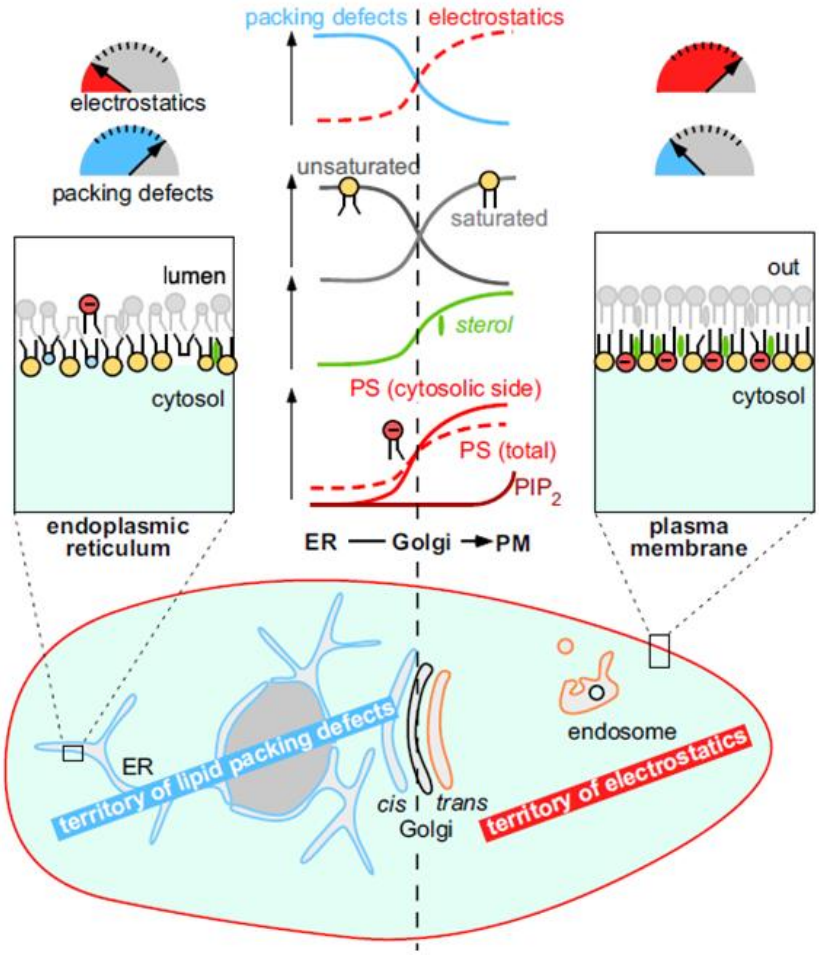

Figure 8. Division of eukaryotic cells in two territories.

Early regions of the secretory pathway such as the ER and *cis*-Golgi display a high level of unsaturated lipids and its biophysics is mainly governed by membrane packing defects. Late membranes such as *trans*-Golgi and the PM are densely packed and rich in anionic phospholipids, therefore making it the territory of electrostatics. Illustration from (Bigay and Antonny 2012).

CONCEPTS FOR ESTABLISHING AN UNEVEN LIPID DISTRIBUTION IN EUKARYOTIC CELLS

Despite their different compositions, organelles perpetually exchange parts of their membrane by vesicular trafficking that allows transport of proteins and nutrients in cells. The constant arrival and departure of material necessitates mechanisms to regulate its lipid homeostasis, i.e. to keep its overall lipid composition and uneven distribution constant.

The mechanisms implied in establishment differences in lipid compositions between subcellular compartments can be divided in three classes: The first class is lipid metabolism, i.e. lipids are produced or modified at different places inside the cell. The second class is lipid transport between bilayers of a single bilayer, which is required for establishing transbilayer asymmetry. The third class is vesicular or non-vesicular mechanisms that deliver lipid molecules specifically between membranes.

Spatial differentiation through lipid metabolism

Glycerophospholipid biosynthesis routes

Synthesis of phosphatidic acid and diacylglycerol

PA is synthesized on the cytosolic face of the ER from glycerol-3-phosphate by acylation of the free 1- and 2-hydroxyl groups with fatty acids activated in the form of acyl-CoA (Coenzyme A). A single acylation yields lysoPA, a subsequent, second acylation yields PA. Dephosphorylation of PA produces DAG, the precursor for GPL biosynthesis *via* the Kennedy pathway (see below) and for biosynthesis of triacylglycerol (TAG), a storage lipid. PA can also be nucleotidylated with cytosine-triphosphate (CTP) by phosphatidate cytidylyltransferase yielding CDP-DAG, the precursor for GPL synthesis *via* the *de novo*-pathway (see below) and cardiolipin biosynthesis in mitochondria (Henry, Kohlwein *et al.* 2012).

Functionalization of different GPL species

In order to obtain fully functional GPLs, a headgroup has to be added to the DAG precursors. In eukaryotic cells, there are two pathways of GPL synthesis: In the **Kennedy pathway**, the major GPL biosynthesis pathway in higher eukaryotes, PC is synthesized by the addition of CDP-choline to DAG and in a reaction catalyzed by CPT1 (cholinephosphotransferase 1), whereas EPT1 (ethanolaminephosphotransferase 1) assures the synthesis of PE from DAG and CDP-ethanolamine. PS is subsequently synthesized from PC and PE, by swapping the headgroups for serine by PS synthases PSS1 and PSS2, respectively. Counter-reaction exist in which PS is decarboxylated, yielding PE, that can undergo subsequent tri-methylation, yielding PC. These reactions are catalyzed by PS decarboxylases (PSD) and PE-methyl transferases (PEMT), respectively. PI is synthesized following the so called ***de novo* pathway** from CDP-DAG and *myo*-inositol (Daum, Lees *et al.* 1998; Vance and Steenbergen 2005; Gibellini and Smith 2010) (**Figure 9**).

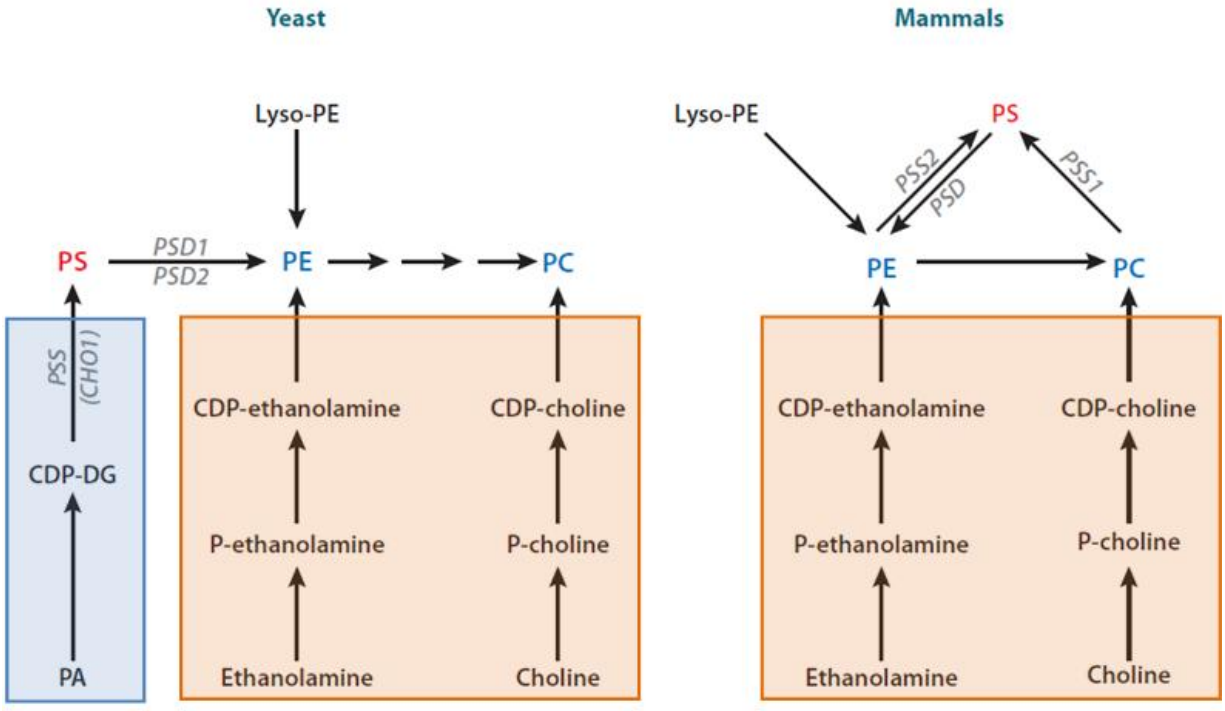

Figure 9. GPL synthesis pathways

All eukaryotes use the **Kennedy pathway** (orange boxes), but budding yeast can also produce PS via the ***de novo* pathway** (blue box) and PE and PC by decarboxylation and successive methylation. In Mammalia and yeast, PI is synthesized from CDP-DAG and *myo*-inositol, like PS in yeast (not shown). Illustration modified from (Leventis and Grinstein 2010)

The budding yeast *S. cerevisiae* possesses the same synthesis machinery, but additionally, it disposes of a *de novo* PS synthase, Pss1p (Cho1p), which synthesizes PS directly from CDP-DAG and *L*-serine. Despite the fact that the Kennedy pathway machinery is fully functional in yeast, it exploits mainly the *de novo* pathway and synthesizes most of its PC and PE by modifying the PS headgroup. The PS synthase Pss1p hence has to ensure the production of the majority of the total GPL in yeast, with PS thus being the key intermediate for bulk GPL synthesis. The syntheses of PS and PI share a common precursor, CDP-DAG, and its limited availability therefore restrains global GPL synthesis (Leventis and Grinstein 2010). For PE biosynthesis by decarboxylation *S. cerevisiae* encodes two PSDs (Psd1p and Psd2p) and two PEMTs, Cho2p and Opi3p. The former catalyzes the first and the latter catalyzing mainly the two other methylation steps. Both Kennedy pathway and *de novo* pathway enzymes are localized to the cytosolic face of the smooth ER in yeast and human (Daum, Lees *et al.* 1998; Vance and Steenbergen 2005; Leventis and Grinstein 2010) (**Figure 9**).

Of the abovementioned enzymes, PS decarboxylases are the only not to be localized at the ER but at the IMM (mammalian PSID and yeast Psd1p) and Golgi/endosomes (yeast Psd2p) (Leventis and Grinstein 2010). It is noteworthy that for budding yeast, an efficient transfer of PS from the ER to mitochondria and Golgi/endosomes is essential, as decarboxylation of PS and methylation of PE are the major sources of PE and PC, respectively. The lipid export/import appears to be favored by the localization of the concerned enzymes: They are not homogenously distributed within the ER but are rather enriched at parts of the ER, called **membrane contact sites** (MCSs) that encounter other membrane-bound compartments (Helle, Kanfer *et al.* 2013). These particular sites and their importance in lipid transport will be discussed in detail later. Human PS synthases PSS1 and PSS2, for example, are enriched in mitochondria-associated membranes (MAM) (Stone and Vance 2000) as well as its yeast counterpart Pss1p which is additionally found in the PM-associated membrane (PAM), thus in proximity of another organelle requiring PS import (Gaigg, Simbeni *et al.* 1995; Pichler, Gaigg *et al.* 2001).

Mammalian PI synthase activity has recently been localized to highly dynamic, ER-derived structures termed PI-Producing ER-derived Organelles or PIPEROsomes that would directly supply other organellar membranes with PI by ample contacts (Kim, Guzman-Hernandez *et al.* 2011). PI is an essential lipid for budding yeast that produces significantly more of this lipid than higher eukaryotes. The function of PI as a negatively charged building

block in membranes might be taken over by PS, thus the importance of PI in yeast might be linked to its function as a precursor for PIP and morevover, for sphingolipid synthesis or as basis of glycosylphosphatidylinositol (GPI)-anchored proteins (Daum, Lees *et al.* 1998).

Phosphoinositide biosynthesis pathways

Synthesis and localization of phosphoinositide species

PIPs are synthesized from PI by different kinases (PIK) that allow the localized and specific creation of PIP pools (**Figure 10**). PI(3)P is synthesized by class II and class III PI3K in the early endosomal system and regulates its dynamics during endocytosis and autophagy. In yeast, both PI(3)P and PI(3,5)P_2 are localized to the vacuole (the yeast counterpart of the endosomal/lysosomal compartment in higher eukaryotes) where they are synthesized by the class III PI3K Vps34 and the PI5K Fab1, respectively, two non-essential enzymes (Mayinger 2012).

In mammalian cells, PI(4)P is synthesized from PI by four PI4K (PI4KIIIα, PI4KIIIβ PI4KIIα and PI4KIIβ, also named, PI4KA, PI4KB, PI4K2A and PI4K2B respectively)and labels the Golgi as well as the PM. Golgi and PM-localized PI4K produce functionally distinct pools of PI(4)P: PI4KIIIβ (Pik1p in yeast) creates the most considerable pool in the Golgi apparatus and thus governs Golgi function in secretion *via* multiple PI(4)P effectors (Audhya, Foti *et al.* 2000; Tan and Brill 2014). Pik1p is localized to the Golgi by interaction with Frq1p, and is rapidly detached from Golgi membranes under glucose starvation conditions, leading to an arrest of vesicular trafficking (Faulhammer, Kanjilal-Kolar *et al.* 2007). PI4KIIIα (Stt4p in yeast) is targeted to the PM by interaction with Sfk1p and also with Efr3p *via* Ypp1p, which together regulates Stt4p localization and activity (Baird, Stefan *et al.* 2008; Wu, Chi *et al.* 2014). The endosomal/lysosomal PI(4)P pool synthesized by PI4KIIα and PI4KIIβ (only one homolog in yeast, Lsb6p) is minor and non-essential compared to the others, and regulates endosomal function (Han, Audhya *et al.* 2002; Shelton, Barylko *et al.* 2003; Jovic, Kean *et al.* 2014). Recently, a novel highly specific and sensitive probe for PI(4)P determination based on the P4M domain of the *Legionella pneumophilia* SidM protein has been developed. Utilization of this probe revealed a broader distribution of PI(4)P, promising a more detailed insight into dynamics of PI(4)P distribution (Del Campo, Mishra *et al.* 2014; Hammond, Machner *et al.* 2014; Hubber, Arasaki *et al.* 2014).

PM localized PI(4)P serves as a precursor for synthesis of $PI(4,5)P_2$ by PIP kinases (PIP5K, Mss4p in yeast), and PI(4)P for $PI(4,5)P_2$ synthesis can originate from both the PI4KA (Stt4p) and PI4KB (Pik1p) pools. PI(4)P together with $PI(4,5)P_2$ makes up to 90 % of cellular PIPs in yeast (Audhya, Foti *et al.* 2000; Audhya and Emr 2002; Tan and Brill 2014). Phosphorylation of PI(4)P and $PI(4,5)P_2$ by class I PI3K yields $PI(3,4)P_2$ and $PI(3,4,5)P_3$, respectively, two short-lived regulators of cell survival and growth, which are not found in yeast due to the lack of a class I PI3K (Odorizzi, Babst *et al.* 2000; Mayinger 2012).

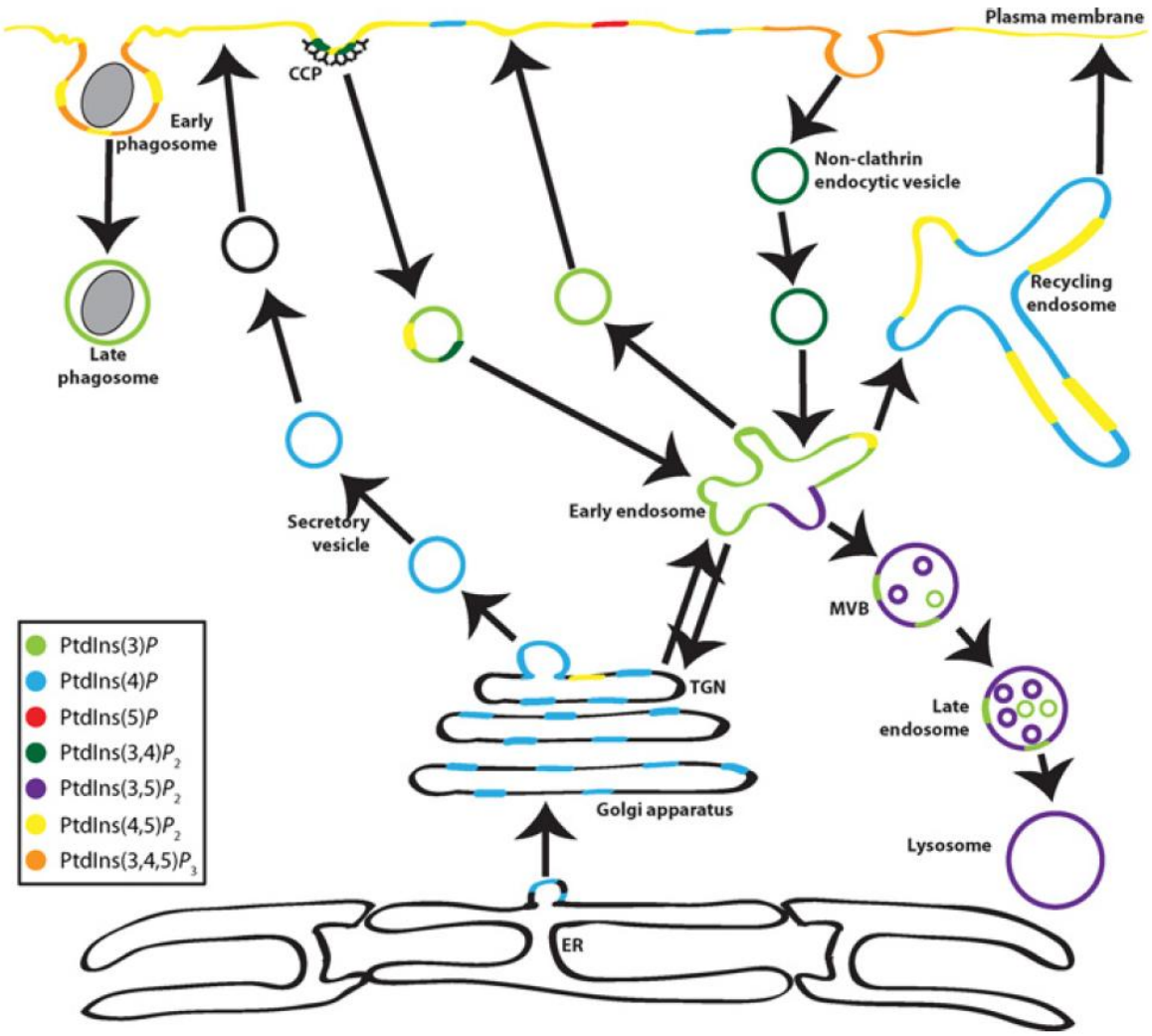

Figure 10. PIP distribution in Mammalia

PI(3)P is found on early endosomal compartments whereas $PI(3,5)P_2$ is localized to late endosomes and lysosomes. Two different pools of PI(4)P highlight the Golgi and the PM which also displays $PI(4,5)P_2$. PI(5)P and the short lived $PI(3,4,5)P_3$ are found at the PM. Illustration from (Billcliff and Lowe 2014).

Phosphoinositide catabolism

PIPs are hydrolyzed by more or less specific PIP phosphatases, allowing interconversion of PIP species and regulation of PIP controlled processes. Sac1p shall be the only PIP phosphatase detailed here due to its implication in PI(4)P hydrolysis; for details on other PIP phosphatases see (Billcliff and Lowe 2014).

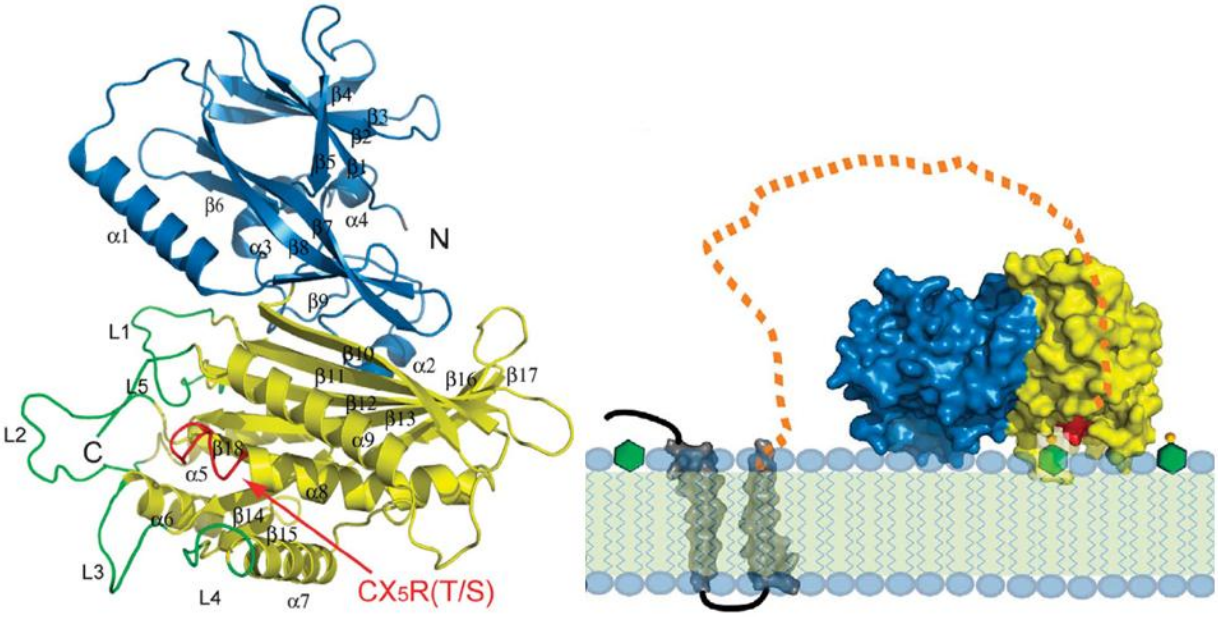

Figure 11. Crystal structure and model of the budding yeast PIP phosphatase Sac1p.

Left: Ribbon diagram showing the structure of the cytosolic portion (residues 1-503) of Sac1p with numbered secondary structure elements. The N-terminal domain (1-182) is shown in blue and the catalytic domain (183-503) in yellow. The catalytic motif $CX_5R(T/S)$ in the P-loop of the catalytic domain is shown in red and protruding loops around the catalytic motif are green. **Right**: Surface representation of the cytosolic portion (yellow and blue) attached to its transmembrane domains (grey) by a flexible linker (spotted in orange). The catalytic site recognizes PI(4)P (green hexagon with phosphate as yellow sphere) and hydrolyses it to yield PI (green hexagon). Illustrations from (Manford, Xia *et al.* 2010).

Sac1p is a double-spanning transmembrane protein that is localized to the ER, but can be shuttled to the Golgi under glucose starvation conditions where it is retained by interaction with Vps74 until reestablishment of normal growth conditions (Konrad, Schlecker *et al.* 2002; Wood, Hung *et al.* 2012; Cai, Deng *et al.* 2014). It is the major PIP phosphatase in budding yeast and controls mainly PI(4)P levels. The crystal structure of its cytosolic portion (1-503) has been solved and it displays two domains, the N-terminal SacN domain (1-182) and the catalytic phosphatase domain (183-503) (PDB entry: 3LWT) (Manford, Xia *et al.* 2010) (**Figure 11**). The phosphatase domain is localized in a loop (P-loop) and displays a $CX_5R(T/S)$

motif around Cys392, its catalytic motif. Mutations of Cys392 yield a catalytically inactive Sac1p in which localization and shuttling is conserved. Just as deletion of Sac1p, this mutation leads to accumulation of PIPs (Konrad, Schlecker *et al.* 2002; Tahirovic, Schorr *et al.* 2005; Manford, Xia *et al.* 2010). Sac1p *in vitro* hydrolyzes PIPs with relatively little specificity, but *in vivo* PI(4)P is the main substrate, and PI(4)P from both Stt4p and Pik1p are hydrolyzed (Tahirovic, Schorr *et al.* 2005; Faulhammer, Kanjilal-Kolar *et al.* 2007). Hydrolysis activity is increased by allosteric activation by anionic phospholipids, particularly PS (Zhong, Hsu *et al.* 2012).

It has been hypothesized that ER-resident Sac1p could hydrolyze the Stt4p PI(4)P pool at ER-PM contact sites. A 80 amino acid (aa) stretch at the C-terminus of the catalytic domain is unstructured, and initially it was thought that this stretch could serve as a linker allowing the catalytic domain to act *in trans* of its transmembrane anchor at ER-PM MCSs (Manford, Xia *et al.* 2010; Stefan, Manford *et al.* 2011). Recent findings showed however that this segment is essential for substrate recognition and catalytic activity, thus challenging the hypothesis of *in trans* activity (PDB entry: 4TU3) (Cai, Deng *et al.* 2014). Sac1p related phenotypes do not only concern vesicular trafficking; in ΔSac1 yeast strains the levels of complex sphingolipids are decreased, probably due to the importance of its substrate, PI, for complex sphingolipid synthesis (Brice, Alford *et al.* 2009). Additionally, ΔSac1 mutants accumulate PS in the ER at the expense of the PM in a manner independent of the *de novo* synthesis of PE and PC by PS decarboxylases, indicating an implication of Sac1p in ER-to-PM PS transport (Tani and Kuge 2014). Localized synthesis and hydrolysis by PI-/PIP-kinases and PIP-phosphatases, respectively, thus allow spatially controlled distribution of PIPs and maintenance of their gradients.

Sphingolipid biosynthesis

Long-chain base and ceramide synthesis

Ceramide has the same role for sphingolipids that DAG has for GPLs in that it forms the backbone for sphingolipids. It induces the major difference between the two phospholipid subfamilies: DAG is based on a glycerol backbone with two acyl chains. Sphingolipids have only one acyl chain, attached to the 2-amine function of the sphingoid backbone. The sphingoid backbone (the long chain base LCB), takes over the role of both the

glycerol and one acyl chain in DAG (see **Figure 4**) (Schneiter 1999). This sphingoid backbone is synthesized from a common precursor for all phospholipids, acyl-CoA that in the case of sphingolipids is coupled to serine by the ER enzyme serine palmitoyltransferases (SPT in human, Lcb1p and Lcb2p in *S. cerevisiae*) yielding ketodehydrosphingosine that is further reduced to dehydrosphingosine. This molecule is in turn *N*-acylated by ceramide synthase (CerS in human, Sur2p in budding yeast) to yield ceramide in the ER (Dickson and Lester 1999; Tidhar and Futerman 2013).

Metabolization of ceramide into sphingolipids

The synthesis of complex sphingolipids in both mammalia and yeast takes place in the *trans*-Golgi lumen. Ceramide has a no polar headgroup; it is therefore rapidly flipped between membrane leaflets, allowing lumenal metabolization. Mammalia synthesize two classes of complex sphingolipids: SMs and glycosphingolipids (see **Figure 4**). SMs are synthesized from ceramide by SM synthase (SMS). Glycosphingolipid biosynthesis necessitates glucosylceramide as precursor that is synthesized in the *cis*-Golgi from ceramide by glucosylceramide synthase (GCS) and transported by FAPP2 (Four Phosphate Adaptor Protein 2, see

Glycolipid transfer proteins and FAPP proteins: glycol(sphingo)lipid transporters) to the *trans*-Golgi, where glycosphingolipid synthesis occurs, mediated by multiple glycosyl-transferases (Funato and Riezman 2001).

In budding yeast, the number of complex sphingolipids is reduced to three, all of which have modified forms of inositol as their polar head group. For their synthesis ceramide is transported by both vesicular and non-vesicular pathways towards the Golgi apparatus. (Funato, Vallee *et al.* 2002) Transfer of inositol phosphate from phosphatidylinositol to ceramide for formation of inositol phosphorylceramide (IPC, see **Figure 4**) is catalyzed by the essential protein Aur1p and highly sensitive to the equilibrium between PI and PI(4)P, as perturbations lead to decreased synthesis of complex sphingolipids (Brice, Alford *et al.* 2009). Mannosylation to form mannosyl-inositol phosphorylceramide (MIPC) and further conversion from MIPC to mannosyl-diinositol phosphorylceramide ($M(IP)_2C$) with PI also occur in the Golgi complex (Brice, Alford *et al.* 2009). Finally, complex sphingolipids are

transported to the PM, where they are most abundant and where they tightly associate with sterol.

Sterol: biosynthetic and uptake routes

Sterol biosynthesis in eukaryotic cells

The biosynthesis pathway of sterols is complex and necessitates over 20 enzymes. Briefly, three molecules of acetyl-CoA are condensed in the mevalonate pathway by HMG-CoA (3-Hydroxy-3-methylgutaryl-CoA) reductase, a key enzyme in the sterol biosynthesis pathway. Further decarboxylation and reduction yields 3-isopentenyl pyrophosphate. Geranyl transferases condense three molecules of 3-isopentenyl pyrophosphate into farnesyl pyrophosphate, and squalene synthase condenses two farnesyl pyrophosphates into squalene. After epoxidation, lanosterol synthase catalyzes the formation of lanosterol, the first molecule in the biosynthesis pathway with the characteristic four-ringed sterol structure. The further pathways differ slightly between mammalia and yeast, as cholesterol is the most important sterol species in mammalia, whereas yeast produces mainly ergosterol. Notwithstanding the differences in the synthesis pathways, both mammalian and yeast sterol biosynthesis take place in the ER, making efficient sterol sorting for functionalization of subcellular membranes (Henneberry and Sturley 2005) (**Figure 12**). However, whereas the syntheses of sphingolipids and different GPL species are tightly interconnected, sterol biosynthesis only shares its basic precursor acetyl-CoA with their respective biosynthesis pathways.

Degrella *et al.* showed that in the case of newly synthesized sterols in mammalian cells, the transport of sterol is independent of vesicular trafficking and is energy-dependent (DeGrella and Simoni 1982). Menon and coworkers were able to show that in yeast, just as in mammalian cells, newly synthesized sterols are transported by non-vesicular, energy-dependent trafficking pathways towards the PM (Baumann, Sullivan *et al.* 2005).

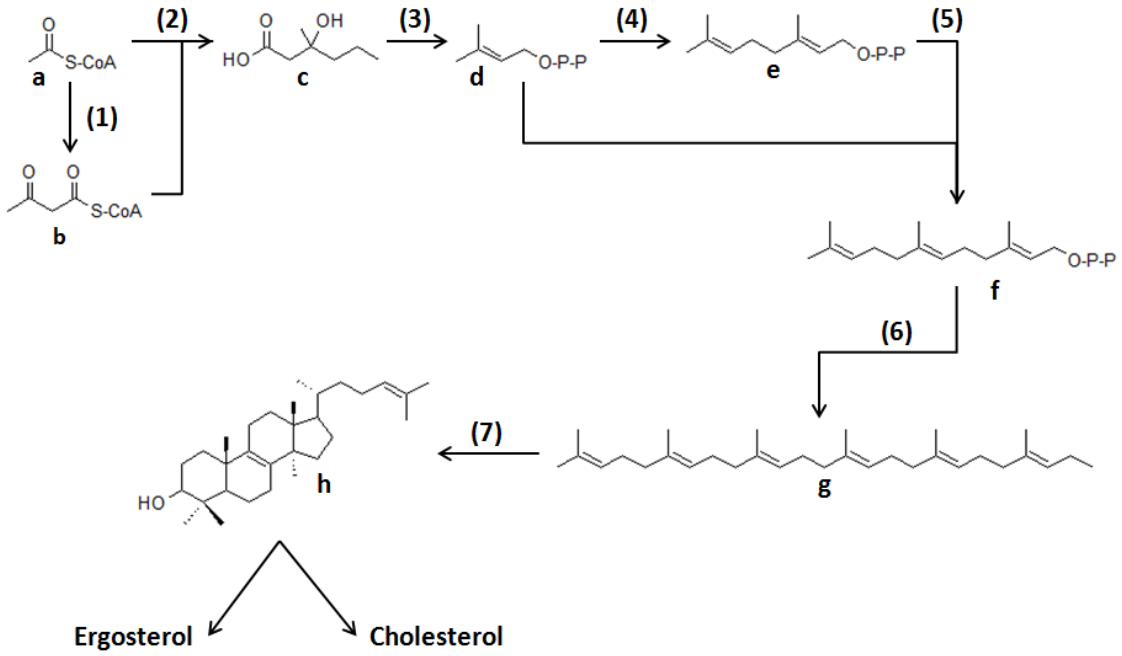

Figure 12. Short overview of the sterol biosynthetic pathway

Summarized sterol biosynthesis pathway: **(1)** Acetoacetyl-CoA **(b)** is synthesized from two molecules of acetyl-CoA **(a)**, addition of another acetyl-CoA **(2)** leads to formation of mevalonic acid **(c)**. The last step is rate limiting and catalyzed by HMG-CoA reductase, hence a key enzyme for sterol. Isopentenyl pyrophosphate (IPP) **(d)** formation requires three steps **(3)**. It is then dimerized **(4)** to yield geranyl pyrophosphate **(e)**, condensation of another IPP molecule **(5)** gives farnesyl pyrophosphate **(f)**. Squalene **(g)** is formed from two farnesyl pyrophosphate molecules **(6)**. After squalene epoxidation, lanosterol synthase catalyzes the cycle formation **(7)** to yield lanotsterol **(h)**, the first intermediate in the biosynthesis with a steroid backbone. Biosyntheses of ergosterol and cholesterol (**Figure 5**) diverge starting from lanosterol and are not further detailed here. For precise descriptions of the pathways see (Nes 2011).

Uptake of exogenous sterol

All eukaryotic cells are capable of both synthesizing their own sterols and taking them up from their environment. In mammalia, the major sterol source is receptor-mediated uptake of VLDL (Very-Low Density Lipoprotein) and LDL (Low-Density Lipoprotein). The steryl ester containing lipoproteins bind to LDL receptor (LDLR) and are then internalized by endocytosis in clathrin-coated pits and further transported to the late endosome (LE)/lysosome (LY) where sterol esters are hydrolyzed by an acidic lipase (Mesmin and Maxfield 2009). In a subtype of lysosomal storage disorders, the Niemann-Pick type C disease, mutations in two proteins (Niemann-Pick type C (NPC) 1 and 2) have been identified as the origin of the disease. NPC1 and NPC2 are structurally unrelated and play a role in desorption

of endogenous sterol from multivesicular body vesicles in the late endosomal/lysosomal (LE/LY) system (Ikonen and Holtta-Vuori 2004). NPC1 is an integral LE/LY protein with a putative transmembrane sterol sensing domain (SSD) and an N-terminal lumenal domain (NTD) that is capable of transporting sterol *in vitro*, as is the shorter NPC2 (Kwon, Abi-Mosleh *et al.* 2009). Transport of sterol by NPC2 is accelerated in presence of the endosomal lipid LBPA, and NPC2 also accelerates the transport of sterol by NPC1 (Infante, Wang *et al.* 2008; Xu, Farver *et al.* 2008). Structural insights on both proteins indicate a "hand-off" of a single sterol molecule between NPC2 and NPC1 by direct interaction, but efforts to structurally elucidate this mechanism have failed so far (Wang, Motamed *et al.* 2010). Their activity might be to make endogenous sterol accessible for other sterol transfer proteins for distribution from the LE/LY system, necessary for distributing sterol to its subcellular localization (Mesmin, Antonny *et al.* 2013).

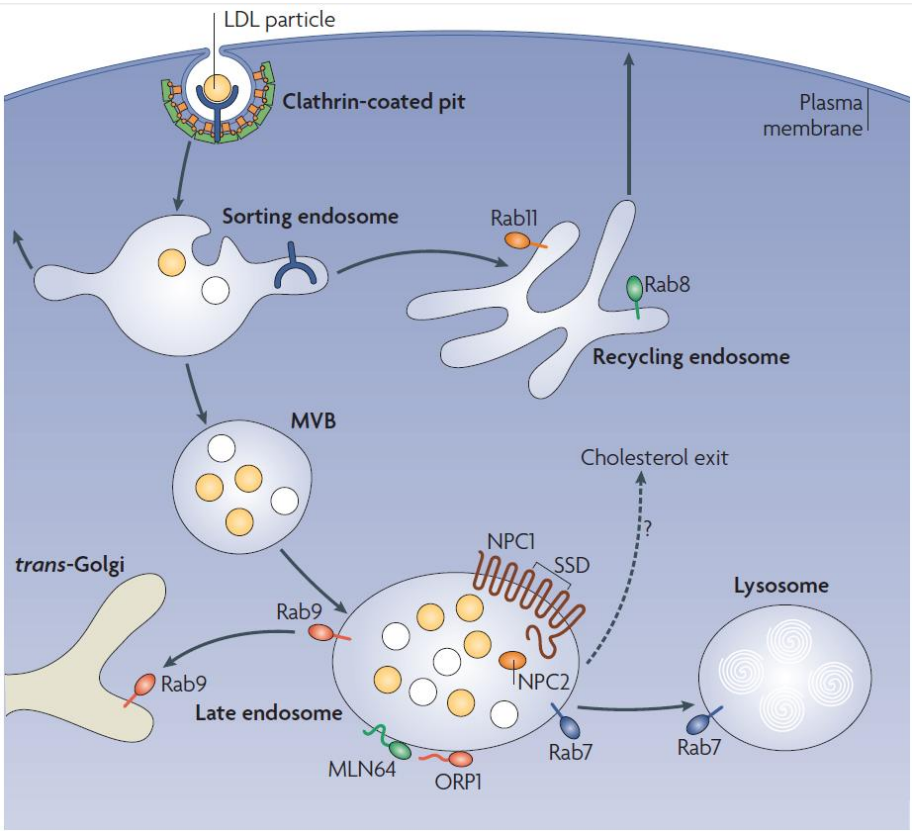

Figure 13. Mechanism of the uptake of exogenous cholesterol in mammalian cells.

Cholesterol-ester laden LDL particles are taken up by receptor-mediated endocytosis in clathrin-coated pits. The coat and the receptor are recycled *via* the recylcling endosome, highlighted by Rab8 and Rab11. Endocytotic vesicles then fuse to multivesicular bodies (MVBs) that maturate into late endosomes, where sterol esters are hydrolyzed and sterol is sorted by not yet fully elucidated mechanisms. However the sorting is dependent on NPC1 and NPC2 and mediated by MLN64/STARD3 ORP1L and the Rab GTPases Rab7 and Rab9. Illustration from (Ikonen 2008).

In budding yeast, sterol uptake is not receptor mediated, but sterols are absorbed directly from the medium. The ATP (adenosine triphosphate)-binding cassette (ABC) transporters Aus1p and Pdr11p are implied in sterol uptake, but their mechanism of action remains to be identified (Wilcox, Balderes *et al.* 2002). Under normal conditions the amount of sterol absorbed from the medium is negligible. It is only when yeast cells are grown under hypoxic conditions that the lack of molecular oxygen necessary for sterol biosynthesis induces a dependency on sterol uptake from the medium, making them conditional sterol auxotrophs (Jacquier and Schneiter 2012).

Uptake or biosynthesis? – The feedback regulation of sterol metabolism

As mammalian cells can use both intrinsic and exogenous cholesterol, the biosynthetic route needs to be slowed down when cholesterol uptake is high and *vice versa*. In higher eukaryotes, this regulation occurs through a transcriptional feedback on cholesterol levels by SREBP (Sterol Regulatory Element Binding Protein) in mechanisms that have been discovered and comprehensively described by the Brown and Goldstein lab (Brown and Goldstein 2009). Briefly, when ER cholesterol levels are normal (5% of total lipid), SREBP is localized to the ER by interaction with cholesterol-binding Scap (SREBP Cleaving Activation Protein). When cholesterol concentration in the ER decreases below 5%, Scap undergoes a conformational change, releasing the SREBP-Scap complex from the ER and it is subsequently transported to the Golgi by COPII-dependent vesicular transport. In the Golgi apparatus the N-terminal transcriptional domain of SREBP is cleaved and transported to the nucleus. The SREBP transcriptional factor there activates the transcription of both cholesterol biosynthetic enzymes and LDL-receptors, which ultimately leads to increasing cellular cholesterol levels (Brown and Goldstein 2009; Raychaudhuri, Young *et al.* 2012).

The origins of transbilayer asymmetry

Phospholipid synthesis is *per se* asymmetric as the lipid synthesizing enzymes are necessarily located on either the lumenal or the cytoplasmic side of an organellar membrane. Sterols, DAG and ceramide do not have a polar headgroup and therefore can equilibrate rapidly between membrane leaflets (see Transbilayer asymmetry and anionic lipids). This is not the case for sphingolipids and GPLs; their localization is therefore fixed to the side of the membrane where they are synthesized, unless they are transported.

Due to the lumenal localization of their biosynthesis, complex sphingolipids are trapped at the lumenal face of the Golgi, as their headgroups reduce flipping. Upon transport to the PM by vesicular trafficking, they are thus accumulated on the exoplasmic face. The mostly saturated sphingolipids segregate sterols, hence explaining one aspect of PM transbilayer asymmetry (Funato, Vallee *et al.* 2002; Holthuis and Menon 2014).

Biosynthesis of GPLs on the cytoplasmic side of the Golgi confers PE, PI and PS to the face they are ultimately enriched in at the PM. Yet newly synthesized GPLs at the ER are rapidly equilibrated between membrane leaflets to prevent excessive curving. This is mediated by **scramblases** that are capable of equilibrating bidirectionally the two leaflets without energy consumption and without ligand specificity (Holthuis and Menon 2014). However, the ER scramblase has not yet been identified, but its presence inferred from the absence of membrane deformation upon synthesis of new phospholipids (Devaux, Herrmann *et al.* 2008).

Intriguingly, PS displays a pronounced asymmetric distribution, with an ER lumenal leaflet concentration higher than at the cytosolic face. How exactly PS is sequestered there is not fully elucidated. Interestingly, PS makes its way back to the surface at the *trans*-Golgi apparatus (Fairn, Schieber *et al.* 2011) (**Figure 14**). Transbilayer movement of PS in the *trans*-Golgi is mediated by type IV P-type ATPases (P4-ATPases), **flippases** that catalyze movement from the lumenal to the cytoplasmic face of a bilayer. Movement in the opposite direction is mediated by **floppases** from the ABC transporter family. Both flippases and floppases require energy in the form of ATP for function (Daleke 2003; Hankins, Baldridge *et al.* 2014).

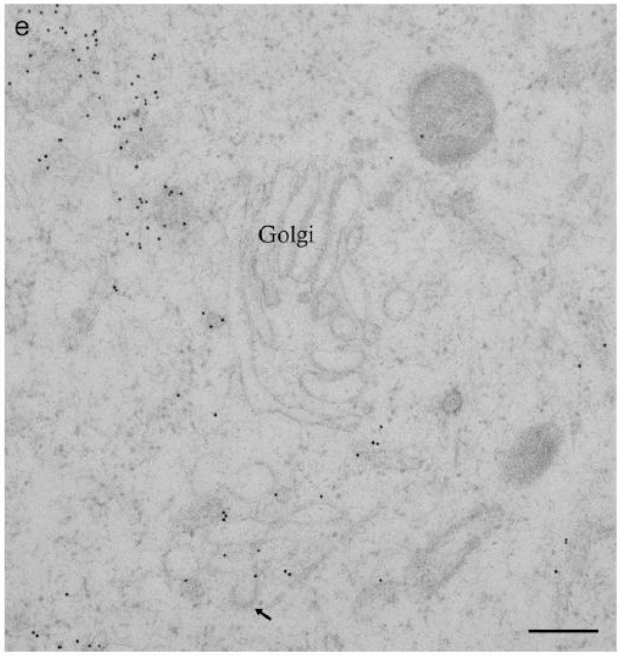

Figure 14. PS flipping on the *trans*-Golgi.

Thin section electron micrographs of BHK cells expressing GFP-$C2_{Lact}$ stained with anti-GFP gold particles. Golgi cisternae show hardly any labeling, whereas tubulated and vesicular structures close to it, putative TGN elements, display PS on the cytoplasmic face (arrow). Scale bar 200 nm. Illustration from (Fairn, Schieber *et al.* 2011).

The best studied P4-ATPase is *S. cerevisiae*'s Drs2p. It is implied in vesicle formation on the *trans*-Golgi and has therefore revealed an interesting link between vesicular trafficking and transbilayer asymmetry. Drs2p is a transmembrane protein translocating PS and, to a lesser extent, PE. Its flipping activity is dependent on its glycosylated partner Cdc50p and increased by binding of PI(4)P from the Pik1p *trans*-Golgi network (TGN) pool (Natarajan, Liu *et al.* 2009; Jacquot, Montigny *et al.* 2012). This PI(4)P-binding is mediated by a C-terminal domain showing similarity to Vps36p split PH domain (Natarajan, Liu *et al.* 2009). Drs2p is capable of creating a transbilayer PS gradient, ultimately leading to membrane deformation, as shown recently by Xu *et al.* using a +ALPS (modified amphipathic lipid packing sensor) motif of the ArfGAP (GTPase-activating protein) Gcs1p (Xu, Baldridge *et al.* 2013). Further findings suggest that the curvature induced rather than just presence of PS are required for vesicle formation on the TGN (Takeda, Yamagami et al. 2014). Despite these detailed findings on the function of Drs2p-mediated PS flipping, the molecular mechanism of its ATPase activity is not yet fully elucidated (Hankins, Baldridge et al. 2014). Yet, it has been hypothesized that the PS headgroup would be specifically recognized by transmembrane domains whose conformation is changed upon ATP hydrolysis pulling the PS headgroup

between the transmembrane domains towards the opposite face of the membrane (Baldridge and Graham 2012; Baldridge and Graham 2013). However, PS ultimately reaches PM where its asymmetric accumulation on the cytoplasmic face (**Figure 15**) is conserved. In mammalian cells, the PM scramblase is activated upon Ca^{2+}-binding, leading to presentation of PS at the extracellular face as an apoptotic 'eat me' signal (Bratton, Fadok *et al.* 1997). Regardless, as for the ER scramblase, the identity of the PM scramblase is not yet confirmed (Hankins, Baldridge *et al.* 2014).

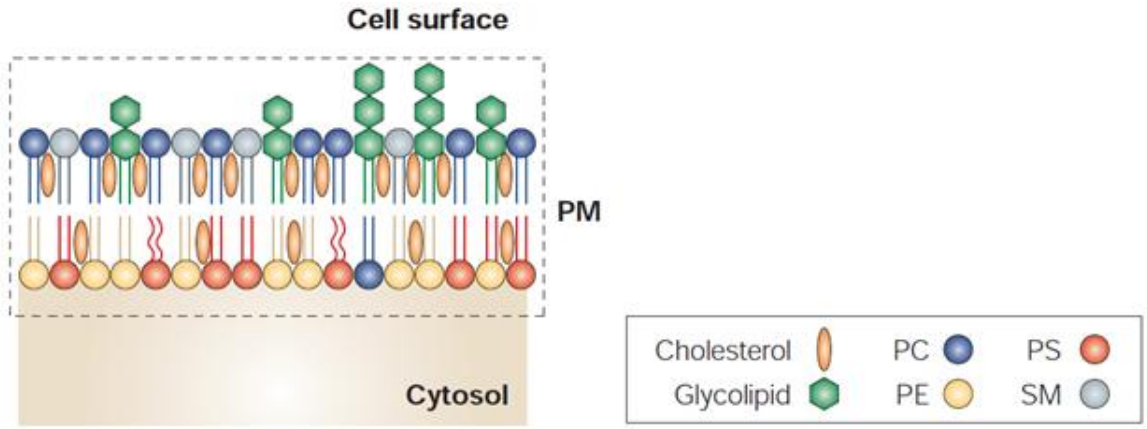

Figure 15. Transbilayer asymmetry at the plasma membrane.

The two leaflets of the PM have fundamentally different lipid compositions: Cholesterol (orange ovals), SM (grey), glycerosphingolipids (green) and PC (blue) are enriched on the exoplasmic face, whereas the cytoplasmic face is rich in PS (red) and PE (yellow) and contains little sterol and PC. Illustration modified from (Holthuis and Levine 2005).

Transbilayer asymmetry of organellar membranes can thus originate from lipid metabolism and thermodynamic trapping or lipid translocation by energy-dependent transporters. Another possibility to create asymmetric membranes by soluble lipid transporters will be described below. (See Hypotheses on the mechanisms of non-vesicular lipid transfer)

Lipid transport between membranes

Lipid transport by vesicular trafficking

The secretory pathway

The archetypal function of the secretory pathway is the sorting and modification of proteins synthesized in the ER. Transmembrane (TM) proteins are embedded in the membrane by the translocon during the translation process. If they do not bear an ER-retention signal, they are sorted towards the Golgi for *post*-translational modification and eventually further towards the PM. The recruitment of COPII coat proteins to adaptors on ER exit sites (ERES) allows formation of vesicles containing protein cargo either in the vesicles membrane (TM proteins) or inside the vesicles (soluble cargo). The vesicle bud off the membrane and the vesicles are uncoated before SNARE (SNAP (Soluble *N*-ethylmaleimide-sensitive factor Adaptor Protein) Receptor)-mediated fusion with ER-Golgi Intermediate Complex (ERGIC).

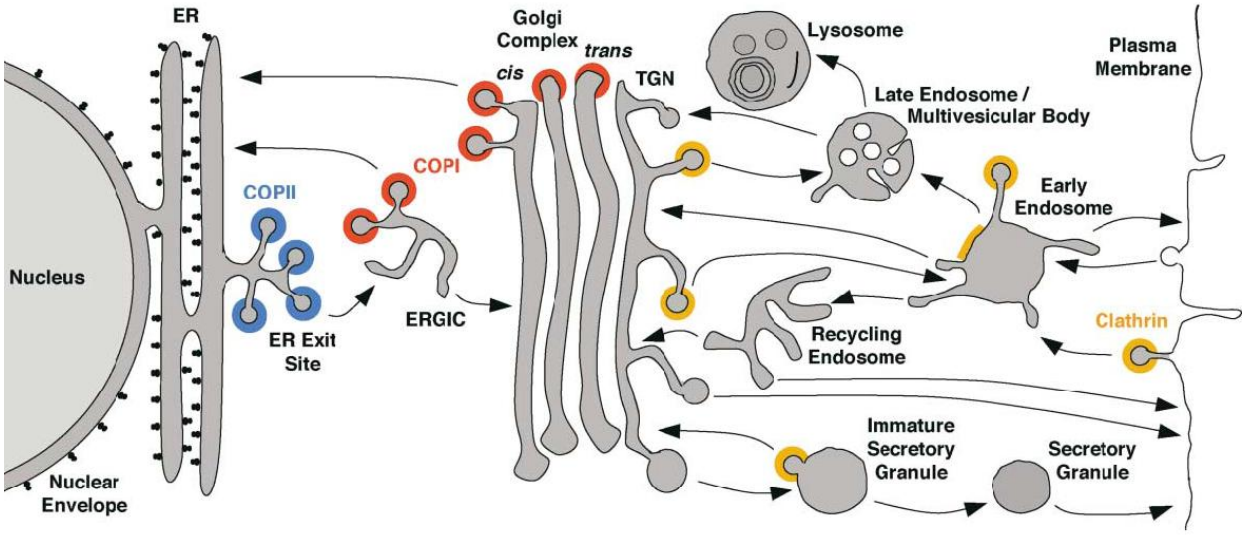

Figure 16. The secretory pathway.

Vesicles traffic between organelles depending on their protein coat. COPII-coated vesicles transport protein cargo from the ER to the Golgi and COPI-coated vesicles in the opposite direction; Clathrin-coated vesicles shuttle between Golgi, PM and endosomal compartments. Secretory vesicles are devoid of protein coats. Illustration from (Bonifacino and Glick 2004).

Sorted proteins required for vesicle formation and missorted proteins are targeted back to the ER in retrograde transport in COPI-coated vesicles for recycling. Cargo destined for anterograde transport is targeted to the Golgi apparatus. Two models exist to describe

transport in the Golgi: The first model predicts anterograde vesicular transport of cargo to a static *cis*-Golgi; the second model predicts fusion of vesicles with the ERGIC to form a new *cis*-Golgi whereas the *cis*-Golgi maturates into *medial*-Golgi, etc., a process termed cisternal maturation. These models can be extrapolated to the entire Golgi apparatus whose protein and lipid composition varies significantly between *cis*- and *trans*-side. Both models require vesicular trafficking, anterograde trafficking of cargo in the case of a static Golgi or retrograde trafficking of Golgi-resident proteins in the dynamic Golgi. Ultimately, cargo reaches the *trans*-Golgi and the tubular network structure of the TGN from where it can be sorted to different loci of the cell. Cargo can be sorted in vesicles coated with clathrin towards endosomes and further towards lysosomes. Cargo destined to the PM is sorted in uncoated secretory vesicles that bud off the Golgi and finally reach the PM to which they are fused by SNARE-mediation. Soluble cargo is secreted into the exoplasmic space upon fusion of secretory vesicles with the PM. Clathrin-mediated endocytosis (CME) allows retrieval of wrongfully sorted proteins and uptake of exogenous molecules into the cell. CME vesicles are targeted to the TGN from which they are sorted to different cellular loci (**Figure 16**) (Bonifacino and Glick 2004; Johansen, Ramanathan *et al.* 2012; Faini, Beck *et al.* 2013; Kienzle and von Blume 2014).

Lipid selectivity in vesicular trafficking

Vesicular trafficking exchanges large amounts of membrane material between organelles and is thus essential for bulk lipid transport. One hypothesis for explaining the conservation of organellar membrane integrity is lipid selectivity in vesicular trafficking: Vesicles are enriched in or depleted of, respectively, lipids, that are more or less abundant, respectively, in the target membrane, during vesicle formation (van Meer, Voelker *et al.* 2008; Diaz-Rohrer, Levental *et al.* 2014). Preferential interaction of secreted or resident proteins with lipids or lipid microdomains would allow such accumulation or depletion, respectively, of lipids in vesicles budding off an organelle. This mechanism would increase the directionality of vesicle trafficking from a lipid point of view; however, only in few cases lipids were shown to accumulate in transport vesicles.

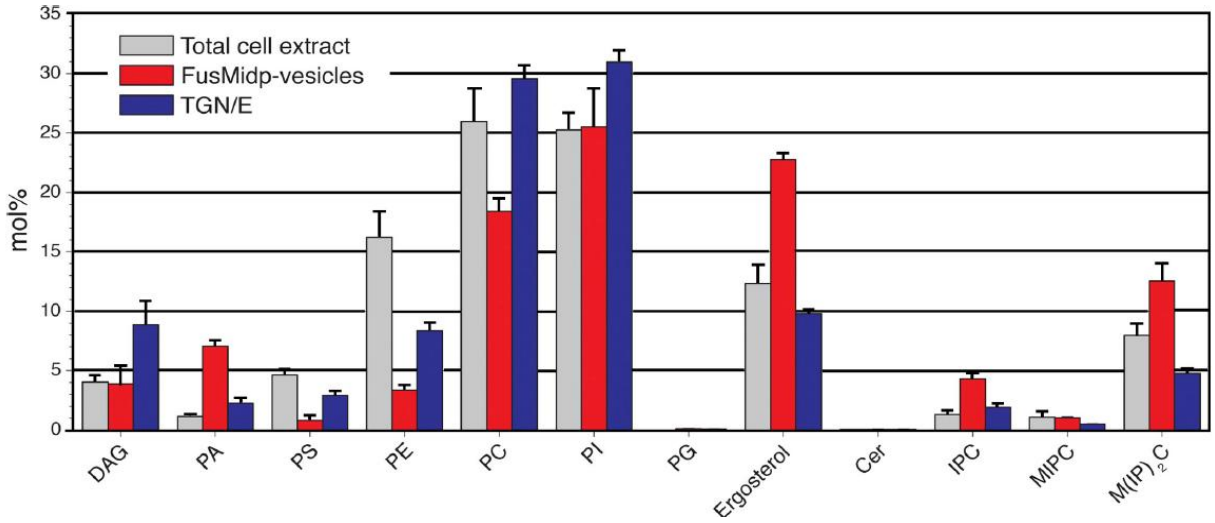

Figure 17. Lipidomic analysis of immunoisolated Golgi-derived vesicles.

Comparison of the overall lipid composition of total cell extracts (grey), immunoisolated Golgi vesicles (FusMidp-vesicles, red) and TGN/Endosomes extract (blue). Values are represented as mol% of total lipid. The FusMidp-vesicles are enriched in PA, ergosterol and sphingolipids and depleted of DAG, PS, PE and PC. Illustation from(Klemm, Ejsing *et al.* 2009).

Klemm *et al.* found that vesicles originating from the budding yeast TGN, immunoprecipitated with a chimeric FusMidp protein containing a 9x myc-tag, are enriched in ergosterol and complex sphingolipids and are in a higher state of order compared to the extracted TGN fractions, as determined by lipidomics (**Figure 17**) and C-Laurdan spectrophotometry, respectively. Notwithstanding the clear difference between the two isolates, the authors were limited by the absence of yeast TGN markers and used Gap1p for immunoisolation, a protein that is known to shuttle between the TGN and endosomal compartments. Whether the observed differences between the two isolates are therefore biased could not be fully excluded by the authors (Klemm, Ejsing *et al.* 2009). Similar observations have been made on COPI-coated vesicle that were found to be enriched in one particular SM species by specific interaction with the transmembrane domain of a COPI machinery protein, a feature that appears to be conserved among certain transmembrane proteins (Contreras, Ernst *et al.* 2012). The ability of sterol and sphingolipids to segregate into microdomains has been proposed as a mean to use recognition of either sterol or sphingolipids to accumulate the other in turn (Brugger, Sandhoff *et al.* 2000). As a matter of fact, introducing sphingolipids not capable of segregation into microdomains affected Golgi secretion (Duran, Campelo *et al.* 2012). Whether this is actually due to the absence of microdomain formation or overall Golgi lipid perturbation awaits further elucidation.

Mioka *et al.* observed using a fluorescent PS probe (mRFP-$C2_{Lact}$) in *S. cerevisiae* that PS accumulates on secretory vesicles budding off the TGN. However, no major perturbation of PM PS was observed under these conditions (Mioka, Fujimura-Kamada *et al.* 2014). Intriguingly, the secretory vesicles originating from the TGN immunoisolated by Klemm *et al.* were depleted of rather than enriched in PS, challenging these hypotheses; though two distinct populations of secretory vesicles might exist for delivering ergosterol and PS (Klemm, Ejsing *et al.* 2009; Mioka, Fujimura-Kamada *et al.* 2014).

However, there are membranes that are not connected to the endomembrane system, such as peroxisomes and particularly mitochondria. Their lipid homeostasis during growth can thus not only be explained by vesicular trafficking events. Additionally, lipid transfer towards other subcellular compartments still occurs in conditions where vesicular trafficking is blocked. Non-vesicular transport mechanism are therefore required for maintaining lipid homeostasis (Lev 2010) (see below).

Non-vesicular lipid transfer between organelles

Hypotheses on the mechanisms of non-vesicular lipid transfer

Non-vesicular lipid transfer can occur *via* passive and active pathways. Free diffusion of lipids between membranes across the aqueous phase can be neglected for lipid homeostasis as it is a very slow process (See Transbilayer asymmetry and anionic lipids). Such passive lipid transfer could occur when it is collision-mediated; i.e. two membranes come close enough to bypass the aqueous diffusion barrier, eventually activated by protrusion of a lipid from one membrane (Lev 2010).

Alternatively, **lipid transfer proteins** (LTPs) could ensure the maintenance of lipid homeostasis by actively shuttling lipids between membranes, eventually facilitated by their close apposition (Helle, Kanfer *et al.* 2013). LTPs would extract lipids from one membrane, shield it from the aqueous environment, target an acceptor membrane and deliver lipids, and therefore impact lipid distribution in cells. The existence of these protein-mediated, non-vesicular mechanisms is undoubted, as lipid transfer still occurs under conditions in which vesicular trafficking is blocked (Kaplan and Simoni 1985; Vance, Aasman *et al.* 1991). However, only a small number of LTPs have been clearly identified so far. They all share an

overall structural arrangement with a lipid-binding pocket that shields the ligand and that is closed by a flexible “lid” region allowing loading and unloading of its lipid cargo (Lev 2010) (**Figure 18**).

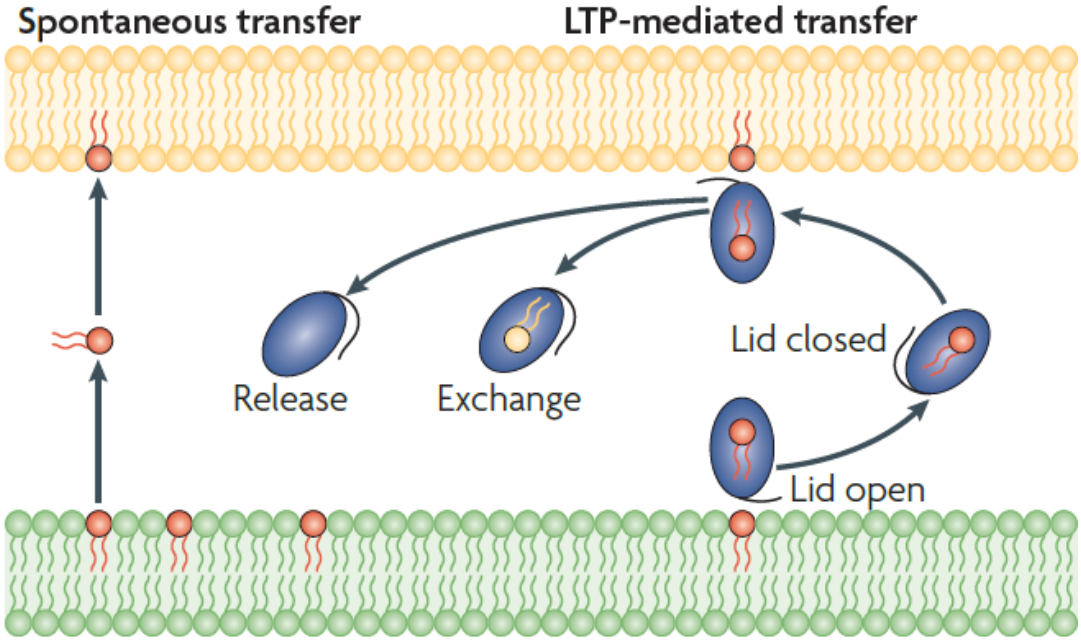

Figure 18. Mechanism of non-vesicular lipid transport.

Schematic representation of non-vesicular lipid transfer mechanisms. Spontaneous diffusion of lipids between organellar membranes is a very slow process that accounts only for neglectable amounts of transfer (left). LTPs extract lipids from one membrane and insert it into another, shielding the lipid in pocket while crossing the cytosol; they might work as lipid exchangers (right). Illustration modified from (Lev 2010)

For virtually all organellar membranes, close appositions (intermembrane distance 10-30 nm) with the ER have been observed. These appositions are probably not tight enough to allow (hemi-) fusion or monomeric spontaneous lipid transfer, but are hypothesized to kinetically favor transport of lipid molecules by LTPs due to decreased diffusion distances (Lev 2010). Those regions of the ER are particularly enriched in proteins implied in lipid biosynthesis and, additionally, multiple LTPs or putative LTPs preferentially localize to these MCSs. These contacts are relatively stable, whereas their surface can vary upon recruitment of additional tethers or depending on the cell cycle. MCSs are induced by tethering factors able to bind two membranes at the same time, directly or indirectly. These tethering factors have been identified for a large number of contact sites (Helle, Kanfer *et al.* 2013).

Generally, LTP activity will always be subject to a lipid concentration gradient, i.e. they could equilibrate lipid concentration between membranes, but not transport lipids against a concentration gradient. As such gradients exist, for example for sterol, sphingolipids and PS, that are synthesized at the ER but accumulate at the TGN and PM, there must be a way to provide energy to the transporters allowing transport up the concentration gradient. There are several hypotheses and explanations for lipid transport against a concentration gradient:

In order to allow lipid transport against a lipid concentration gradient, lipid biosynthesis could thus be restricted to sites of LTP activity. The lipid concentration would thus be sufficiently elevated locally, reversing the overall gradient between organellar membranes. Such elevated lipid synthase activity has been shown for certain MCSs (Pichler, Gaigg *et al.* 2001; Maeda, Anand *et al.* 2013).

Metabolization of transported ligands also sustains a lipid gradient by substrate consumption. This is the case, for example, for the CERT-mediated transport of ceramide that is metabolized into SM in the Golgi targeted by CERT (Hanada, Kumagai *et al.* 2003) (See StAR-related lipid transfer (START) proteins) and would be the case for transport of PS to sites of decarboxylation by PSDs.

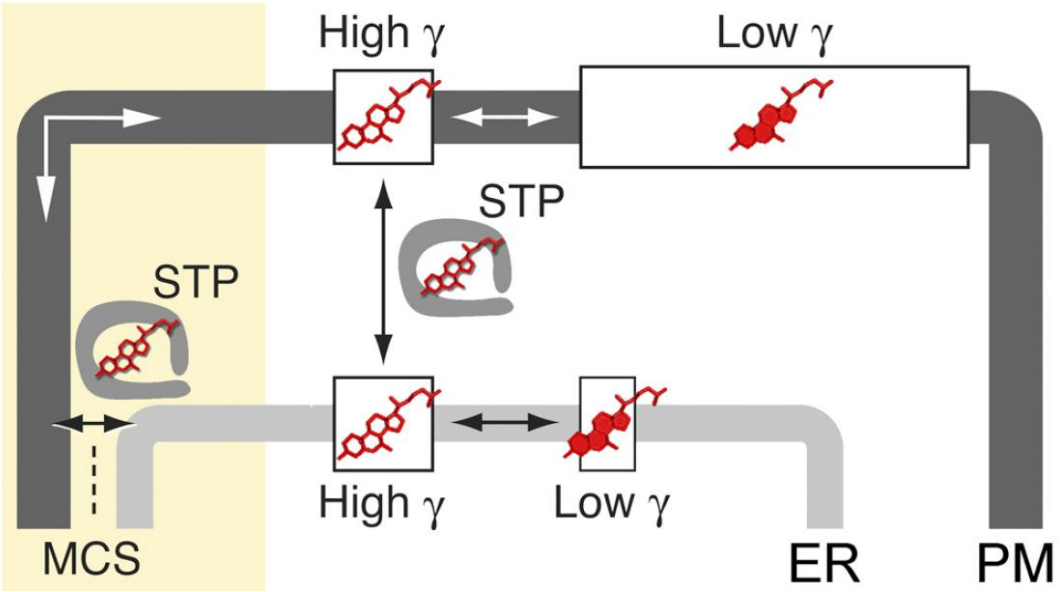

Figure 19. High and low activity sterol pools in the ER and the PM.

Two pools of sterols exist in membranes, one with a high (empty sterol, red) and one with a low (filled sterol, red) chemical activity γ. The portion of the low γ pool at the PM is greater as compared to the ER due to their different lipid saturation levels. This allows sterol transfer proteins (STPs) equilibration between the high γ pools of ER and PM, at MCSs or by diffusion across the cytosol, thus increasing the net sterol at the PM despite the concentration gradient. Illustration from (Beh, McMaster *et al.* 2012).

For sterol transport, a long-standing hypothesis is that LTPs convey this lipid in a bidirectional manner between the ER and late membranes. Sterol forms condensed complexes with sphingolipids and saturated GPLs (**Figure 7**) and these condensed complexes have a lower chemical activity compared to 'free' sterol in a membrane. Chemical activity α is defined by $\alpha = \gamma \cdot c$, with c being the concentration and γ the chemical activity coefficient. Therefore two sterol pools would exist in membranes, one with a low (low γ, in condensed complexes, low extractability) and one with a high (high γ, 'free' sterol, high extractability) activity. Sterol would be equilibrated between the low and high activity pools in ratios defined by the saturation level. The portion of the low activity pool in the TGN and PM would be greater as compared to the ER because of the late membranes' higher acyl chain saturation levels. It is considered that LTPs transport sterol in a bidirectional manner between the high activity pools of the ER and late membranes. However, this would not result in a simple equilibration between membranes but would allow a net sterol transport towards TGN and PM against the sterol concentration gradient. This is due to the fact that the sterol gradient is being outweighed by the chemical affinity gradient. In other words, the low γ pool act as a trap for sterol coming from the ER, resulting in the creation of a sterol gradient (Sullivan, Ohvo-Rekila *et al.* 2006; Georgiev, Sullivan *et al.* 2011; Beh, McMaster *et al.* 2012; Mesmin, Antonny *et al.* 2013) (**Figure 19**).

Alternatively, non-vesicular lipid transport could be targeted in a vectorial manner; i. e. be driven by a coupling to another event giving the transport directionality independent of the concentration gradient. Such coupling could be obtained by counterexchange of lipids, in which one molecule's concentration gradient provides directionality for another lipid's transport (de Saint-Jean, Delfosse *et al.* 2011; Mesmin, Antonny *et al.* 2013).

The following chapter shall give an overview of some of the so far identified lipid transfer proteins and their implication in or activity at MCSs. The great importance of these membrane junctions in Ca^{2+} homeostasis will not be detailed; for a review see (Helle, Kanfer *et al.* 2013).

Lipid transport by cytosolic carriers: Lipid transfer proteins

StAR-related lipid transfer (START) proteins: cholesterol and ceramide transporters

The START protein family regroups 15 proteins in human (**Figure 20**), its founding member **StAR** (Steroidogenic Acute Regulatory Protein, STARD1) is a mitochondrial cholesterol transporter essential for steroidogenesis. Its ≈ 210 aa StAR-related lipid transfer (START) domain is the common feature of all START domain containing proteins (STARD1-STARD15); intriguingly, this conserved domain binds a plethora of different lipids. STARD1, D3, D4, D5, D6 bind to cholesterol, whereas STARD2, D7 and D10 bind GPLs (PC and/or PE); STARD11/CERT is a ceramide transporter, and there is still some uncertainty concerning the ligands of STARD8, D9, D12, D13, D14 and D15. Interestingly, budding yeast has no homologs of START proteins, their role must therefore be compensated by other lipid transport proteins (Alpy and Tomasetto 2014).

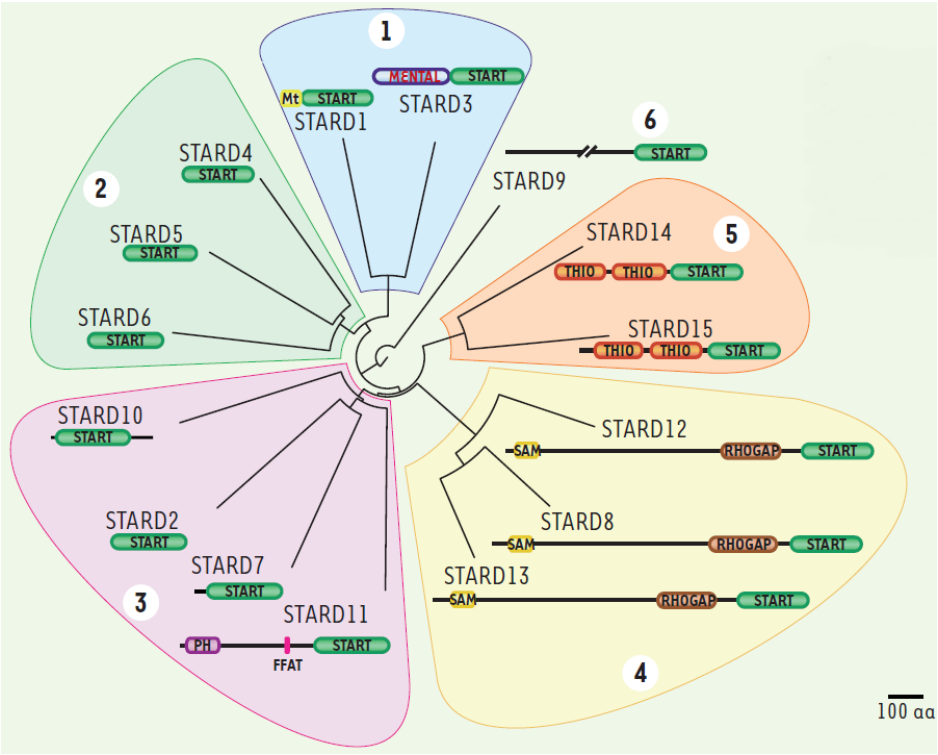

Figure 20. Phylogenetic analysis of the human START proteins.

The START proteins can be divided into six subfamilies based on their sequence alignments. All START proteins display a START domain (green). Other domains found are Mt (mitochondrial targeting sequence), MENTAL (MLN64 N-terminal), PH (pleckstrin homology), FFAT (two phenylalanines in an acidic tract), SAM (sterile alpha motif), RHOGAP (Rho GTPase activation) and THIO (Acyl-CoA thioesterase). Illustration modified from (Alpy, Legueux *et al.* 2009).

STARD11/CERT (Ceramide transfer protein), the best studied START protein and the first described genuine LTP, localizes to the **membrane contact site between the ER and the TGN** (ER-TGN contact sites) (Hanada, Kumagai *et al.* 2003) (**Figure 21**). Despite the fact that the ER and the Golgi apparatus are linked to another by vesicular trafficking, the reticulated network of the ER also displays direct connection with the *trans*-Golgi compartment in mammalian cells (Peretti, Dahan *et al.* 2008) and have been shown to harbor LTPs: The phosphatidylinositol transport protein (PITP) Nir2 localizes there, as well as the glycosylceramide transporter FAPP2 (Four-phosphate [PI(4)P] adaptor protein), the START family ceramide transporter CERT, and the Oxysterol-Binding Protein OSBP (Litvak, Dahan *et al.* 2005; Perry and Ridgway 2006; D'Angelo, Polishchuk *et al.* 2007) (See below). Even though they are members of different protein families, the latter three share a common architecture: In addition to their lipid-binding domain, they bear a FFAT (two phenylalanines in an acidic tract) motif that mediates binding to the type II ER-resident VAMP-associated protein A (VAP-A) and a PH domain that binds PI(4)P to target the *trans*-Golgi membrane (Peretti, Dahan *et al.* 2008).

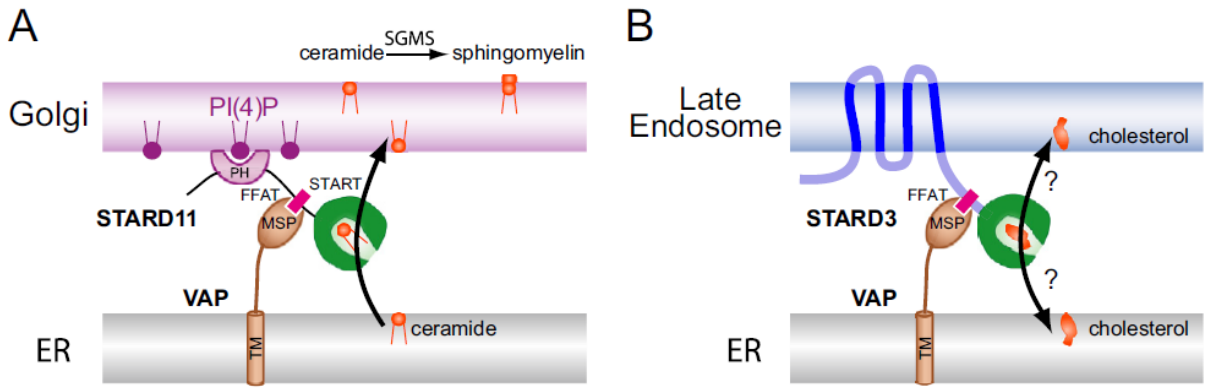

Figure 21. Membrane tethering and lipid transport by START protein

Both STARD11/CERT **(A)** and STARD3/MLN64 **(B)** are capable of tethering the ER to a second organelle. STARD11/CERT binds ER and Golgi membranes by VAP-recognition *via* its FFAT motif and PI(4)P-recognition *via* its PH domain, respectively. Its START domain shuttles ceramide from the ER to the Golgi where it is metabolized into SM. STARD3/MLN64 is a late endosomal transmembrane protein that additionally binds to ER membranes by recognition of VAP *via* its FFAT motif and hence allows tethering of these membranes. Cholesterol transport by its START domain is currently studied in our lab. Illustration from (Alpy and Tomasetto 2014).

CERT can thus serve as an ER-*trans*-Golgi tether and transports ceramide molecules inside its START domain from its site of biosynthesis in the ER to the *trans*-Golgi where ceramide is metabolized to form SM and glucosylceramide (**Figure 21**). In cells, ceramide transport would thus be sustained by a thermodynamic trap as ceramide metabolization into SM and glucosylceramide allows maintenance of a ceramide gradient between the ER and *trans*-Golgi (Hanada, Kumagai *et al.* 2003). *In vivo*, CERT transports ceramide with a rate of about 4 lipids/protein per minute (Kudo, Kumagai *et al.* 2008) and this transport is regulated by phosphorylation of CERT. Different phosphorylation sites have been identified which upon protein kinase activity can induce increased membrane tethering or autoinhibition of CERT (Kumagai, Kawano *et al.* 2007; Kumagai, Kawano-Kawada *et al.* 2014). Complete disruption of its function either in tethering or in transport leads to accumulation of ceramide in the ER and a depletion of cellular SM that can be compensated by expression of a wild type (WT) form of CERT (Hanada, Kumagai *et al.* 2003) (**Figure 22**).

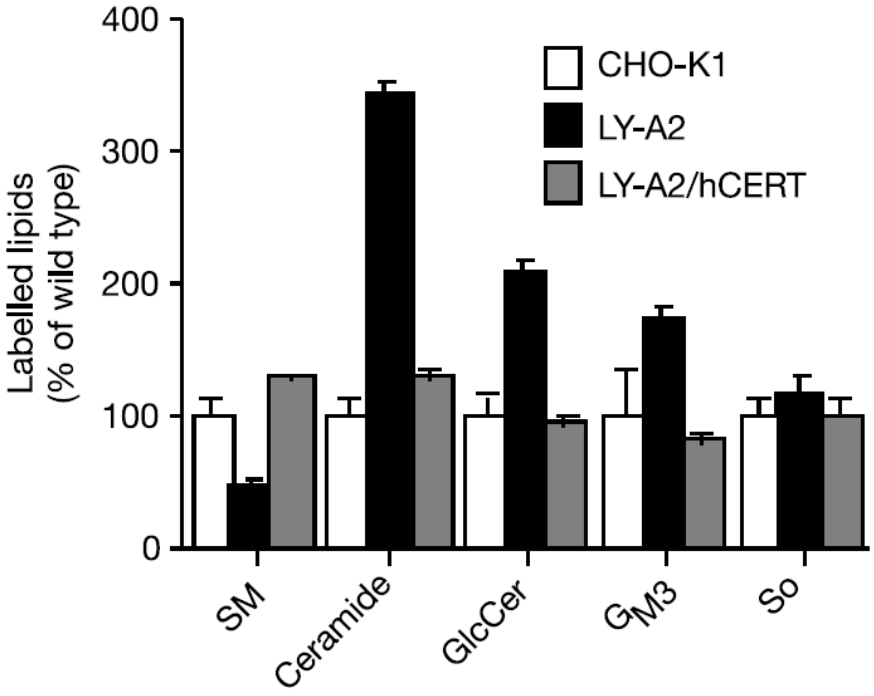

Figure 22. CERT control sphingolipids homeostasis in mammalian cells.

TLC analysis of total lipids after metabolic labeling of sphingolipids with [^{3}H]sphingosine in Chinese hamster ovary (CHO) cells. CERT-depleted cells (LY-A2, black) have decreased SM levels, compared to WT (CHO-K1, white) whereas its precursor ceramide is accumulated, just as glucosylceramide (GlcCer), N-acetyl neuraminyl lactosylceramide (GM3) and sphingosine (So). Expression of human CERT restores wild-type levels (LY-A2/hCERT, grey). Illustration from (Hanada, Kumagai *et al.* 2003)

Another STARTD protein, **STARD3/MLN64** (Metastatic Lymph Node 64) is anchored to endosomal membranes *via* its N-terminal MENTAL domain (Zhang, Liu *et al.* 2002), whereas its C-terminal cytosolic START domain can extract and bind a single cholesterol molecule and transport sterol between membranes *in vitro* (Tsujishita and Hurley 2000). STARD3NL is identical to STARD3, except that it lacks the START domain (Alpy, Wendling *et al.* 2002). Their common part regulates the localization of these two proteins: MENTAL anchors the protein to endosomal membranes and a short FFAT motif allows interaction with the ER-resident VAP-A and VAP-B. Simultaneous targeting of two membranes is a prerequisite for tethering two organelles and STARD3 and MENTAL thus allow the formation of junctions **between the ER and endosomes** (**Figure 21, Figure 31**). The FFAT motif is not canonical as the FFAT found in STARD11/CERT or OSBP but was nonetheless able to bind VAP proteins *in vivo*. Overexpression of STARD3 or STARD3NL significantly increases the surface of ER-endosome contact sites in HeLa cells (Zhang, Liu *et al.* 2002; Alpy, Rousseau *et al.* 2013). Whether the START domain allows active sterol transport by STARD3 at ER-endosome contact sites from ER to endosomes or *vice versa* is currently examined by our lab.

STARD4 is a cholesterol-binding START protein that, in contrast to the abovementioned START proteins and, like STARD5 and STARD6, features only the START domain. The crystal structure shows that the fold of the START domain between STARD3 and STARD4 is conserved and that both display a hydrophobic tunnel for accommodating a single cholesterol molecule (PDB entry: 1JSS) (Tsujishita and Hurley 2000; Romanowski, Soccio *et al.* 2002). *In vitro* the STARD4 has been shown to extract sterol from artificial membranes, bind sterol with a 1:1 stoichiometry and rapidly equilibrates sterol between membranes (Mesmin, Pipalia *et al.* 2011). In cells, cytosolic STARD4 equilibrates cholesterol between the endosomal recycling compartment (ERC) and the ER. Whether this is due to a specific ER-targeting or to the cholesterol gradient between the two compartments is not clear, as STARD4 overexpression can be phenocopied by the microinjection of methyl-β-cyclodextrin (β-MCD), an unspecific sterol transporter, albeit at higher concentrations than STARD4. In the case of a targeted transport, STARD4 would allow feedback to SREBP-2 on exogenous cholesterol uptake and, in fact, STARD4 depletion leads to an SREBP-2 dependent increase in free cholesterol levels in cells (**Figure 23**). Further experimental evidence is required for proving this hypothesis (Mesmin, Pipalia *et al.* 2011).

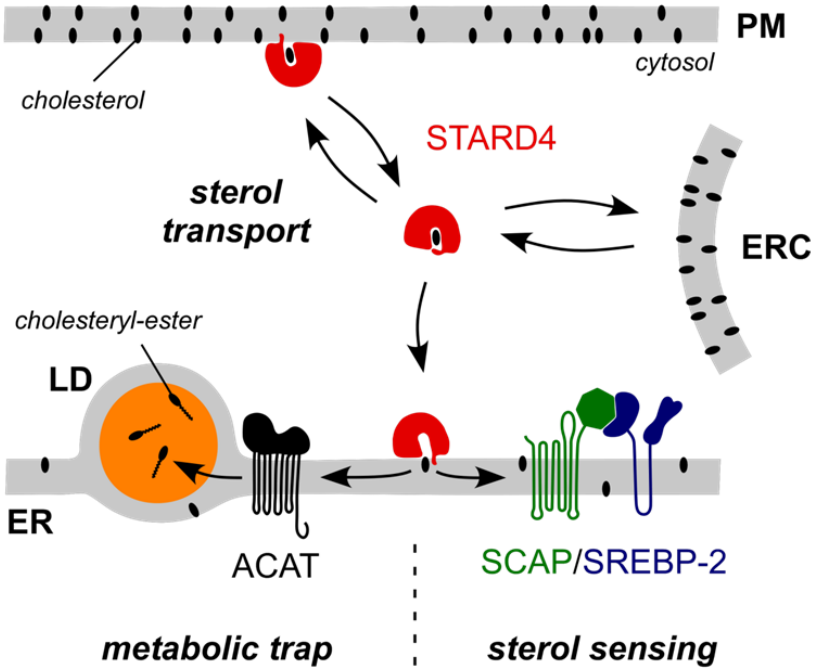

Figure 23. STARD4 equilibrates cholesterol between organelles as cytosolic transporter.

STARD4 rapidly equilibrates cholesterol concentration gradients between the endocytic recycling compartment (ERC) and the ER. Its activity as soluble cholesterol transporter could allow rapid feedback on cellular cholesterol levels to regulate sterol biosynthesis *via* the SCAP/SREBP-2 system and cholesterol esterification *via* ACAT in lipid droplets (LD). Illustration from (Mesmin, Antonny *et al.* 2013).

Glycolipid transfer proteins and FAPP proteins: glycol(sphingo)lipid transporters

Glycolipid transfer protein (GLTP), a small human protein conserved in higher eukaryotes, was among the first LTPs identified for their activity in glycolipid transport *in vitro* (Metz and Radin 1982). The *in vitro* transport activity is influenced by the lipid packing of membranes, glycolipids were found to be preferentially transported toward densely packed membranes, alike those towards which the ligand is transported *in vivo*. However, the function of this protein *in vivo* is not clearly assessed due to its low abundance and the low level of glycolipids (Nylund, Kjellberg *et al.* 2006; Tuuf and Mattjus 2014). Nevertheless, its homolog GLTP domain-containing protein 1 (GLTPD1 or ceramide-1-phosphate transfer protein CPTP) showed selective transport of ceramide-1-phosphate (C1P), and no inhibition by ceramide or sphingosine-1-phosphate was observed. Ceramide is phosphorylated by ceramide kinase CERK at the TGN, and CPTP was found to localize there, it could thus regulate the TGN C1P pool and the inflammatory response induced by C1P (Simanshu, Kamlekar *et al.* 2013).

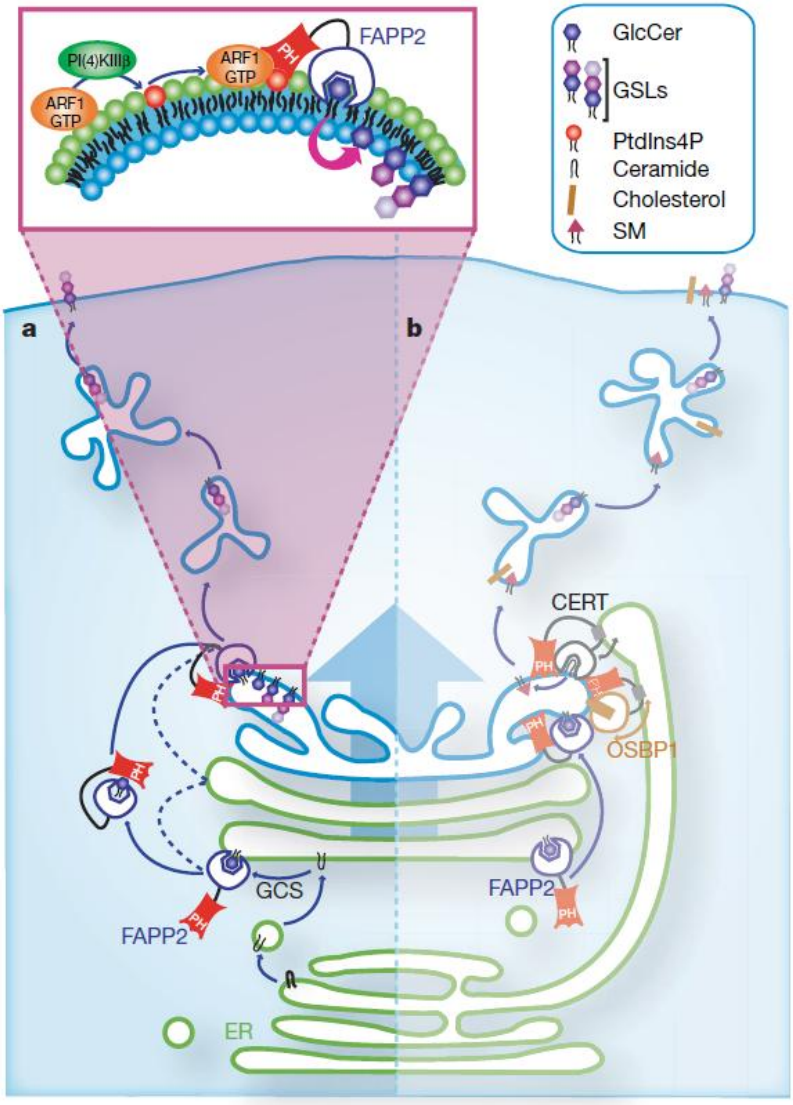

Figure 24. Working model for FAPP2 glucosylceramide transport.

FAPP2 transports glucosylceramide from the *cis*- to the *trans*-Golgi region, where FAPP2 is targeted by its PH domain and where glucsylceramide is metabolized to form glycosphingolipids. Two hypotheses are shown for transport by FAPP2: Transport independent of **(a)** or in concert with other LTPs (CERT, OSBP) at ER-Golgi contact sites **(b)**. Illustration from (D'Angelo, Polishchuk *et al.* 2007).

Human FAPP1 and FAPP2 (Four-phosphate [PI(4)P] adaptor proteins 1 and 2) were initially identified owing to their PH domain that interacts with PI(4)P and the small GTPase Arf1 (in a GTP-bound state), but a detailed analysis revealed a GLTP-like domain at the C-terminus of FAPP2. It also displays a FFAT motif, yet the sequence is unconventional resulting in weaker VAP-binding (Godi, Di Campli *et al.* 2004; Mikitova and Levine 2012). Nevertheless, the overall geometry would thus be shared with STARD11/CERT, allowing an activity at ER-Golgi contact sites, even though experimental evidence for such localization is lacking (**Figure 21**). FAPP2 has been shown to bind glucosylceramide, the precursor of glycosphingolipid

biosynthesis, and transport it *in vitro* between artificial membranes and *in vivo* between *cis*-Golgi and *trans*-Golgi (D'Angelo, Polishchuk *et al.* 2007). This transport activity was revealed to be essential for glycosphingolipid biosynthesis, which is surprising as the vesicular trafficking between *cis*- and *trans*-Golgi is important, but apparently not sufficiently efficient for glucosylceramide transport. The authors of the study also assayed the effect of PI(4)P metabolism on FAPP2 activity and showed that PI(4)P recognition by FAPP2 was vital for its function, thus revealing a control of PIP metabolism on sphingolipid homeostasis (D'Angelo, Polishchuk *et al.* 2007) (**Figure 24**).

Sec14p, the Sec14-homology (Sfh) proteins: PI transporters

Sec14 is a budding yeast lipid-binding protein that was first identified in a screening for secretion-deficient mutants (Novick, Field *et al.* 1980) and for its capacity of transferring PI and PC between membranes *in vitro* (Bankaitis, Malehorn *et al.* 1989; Gnamusch, Kalaus *et al.* 1992). Several homologous proteins have since been identified in multiple different eukaryotic species and crystal structures have given insight into ligand binding *via* their conserved CRAL_TRIO domain. These homologous proteins were named Sfh proteins (**S**ec **F**ourteen **h**omologs), yet it is important to emphasize that not all Sfh proteins are also PI/PC exchange proteins (Bankaitis, Mousley *et al.* 2010).

Sec14p is an essential protein in yeast. Its depletion leads to the accumulation of PC and depletion of PI, PI(4)P and PS in Golgi membranes and to *post*-Golgi secretory defects (McGee, Skinner *et al.* 1994; Hama, Schnieders *et al.* 1999). Interestingly, deletion of specific proteins can bypass the essential requirement for Sec14p, amongst which three are implied in Kennedy pathway PC biosynthesis (Cpt1, Cct1p and Cki1p) and two in PI(4)P metabolism (Sac1p, Pik1p when overexpressed). The Sec14-bypass phenotype of Osh4p will be described below (McGee, Skinner *et al.* 1994; Fang, Kearns *et al.* 1996; Hama, Schnieders *et al.* 1999; Xie, Fang *et al.* 2001; Fairn, Curwin *et al.* 2007). Thus, the control of Golgi lipid homeostasis, particularly of PI(4)P, seems to be an essential function of Sec14p, but whether this is based on active lipid transfer is yet to be proven and the hypothesis has been challenged. It is nevertheless clear that Sec14p teams with Pik1p to maintain a proper Golgi PI(4)P level (Fairn, Curwin *et al.* 2007).

The lipid-binding capacity of Sec14p and Sfh proteins has been clearly established (**Figure 25**). Yet, it has not been proven whether all or only subsets are genuine lipid transfer proteins. The Sfh proteins in budding yeast and human have been found to influence most PIP signaling pathways, linking PIP metabolism with lipid droplet regulation in the case of Sfh3 or PS decarboxylation pathway for PC synthesis in the case of Sfh4 (Wu, Routt *et al.* 2000; Ren, Pei-Chen Lin *et al.* 2014). As an alternative hypothesis for their function, a "nanoreactor" role in regulating PIK activity by controlling its substrate accessibility has been proposed for the founding member Sec14p, a hypothesis that needs to be clarified and might be extrapolated to the whole protein family (Bankaitis, Ile *et al.* 2012).

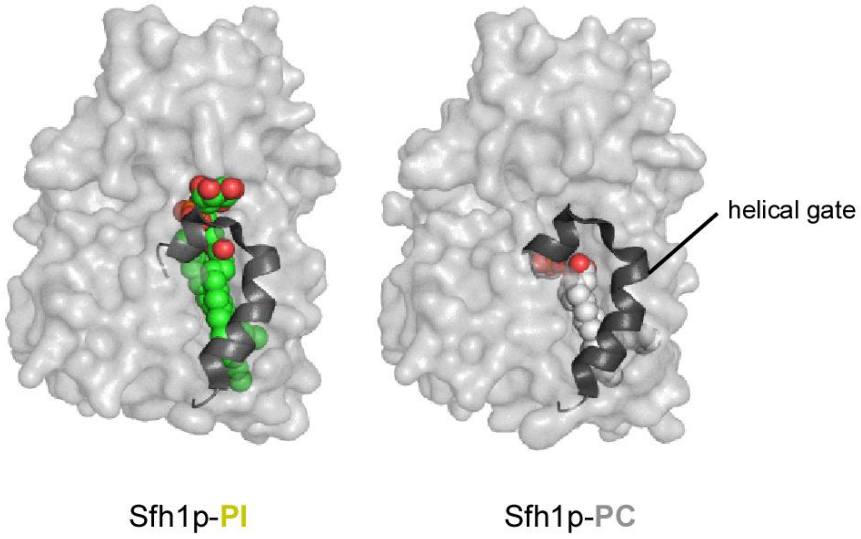

Figure 25. Lipid-binding in Sfh proteins

Sfh1p, the closest homolog of Sec14p, binds both PI and PC in a lipid-binding pocket closed by a helical gate that is opened in the apo-form (not shown). The two lipid ligands are recognized by different residues of the binding pocket, making binding both ligand impossible. Illustration from (Drin 2014).

A similar function has been proposed for human Nir2 as it also regulates Golgi PI levels at ER-TGN junctions and *post*-Golgi secretion similar to Sec14p, despite the fact that Nir2 does not belong to the Sec14 superfamily (Litvak, Dahan *et al.* 2005; Kim, Kedan *et al.* 2013). Interestingly, Nir2 is anchored *via* an interaction of its FFAT motif with VAP to the ER, not unlike CERT and OSBP, thus necessitating a close membrane contact for ensuring its function (Peretti, Dahan *et al.* 2008) (**Figure 54**).

The TULIP superfamily and SMPs: Infrastructure without lipid transport?

The **Tu**bular **Lip**id-binding (TULIP) superfamily encompasses proteins that are not characterized by sequence conservation but rather by a general geometric feature: A long hydrophobic tunnel capable of binding and transporting various lipids (Kopec, Alva *et al.* 2010). The functions of these proteins are diverse: Human CETP and PLTP for example are capable of transporting cholesteryl esters and phospholipids, respectively, between lipoproteins, thus in the extracellular medium (Albers, Vuletic *et al.* 2012; Pirillo, Norata *et al.* 2013). A screen of full genomes for TULIP revealed homology of certain intracellular proteins that were called **S**ynaptotagmin-like, **M**itochondrial and Lipid-binding **P**roteins (SMPs) (Lee and Hong 2006; Kopec, Alva *et al.* 2010). Intriguingly, numerous SMPs (all of them in budding yeast) localize *via* their SMP domain to membrane contact sites that have been proposed to facilitate non-vesicular lipid transfer. Additionally, SMPs can recognize lipids and are essential, yet not sufficient for MCS formation, and their TULIP homologs are capable of lipid transfer, but nonetheless there is currently no evidence of the implication of SMPs in active lipid transfer (Toulmay and Prinz 2013; Schauder, Wu *et al.* 2014).

The first subgroup of SMPs is constituted by the synaptotagmin-like proteins. These proteins all possess Ca^{2+}-dependent lipid-binding C2 domains like synaptotagmin, but are additionally equipped with a SMP domain, such as the extended synaptotagmins E-Syt1, 2, 3 and their yeast homologs the tricalbins Tcb1, 2, 3 (Manford, Stefan *et al.* 2012; Giordano, Saheki *et al.* 2013). Interestingly, both the E-Syts and the tricalbins have been implied in the formation of **membrane contact sites between the ER and the PM** (ER-PM MCS). In budding yeast, large parts of the PM have an underlying network of ER called or cortical ER (cER) that copurifies with the PM as PAM (Manford, Stefan *et al.* 2012). Analysis of the PAM fraction of the ER revealed a high abundance of enzymes implied in GPL biosynthesis such as Pss1p and Pis1p, but also sterol biosynthetic enzymes such as Erg9p (Pichler, Gaigg *et al.* 2001). In most higher eukaryotes, the ratio of ER associated with the PM is significantly lower than in yeast. Yet some cell types display equally elevated ratios such as muscle cells and neurons (Henkart, Landis *et al.* 1976). In all eukaryotes, the products (PS, PI and squalene (when further metabolized into ergosterol)) of all of the abovementioned enzymes are enriched in the PM compared to the ER, indicating an implication of these regions of the ER in transport of lipids towards the PM (Pichler, Gaigg *et al.* 2001).

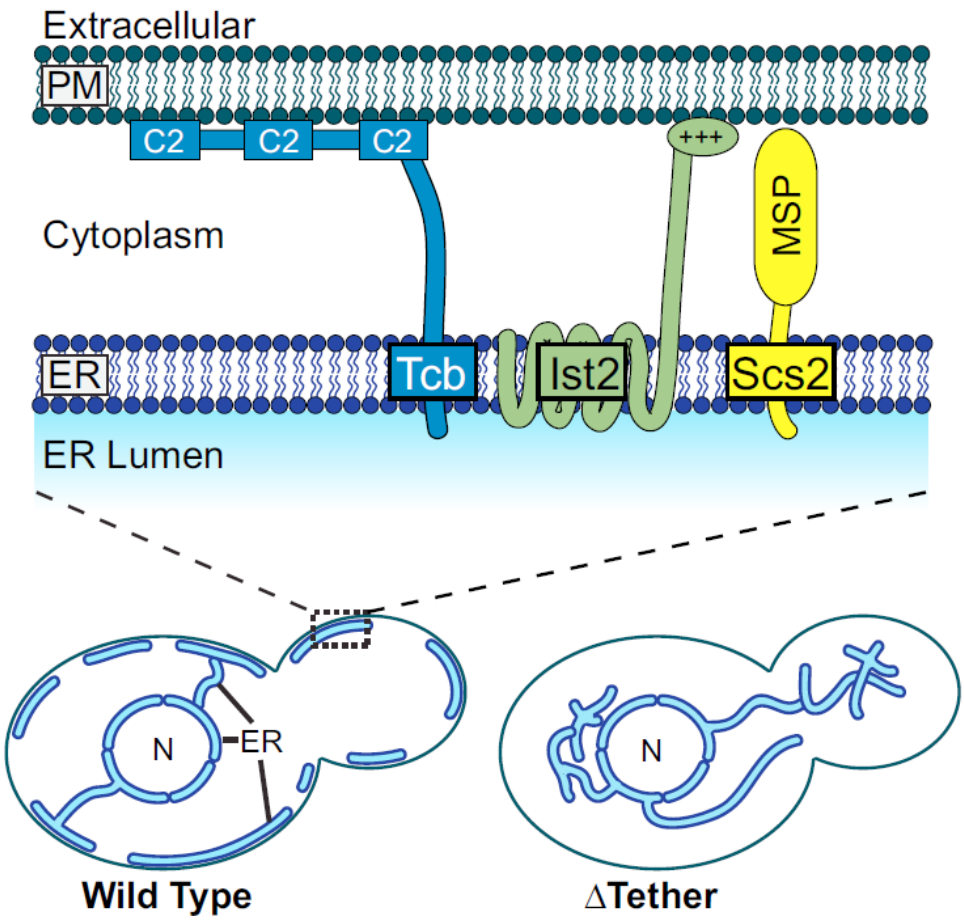

Figure 26. Tethering cortical ER and PM to form ER-PM MCSs.

Top: Three tricalbins (Tsbs), Ist2p and Scs2p are essential for ER-PM tethering and contact site formation. These ER-transmembrane proteins are capable of binding the PM: Tricalbins *via* its multiple lipids-binding C2 domains and Ist2p *via* a polybasic tails. The VAP Scs2p does not directly bind the PM but can serve as anchor for proteins interacting with the PM. Bottom: Large parts of the yeast ER are cortical, i.e. closely apposed to the PM. Deletion of the abovementioned proteins leads to a complete loss of the contacts. Illustration from (Manford, Stefan *et al.* 2012).

Manford *et al.* have identified several conserved ER-PM tethering factors whose deletion leads to collapsing of the ER and loss of contact site-dependent activities (**Figure 26**). All these tethers (Ist2p, the VAP proteins Scs2p and Scs22p, and the tricalbins Tcb1p, Tcb2p, and Tcb3p) are ER-resident proteins and a subset of them are bifunctional, i. e. they directly interact with the PM *via* multiple lipid-binding C2 domains (Tcb1-3p) or a polybasic motif (Ist2p) (Manford, Stefan *et al.* 2012). Deleting the human E-Syts leads to loss of ER-PM contact sites, which implies that these proteins have the same function as the tricalbins in yeast; regardless the fact that the E-Syts are no transmembrane proteins but anchored to the ER *via* insertion of a hairpin motif (Schauder, Wu *et al.* 2014). Interestingly, deletion of the SMP domain in Tcb2p leads to loss of MCS localization, indicating its role in tethering, even

though its precise function remains unknown (Manford, Stefan *et al.* 2012). VAP proteins do not interact directly with the PM but displays a binding site for a FFAT motif an could thus mediate indirect membrane tethering *via* FFAT-containing proteins (Mikitova and Levine 2012).

The multitude and conservation of ER-PM tethering factors highlights the diversity of this contact site as well as its importance for cell function that is assured by this redundancy. Notwithstanding their lipid-binding features and the importance of SMPs in ER-PM tethering, evidence on lipid transport by the SMP domains is still lacking (Toulmay and Prinz 2012); though recent findings of the De Camilli lab allowed them to posit two possible mechanisms: Either could SMP dimers form a tunnel for lipids or the tunnel could serve as lipid-binding pocket shuttling between membranes (Schauder, Wu *et al.* 2014).

The second subgroup of SMPs is formed by mitochondrial proteins as three mitochondrial yeast proteins were identified in the screen: Mmm1p, Mdm12 and Mdm34, implied in **ER-mitochondria contact sites** (ER-mito MCSs).

Membrane contacts between the ER and mitochondria were the first contact sites identified by electron microscopy. Upon isolation of mitochondria, parts of the ER are co-purified that were named mitochondria associated membranes (MAM) (Tatsuta, Scharwey *et al.* 2014). These MAM fractions are, not unlike the PAM fractions, enriched in lipid biosynthesizing enzymes, which indicated an implication of these contacts in lipid transport (Stone and Vance 2000). Mitochondria are only partially capable of synthesizing the lipids necessary for their growth and are not connected *via* vesicular trafficking to the endomembrane system. Additionally, as mentioned before, the inner IMM is one of the two loci of PS decarboxylation for PE and PC biosynthesis in the Kennedy pathway and mitochondrial PS import depends on non-vesicular mechanisms. (Leventis and Grinstein 2010) Altogether, these findings indicate in implication of ER-mitochondria contact sites in lipid transport. Besides, Ca^{2+} homeostasis in mitochondria is essential for mitochondrial ATP synthesis, and given the low affinity of the mitochondrial Ca^{2+}-uptake system, membrane contact with the ER would allow a local increase of Ca^{2+} concentration upon ER Ca^{2+} release, thus increase the signaling efficiency; the Ca^{2+}-related findings will not be further discussed here. For a recent review see (Helle, Kanfer *et al.* 2013).

Several ER-resident proteins interact physically with mitochondrial proteins and have thus been proposed as ER-mitochondria tethers, but the nature of the key tethering complex

has not yet clearly been defined. The **ER**-**M**itochondria **E**ncounter **S**tructure (ERMES) (**Figure 27**) is a potential candidate: ERMES is a heterotetrameric complex of soluble Mdm12p, two OMM proteins Mdm10p and Mdm34p and ER-resident Mmm1p (Kornmann, Currie *et al.* 2009). Three of these four proteins (Mmm1p, Mdm12p and Mdm34p) bear a SMP domain, but it has been impossible so far to show their direct effect on lipid transport. Intriguingly, deleting the SMP domain of Mmm1p leads to loss of ER-mitochondrion MCS localization, and deleting any of the ERMES subunits affects mitochondrial function in PC synthesis by PS decarboxylation, but phenotypes can be rescued by expression of an artificial construct that has only tethering activity (ChiMERA) (Kornmann, Currie *et al.* 2009). Nguyen *et al.*, however, showed that deletion of ERMES subunits did not affect mitochondrial PS decarboxylation (Nguyen, Lewandowska *et al.* 2012). These findings lead to the conclusion that contact of the mitochondria with the endomembrane system is essential and SMP-mediated, but ERMES does not directly intervene in lipid trafficking towards mitochondria (Kornmann, Currie *et al.* 2009; Toulmay and Prinz 2012).

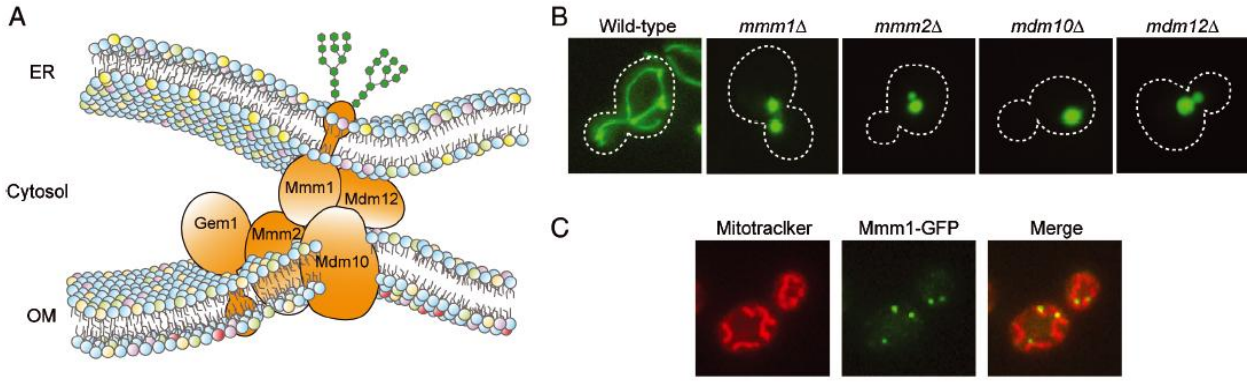

Figure 27. The ERMES complex between the ER and the outer mitochondrial membrane.

(A) Molecular architecture of the ERMES complex and its four subunits Mdm10p, Mdm12p, Mmm1p and Mmm2p. **(B)** GFP labeled mitochondria upon deletion of ERMES subunits show loss of the tubular structure found in WT mitochondria. **(C)** Colocalization of mitotracker (RFP, red) and Mmm1p-GFP shows punctuate structures, presumably ER-mitochondria contact sites. Illustration from (Tamura, Sesaki *et al.* 2014).

Mitochondria are not only connected to the ER but also display contacts with vacuoles in yeast. This interaction is mediated by **vCLAMP (vacuole and mitochondria patch)**, a protein complex containing the non-essential HOPS (homotypic fusion and protein sorting) tethering complex subunit Vps39 (Honscher, Mari *et al.* 2014). Recent findings on ERMES indicate an important role of this complex in tethering: Deletion of ERMES components does not lead to loss of mitochondrial PC synthesis activity, but deletion of both ERMES and

vCLAMP subunits is lethal. These results indicate that a mitochondrial connection to the vacuole can compensate loss of an ER connection and *vice versa*, thus underlining the importance of ERMES for ER-mitochondria tethering (Elbaz-Alon, Rosenfeld-Gur *et al.* 2014).

A third subgroup is just emerging as Toulmay and Prinz identified and characterized another yeast SMP, Nvj2p, that is localized to sites of contact between the nucleus and the vacuole called **nucleus-vacuole junction** (NVJ) (Toulmay and Prinz 2012) (**Figure 28**).

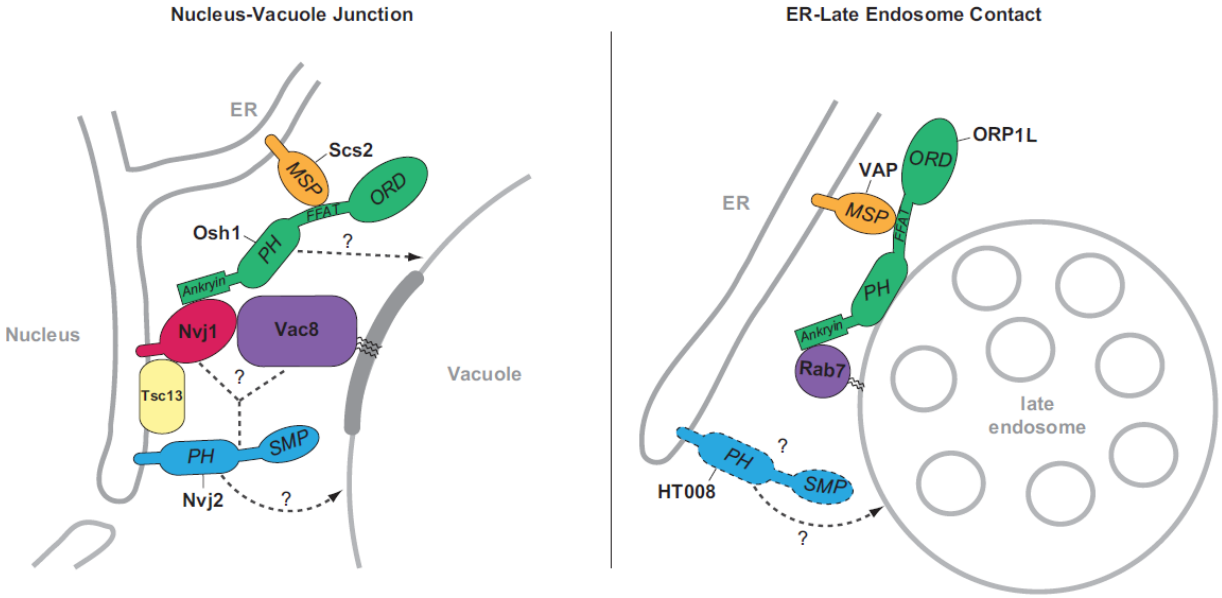

Figure 28. Comparison of yeast NVJ and mammalian ER-late endosome contact site.

Both late endosomes and vacuoles, the yeast equivalent of late endosomes/lysosomes, interact with the ER. The interaction between ORPs and VAPs appears to be conserved, whereas other tethering factors remain to be identified. Illustration from (Honscher and Ungermann 2014).

The vacuole, the equivalent in budding yeast of the higher eukaryote lysosomes, is connected to the nuclear envelope, which is continuous with the ER and the inner nuclear membrane. In stationary growth phase, this Nucleus-Vacuole junction (NVJ) becomes enlarged in order to perform an autophagic event called piecemeal microautophagy of the nucleus (PMN), in which small portions of the nucleus are digested in the vacuole (Kvam and Goldfarb 2004). The architecture of this contact site is surprisingly simple as only two proteins are required for its formation: Nucleus-vacuole junction 1 (Nvj1p) – that binds the inner nuclear membrane, spans the perinuclear space and the nuclear envelope – binds *via* its cytosolic domain to Vac8, a soluble protein that is anchored to the vacuole by N-terminal myristoylation and palmitoylation. The interaction of these two proteins is sufficient for

tethering and deletion of either one leads to complete dissociation of the MCSs (Kvam and Goldfarb 2004). Other proteins are targeted to the NVJ by interaction with Nvj1p such as Tsc13p and Osh1p, but are not required for its formation. Tsc13p is an essential very long chain fatty acid (VLCFA) synthase, required for efficient PMN, eventually by locally modifying the membrane composition with VLCFA. Osh1p was the first Osh protein to be localized to a MCS, although its NVJ-localization is transient for PMN and it is otherwise Golgi-localized (Levine and Munro 2001). The human ORP1 displays geometry similar to Osh1p and seems to be implied in contact sites between the ER and late endosomes, a contact site that might be functionally equivalent to the NVJ (Johansson, Lehto *et al.* 2005) (See Mammalian Oxysterol-Binding Protein and OSBP-related proteins: Only sterol transporters? and The long Osh proteins: Osh1p, Osh2p and Osh3p). The SMP domain-containing Nvj2p is targeted to the NVJ by its SMP domain, but its deletion does not seem to affect NVJ formation or PMN, nor could a lipid transfer activity be identified for Nvj2p (Toulmay and Prinz 2012).

Mammalian Oxysterol-Binding Protein and OSBP-related proteins: Only sterol transporters?

On the quest for events regulating cholesterol biosynthesis, oxidized sterol metabolites (oxysterols, precursors of steroid hormones and bile acids) were identified as potent inhibitors. 25-OH blocks HMG-CoA reductase activity in nanomolar concentrations in cells (Taylor and Kandutsch 1985). Interaction with this inhibitor allowed the isolation of the first oxysterol-binding protein from hamster liver cytosol, as well as the identification of the human Oxysterol-Binding Protein (OSBP) (Taylor and Kandutsch 1985; Dawson, Ridgway *et al.* 1989; Levanon, Hsieh *et al.* 1990).

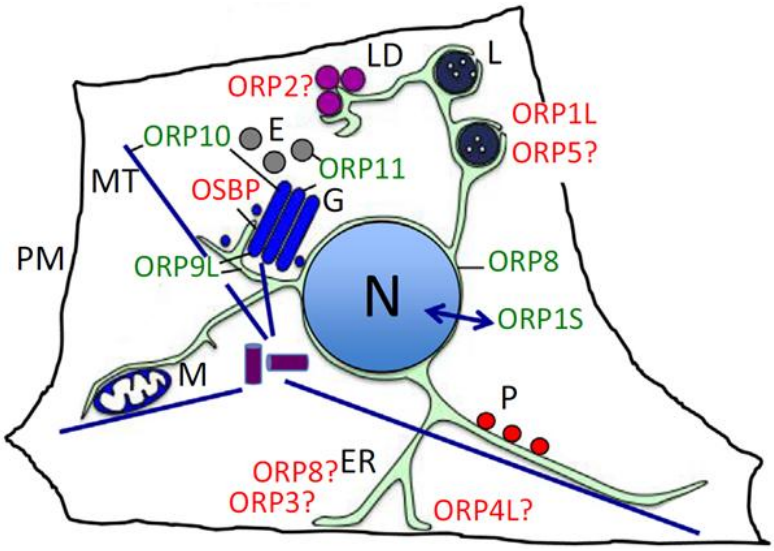

Figure 29. Localization of human ORPs.

ORPs identified at MCS are labeled in red, green ORPs have not been assigned to any MCS so far. Abbreviations are: E for endosomes, ER for endoplasmic reticulum, G for Golgi apparatus, L for lysosomes, LD for lipid droplets, M for mitochondria, MT for microtubules, P for peroxisomes (Olkkonen and Li 2013).

Screening eukaryotic genomes for sequence homologs of OSBP revealed that the OSBP-related protein (ORP) family is conserved among eukaryotic species, from higher eukaryotes (human, mouse, zebrafish) (Lehto, Laitinen *et al.* 2001; Anniss, Apostolopoulos *et al.* 2002; Liu, Boukhelifa *et al.* 2008; Zhou, Wohlfahrt *et al.* 2014) to yeast (Beh, Cool *et al.* 2001) (See *S. cerevisiae* OSBP homologs: The Osh protein family).

In human cells, twelve ORP genes code for 16 splicing variants and only a subset of the proteins' functions has been detailed so far (**Figure 29**, **Figure 30**). All ORPs share a C-terminal, ≈ 350 aa long **OSBP-related domain (ORD)** with a highly conserved fingerprint motif (EQVSHHPP) and most of them also display N-terminal domains. In these additional parts membrane- and protein interacting domains have been identified, such as PH domains

and Ankyrin repeats. ORP5 and ORP8 are particular as they are anchored with a C-terminal transmembrane segment to the ER (Olkkonen and Li 2013) (**Figure 30**). Most of the ORPs were found to bind oxysterols or sterols, yet with dramatically varying affinities (Suchanek, Hynynen *et al.* 2007).

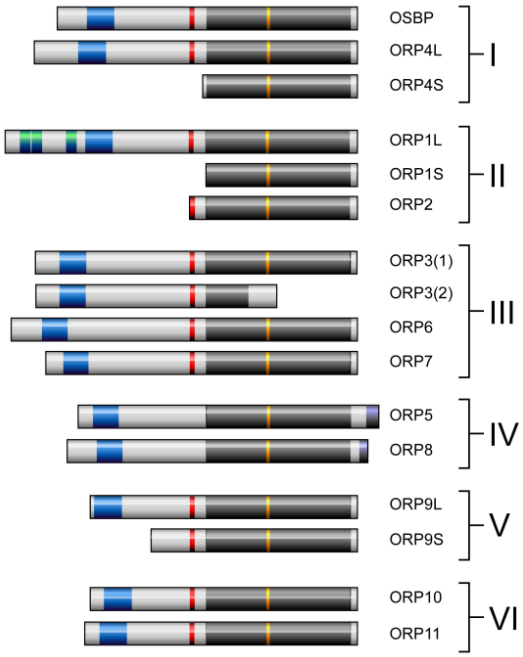

Figure 30. Overall domain structure of human OSBP-related proteins.

The sixteen splicing variants of the twelve human OSBP-related proteins classified in six subfamilies based on sequence homology. PH domains are represented in blue, FFAT motifs in red, ankyrin repeats in green, transmembrane segments in purple and the OSBP-related domain (ORD) in which the "fingerprint motif" (EQVSHHPP, yellow) is highlighted, in grey.

The founding member **OSBP** displays a PH domain in addition to its ORD, as well as a short FFAT motif to interacts with the ER-resident VAP-A (Levine and Munro 2002; Mikitova and Levine 2012). Dual targeting of PI(4)P-containing membranes by the PH domain and binding of an ER-resident protein with the FFAT motif allows OSBP to populate the ER-TGN junction (Perry and Ridgway 2006). The activity of OSBP for formation of such contact sites is higher compared to two other proteins with the same domain geometry (CERT and FAPP2, see StAR-related lipid transfer (START) proteins and Glycolipid transfer proteins and FAPP proteins: glycol(sphingo)lipid transporters), as OSBP helps to recruit them to the ER-Golgi contact sites. Interestingly, OSBP is found exclusively on the Golgi when cells are treated with 25-OH (Ridgway, Dawson *et al.* 1992). Binding of oxysterols was the leitmotif for ORP identification, yet binding of other sterols was hypothesized and OSBP also binds cholesterol with varying affinities depending on its phosphorylation state (Wang, Weng *et al.* 2005; Goto,

Liu *et al.* 2012). Ngo and Ridgway were able to demonstrate that OSBP is also capable of transporting cholesterol between artificial membranes *in vitro* (Ngo and Ridgway 2009). Finally, it was not clear whether OSBP was a sterol LTP or a 25-OH sensor.

Human **ORP1** is found in cells in two different splicing variants, ORP1S and ORP1L, the latter, longer version displaying N-terminal extensions comprising ankyrin repeats, a FFAT motif and a PH domain that are lacking in ORP1S. Both short and long versions of ORP1 bind sterols, but their localizations are distinct, as ORP1S is mainly cytosolic whereas ORP1L associated with endosomal compartments through interaction of its ankyrin repeats with the small GTPase Rab7 (Johansson, Bocher *et al.* 2003; Johansson, Lehto *et al.* 2005; Suchanek, Hynynen *et al.* 2007). Rab7 is bound to its effector RILP (Rab7-interacting lysosomal protein) and the dynein motor $p150^{Glued}$. Tethering of late endosomes to the ER through ORP1L by binding both membranes is controlled by endosomal cholesterol levels sensed by ORP1L (**Figure 28**, **Figure 31**). Increasing endosomal cholesterol levels increase the tethering, allowing dissociation of the Rab7-RILP-$p150^{Glued}$ complex and movement of endosomes along microtubules for LE repositioning (Rocha, Kuijl *et al.* 2009; van der Kant, Fish *et al.* 2013). Interestingly, the LE population bound by ORP1L also contains the sterol exporter NPC1 (See Uptake of exogenous sterol), whereas the LE population bound by STARD3 is distinct from the first since it does not contain NPC1 but the ABC3 sterol exporter (Alpy, Rousseau *et al.* 2013; van der Kant, Zondervan *et al.* 2013). Therefore, two different populations of LE can encounter the ER by different mechanisms, which would allow cholesterol transport at different levels of the endocytic pathway (van der Kant, Zondervan *et al.* 2013). Yet for both putative sterol export proteins, STARD3 and ORP1L, their lipid transport activity has been shown only indirectly.

ORP5 might be another player in the endosomal cholesterol efflux, as it physically interacts with NPC1 on late endosomes and thus at LE-ER contact sites as ORP5 displays a C-terminal transmembrane domain that is anchored into the ER membrane (**Figure 31**) Knockdown of ORP5 affects the cholesterol distribution in NPC fibroblasts leading to endosomal cholesterol accumulation, whereas knockdown of both NPC1 and ORP5 induces a diffuse sterol distribution (Du, Kumar *et al.* 2011). ORP5 binds oxysterols and cholesterol, yet recent findings suggested that ORP5 transports PS rather than cholesterol, challenging the hypothesis that ORP5 is a sterol transporter (Suchanek, Hynynen *et al.* 2007; Du, Kumar *et al.* 2011; Maeda, Anand *et al.* 2013).

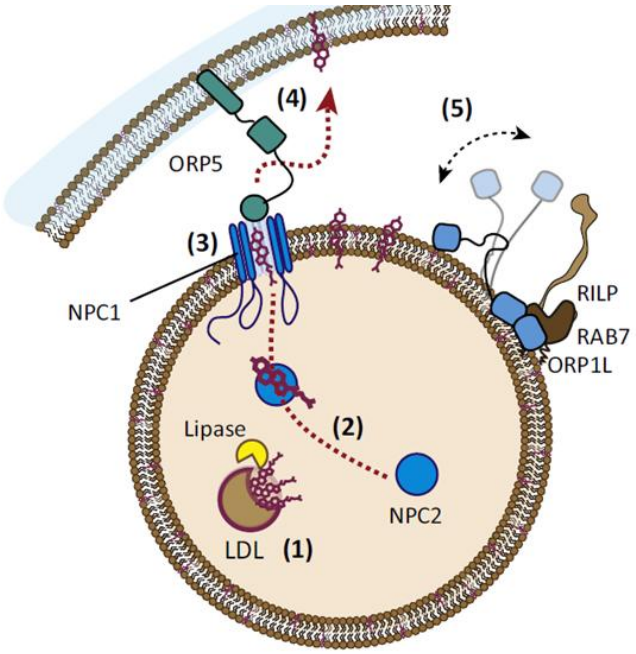

Figure 31. Working hypothesis for the interplay of ORP1L and ORP5 on late endosomes

Inside late endosomes, LDL particles are hydrolyzed by an acidic lipase **(1)** and release free cholesterol that is bound by NPC2 **(2)** and handed off to NPC1 that exports cholesterol from late endosomes **(3)**. ORP5 would then shuttle cholesterol to the ER **(4)**, just as ORP1L **(5)** that additionally relocalizes the LEs *via* the Rab7-RILP-p150^{Glued} (not shown) complex. Figure modified from (Neefjes and van der Kant 2014).

ORP2, an ORP displaying only an ORD, which also binds oxysterols or cholesterol has been found localized to lipid droplets (LD), and its depletion affected neutral lipid metabolism, implicating a role in LD homeostasis (Suchanek, Hynynen *et al.* 2007; Hynynen, Suchanek *et al.* 2009). Previous findings on ORP2 by overexpression had associated it with efflux of cholesterol from the ER without any change of PM cholesterol, findings that could be reconciled by a hypothesis on cholesterol efflux from the ER towards LD (Hynynen, Laitinen *et al.* 2005; Hynynen, Suchanek *et al.* 2009).

A short and a long version exist for **ORP9**: the long version ORP9L displays a PH domain, a FFAT motif and the ORD, thus sharing the OSBP domain structure, whereas the shorter ORP9S lacks the PH domain (Ngo and Ridgway 2009). Cholesterol transport activity has been shown *in vitro* and *in vivo* for ORP9L and ORP9S, which is increased in presence of PI(4)P. ORP9L localizes to ER-TGN contact sites in a VAP-A dependent manner, where ORP9L would transport cholesterol from the ER to the TGN. On the contrary, the short variant ORP9S is mainly cytosolic and affects vesicular trafficking (Ngo and Ridgway 2009; Ling, Hayano *et al.* 2014; Liu and Ridgway 2014).

S. cerevisiae OSBP homologs: The Osh protein family

Common features of the Osh proteins

In a hallmark publication, Beh *et al.* screened the entire yeast genome for homologs of OSBP and identified seven proteins (some of which had already been identified previously) that were named **Osh1-7p**. They all share an OSBP-related domain (ORD) that is well conserved from human to yeast, including the "fingerprint" signature motif EQVSHHPP. Based on the sequence similarity of Osh proteins, they can be divided into four subfamilies, pairing Osh1p and Osh2p; Osh3p; Osh4p and Osh5p; Osh6p and Osh7p. An alternative subdivision is the classification into "long" (Osh1-3p, integrating a C-terminal ORD and additional domains) and "short" (Osh4-7p, no domains other than the ORD) Osh proteins (**Figure 32**, **Figure 33**).

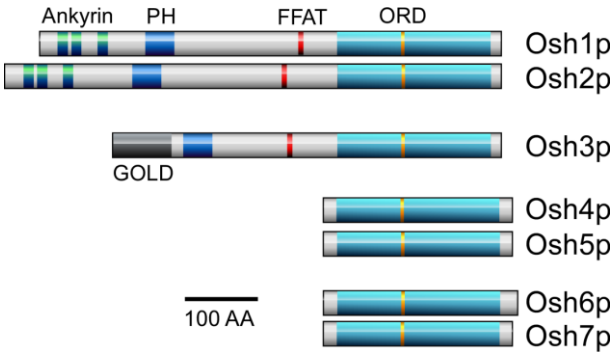

Figure 32. Overall domain structure of Osh proteins.

The seven yeast Osh proteins divided in long and short Osh proteins (Osh1p-3p) and in sequence similarity-based subfamilies (Osh1p-2p; Osh3p; Osh4p-5p; Osh6p-7p). The long Osh proteins display pleckstrin homology (PH, blue) domains and an FFAT (two phenylalanines in an acidic tract, red) motif. Osh1p and Osh2p additionally dispose of N-terminal Ankyrin repeats (green) and Osh3p of a Golgi dynamics (GOLD) domain. Osh4p-7p are devoid of these N-terminal extensions and only have an OSBP-related domain (ORD, cyan) in which the "fingerprint motif" (EQVSHHPP, yellow) is highlighted.

Based on early findings on OSBP, they analyzed every possible combination of deletion of Osh proteins, mainly to identify sterol-related phenotypes. In certain Osh deletion strains they identified resistance to nystatin, a drug specifically permeabilizing the PM in the presence of ergosterol. Nystatin resistance thus indicates absence of ergosterol from the PM. Yet total sterol levels of the Osh deletion strains were increased rather than decreased, indicating deficiencies in the transport of sterol towards the PM, resulting in intracellular accumulation of sterol. This lead the authors to the hypothesis that certain Osh proteins play an important role in PM sterol supply. Intriguingly, single deletion of one of the

seven Osh proteins had no effect on viability under normal growth conditions, and only multiple deletions impaired growth. Interestingly, any Osh protein (except Osh1p) is capable of restoring viability in a yeast strain depleted of all other Osh proteins, indicating that they share a common, essential function. These experiments were the cornerstone for all subsequent research on Osh proteins that is detailed in the following chapter (Beh, Cool *et al.* 2001).

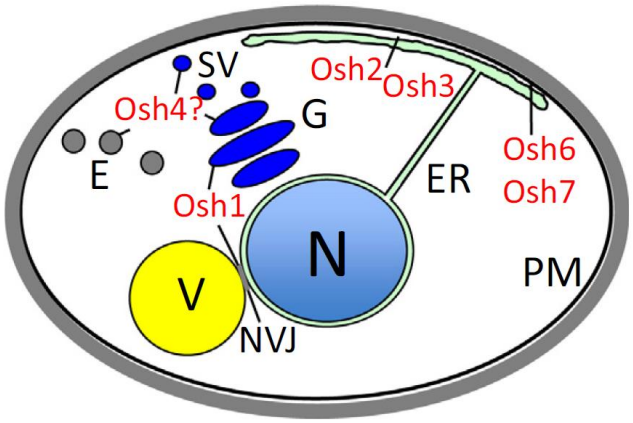

Figure 33. Localization of the Osh proteins in *S. cerevisiae*

Osh1p localizes to the nucleus vacuole junction (NVJ) and to the Golgi, Osh2p, Osh3p, Osh6p and Osh7p are found in the cell periphery, at putative ER-PM contact sites. Osh4p and Osh5p (not shown) localize to puncta, most probably secretory vesicles and the TGN or endosomal compartments. Illustration from (Olkkonen and Li 2013).

Further results of the same authors found an implication for the Osh protein family in cell polarization and polarized secretion and in secretory events in general. As explanation, they postulated sterol-dependent alterations of membrane composition (Beh and Rine 2004; Kozminski, Alfaro *et al.* 2006). Following experiments to prove the importance of the entire Osh family in sterol transport in cells produced contradictory results: Raychaudhuri *et al.* analyzed Osh function using a yeast strain capable of sterol uptake under normoxic (aerobic) conditions (upc2-1) and exogenous cholesterol. They found that functional Osh proteins are required for efficient sterol transport from the PM to the ER and sterol esterification, contradictory to the abovementioned findings (Raychaudhuri, Im *et al.* 2006). However, Georgiev and coworkers initially found that PM-to-ER sterol transport was affected after Osh deletion (Sullivan, Ohvo-Rekila *et al.* 2006),yet later revised their first communication and showed that PM-to-ER and ER-to-PM transport was unaffected by the absence of all Osh proteins (Georgiev, Sullivan *et al.* 2011).

The long Osh proteins: Osh1p, Osh2p and Osh3p

Osh1p and **Osh2p** are the Osh proteins sharing the highest sequence homology with OSBP. Despite the high sequence homology between the two proteins (55% identity, 71% similarity), the initial study were distinct, as Osh1p was identified as the only cold-sensitive Osh deletion mutant on minimal medium lacking tryptophan. Second, it has been found that any Osh protein except Osh1p is sufficient for yeast viability (Beh, Cool *et al.* 2001).

Analyzing the sequences of Osh1p and Osh2p revealed that in addition to their C-terminal ORD, they also integrate a PI(4)P-binding PH domain, a FFAT motif and three N-terminal ankyrin repeats, which are implied in protein-protein interactions, thus making them part of the "long" Osh proteins (1188 aa for Osh1p, 1283 aa for Osh2p) (Schmalix and Bandlow 1994; Beh, Cool *et al.* 2001). A study by Levine and Munro analyzed the localizations of Osh1p and Osh2p by fluorescence microscopy and revealed a peripheral localization of Osh2p in buds and at the bud neck, whereas Osh1p was located to central puncta. They subsequently identified the localization of Osh1p more precisely, showing that Osh1p is targeted to both the Golgi compartment by its PH domain and to the NJV by interaction between its ankyrin repeats and Nvj1 (**Figure 28**). Intriguingly, the ankyrin repeats of Osh2p do not target the NVJ, even as chimera with the Osh1p-ORD (Levine and Munro 2001). Kvam and Goldfarb showed that Osh1p is not required for PMN at NVJs, but that deletion of the entire Osh family perturbs PMN, underlining again the functional redundancy of Osh proteins (Kvam and Goldfarb 2004). Interestingly, the localization of the N-terminal extensions of Osh1p and Osh2p were distinct from the full-length proteins, indicating a role for the ORD in localization. The GFP-fused PH domains of Osh1p and Osh2p target spatially distinct PI(4)P pools *in vivo:* PH-Osh1p labels the Pik1p-derived Golgi pool whereas Osh2p-PH binds both Pik1p-derived Golgi and Stt4p-derived PM pools of PI(4)P, making it a valuable tool for following PI(4)P *in vivo* (Levine and Munro 2001; Roy and Levine 2004).

Osh3p is the third "long" (996 aa) Osh protein that forms a proper subfamily. Its sequence displays an N-terminal Golgi dynamics domain (GOLD), a FFAT motif, a PH domain and the C-terminal ORD (Levine and Munro 2001). Stefan *et al.* found that Osh3p localizes to cortical patches of the cell, which have been identified as ER-PM contact sites, by preferential interaction between its PH domain and the PM-localized Stt4p PI(4)P pool and by physical interaction with the VAP proteins Scs2p and Scs22p (Stefan, Manford *et al.* 2011). This discovery might partially explain the importance of Scs2p for ER-PM membrane

tethering (Stefan, Manford *et al.* 2013) (**Figure 26**). The authors hypothesized that Osh3p might through this tethering activity allow the ER-resident PI(4)P phosphatase Sac1 to act *in trans* on the PM and hydrolyze PI(4)P (Manford, Xia *et al.* 2010; Stefan, Manford *et al.* 2011), but recent findings challenge this hypothesis: The linker that would allow Sac1 to act in *trans* is implied in substrate recognition and would thus be shorter than assumed by the authors and not long enough to reach the PM (Cai, Deng *et al.* 2014). Besides, the authors gave no explanation on the necessity to down-regulate PI(4)P directly at the PM where it is synthesized. The crystal structure of Osh3p-ORD has recently been solved (PDB entry: 4INQ) (Tong, Yang *et al.* 2013). Unlike in Osh4p, a sterol molecule cannot be accommodated inside the lipid-binding pocket of Osh3p, explaining the previous finding that Osh3p is not capable of transferring sterols. Yet, Osh3p alike Osh4p is capable of binding PI(4)P in a conserved binding site (Tong, Yang *et al.* 2013).

This finding further clarifies the link between Osh3p and Sac1p reported by Stefan *et al.* (Stefan, Manford *et al.* 2011). Another intriguing hypothesis for the function of Osh3p was presented by Tavassoli *et al.,* who found that ER-PM tethering by the Osh3p-interacting VAP Scs2p is required for the function of the PEMT Opi3p, an effect alleviated by Osh3p overexpression, and that Osh3p would thus present PE or phosphatidyl methyl-ethanolamine (PME) to Opi3p, or ultimately transport PC to prevent its accumulation in the ER (Tavassoli, Chao *et al.* 2013).

The short Osh proteins: Osh4p, Osh5p, Osh6p and Osh7p

Osh4p was the first Osh protein identified, yet under its alias Kes1 (**K**r**e**11 **s**upressor), and **Osh5p** was subsequently identified as **h**omolog of K**es**1 (Hes1). The products of the Osh4p and Osh5p genes are surprisingly alike, sharing a sequence identity of 70% and over 80% similarity. They are “short” Osh proteins, meaning that they have no clearly identified domain other than the ORD. Deletion of both Osh4p and Osh5p lead to a resistance to the ergosterol specific drug nystatin leaving the total amount of ergosterol unaffected, indicating a role of these proteins in PM ergosterol supply or organization (Jiang, Brown *et al.* 1994) .

Intriguingly, Osh4p was found by Bankaitis and colleagues to rescue the effect of Sec14p-deletion. As mentioned before, Sec14p is a PC/PI exchanger that regulates the lipid composition at the Golgi level and downstream secretory processes. Its deletion is lethal

unless other proteins are simultaneously deleted. Among these protein deletions resulting in a Sec14p-bypass phenotype they identified Osh4p, whereas, intriguingly, Osh5p had no such effect despite its high sequence similarity with Osh4p, even at higher expression rates (Fang, Kearns et al. 1996).

The authors further characterized Osh4p and found it to be cytosolic, but also localized it at the Golgi complex. It has been suggested that Osh4p binds to the Golgi-localized Pik1p-derived PI(4)P pool and that this targeting is perturbed if either synthesis or hydrolysis (by Sac1p) of Golgi-PI(4)P is perturbed (Li, Rivas et al. 2002; Fairn, Curwin et al. 2007). A partial explanation for the Sec14-bypass phenotype caused by Osh4p deletion has been provided: Silencing Sec14p lead to a decrease of the availability of PI(4)P at the Golgi, mainly because Sec14p works with Pik1p to yield PI(4)P at this organelle. It was therefore suggested that Osh4p is lethal in Sec14p-deficient strains, because, due to its high endogenous expression, it monopolizes all the remaining Golgi PI(4)P molecules at the expense of other PI(4)P-binding proteins essential for *post*-Golgi vesicle biogenesis (Fairn, Curwin *et al.* 2007; LeBlanc and McMaster 2010). However, it was not understood how Osh4p binds PI(4)P. As shown later by structural analysis, Osh4p does not have any known PIP-binding domain such as a PH domain as suggested by Bankaitis and co-workers (Li, Rivas *et al.* 2002). Beside this, *in vitro* binding assays failed to prove that Osh4p could distinguish a PI(4)P- from a PI(4,5)P_2-containing membrane (Li, Rivas *et al.* 2002; Fairn and McMaster 2005; Schulz, Choi *et al.* 2009). More intriguingly, overexpressing Osh4p was observed to merely reduce the cellular level of PI(4)P (Fairn, Curwin *et al.* 2007). Altogether, these data suggested a strong link between Osh4p and PI(4)P metabolism.

Yet these data remain difficult to reconcile with other observations suggesting that Osh4p was a sterol transporter (Fairn, Curwin *et al.* 2007). First, in 2005, the group of James Hurley solved the crystal structure of Osh4p in complex with different sterols and oxysterols (Im, Raychaudhuri et al. 2005). This was naturally considered to be an important leap towards the understanding of Osh proteins function. The three-dimensional structure revealed a novel fold that was subsequently shown to be conserved in other Osh proteins (**Figure 34**). Osh4p displays a near-complete β-barrel of 19 sheets surrounding a hydrophobic cavity inside that accommodates a single sterol molecule in a head-down conformation. Osh4p was crystallized in complex with different sterols (cholesterol, ergosterol and oxysterols) with a 1:1 stoichiometry. The sterol 3-OH moiety makes direct and water-

mediated contacts with polar residues (Q96, Y97) at the bottom of the pocket. The sterol-binding site is locked by a flexible N-terminal lid region of 29 amino-acids (PDB entry: 1ZHZ) (Im, Raychaudhuri et al. 2005). When Osh4p is empty, the lid is unfolded and leaves the pocket accessible.

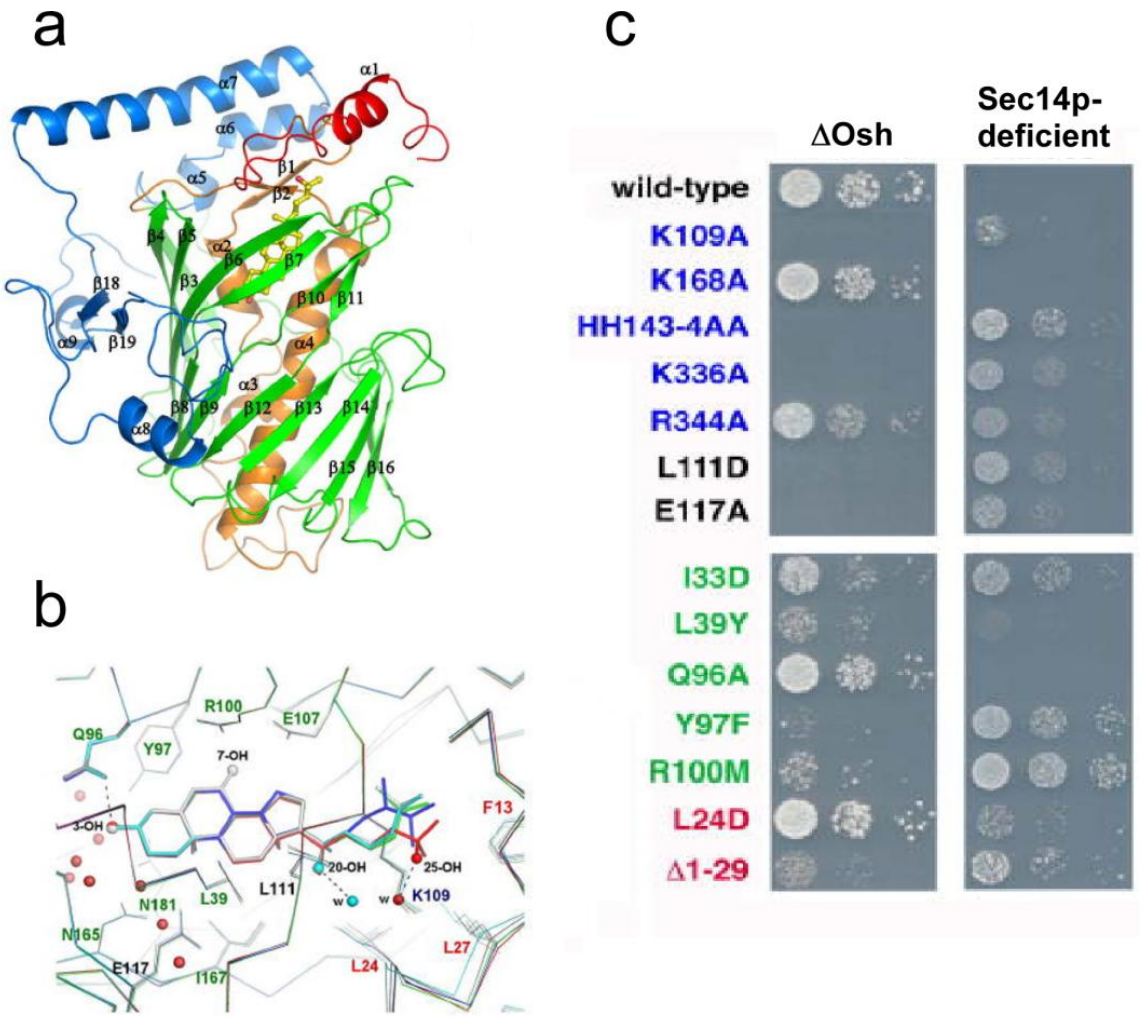

Figure 34. Crystal structure of Osh4p and analysis of mutations in ΔOsh and Sec14-*ts* backgrounds

(a) The overall structure of Osh4. The N-terminal lid (1–29) is red, the central helices (30–116) orange, the β-barrel (117–307) green, and the C-terminal sub-domain (308–434) cyan. **(b)** Superposition of five sterols in the binding site. 7-HC is colored grey, 20-HC cyan, 25-HC red, cholesterol green and ergosterol blue. Hydroxyl groups in the sterols are shown in spheres. Hydrogen bonds are shown in dashed lines. **(c)** Plasmids encoding Osh4 mutants were introduced into CBY926 (4) (ΔOsh) and NDY93 (Sec14-*ts*). The strains were grown at permissive temperature (23 °C) and dilution series were incubated at 37 °C. Illustration modified from (Im, Raychaudhuri *et al.* 2005).

These results suggested that Osh proteins adopt two distinct conformations: an empty form that might target a donor membrane to extract sterol and a sterol-bound form that recognizes an acceptor membrane to supply it with sterol. Further results from the same

group showed that Osh4p transports radioactively labeled cholesterol, albeit at slow speed, between artificial membranes *in vitro*, and that this activity was slightly accelerated by charged phospholipids such as PS and PI(4,5)P_2 (Raychaudhuri, Im et al. 2006). Interestingly, we found that the lid of Osh4p could alternatively fold into an ALPS motif that senses lipid-packing defect, suggesting ability for Osh4p to extract sterol from curved membranes (Drin, Casella *et al.* 2007).

Yeast complementation assays showed that Osh4p rescues ΔOsh strains lacking the entire Osh family (Beh, Cool *et al.* 2001; Beh and Rine 2004) likely by restoring proper ergosterol levels in the PM. This suggested that Osh4p transfers sterol to the PM. However, as mentioned above, the exact role of Osh4p and other Osh proteins in sterol distribution was rapidly disputed (See above). Nevertheless, Im and coworkers identified mutants shown to be unable to bind radioactive cholesterol *in vitro* (Y97F and R100M) to phenocopy the WT form of Osh4p in ΔOsh strains, thus suggesting that Osh4p acts as a sterol transporter. However, mutation of a neighboring residue (Q96A), that shows even stronger interaction with the ergosterol molecule in Osh4p was found to bind to sterol *in vitro* and to behaves like WT Osh4p in ΔOsh strains, questioning notably the results obtained with the Y97F mutant (Im, Raychaudhuri et al. 2005; Singh, Brooks et al. 2009). Moreover, subsequent results showed that the Y97F mutant is not a loss-of-function mutant of Osh4p in a study observing the repressive role of Osh4p function on exocytosis leading the authors to the conclusion that sterol transport is not an essential function of Osh4p (Alfaro, Johansen et al. 2011; Beh, McMaster et al. 2012). However, these studies aimed to examine mainly the impact of Osh4p on PI(4)P metabolism at the Golgi level.

Hurley and coworkers were intrigued by residues that are not directly implied in sterol recognition but that are strictly conserved in ORP/Osh proteins (Im, Raychaudhuri *et al.* 2005) such as H143A/H144A residues that belong to the ORD signature “EQVSHHPP“ and other residues, strictly conserved among the ORP/Osh protein such as K109 and K336. Intriguingly, the H143/H144AA double mutant, the K109A or K336A mutant do not have, unlike WT Osh4p, any lethal effect in Sec14p-deficient strains and, inversely, do not restore the viability of ΔOsh strains as Osh4p WT does (**Figure 34**). No clear explanation was given for these observations because most of these mutants were found to bind cholesterol as efficiently as the WT form.

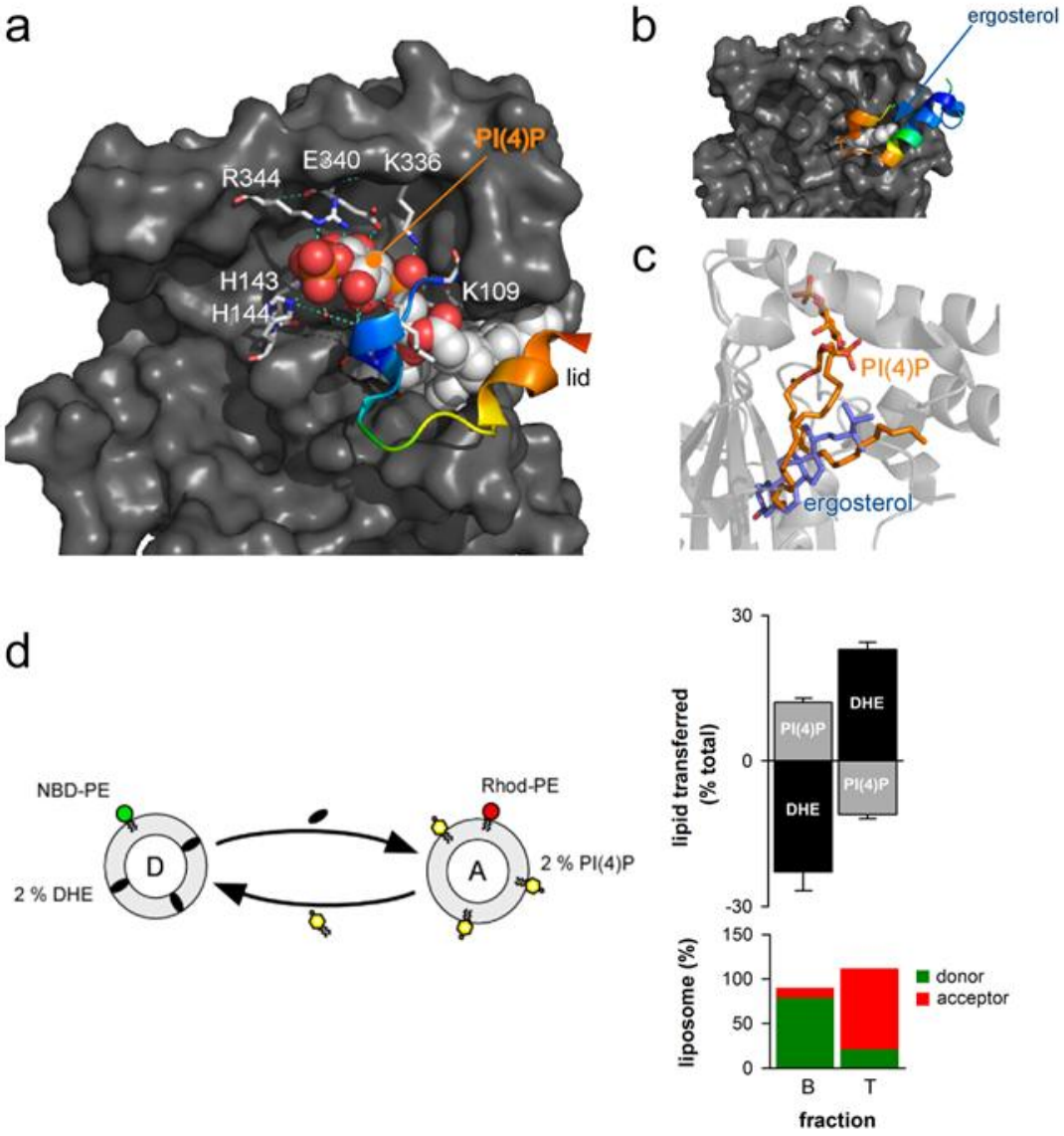

Figure 35. Structural aspects of Osh4p PI(4)P recognition and PI(4)P transport assay

(a) Close-up view of the PI(4)P binding site. PI(4)P is shown in grey with oxygen in red and phosphorus in orange. The residues that interact with the polar-head are represented in stick with oxygen in red and nitrogen in blue. The H-bonds are represented by cyan dashed lines, the water molecules are represented as red dots. The lid is colored with the B factor of Cα. **(b)** Structure of Osh4p bound to ergosterol. **(c)** Superposition of PI(4)P (colored in orange) and ergosterol (blue) molecules in Osh4p. The backbone of Osh4p is shown in light grey **(d)**. Sucrose-loaded DOPC/DHE liposomes (98:2 mol/mol, 0.5 mM lipids, labeled with 0.1% mol NBD-PE) were incubated with DOPC/PI(4)P liposomes doped with [^{32}P]PI(4)P (98:2 mol/mol, 0.5 mM lipids, labeled with 0.1 mol% Rho-PE). After centrifugation on a sucrose gradient, a bottom and top fraction were collected. The fluorescence of NBD-PE, Rho-PE, and DHE was measured and PI(4)P radioactivity was counted for each fraction. (B, bottom) The relative amount of donor and acceptor liposomes in each fraction is shown. (B, top) The gain or loss of DHE and PI(4)P (in percentages) for each liposome population. Data are represented as mean ± SEM (*n* = 2) Illustration in (d) modified from (de Saint-Jean, Delfosse *et al.* 2011).

Using novel real-time assays based on the use of dehydroergosterol (DHE), a close fluorescence analogue of ergosterol, our group addressed the influence of membrane composition on the ability of Osh4p to extract, deliver or transport sterol. Our major result was to unveil that PI(4)P specifically inhibits sterol extraction because PI(4)P is itself efficiently extracted by Osh4p (de Saint-Jean, Delfosse et al. 2011). We solved the structure of the Osh4p-PI(4)P complex and revealed how sterol and PI(4)P molecules, whose chemistry is unrelated, compete with each other (**Figure 35a, b**). This competition is explained by the fact that one PI(4)P acyl chain occupies the same pocket that sterol is bound to (**Figure 35a, b**). The polar head of PI(4)P lies in an adjacent shallow pocket: The phosphate groups at position 1 and 4 of the inositol ring contact exposed residues, notably K109, N112, K336, E340 and R344 residue and the H143/H144 pair. Compared to the sterol-bound form, the lid adopts a slightly different conformation to shield the PI(4)P molecule (**Figure 35a, b**). Importantly, we show that Osh4p exchanges DHE for PI(4)P and, thereby, can transport these two lipids between two distinct membranes along opposite routes (de Saint-Jean, Delfosse *et al.* 2011).

These findings lead us to the development of our current working model (**Figure 36**) We suggest that Osh4p uses the PI(4)P gradient at the ER/Golgi interface maintained by Pik1p and Sac1p to supply the *trans*-Golgi with sterol. In our model, Osh4p extracts sterol from the ER, then releases it by counterexchange with PI(4)P at the Golgi, and transports PI(4)P from the Golgi to the ER. The ATP-dependant production of PI(4)P by Pik1p would energetically drive sterol/PI(4)P cycles by Osh4p, thereby promoting the active release of sterol into the *trans*-Golgi and the creation of a sterol gradient. More generally, we propose for the first time a model to explain how lipids can be transported along an one-way route between organelles against their concentration gradient, and, as PI(4)P synthesis depends on ATP, why non-vesicular sterol transport processes were found to rely on energy (de Saint-Jean, Delfosse et al. 2011).

This model could explain why Osh4p expression is lethal in Sec14p-deficient yeast (Fang, Kearns *et al.* 1996; Fairn, Curwin *et al.* 2007). Osh4p does not reduce the availability of Golgi PI(4)P by solely binding this lipid but by extracting and transferring PI(4)P from the Golgi to the ER where Sac1p resides. This also easily explains why the overexpression of Osh4p reduces cellular PI(4)P levels and why, on the contrary, silencing Osh4p provokes a notable increase in cellular PI(4)P level similar to what is observed for Sac1p-deficient yeast

(Stefan, Manford *et al.* 2011) (**Figure 34**). Strikingly, we observed *in vitro* that the mutants K109A, H143A/H144A and K336A were unable to bind to PI(4)P. As mentioned above, these exact same mutants are those that are not lethal in Sec14p-deficient yeasts. We thus propose that these mutants lost their ability to extract PI(4)P from the Golgi and to convey this lipid to the ER. In line with this, a report by LeBlanc and McMaster (LeBlanc and McMaster 2010) showed that the K109A mutant does not lower the amount of PI(4)P in yeast as WT Osh4p does. Eventually, we could explain why the H143/H144AA, the K109A or K336A mutants do not restore viability of ΔOsh strains: Unable to bind PI(4)P, they would not exchange sterol for PI(4)P on the Golgi surface and, thus, would not properly release sterol into late membranes.

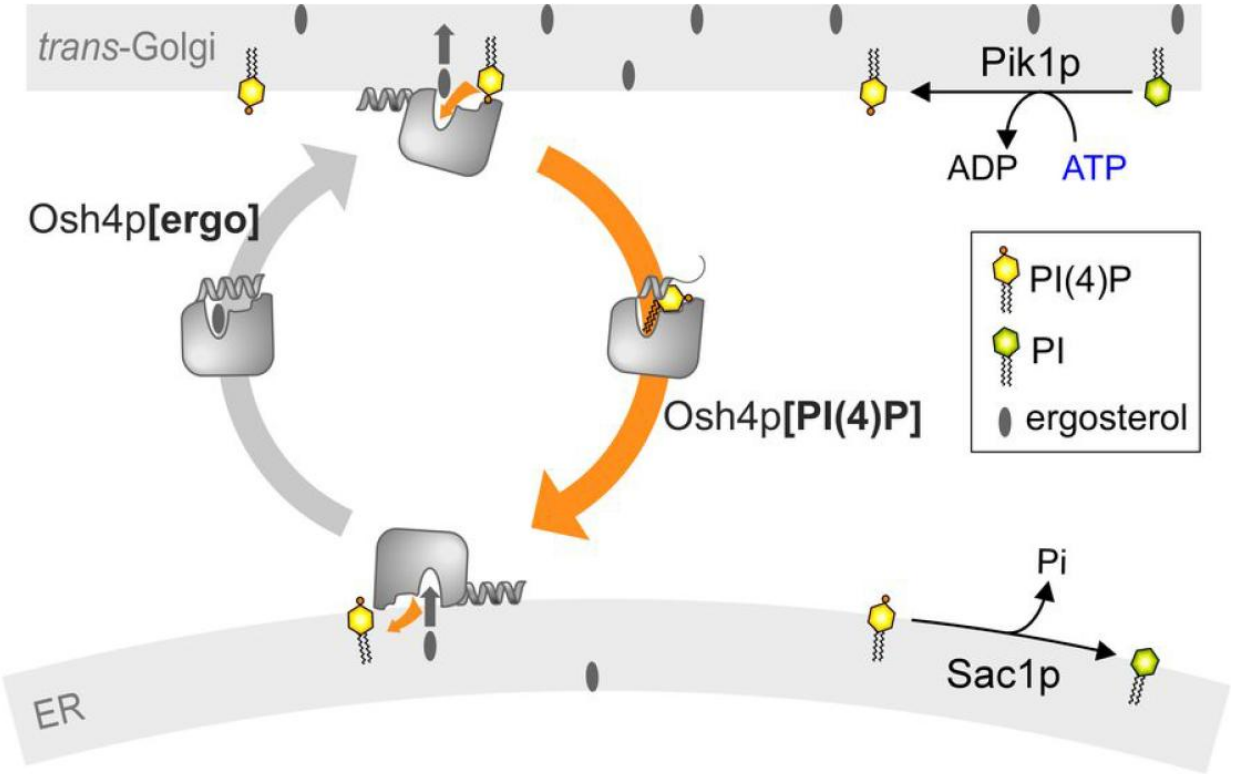

Figure 36. Working model for the lipid exchange function of Osh4p.

Our working model is based on the findings of (de Saint-Jean, Delfosse *et al.* 2011); **Figure 1** of the submitted manuscript "A phosphatidylinositol 4-phosphate-powered exchange mechanism to create a lipid gradient between membranes". Ergosterol is synthesized at the ER. Osh4p transports ergosterol from the ER to the *trans*-Golgi and PI(4)P in the opposite direction. ATP-dependent phosphorylation of PI into PI(4)P by Pik1p and the hydrolysis of PI(4)P by Sac1p allow multiple sterol/PI(4)P transport cycles by Osh4p. The maintenance of the PI(4)P gradient would allow in turn the vectorial transport of sterol and, thereby, the creation and maintenance of a sterol gradient between the ER and the Golgi by Osh4p.

Interestingly, our model might also explain further interesting observations: The control of Golgi PI and PI(4)P is essential for *post*-Golgi secretion. The ability of Osh4p to transfer PI(4)P from the Golgi to the ER might explain why Osh4p has been defined as a repressor of the biogenesis of exocytotic vesicles, relying on PI(4)P (Audhya, Foti *et al.* 2000). However, Osh4p was found to interact genetically and physically with the Rho GTPases Rho1 and Cdc42 as well as with the Rab GTPase Sec4p, regulators of polarized exocytosis (Kozminski, Alfaro et al. 2006). Additionally, Osh4p colocalizes in a PI(4)P-dependent manner to proteins of the exocyst complex and was found to be required for the Cas1-mediated removal of Golgi-derived PI(4)P from secretory vesicles (Alfaro, Johansen et al. 2011). PI(4)P is required on secretory vesicles budding off the Golgi for interaction of Ypt31/32p with Sec2p, which in turn activates Sec4p, controlling delivery and tethering of secretory vesicles *via* the exocyst complex. For this tethering the exocyst subunit Sec15p is required to bind to Sec2p in a site that overlaps with the Sec2p Ypt31/32p-binding site; in order to allow tethering with the PM Ypt31/32p thus needs to be dissociated from Sec2p (Mizuno-Yamasaki, Medkova et al. 2010). Osh4p controls this switch of Sec2p between Ypt31/32p and Sec15p by removing PI(4)P from secretory vesicles and thus promotes dissociation of Ypt31/32p from Sec2p (Ling, Hayano et al. 2014). PI(4)P hydrolysis by Sac1p is required for this activity, indicating that Osh4p therefore would not only remove PI(4)P from secretory vesicles but also make it available for the phosphatase (Ling, Hayano et al. 2014).

To sum up, we propose that Osh4p ensures sterol/PI(4)P exchange cycles at the ER/late membrane interface and that any deregulation of this activity has subtle effects on the exocytosis process. The sterol/PI(4)P exchange activity, in context where Golgi PI(4)P is lacking, might promote even more severe reduction of PI(4)P level in this compartment resulting in an blockade of exocytotic vesicle biogenesis. On the contrary, any arrest of the sterol/PI(4)P exchange through the silencing of Osh4p, would block the tethering of exocytotic vesicles with the PM. Interestingly, recent evidence also suggests that the deregulation of Sac1p, Pik1p or Osh4p has an effect on cellular sphingolipid levels (Brice, Alford et al. 2009; LeBlanc and McMaster 2010; Mayinger 2012). A likely hypothesis is that the PI/PI(4)P balance, at the ER level, depends on the activity of these three proteins and that this balance is crucial for sphingolipids synthesis as such a process directly relies on the availability of PI coming from the ER.

The two other short Osh proteins **Osh6p** and **Osh7p** have a sequence identity alike Osh4p and Osh5p (70% identity, 80% similarity), yet the conservation level between the two subfamilies is lower (Beh, Cool *et al.* 2001). Most research effort has been intended for Osh6p, neglecting Osh7p due to its high sequence similarity and thus functional conservation, but considering the differences in Osh4p- and Osh5p-related phenotypes, more detailed analysis of Osh7p could reveal functional differentiation between Osh6p and Osh7p.

Osh6p and Osh7p are cytosolic proteins that are also enriched at cortical patches of the ER, presumably ER-PM contact sites, as determined by fluorescence microscopy. Wang *et al.* found Osh6p to be a major regulator of cellular ergosterol, as its deletion lead to increase and its overexpression to decrease of total ergosterol (Wang, Duan *et al.* 2005; Wang, Zhang *et al.* 2005). This was underlined by findings showing both Osh6p and Osh7p interacting with the vacuolar yeast NPC1 homolog Ncr1p in an Arv1p-dependent manner, yet the impact on Arv1p on sterol homeostasis appears to be minor as recently reported (Du, Kumar *et al.* 2011; Georgiev, Johansen *et al.* 2013).

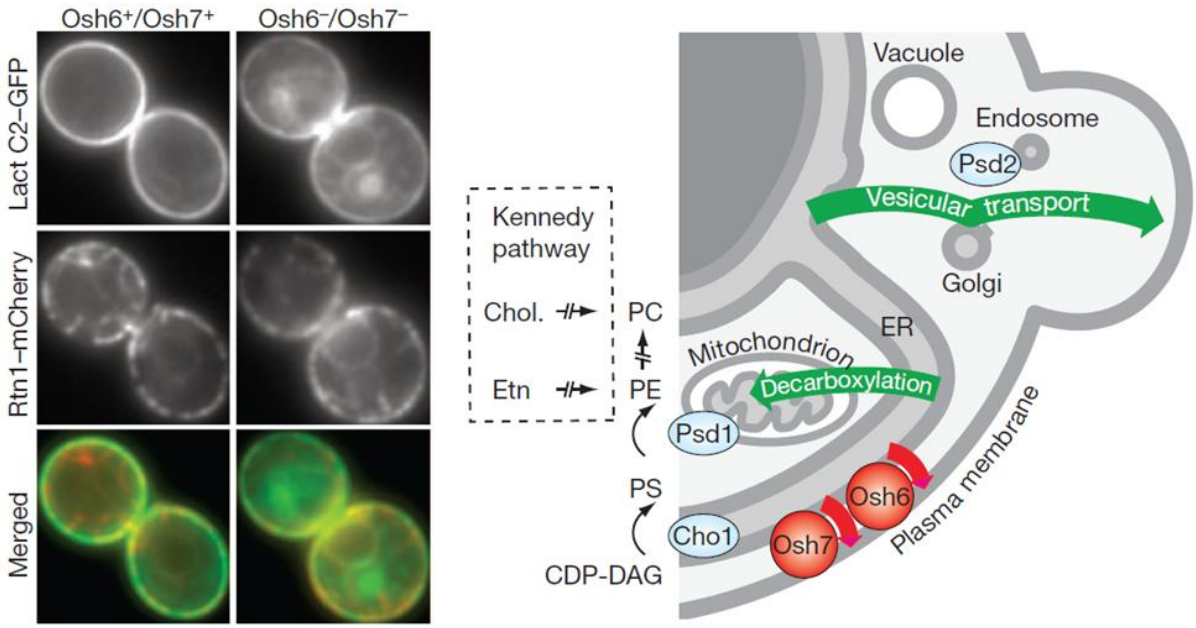

Figure 37. Osh6/7p are PS transporters

Left: Yeast strains without Osh6p and Osh7p ($Osh6^-/Osh7^-$) show decreased PS levels at the PM compared to WT ($Osh6^+/Osh7^+$) as observed using a genetically encoded PS probe ($GFP\text{-}C2_{Lact}$). PS levels are decreased by 30 % whereas they are in increased in the ER, highlighted by Rtn1-mCherry. **Right:** Model showing different PS transport pathways that are Osh6/7p-dependent (red) or -independent (green). Illustration modified from (Maeda, Anand *et al.* 2013).

However, a recent study and our own results will show that Osh6p is clearly not capable of interaction with ergosterol (Maeda, Anand *et al.* 2013) (**Figure 46**). Osh6p rather binds PS in its conserved hydrophobic pocket and transports newly synthesized PS from the ER towards the PM (Maeda, Anand *et al.* 2013) (**Figure 37**). Deletion of both Osh6p and Osh7p is necessary for affecting PS transport, indicating a functional redundancy between the two proteins (Maeda, Anand *et al.* 2013). PS transport towards sites of polarized growth is also mediated by vesicular trafficking, whether these vesicular and non-vesicular transport pathways are coupled awaits further elucidation (Fairn, Hermansson *et al.* 2011; Mioka, Fujimura-Kamada *et al.* 2014). The Osh protein family is not implied in PS transport towards Psd1p or Psd2p for PE and PC synthesis and yet total PS levels in Osh deletion mutants are significantly decreased favoring PE and PC synthesis, underlining the importance of Osh proteins in alternative PS trafficking routes like those shown by Maeda *et al.* (Raychaudhuri, Im *et al.* 2006; Maeda, Anand *et al.* 2013). Albeit the clear effect of Osh6p and Osh7p on ER-PM PS transport, this is not an essential function as ablation of both proteins is not lethal. Also, both proteins can restore cell growth in mutants lacking all other Osh proteins, whereas Osh7p bearing mutations in residues not affecting PS binding (HH159/160AA) fails to do so, indicating further essential functions for Osh6p and Osh7p (Tong, Yang *et al.* 2013).

Recent Structural aspects of Osh protein lipid binding

The intriguing finding that Osh4p does not only bind sterols (Im, Raychaudhuri et al. 2005) but also PI(4)P (de Saint-Jean, Delfosse et al. 2011) represented a paradigm shift in ORP/Osh research as for the first time a non-sterol lipid ligand was found to bind to an Osh protein. Crystal structures of Osh3p-ORD (PDB entry: 4IC4), the Osh3p-ORD-PI(4)P complex (PDB entry: 4INQ) (Tong, Yang et al. 2013) and the Osh6p-PS complex (PDB entry: 4B2Z) (Maeda, Anand et al. 2013) showed that the overall fold of Osh proteins is well conserved, as well as the PI(4)P-binding site (de Saint-Jean, Delfosse et al. 2011; Tong, Yang et al. 2013). The second GPL ligand found to bind to an Osh protein was PS in Osh6p, but whether PS-binding is structurally conserved in Osh proteins has not been shown so far (Maeda, Anand et al. 2013). Intriguingly, the ORP/Osh fingerprint motif found to be implied in PI(4)P binding in Osh4p and Osh3p, but does not interact with the PS molecule in the Osh6p structure nor with sterol in the Osh4p structure (Im, Raychaudhuri et al. 2005; de Saint-Jean, Delfosse et al.

2011; Maeda, Anand et al. 2013). As the geometry of the PI(4)P binding site is conserved in Osh6p, this leads to the intriguing question whether Osh6p can also bind PI(4)P. Moreover, does it bind PS and PI(4)P in the same mutually exclusive manner than for ergosterol and PI(4)P in Osh4p?

Hypothesis for ORP/Osh protein function and objectives

Sterols are unevenly distributed in eukaryotic cells: Sterols are scarce at the ER, where they are synthesized, whereas they are enriched at the TGN and PM. In yeast and human cells, the uneven distribution of sterols, ergosterol in yeast and cholesterol in human, plays a key role as sterols render membranes more rigid in presence of saturated phospholipids. The accumulation of sterol species at the PM thus allows formation of a rigid barrier shielding the cell from external influence (van Meer, Voelker *et al.* 2008). Early studies from the Simoni group suggested that sterol is rapidly transferred ($t_{1/2}$ ≈10 min) from the ER to PM mostly along non-vesicular routes in an energy-dependent manner (DeGrella and Simoni 1982). Likewise, ER-to-PM transfer of ergosterol, the major sterol in yeast, takes place along non-vesicular routes (Baumann, Sullivan *et al.* 2005). Whereas the trafficking in the secretory pathway is well established and defined, little is known about the non-vesicular trafficking of lipids and sterols inparticular (Drin 2014). Among the LTPs that could be able to serve as sterol transporters are the ORP/Osh proteins (Beh, Cool *et al.* 2001; Lehto, Laitinen *et al.* 2001). Whether ORP/Osh proteins participate in active sterol transport *in vivo* and how their activity is regulated is largely unknown (Raychaudhuri, Im *et al.* 2006; Alfaro, Johansen *et al.* 2011; Georgiev, Sullivan *et al.* 2011). Yet the current opinion on sterol transport proteins considers the chemical potential gradient sufficiently powerful for the establishment of sterol concentration gradient by random shuttling (Sullivan, Ohvo-Rekila *et al.* 2006; Beh, McMaster *et al.* 2012) (**Figure 19**).

Our group has proposed an alternative hypothesis: We posit that Osh4p exchanges newly synthesized sterols from the ER for PI(4)P at the *trans*-Golgi. Anterograde sterol transport is fueled by retrograde PI(4)P transport and PI(4)P hydrolysis (de Saint-Jean, Delfosse *et al.* 2011) (See our working model (**Figure 36**)). We therefore wanted to test this model by very precise quantitative analysis. One of our goals was to **measure whether Osh4p acts as an efficient sterol/PI(4)P counterexchanger, i.e. by coupling intimately the transport of its two lipid ligands in opposite directions between two membranes.** We further aimed to **define whether the maintenance of a PI(4)P gradient by PI(4)P hydrolysis provides additional energy for sterol transport to Osh4p.** Ultimately we wanted to **provide evidence that this mechanism allows Osh4p to transport sterol against its concentration gradient.**

MCSs are specialized zones in which the ER membrane is closely apposed to the membrane of a second organelle (10–20 nm apart), and are increasingly considered as essential hubs for the transport of lipids. In higher eukaryotes, MCSs between the ER and *trans*-Golgi are notable because they host various LTPs, including OSBP, CERT and Nir2, which play major roles for the remodelling of the Golgi membrane. OSBP has been shown to bind and/or transport oxysterols and cholesterol with varying affinities (Wang, Weng *et al.* 2005). Besides, it targets both the ER and the *trans*-Golgi network by interaction of its FFAT motif with VAP-A and by coincidence detection of both PI(4)P and Arf1 with its PH domain (Levine and Munro 2002; Mikitova and Levine 2012). OSBP is mostly cytosolic, but binding to its high affinity ligand 25-OH rapidly targets the protein to the Golgi (Ridgway, Dawson *et al.* 1992). Our lab was interested in determining the actual function of OSBP. At one point, **we aimed to demonstrate that OSBP is also capable of counterexchanging PI(4)P for cholesterol and that this activity determines its function at ER-Golgi contact sites.**

Recent structural insight gave proof that sterol binding is not a common feature of the ORP/Osh proteins (Maeda, Anand *et al.* 2013; Tong, Yang *et al.* 2013). The recognition of PI(4)P, however, might be better conserved (de Saint-Jean, Delfosse *et al.* 2011; Tong, Yang *et al.* 2013). The demonstration of a conserved PI(4)P-binding mode in ORP/Osh proteins could thus help to identify a common mechanism of function, and be (possibly related to) the common essential function of Osh proteins in budding yeast (Beh, Cool *et al.* 2001).

PS has been identified as ligand for Osh6/7p and potentially for ORP5 and ORP10; Osh6/7p have additionally been shown to transport PS from the ER to the PM (Maeda, Anand *et al.* 2013). **We wanted to study whether Osh6/7p are capable of binding PI(4)P and counterexchanging it for PS between membranes, and whether this transport is favored by PI(4)P metabolism, in the same manner as for sterol/PI(4)P counterexchange by Osh4p, allowing Osh6/7p to create a PS gradient between the ER and PM.**

Using fluorescence-based lipid transfer assays in a reconstituted system of reduced complexity we aimed to follow the effects of ORP/Osh proteins on transport of lipid species. We developed, in addition of using well-established techniques, novel fluorescence-based lipid transport assays *in vitro*, to examine with a high temporal resolution the ability of ORP/Osh proteins to transport sterol and PI(4)P in opposition direction between two distinct membranes. Such reconstituted system allows the observation of a strictly controlled variable under constant control of all factors, excluding unwanted compensatory effects.

We provide insight in the conservation of the proposed mechanism between budding yeast and human as well as proof for the capability of Osh4p to transport sterol against its concentration gradient using PIP metabolism as energy source.

MATERIALS AND METHODS

RECONSTITUTIVE APPROACH:

ASSAYING LIPID TRANSFER *IN VITRO*

Lipid homeostasis is very rapid and highly dynamic. Qualitative detection of the lipid transport activity of protein *in vivo* is usually based on fluorescence-labeled, specific lipid-interacting protein domains (GFP-Annexin V, GFP-$C2_{Lact}$, GFP-PH_{FAPP}) or naturally fluorescent lipids (DHE), but quantification of lipid transport remains difficult, so that kinetics and interplay in the case of lipid exchange cannot be easily assayed. Fluorescence-labeled lipid molecules are to be used with caution as the presence of a fluorescent moiety might influence the physical-chemical properties of lipids in both membrane insertion and recognition by LTPs. Isotope labeling allows quantification of lipid transport by membrane fractionation, lipid extraction and autoradiography, but the low time resolution prevents detailed insight into the kinetics of lipid transport mechanisms.

Therefore, to fully understand the biochemistry of ORP/Osh proteins, it is necessary to use a pure *in vitro* approach. We use artificial membranes of defined composition, small fluorescence-labeled lipid probes and recombinant proteins to follow lipid transport by fluorescence measurement under controlled conditions. Despite the fact that our system does not perfectly mimic a cellular context, it allows us to measure with an unprecedented precision the lipid transport activity of proteins. This precision is required to detect kinetic coupling in lipid counterexchange, as compensatory or regulatory events possibly occurring *in vivo* might prevent us from detecting such coupling. Once biochemically demonstrated, proof from *in vivo* experiments is however required to ascertain the validity of the hypothesis in living cells. This validation has been achieved for certain findings (see Results) or is currently ongoing.

Liposomes

In order to measure transport of lipids between lipid membranes we need to control the lipid composition of those membranes. We use spherical vesicles with a defined diameter (liposomes) and of defined composition that are produced from lipid films by suspension in buffer and extrusion. Lipids were purchased from Avanti Polar Lipids, except DHE, which was purchased from Sigma-Aldrich. The lipids solubilized in an organic solvent (chloroform, methanol or more complex mixtures) were mixed in the desired molar ratios and the organic solvent was evaporated under reduced pressure in a rotative evaporator. The dried films were hydrated in buffer (120 mM K acetate, 50 mM Hepes, pH = 7.2) with small glass beads under rigorous agitation and the suspension subsequently underwent five freeze-thaw cycles (flash freezing in liquid nitrogen and thawing in a water bath at 37 °C) in order to obtain multilamellar vesicles (MLVs). MLVs were then extruded into small unilamellar vesicles (SUVs) by passing them 21-times through a polycarbonate filter with pores of defined size (usually 0.2 µm) using a mini-extruder (Avanti Polar Lipids). To produce liposome of varying diameter liposomes were sequentially extruded through filters with decreasing pore size (0.4 µm, 0.2 µm, 0.1 µm, 0.05 µm and 0.03 µm). Dynamic light scattering (DLS) was used to define the size distribution and average size of these unilamellar vesicles.

Protein purification

In order to obtain high grade recombinant protein for our measurements, we used isopropyl β-D-1-thiogalactopyranoside (IPTG)-induced overexpression from pET-24b (+) (Sac1p) or pGEX-4-T3 (all other proteins) plasmids in BL21 Gold cells (*Escherichia coli*). Mammalian protein (PH_{FAPP}, $C2_{Lact}$) overexpression was induced with 1 mM IPTG for 4 h at 37 °C, whereas yeast proteins were induced with 1 mM IPTG over night at 30 °C. Cells were harvested by centrifugation, washed with phosphate buffered saline (PBS) and again sedimented. Bacteria pellets were stored at -20 °C prior to purification. For purification, cells were suspended in lysis buffer (150 mM NaCl, 50 mM Tris.HCl pH = 7.4) and lysed in a French Press in the presence of a protease inhibitor cocktail (EDTA-free protease inhibitor tablets (Roche), pepstatin, bestatin, phosphoramidon and PMSF) and 2 mM dithiothreitol (DTT) to

prevent oxidation. The lysate was treated with DNase I to remove longer DNA strands prior to ultracentrifugation. For GST-tagged proteins, the supernatant was applied to Glutathione sepharose beads (GE Life Sciences) and bound protein washed three times with lysis buffer containing DTT. The GST-tag was cleaved by thrombine (Roche) treatment over night. Eluted fractions were concentrated and further purified by on size exclusion chromatography (Sephacryl S-300, GE Life Sciences). For His_6-tagged proteins, the supernatant was applied to Ni-NTA Agarose (Qiagen), the beads washed, protein eluted with 20 mM, 50 mM imidazole and the concentrated eluate further purified by size exclusion chromatography (Sephacryl S-300, GE Life Sciences) to remove imidazole. All proteins were assayed by Bradford assay, absorbance at λ = 280 nm and gel assay using SyproOrange (Life technologies).

Flotation assays

Binding of protein on membranes and its lipid specificity were assayed by flotation assays that have been described previously. Briefly, proteins (750 nM) were incubated with NBD-PE containing liposomes (750 µM total lipids) in 150 µl HKM buffer at room temperature for 5 min. The suspension was adjusted to 30% sucrose by mixing 100 µl of a 75% (w/v) sucrose solution in HKM buffer and overlaid with 200 µl HKM containing 25% (w/v) sucrose and 50 µl sucrose-free HKM. The sample was centrifuged at 240,000 g in a swing rotor (TLS 55 Beckmann) for 1 h. The bottom (250 µl), middle (150 µl) and top (100 µl) fractions were collected. The top fractions were analyzed by SDS-PAGE using Sypro-Orange staining and a FUJI LAS-3000 fluorescence imaging system (Bigay and Antonny 2005).

Fluorescence and FRET

PI(4)P detection by NBD-PH_{FAPP}

Multiple proteins are specifically localized to PI(4)P containing membrane compartments *via* PI(4)P-interacting domains and have been described above (See Synthesis and localization of phosphoinositide species). The approximately 100 aa long pleckstrin homology (PH) domains can simultaneously bind PIPs and/or small G proteins. PH domains are abundant and found in LTPs, such as FAPP1, FAPP2, CERT and ORPs, but also in

phospholipase Cδ (PLCδ), and have been used extensively to study localizations of PIPs *in vivo*. GFP-labeled PH domains of PLCδ identifies PM PI(4,5)P_2, whereas PH domains of FAPP1, OSBP and CERT target Golgi PI(4)P and GFP-PH_{Osh2p} highlights both Golgi and PM PI(4)P (Roy and Levine 2004; Lemmon 2008; Lenoir and Overduin 2013).

Crystal and NMR structures of several PH domains have been solved, yet the data for FAPP1 is most complete. A first solution NMR structure (PDB entry: 2KCJ) solved by Lenoir *et al.* revealed a seven-stranded β-barrel capped by an α-helix with a hydrophobic wedge between the first two β-stands (Lenoir, Coskun *et al.* 2010), confirmed by a crystal structure (PBD entry 3RCP) (He, Scott *et al.* 2011). Incubation of PH_{FAPP1} with lipid/detergent micelles showed a resonance shift for the residues of the loop, and molecular docking of PH_{FAPP1} showed a deep insertion of this wedge into a model membrane (Lenoir, Coskun *et al.* 2010). They also identified the PI(4)P-interacting residues by molecular docking, and this identification was confirmed by the resolution of the structure of PH_{FAPP1} bound to soluble di-C6 PI(4)P (Lenoir, Coskun *et al.* 2010; He, Scott *et al.* 2011). Arf1-binding depends on the bound nucleotide as only Arf1-GTP is bound on the outside of the β-barrel as determined by resonance shift and molecular docking (He, Scott *et al.* 2011). Recently the structure of the ternary complex PH_{FAPP1}/PI(4)P/Arf1 bound to a small bicelle surface has been presented by Liu *et al.*, resuming and confirming the previous findings (**Figure 38**) (Liu, Kahn *et al.* 2014).

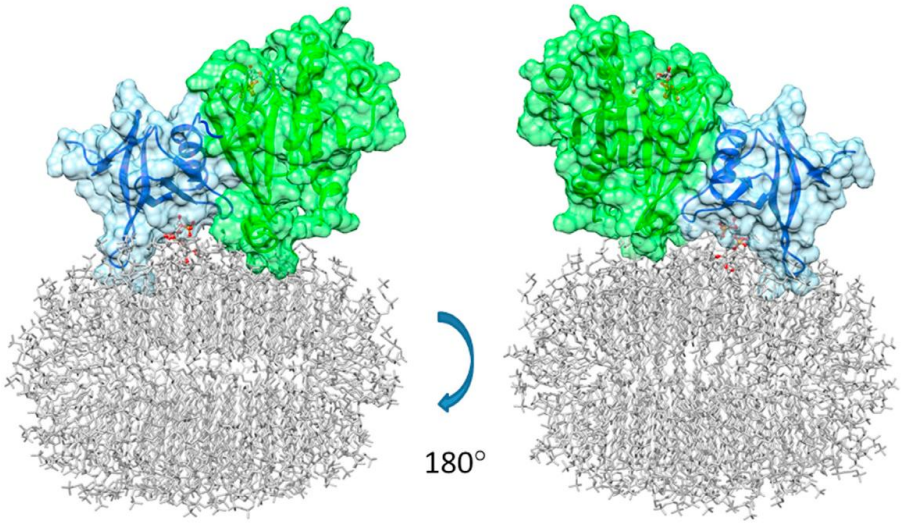

Figure 38. Ternary complex PHFAPP1/PI(4)P/Arf1 on a small bicelle.

Haddock molecular docking model illustrating the interactions of PH_{FAPP1} (blue), PI(4)P (sticks in the bicelle) and Arf1 (green) with GTPγS (sticks in Arf1). PH_{FAPP1}/PI(4)P models and PH_{FAPP1}/Arf models are superimposed for the ternary complex and combined with an Arf1/bicelle model. The deep insertion of the wedge into the bicelle is well illustrated in the right representation. Illustration from (Liu, Kahn *et al.* 2014).

We wanted to develop a fluorescent tool that would recognize PI(4)P-containing membranes and reflect binding by a change in fluorescence. We thus mutated the solvent-exposed T13 residue localized in the hydrophobic wedge of PH_{FAPP} into a cysteine and replaced other solvent-exposed cysteines to serine (mutations C37S and C94S). This series of mutations allowed us to chemically label specifically the C13 residue with an environment sensitive probe, nitrobenz-2-oxa-1,3-diazole (NBD). N-((2-(iodoacetoxy)ethyl)-N-Methyl)amino-7-Nitrobenz-2-Oxa-1,3-Diazole (IANBD, Molecular Probes®, Life Technologies) is a reagent which rapidly condenses with thiols attaching the NBD moiety (**Figure 39a**). Insertion of this moiety into a lipid bilayer modifies the emission wavelength and intensity of its fluorescence (**Figure 39d**).

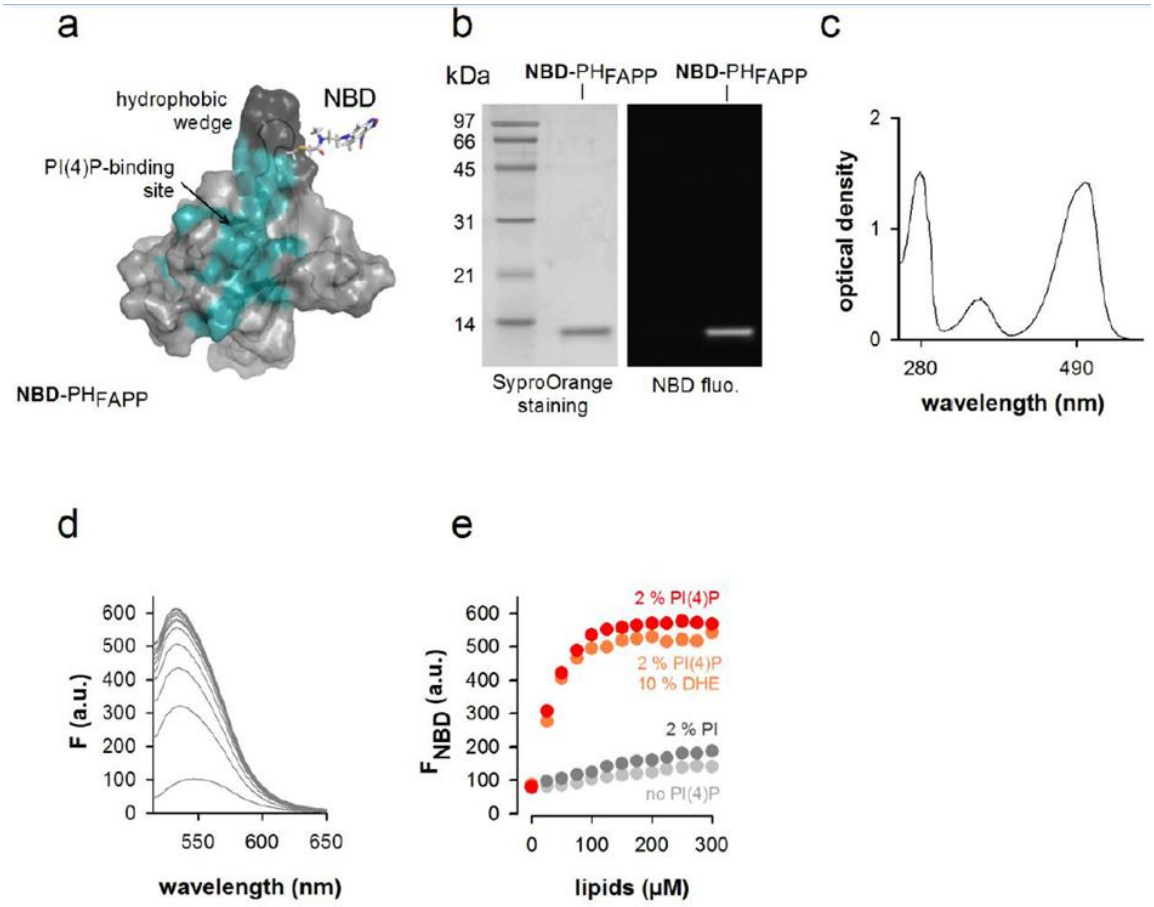

Figure 39. Characterization of lipid recognition and fluorescence of NBD-PH_{FAPP}

See text and figure legend for figure S2 of the submitted manuscript for details.

We used IPTG-induced overexpression from a pGEX-4-T3 plasmid in *E. coli* to produce a GST-PH_{FAPP} construct bearing the abovementioned mutations and purified it using glutathione sepharose beads (GE healthcare), as described above, but in presence of 2 mM DTT in order to prevent cysteine oxidation. DTT was removed by gel filtration on a NAP-10

column (GE healthcare) before incubating the protein with a 10-fold excess of IANBD (life technologies) dissolved in N,N-dimethylformamide (DMF). After quenching with L-cysteine (10-fold excess over IANBD incubation) and intensive washing in DTT-containing buffer to remove unbound probe, the NBD-PH_{FAPP} was further purified on size exclusion chromatography (Sephacryl S-200, GE Life Sciences) and assayed, revealing a complete labeling of PH_{FAPP} by comparing its absorbance at 280 nm over 480 nm (**Figure 39b,c**). Incubating NBD-PH_{FAPP} with liposomes containing 4 mol% of PI(4)P induced a blue-shift (542-529 nm) of the emission maximum and increased its fluorescence intensity six fold compared to liposomes devoid of PI(4)P (**Figure 39d,e**).

Recognition of phosphatidyl-*L*-serine with NBD-$C2_{Lact}$

The function of PS, the most abundant negatively charged phospholipid, is strictly dependent on its localization, thus multiple strategies have been developed to analyze its distribution. First insight came from subcellular fractionation and detection of PS by thin layer chromatography (TLC). Notwithstanding the importance of this technique, organelle isolation always bears the risk of cross-contamination. Additionally, this technique does not give any information on the sidedness of PS and the temporal resolution is reduced. Different fluorescent probes have thus been developed for PS detection *in vivo*. Headgroup or side-chain fluorescence-labeled PS derivatives can mimic endogenous PS in membranes, but protein interaction with PS might be affected by chemical lipid modification. The C2 domain of Annexin V recognizes PS and can easily be tagged and genetically expressed, but its binding is not specific for PS as it also recognizes other anionic phospholipids (PI, PA) and requires high Ca^{2+} concentrations, thus making it an adequate tool for measuring extracellular PS (an apoptotic signal), but limiting its application for intracellular measurements (Leventis and Grinstein 2010; Kay, Koivusalo *et al.* 2012).

Lactadherin is a glycoprotein secreted into milk by mammalian mammary epithelial cells. It bears a discoidin-like C2 domain that stereospecifically recognizes phosphatidyl-*L*-serine independent of Ca^{2+}. Lactadherin C2 domains with fluorescent tags have recently been used to detect PS *in vivo* (Yeung, Gilbert *et al.* 2008; Fairn, Schieber *et al.* 2011). The crystal structure of the C2 domain of bovine Lactadherin has been solved by Gilbert and coworkers (PDB entry: 3BN6), showing a β-barrel core as found in other discoidin-like C2 domains, but

the Lactadherin C2 domain has particular membrane-interacting spikes. The PS-binding site was determined by molecular modeling, and these findings were confirmed by a recent ^{13}C- and ^{15}N-NMR structure of human Lactadherin in complex with soluble di-C6:0 PS (Shao, Novakovic *et al.* 2008; Yeung, Gilbert *et al.* 2008; Kay, Koivusalo *et al.* 2012; Ye, Li *et al.* 2013).

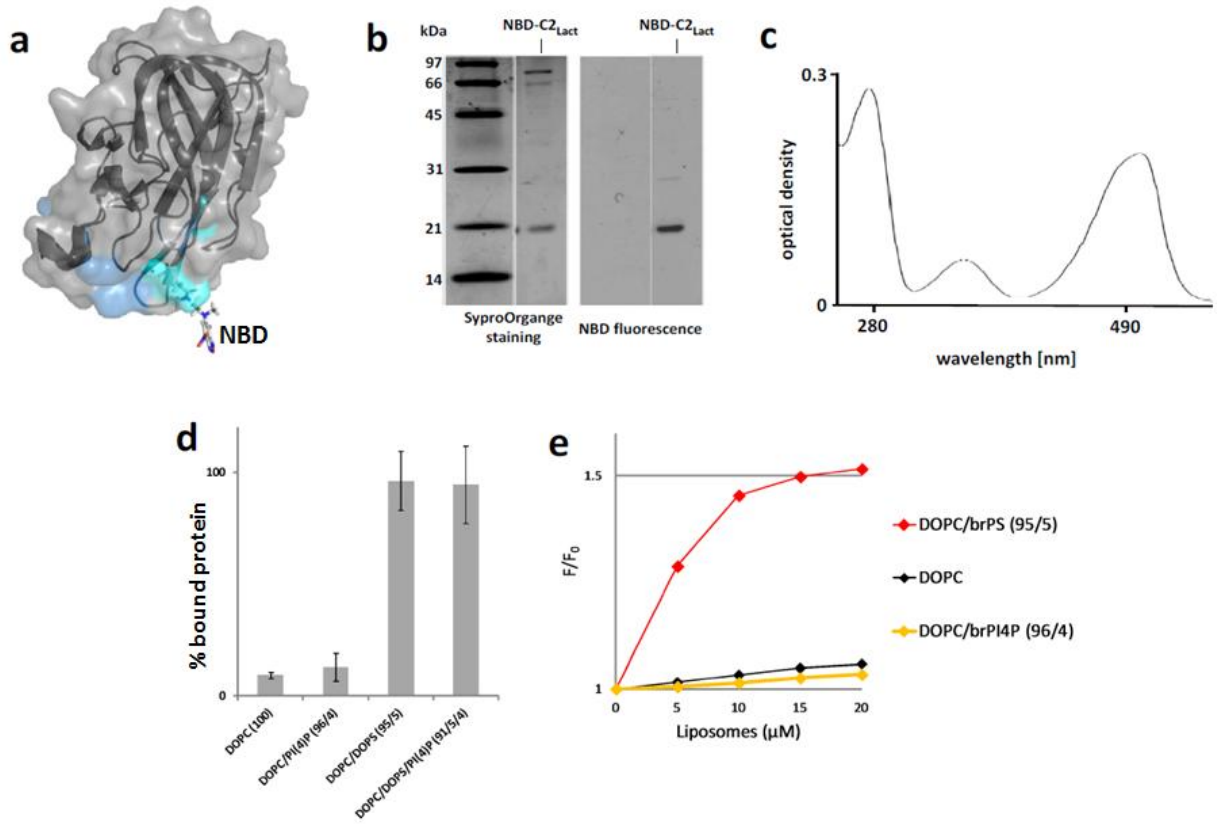

Figure 40. Characteristization of lipid recognition and fluorescence of NBD-C2$_{Lact}$

(a) Tridimensional model of the NBD-labeled C2$_{Lact}$ based on the NMR structure of the crystal structure of the C2 domain of bovine Lactadherin (PDB entry: 3BN6). The solvent-exposed cysteines C240 and C427 are mutated for alanines, histidine H352 is replaced by a cysteine. An N,N'-dimethyl-N-(thioacetyl)-N'-(7-nitrobenz-2-oxa-1,3-diazol-4-yl)ethylenediamine moiety (in stick, with carbon in grey, nitrogen in blue and oxygen in red), built manually and energetically minimized, is grafted to the thiol function of C352. The figure is prepared with PyMOL (http://pymol.org/). **(b)** SDS-PAGE of purified NBD-C2$_{Lact}$. The gel was directly visualized in a fluorescence imaging system to identify labeled proteins (right picture) and then stained with Sypro Orange to visualize all proteins and molecular weight markers (left picture). Unrelated bands have been excised. **(c)** UV-visible absorption spectrum of NBD-C2$_{Lact}$. Considering a purity grade of 100% for the protein, the optical density value at 280 nm (Trp) and 495 nm (IANBD) indicate that the C2 domain was labeled with the probe at a 1:1 ratio. **(d)** Flotation assays showing binding of C2$_{Lact}$ (1µM) to extruded 0.2 µm liposomes (1 mM total lipid) depending on their lipid composition. Values are the means two independent experiments ± SEM. **(e)** NBD fluorescence intensity measured at 525 nm as function of total lipids concentration and for different membrane compositions (in mol/mol). NBD-C2$_{Lact}$ only binds to PS -containing liposomes and this interaction is not impaired when membrane contains PI(4)P.

The identification of PS- and membrane-interacting residues allowed us to modify the C2 domain (residues 270-427) of bovine Lactadherin for our purposes as PS probe. Solvent exposed cysteines were mutated by Quikchange mutagenesis (Agilent) into alanines (mutations C270A and C427A) and a histidine residue in the membrane-interacting third spike was mutated to cysteine (H352C) in order to allow chemical labeling with an NBD probe to yield NBD-$C2_{Lact}$. The overexpression, purification and labeling protocols for NBD-$C2_{Lact}$ are identical with those for NBD-PH_{FAPP}. Binding and fluorescent properties were assayed as described for NBD-PH_{FAPP} (**Figure 40**).

FRET-based lipid transfer assays

DNS-PE-based DHE transport assay

The assay has been described elsewhere (de Saint-Jean, Delfosse *et al.* 2011). In brief, FRET (Förster Resonance Energy Transfer) is measured between DHE and Dansyl-labeled lipids (DNS-PE) at λ = 510 nm (emission slid width = 10 nm) upon excitation of DHE at λ = 310 nm (excitation slid width = 1.5 nm) using a 0.6 neutral filter. At 30 °C, 200 µM liposomes (0.2 µm extrusion) containing 2.5 mol% DNS-PE and 5 mol% DHE were incubated with 200 µM of a population of liposomes without DNS-PE (0.2 µm extrusion), containing or not 4 mol% PI(4)P and FRET is measured after addition of 200 nM protein in a stirred quartz cuvette (**Figure 41**). Loss of FRET mirrors DHE extraction, and owing to the excess of DHE over Osh proteins extraction is equivalent to transport. For every experimental condition (different DHE gradients, GPL and sphingolipid composition), the obtained kinetics were normalized compared to liposomes of the same overall composition but depleted of DHE as zero.

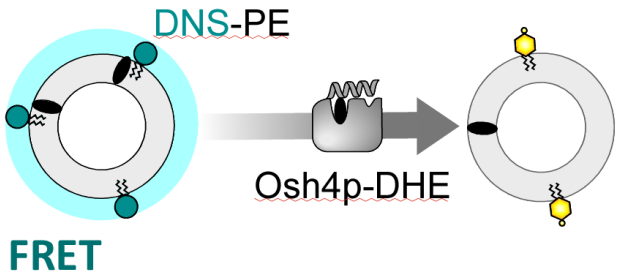

Figure 41. Schematic representation of DHE transport assay with DNS-PE.

NBD-PH_{FAPP}-based PI(4)P transport assay

NBD fluorescence of our NBD-PH_{FAPP} probe upon PI(4)P recognition is quenched by FRET when the liposomes also contain Lissamine Rhodamine B headgroup labeled lipids (Rhod-PE, Avanti Polar Lipids). Two liposome populations were used and only one initially contained PI(4)P and Rhod-PE. We chose to follow the NBD fluorescence increase as it directly mirrors transported PI(4)P. NBD-fluorescence was measured at λ = 530 nm (emission slid width = 10 nm) upon excitation at λ = 460 nm (excitation slid width = 1.5 nm).

For PI(4)P transfer assays, 250 nM NBD-PH_{FAPP} and 200 µM liposomes containing both PI(4)P (4 mol%) and Rhod-PE (2 mol%) (0.2 µm extrusion) were mixed with 200 µM liposomes deprived of PI(4)P and Rhod-PE containing or not 5 mol% DHE (0.2 µm extrusion) at 30 °C in a stirred quartz cuvette. NBD fluorescence was measured after injection of 200 nM Osh proteins (**Figure 42**). For every experimental condition, kinetics were normalized compared to the signal measured with liposomes with the same overall lipid composition, containing equal amounts of PI(4)P, mimicking full equilibration of PI(4)P (2 mol%), but only one of them containing Rhod-PE.

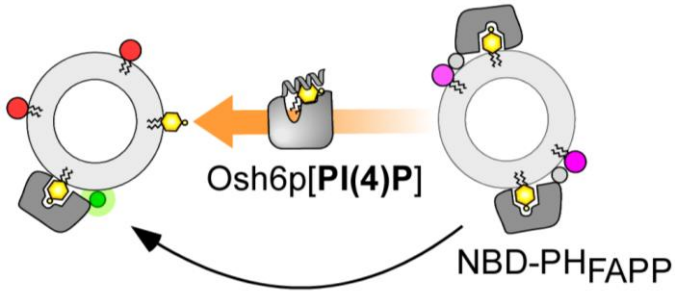

Figure 42. Schematic representation of NBD-PH_{FAPP}-based PI(4)P transport assay.

NBD-PH_{FAPP}-based PI(4)P extraction assay

For PI(4)P extraction assays, 250 nM NBD-PH_{FAPP} and 300 µM liposomes containing 2 mol% (3 µM accessible) PI(4)P were incubated with a stoichiometric amount of Osh protein (3 µM) for 5 min at room temperature and NBD fluorescence spectra emission spectra were measured (500 nm < λ < 650 nm (emission slid width = 10 nm) upon excitation at λ = 460 nm (excitation slid width = 1.5 nm)). A blue-shift was observed upon liposome binding of NBD-PH_{FAPP} (**Figure 39**). Emission maxima before and after incubation with Osh protein were substracted and normalized to a control with liposomes devoid of PI(4)P.

NBD-$C2_{Lact}$-based PS transport assay

As for NBD-PH_{FAPP}, NBD fluorescence of the NBD-$C2_{Lact}$ probe upon PS recognition is quenched by FRET when the liposomes also contain Rhod-PE. Two liposome populations were used and only one initially contained PS and Rhod-PE. NBD-$C2_{Lact}$ equilibrates more slowly than NBD-PH_{FAPP}, but equilibration is nonetheless faster than transport by Osh proteins (not shown). NBD fluorescence increase thus directly mirrors PS transport. NBD-fluorescence was measured at λ = 530 nm (emission slid width = 10 nm) upon excitation at λ = 460 nm (excitation slid width = 1.5 nm).

For lipid transfer assays, 250 nM NBD-$C2_{Lact}$ and 200 µM liposomes containing both PS (5 mol%) and Rhod-PE (2 mol%) (0.2 µm extrusion) were mixed with 200 µM liposomes deprived of PS and Rhod-PE containing or not 5 mol% PI(4)P (0.2 µm extrusion) at 30 °C in a stirred quartz cuvette. NBD fluorescence was measured after injection of 200 nM Osh proteins (**Figure 43**). For every experimental condition, kinetics were normalized compared to liposomes with the same overall lipid composition, containing equal amounts of PS, mimicking full equilibration of PS (2.5 mol%), but only one of them containing 2 mol% Rhod-PE.

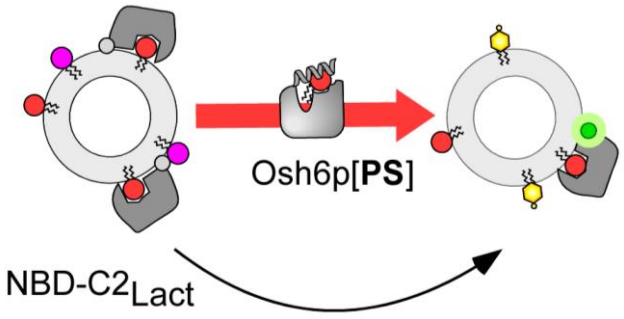

Figure 43. Schematic representation of NBD-$C2_{Lact}$-based PS transport assay.

RESULTS

PART I:

STEROL HOMEOSTASIS IN EUKARYOTIC CELLS

Article I

A phosphatidylinositol 4-phosphate-powered exchange mechanism to create a lipid gradient between membranes

Joachim Moser von Filseck, Stefano Vanni, Bruno Mesmin, Bruno Antonny and Guillaume Drin

Manuscript in revision for Nature Communications

"A phosphatidylinositol 4-phosphate-powered exchange mechanism to create a lipid gradient between membranes"

Based on previous findings on the counterexchange of sterol with PI(4)P by Osh4p we aimed to use a reconstituted system to follow transport of the two lipids in real time. We therefore developed a tool that would allow us to follow transport of PI(4)P under the same conditions as sterol transport and opted for a fluorescence-labeled PH domain. The development and characterization of the NBD-PH_{FAPP} PI(4)P probe is described in detail. (See PI(4)P detection by NBD-PHFAPP and **Figure 36** in the Materials and Methods section and **Article Figure S2**). For the transport assays, we used two distinct populations of DOPC-based liposomes, one population containing 10 µM accessible DHE, mimicking the ER (L_E) and one population containing or not 4 µM accessible PI(4)P, mimicking the *trans*-Golgi (L_G). In order to distinguish the two populations, L_E liposomes contained Dansyl-labeled lipids (DNS-PE) for DHE transport assays and L_G liposomes contained Rhodamine Lissamine A-labeled lipids (Rhod-PE) for PI(4)P transport assays.

Measuring transport kinetics for both DHE and PI(4)P under identical conditions allowed us to reveal a tight coupling of the transport in opposite directions of the two lipids. The initial transport velocity for each ligand is increased by one order of magnitude under conditions where counterexchange is possible (from 1-2 lipids/min to ≈20 lipids/min *per* Osh4p, **Article Figure 2a,b**). The initial transport velocities were similar for both lipids, thus endorsing the hypothesis of a counterexchange. Importantly, altering the affinity of Osh4p for one ligand affected the transport velocities for both ligands in the same manner, another affirmation of an exchange process (**Figure 2c**).

In our assays, we used a molar excess of DHE over PI(4)P. We observed that the DHE transport is slowed down significantly once PI(4)P is equilibrated between the two liposome populations. In cells, PI(4)P is produced by PI4Ks on *trans*-Golgi membranes and the PM and hydrolyzed by the ER-resident PI(4)P phosphatase Sac1p (Tahirovic, Schorr *et al.* 2005; Faulhammer, Kanjilal-Kolar *et al.* 2007), thus creating and maintaining a PI(4)P gradient between early and late membranes. We therefore sought to attach Sac1p to the ER-

mimicking liposome population to hydrolyze delivered PI(4)P into PI and hence maintain the PI(4)P gradient between the ER-like and the Golgi-like populations. Attachment was achieved by integrating Ni^{2+}-displaying lipids (DOGS-NTA-Ni^{2+}) into the ER-like liposomes that interact with a C-terminal His_6-tag on Sac1p. Sac1p attached to liposomes efficiently hydrolyzed PI(4)P and allowed continuing accelerated transport of sterol through maintenance of the PI(4)P gradient (**Article Figure 3**).

In cells, a sterol transporter would have to transport sterol against its concentration gradient to create and maintain this sterol gradient at the ER/Golgi interface. We therefore assayed whether Osh4p could transport DHE between two liposome populations that initially contained the same amount of DHE or even against a preexisting DHE gradient (**Article Figure 4**). In the absence of PI(4)P, transport was slow and followed the gradient, yet counterexchanging DHE for PI(4)P allowed Osh4p to create or even increase the DHE gradient. The effect was transient as, after equilibration of PI(4)P, sterol was transferred back along its gradient. However, the transport of DHE up its gradient was maintained by sustaining the PI(4)P gradient *via* Sac1p. It has long been thought that the creation of sterol gradient could be obtained simply by random transport of sterol and sequestration of transported sterols in membrane rich in saturated GPLs and sphingolipids (Sullivan, Ohvo-Rekila *et al.* 2006; Beh, McMaster *et al.* 2012) We were able to show that the presence of more saturated lipids or SM in Golgi-like membrane favors the accumulation of sterol by Osh4p, against its concentration gradient, but the counterexchange for PI(4)P was essential to observe this (**Article Figure 5**).

We furthermore showed that packing defects induced by phospholipid unsaturation or membrane curvature facilitates DHE extraction from ER-like liposomes. This suggests that the transport of sterols from the ER towards better packed *trans*-Golgi membranes is favored rather than in the opposite direction. Another aspect for this directionality is the dynamics of the lid segment (**Article Figure 6**). Molecular dynamics simulations suggest that in the sterol-bound form, the lid of Osh4p is tightly closed whereas it remains flexible when Osh4p is bound to PI(4)P. We show that on ER-like membranes, i.e. neutral membranes, Osh4p is more prone to deliver PI(4)P rather than DHE, favoring transport of PI(4)P towards these membranes rather than sterol (**Article Figure 7**). This might prevent the back delivery of sterol from the Golgi to the ER.

Our results show that Osh4p disposes of different features that allow it to rapidly exchange two different lipid ligands in opposite directions. Similar affinities for both ligands allow a rapid exchange between them, whereas directionality is provided for the transport by packing defect-favored extraction and delivery as well as by coupling the transport to PIP metabolism. The maintenance of the cellular PI(4)P gradient by kinases and phosphatases can therefore provide both energy and directionality to the anterograde sterol transport. This feature is necessary for efficient transfer of sterol as the chemical affinity gradient alone is not sufficient. Hence, we show that Osh4p displays all the features required for a genuine sterol transporter in cells. The velocities of transport are compatible with a role of Osh4p in providing sterol to late membrane during yeast growth phase. We will demonstrate in a near future how sterol transport activity of Osh4p is coupled *in vivo* to PI(4)P turnover and will help to further elucidate the function and molecular mechanism of other ORP/Osh proteins.

A phosphatidylinositol-4-phosphate powered exchange mechanism to create a lipid gradient between membranes

Joachim Moser von Filseck, Stefano Vanni, Bruno Mesmin, Bruno Antonny and Guillaume Drin*

CNRS, Institut de Pharmacologie Moléculaire et Cellulaire, Université de Nice Sophia-Antipolis, France

*To whom correspondence should be addressed
Guillaume Drin, Institut de Pharmacologie Moléculaire & Cellulaire, Université de Nice Sophia-Antipolis and CNRS, 660 route des lucioles, 06560 Valbonne, France. Tel.: +33 4 93 95 77 72; Fax: +33 4 93 95 77 10; email : drin@ipmc.cnrs.fr

Running title: PI(4)P-driven Osh4p-mediated sterol transport

ABSTRACT

Lipids are unevenly distributed within eukaryotic cells, thus defining organelle identity. How non-vesicular transport mechanisms generate these lipid gradients between membranes remains a central question. With novel biochemical approaches, we demonstrate that Osh4p, a sterol/phosphatidylinositol-4-phosphate (PI(4)P) exchanger of the ORP/Osh family, transports sterol against its gradient between two membranes by dissipating the energy of a PI(4)P gradient. Sterol transport is sustained through the maintenance of this PI(4)P gradient by the PI(4)P-phosphatase Sac1p. Differences in lipid-packing between membranes can stabilize sterol gradients generated by Osh4p and modulate its lipid exchange capacity. The ability of Osh4p to recognize sterol and PI(4)P *via* distinct modalities and the dynamic of its N-terminal lid govern its activity. We thus provide the first direct demonstration that an intracellular lipid transfer protein is structurally designed to actively create a lipid gradient between membranes.

INTRODUCTION

Sterol is a key lipid in eukaryotic cells that, owing to its rigid and planar structure, reduces the flexibility of neighboring lipids, thereby ensuring the impermeability of membranes[1]. The ER, in which sterol is synthesized, displays low sterol levels (<5 mol% of lipids)[2]. Contrastingly, sterol is abundant (up to 40 mol%) in the *trans*-Golgi, endosomes and plasma membrane (PM)[3,4]. This gradient between early and late regions of the secretory pathway is supposed to be mainly established by specialized lipid transfer proteins (LTPs)[5,6] able to transport sterol, insoluble in aqueous media, between membranes[7,8]. Some LTPs for sterol belong to the ORP/Osh family, an evolutionary conserved family in eukaryotes, including oxysterol-binding protein-related proteins (ORP) in human and oxysterol-binding homologue (Osh) proteins in yeast[9]. In higher eukaryotes, members of the START family are also potential LTPs for sterol[10].

Defining the mechanisms by which LTPs create intracellular sterol gradients remains a central issue in membrane biology[7,8]. One model posits that LTPs randomly equilibrate sterol between subcellular membranes by bidirectional shuttling[5,11]. The accumulation of sterol in the *trans*-Golgi and PM would be exclusively driven by its high affinity for saturated glycerophospholipids and sphingolipids[12-14], largely abundant in these compartments [3,15,16]. An alternative hypothesis, suggested by our recent studies on ORP/Osh proteins, is that LTPs actively create sterol gradients by vectorial transport[17,18].

Osh4p is an archetypical LTP whose structure consists of a 19-strand β-barrel defining a sterol-binding pocket[19]. A short N-terminal segment forms a lid that blocks the sterol molecule inside its binding cavity. We revealed that Osh4p can alternatively extract PI(4)P from a membrane. X-ray crystallography indicated that the sterol-binding pocket accommodates the PI(4)P acyl-chains whereas charged residues defining an adjacent pocket recognize the PI(4)P headgroup. The lid, under a different conformation, shields the lipid. Strikingly, we observed that Osh4p transfers sterol and PI(4)P along opposed directions between membranes by counterexchange[17].

PI(4)P is mostly localized in the *trans*-Golgi and PM[20] but is absent from the ER, implying that a steep PI(4)P gradient exists between these distant cellular regions. In yeast this gradient is maintained by spatially-distant enzymes. Pik1p and Stt4p phosphorylate PI into PI(4)P in the *trans*-Golgi and PM, respectively[20], whereas Sac1p, the major phosphatase that degrades PI(4)P into PI[21,22] resides at the ER[23]. Intriguingly, Osh4p downregulates cellular PI(4)P levels and the availability of this lipid on Golgi surface, thereby counteracting Pik1p and Sec14p[24], a PI/PC LTP that teams with Pik1p to yield Golgi PI(4)P[25]. Several

reports also suggest that Osh4p supplies the *trans*-Golgi and PM with sterol[26-28]. Consequently, we proposed that Osh4p uses the PI(4)P gradient at the ER/Golgi interface to supply the *trans*-Golgi with sterol. In our model, Osh4p extracts sterol from the ER, then releases it by counter-exchange with PI(4)P at the Golgi, and transports PI(4)P from the Golgi to the ER. The ATP-dependant production of PI(4)P by Pik1p would energetically drive sterol/PI(4)P cycles by Osh4p, thereby promoting the active release of sterol into the *trans*-Golgi and the creation of a sterol gradient (**Fig.1**).

Here, we have tested this model using novel quantitative and real-time assays to measure the transfer of sterol and PI(4)P between liposomes mimicking the ER/Golgi interface. We demonstrate that Osh4p transports sterol at high velocity, and remarkably, even against a sterol concentration gradient, by dissipating a PI(4)P gradient. The maintenance of this PI(4)P gradient over time sustains sterol transport by Osh4p. Differences in lipid-packing between membranes influence the transfer of lipids and stabilize sterol gradients created by Osh4p. Its activity relies on the dynamic of its N-terminal lid. Our results provide the first demonstration that an intracellular LTP has a built-in capacity to actively create a lipid gradient between membranes.

RESULT

Osh4p mediates fast sterol/PI(4)P exchange.

To measure the sterol/PI(4)P exchange capacity of Osh4p, we devised two FRET-based assays with high temporal resolution to quantify sterol transport from ER- to Golgi-like liposomes (L_E and L_G liposome, **Fig.2a**) and PI(4)P transport in the backward direction (**Fig.2b**).

In the first assay, L_E liposomes contained both dehydroergosterol (DHE, 5 mol%) and DNS-PE (2.5 mol%), whereas L_G liposomes incorporated or not 4 mol% PI(4)P. The decrease in FRET between DHE and DNS-PE allows quantifying the transport of DHE by Osh4p (200 nM) from L_E to L_G liposomes[17]. When L_G liposomes were devoid of PI(4)P, the initial DHE transport rate was slow (**Fig.2a**, black trace, 1 ± 0.1 DHE/min *per* protein (mean ± SEM, n=4)). Contrastingly, when L_G liposomes contained PI(4)P, the transport rate was 17 times higher (**Fig.2a**, blue trace, 17.4 ± 1.1 DHE/min *per* protein (n=6)). The efficacy of Osh4p to transport DHE was directly proportional to PI(4)P amounts initially present in L_G liposomes (**Supplementary Fig.1**). These results corroborated our previous observations[17].

To measure the back transport of PI(4)P from L_G to L_E liposomes, we created a PI(4)P-sensor based on the FAPP1 PH domain (PH_{FAPP}). This domain has a binding site for the PI(4)P headgroup and a hydrophobic wedge that inserts into membranes[29]. We produced a PH_{FAPP} domain including a single solvent-exposed cysteine (C13), localized in the hydrophobic wedge, to which we grafted a polarity-sensitive NBD (7-nitrobenz-2-oxa-1,3-diazol) probe (**Supplementary Fig.2a-c**). Incremental addition of liposomes doped with 2 mol% PI(4)P to the NBD-PH_{FAPP} construct resulted in a blue-shift of the maximal emission wavelength of NBD from 542 to 529 nm with a maximal 6-fold increase in intensity (**Supplementary Fig.2d,e**). A similar binding curve was obtained with liposomes containing PI(4)P and high DHE levels (10 mol%). No binding was seen with liposomes devoid of PI(4)P or containing 2 mol% PI. Thus, NBD-PH_{FAPP} is a specific sensor of PI(4)P and its efficiency is independent of sterol levels.

In the transport assay (**Fig.2b**), NBD-PH_{FAPP} (250 nM) was mixed with L_G liposomes doped with 4 mol% PI(4)P and 2 mol% Rhod-PE. The NBD fluorescence was quenched due to a FRET process with Rhod-PE. Adding L_E liposomes did not induce any signal increase: all NBD-PH_{FAPP} copies remained associated with L_G liposomes. The subsequent injection of Osh4p (200 nM) provoked a fast dequenching, indicative of the transport of PI(4)P by Osh4p and translocation of NBD-PH_{FAPP} to L_E liposomes (**Fig.2b**). To quantify this transport, the NBD signal was normalized (see Methods) by taking as reference the NBD signal measured in a condition mimicking full PI(4)P equilibration between L_E and L_G liposomes, each containing 2 mol% PI(4)P (**Supplementary Fig.2f**). With DHE-free L_E liposome, Osh4p transported PI(4)P with an initial rate of 1.9 ± 0.6 PI(4)P/min (n=3) (**Fig.2b**, black trace). Strikingly, with L_E liposomes containing 5 mol% DHE, the transport rate was accelerated by one order of magnitude (22.2 ± 0.7 PI(4)P/min *per* protein (n=8)) resulting in PI(4)P equilibration between the two liposome populations within one minute (**Fig.2b**, orange trace). Remarkably, the initial PI(4)P transport rate was similar to that measured for DHE under the same condition, DHE and PI(4)P being present in distinct membranes. This correlation between lipid transport velocities, measured along apposed direction, strongly indicated that Osh4p is a sterol/PI(4)P exchanger.

Sterol/PI(4)P exchange activity of Osh4p mutants

To further address the coupling between sterol and PI(4)P transport, we tested mutants lacking residues that make major contact either with sterol (Q96A, Y97F)[19] or PI(4)P (K109A, K336E, H143A/H144A)[17]. If the transport of the two lipids relies on a counter-

exchange mechanism, then affecting the binding of one lipid ligand should affect the transport of the second ligand. We first assessed the ability of mutants to extract lipids. Surprisingly, the Q96A and Y97F mutants were not deficient in extracting DHE (**Supplementary Fig.3a**). Mutants belonging to the second group (K109A, K336E, H143A/H144A) properly extract DHE[17] but not PI(4)P (**Supplementary Fig.3b**). Like Osh4p WT, all mutants slowly transported DHE or PI(4)P between membranes in the absence of the second lipid (**Supplementary Fig.3c**). However, in transport assays including both lipids, the K336E and H143A/H144A mutants displayed no sterol/PI(4)P exchange activity compared to Osh4p WT, whereas the K109A mutant retained some residual activity, as indicated by both the initial DHE and PI(4)P transport velocities. (**Fig.2c, Supplementary Fig.3c**). The Y97F mutant (but not the Q96A mutant) was twofold less active than Osh4p WT. Finally, we found that the lidless [30-434]Osh4p mutant was unable to properly extract PI(4)P or DHE and exchange lipids, indicating that the lid is a key structural element for the function of Osh4p (**Supplementary Fig.3a-c, Fig.2c**). This structure-function analysis shows that the sterol and PI(4)P transport processes are intimately coupled and occur efficiently only when Osh4p properly recognizes the two lipids. This confirms that Osh4p is a sterol/PI(4)P exchanger.

Maintaining the PI(4)P gradient sustains sterol transport by Osh4p

The DHE transport kinetic measured in the presence of PI(4)P was biphasic (**Fig.2a**). The first phase corresponds to the sterol/PI(4)P exchange and ends when PI(4)P is equilibrated between liposomes. A similar amount of DHE and PI(4)P is exchanged (~ 2µM, **Fig.2a,b**). The second phase likely corresponds to the slow completion of DHE equilibration by Osh4p since, in our assays, the amount of DHE to be transported is higher than the amount of PI(4)P. Thus Osh4p efficiently transports DHE, by sterol/PI(4)P exchange, from ER to Golgi-like membranes until it has fully equilibrated the PI(4)P gradient, which pre-existed between these membranes.

In cells, PI(4)P gradients between the ER and late membranes are maintained by PI4-kinases and Sac1p[21,23]. This might sustain sterol/PI(4)P exchange cycles by Osh4p. To examine this *in vitro*, we attached a Sac1p[1-522]His_6 construct (200 nM), in which the His-tag substitutes for the TM region, to L_E liposomes doped with DOGS-NTA-Ni^{2+}. Flotation assays indicated that Sac1p[1-522]His_6 was fully and selectively attached to such liposomes (**Supplementary Fig. 4a**).

With Sac1p bound to L_E liposomes and under conditions where L_G liposomes included PI(4)P, the biphasic aspect of the DHE transport kinetics mediated by Osh4p was lost (**Fig.3a,**

cyan trace). The transport of DHE was sustained over time and, at the end of the kinetic, more DHE (1µM) was transferred into L_G liposomes compared to the experiment without Sac1p. This effect is due to the hydrolysis of PI(4)P: an inactive Sac1p mutant (C392S) did not impact DHE transport. Moreover, the stimulatory effect of Sac1p on DHE transport required Sac1p to be immobilized on L_E liposomes. Sac1p in a soluble form did not influence DHE transport. It is thus unlikely that Sac1p works with Osh4p *via* direct protein-protein interactions as suggested previously[30]. In our binding assays, whatever its status (empty or in the presence of ligands), Osh4p was not recruited by Sac1p onto liposomes (**Supplementary Fig. 4b**).

In the PI(4)P transport assay, the increase in NBD-PH_{FAPP} signal, indicative of the transfer of PI(4)P from L_G to L_E liposomes by Osh4p, was followed by a large decay when Sac1p was immobilized on L_E liposomes (**Fig.3b,** dashed line), which was not the case with Sac1p(C392S). Undoubtedly, PI(4)P hydrolysis prevented the relocalisation of NBD-PH_{FAPP} on L_E liposomes, as PH_{FAPP} is unable to detect PI (**Supplementary Fig.2e**), the reaction product. Thus, the NBD trace, resulting from the combination of transport and hydrolysis processes, was no longer a direct readout of the amount of PI(4)P transferred by Osh4p. This amount was estimated by fitting the trace with a kinetic model (see Methods) which integrates the rate of PI(4)P hydrolysis by Sac1p, estimated using a distinct assay (**Supplementary Fig.4c**). This analysis indicated that Osh4p transferred more PI(4)P (~1.7 µM, **Fig.3b**) from L_G to L_E liposomes when Sac1p was attached to L_E liposomes. The model used for fitting procedures seemed adequate since it fairly predicted the DHE kinetic trace in the presence of Sac1p as well as the lipid transport kinetics in the absence of Sac1p (**Supplementary Fig.5a**).Together, these data indicated that the hydrolysis of PI(4)P by Sac1p on ER-like membranes sustains PI(4)P transport by Osh4p. In turn, this transport allows extended transport of sterol in the opposite direction.

Osh4p transports sterol against its concentration gradient by using PI(4)P.

To maintain a sterol gradient intracellularly, Osh4p should be able to deliver sterol from early to late membranes against its concentration gradient. Accordingly, we compared the transport of DHE by Osh4p from L_E to L_G liposomes in three situations: along the DHE gradient as previously measured (**Fig.2**), in the absence of a DHE gradient or against a DHE gradient. For this, we prepared L_E liposomes containing 5 mol% DHE and L_G liposomes incorporating 4 mol% PI(4)P and respectively 0, 5 or 10 mol% DHE. In the first case, the initial DHE transport rate was similar to previous values (~20 DHE/min *per* protein).

Remarkably, in the second case, where DHE was already equilibrated between liposomes, we observed a very fast diminution in FRET signal upon Osh4p injection, corresponding to the transfer of ~1 μM DHE from L_E to L_G liposomes (**Fig.4a,** upper panel, dark blue trace). Moreover, in the third case, a very transient decrease was also observed, implying that Osh4p had transported DHE from L_E to L_G liposomes within the first seconds against its gradient. In each situation, the initial DHE transport was coupled to a backward transfer of PI(4)P of equal velocity and no DHE transport occurred if L_G liposomes were devoid of PI(4)P (**Fig.4a,b**). These observations revealed that Osh4p can create or maintain a sterol gradient between membranes, owing to its sterol/PI(4)P exchange activity.

Initial transport rates indicated that the sterol/PI(4)P exchange was slower when the preexisting L_E-to-L_G sterol gradient was positive and steeper (**Fig.4b**). The FRET signal recovery, after the lipid exchange step, also suggested that DHE was transferred back from L_E to L_G liposomes along its gradient by a PI(4)P-independent slow re-equilibration process. Simulations indicated that the shape of sterol and PI(4)P kinetic traces are primarily influenced by the direction (positive or negative) and steepness of the preexisting DHE gradient (**Supplementary Fig.5b**). The attachment of Sac1p on L_E liposomes improved the transfer of DHE by Osh4p in all conditions (**Fig.4a,** upper panel, blue and cyan traces). Decay of the NBD signal in PI(4)P-transport assays was indicative of Sac1p hydrolysis activity (**Fig.4a,** lower panel). Moreover, a higher density of Sac1p (400 nM) on L_E liposomes was required to help Osh4p operate against a steep DHE gradient, suggesting that an elevated PI(4)P consumption was necessary in that case (**Fig.4a** cyan trace). We conclude that the maintenance of a PI(4)P gradient helps Osh4p to create and maintain a sterol gradient between membranes.

High acyl-chain saturation levels stabilize sterol gradients generated by Osh4p.

The existence of a cellular sterol gradient possibly relies on the sequestration of sterol in the *trans*-Golgi and PM at the expense of the ER[5], due to its higher affinity for saturated glycerophospholipids and sphingolipids[1,31]. This process might help the delivery of sterol by Osh4p in late membranes. We tested this hypothesis by comparing the transport of DHE by Osh4p against its gradient from L_E liposomes made of diunsaturated lipid (DOPC, 5 mol% DHE) to L_G liposomes (including 10 mol% DHE and 4 mol% PI(4)P) made either of DOPC (as before, **Fig.4**), of monounsaturated lipid (POPC) or of a equal amount of DOPC and saturated sphingomyeline (SM).

As shown in the **Figure 5a**, the final amount of DHE transferred by Osh4p into L_G liposomes was higher when the acyl-chain saturation level of these liposomes was superior to that of L_E liposomes (dark blue traces). Sterol seems trapped in L_G liposomes: no return of DHE from L_G to L_E liposomes was observed. However, DHE did not accumulate in L_G liposomes devoid of PI(4)P, demonstrating that the delivery of sterol was primarily conditioned by its exchange with PI(4)P and not its affinity for saturated lipids. The initial transport rate was up to 3 times higher with POPC or SM-containing L_G liposomes, suggesting that the sterol/PI(4)P exchange was facilitated (**Fig.5b**). Concomitantly, the transfer of DHE by Osh4p seemed moderately influenced by PI(4)P hydrolysis. A low density of Sac1p on L_E liposome (200 nM) was sufficient to sustain the delivery of DHE into L_G liposomes made of POPC and Sac1p became almost dispensable with SM-containing L_G liposomes. Thus, the higher affinity of sterol for saturated lipids is a factor that helps Osh4p deliver sterol against its gradient into acceptor membranes.

Lipid-packing defects control sterol/PI(4)P exchange

The ER membrane is neutral, mostly made of unsaturated phospholipids[3] and forms extensive tubules characterized by a positive curvature[32]. Due to its unsaturation level and shape, the ER displays lipid-packing defects, which are known to facilitate sterol desorption[33]. We examined whether the extraction of sterol by Osh4p, which should occur according to our model (**Fig.1**) when Osh4p is in a PI(4)P-bound form, was influenced by these defects. Osh4p[PI(4)P] was incubated with large L_E liposome made of DOPC or POPC and containing 0.5 or 5 mol% DHE (lower and upper sterol concentration in the ER[2]). By measuring the quenching of tryptophan residues, localized near the sterol-binding pocket, by DHE[17], we found that Osh4p[PI(4)P] extracted DHE from DOPC liposomes faster than from POPC liposomes (**Fig.6a**). In each case the extraction process was accelerated when liposomes contained 5 mol% DHE. Eventually we observed that Osh4p extracted more efficiently DHE from POPC liposomes of decreasing radius, i.e of increasing curvature (**Fig.6b**). Thus, Osh4p efficiently exchanges PI(4)P for sterol on neutral membranes displaying lipid-packing defects and containing sterol % similar to that found at the ER.

We further examined whether the membrane curvature influenced the sterol/PI(4)P exchange activity of Osh4p between L_E liposomes made of POPC (with 5 mol% DHE) of defined radii and L_G liposomes made of DOPC (with 4 mol% PI(4)P). With large L_E liposomes ($R > 100$ nm), the initial transport rates were up to twentyfold lower (1.8 ± 0.1 DHE/min and 1.1 ± 0.3 PI(4)P/min *per* Osh4p (n=2-3)) than with large L_E liposomes made of

DOPC (**Fig.2**). With POPC liposomes of decreasing radius (down to ~40 nm), the velocities were partially restored (**Fig.6c,d**). Jointly, these data suggest that the ER, both rich in unsaturated lipid and curved, constitutes a permissive membrane for sterol extraction by Osh4p in the context of sterol/PI(4)P exchange cycles.

The lid controls the release of sterol and PI(4)P into neutral membrane

To better apprehend the sterol/PI(4)P exchange mechanism, we examined how the binding of each lipid to Osh4p affects its structural and dynamical properties by running molecular dynamics (MD) simulations of the protein bound to ergosterol (PDB ID: 1ZHZ) or PI(4)P (3SPW). These simulations indicated that the main contribution to ergosterol binding arises from Van-der-Waals (VdW) interactions (98%, **Fig.7a**). Sterol in its binding pocket is very stable, showing little deviations from its conformation in the crystal (**Fig.7b**).The F42, Q96 and Y97 residues contribute the most to the Osh4p-sterol interaction (**Fig. 7c**). However, each residue only participates to ~7% of the total protein-sterol energy, indicating that the interaction of sterol with Osh4p relies on multiple residues. For PI(4)P, the role of electrostatic interactions was predominant, accounting for 73 % of the total lipid-protein interaction energy (**Fig.7a**). Remarkably, the PI(4)P acyl-chains, despite occupying the sterol-binding pocket, showed a high flexibility compared to ergosterol (**Fig.7b**). In contrast, the polar head of PI(4)P binds tightly to five residues (K109, H143, H144, K336, R344) (**Fig.7b, c**) that alone contribute for 65% of the total PI(4)P-protein interaction energy.

The remarkable difference in dynamics between sterol and the PI(4)P acyl-chains in Osh4p is intimately linked to the behavior of the N-terminal lid. Stable VdW interactions between ergosterol and hydrophobic residues restrain lid movement. In contrast, the lid in the PI(4)P-bound Osh4p is extremely mobile (**Fig. 7d**). This prompted us to examine whether Osh4p liberates more readily PI(4)P than sterol. For this aim we monitored using NBD-PH_{FAPP} to which extent Osh4p, preloaded with PI(4)P, released PI(4)P into DOPC liposomes. If these liposomes were devoid of ergosterol, we observed a slow increase in the NBD signal (**Fig.7e,** gray trace). Contrastingly with liposomes containing 5 mol% ergosterol, the NBD signal reached a plateau within seconds, suggesting that PI(4)P was quickly delivered into membrane by exchange with sterol (**Fig.7e,** black trace). Quantification of PI(4)P by the PH_{FAPP} domain indicated that all Osh4p protein had released PI(4)P. Under identical conditions, but with a different assay[17], we found that Osh4p exchanged DHE with ergosterol very slowly (**Fig.7f**), suggesting that the lid does not readily open when covering sterol. Thus, Osh4p is more prone to deliver PI(4)P than sterol into neutral, ER-like membranes.

DISCUSSION

Identifying the mechanisms that generate lipid gradients between organelles is an important issue in cell biology. By measuring a lipid exchange process with an unprecedented accuracy, we reveal that an intracellular LTPs can create a lipid gradient by dissipating a PI(4)P gradient.

We demonstrate that Osh4p is an efficient LTP only when it acts as a lipid exchanger. In our assays in which sterol (5 mol%) and PI(4)P (4 mol%) are in distinct membranes, Osh4p transports the two lipids along opposite routes with equivalent velocities (~20 lipids/min). Lipid transport is ten-fold slower when one of these two lipids is absent and impairing the affinity of Osh4p for either sterol or PI(4)P systematically reduces both DHE and PI(4)P transport rates.

Under conditions where sterol is already equilibrated between membranes, Osh4p mediates the accumulation of sterol in one membrane at the expense of the other by sterol/PI(4)P exchange. Moreover, Osh4p even transports sterol against a concentration gradient, alike the gradient at the ER/Golgi interface (≤5 mol% in ER[2], 10 mol% in *trans*-Golgi[15]). The lipid exchange rates are lower (~13 and ~ 6 lipids/min, respectively); nevertheless, they remain comparable to the rates measured for other LTPs (STARD4: 7 sterols/min[34]; CERT: 4 ceramides/min[35]). This suggests that Osh4p is a genuine carrier that can create and maintain sterol gradients within cells.

Our kinetic analysis indicates that Osh4p rapidly transports sterol by lipid exchange until it has fully dissipated a pre-existing PI(4)P gradient between membranes. In cells, PI(4)P gradients are maintained over time as PI(4)P is continually synthesized on late membranes and hydrolyzed by Sac1p on the ER[20-23]. *In vitro,* the sterol/PI(4)P exchange activity of Osh4p is sustained in conditions where Sac1p, by hydrolyzing PI(4)P, maintains the PI(4)P gradient.

The final amount of sterol delivered by Osh4p against a sterol gradient is higher in membranes rich in saturated lipids, likely because sterol is sequestered in these membranes. However, the delivery process *per se* remains strictly PI(4)P-dependent. Thus, if Osh4p create sterol gradients, this is not *via* a process primarily driven by the affinity of sterol for saturated lipids, as previously postulated[5,11]. Conversely, the sterol extraction step of the sterol/PI(4)P cycle is facilitated by the unsaturation level and positive curvature of membrane. The ER, both highly tubulated and rich in unsaturated lipid, likely constitutes a permissive membrane for Osh4p to load sterol. Jointly, these results suggest that the difference in lipid packing at

ER/Golgi interface defines an ideal context for PI(4)P-mediated vectorial transfer of sterol by Osh4p.

Menon and colleagues estimated that, during yeast asymmetric division, 60.10^6 sterol molecules should be provided to the PM of the mother cell within 2 hours[11]. Osh4p might significantly contribute to this process. In the same time period, considering its sterol transport rate driven by PI(4)P (5-10 sterols/min *per* protein, against a sterol gradient) and its natural abundance (32.10^3 copies/cell)[36], Osh4p could supply the *trans-Golgi* with 19-38.10^6 sterol molecules, which would be next conveyed by exocytotic vesicles to the PM. The ability of Osh4p to massively deliver sterol by exploiting PI(4)P would explains why its knock-down impacts sterol distribution in the Golgi and PM[26-28,37] and why Osh4p acts as a repressor of exocytosis[38], a process that depends on appropriate Golgi PI(4)P levels[39].

Several mutants, unable to recognize PI(4)P, have no sterol/PI(4)P exchange activity *in vitro*. Interestingly, contrary to Osh4p WT, they do not rescue Osh-depleted strains whose PM lack sterols and are not lethal in Sec14p-deficient strains displaying limited Golgi PI(4)P levels[19]. Likely these mutants cannot import sterol to and export PI(4)P from the Golgi. Other mutants (Q96A, Y97F) lacking residues that interact with sterol, still extract DHE and operate sterol/PI(4)P exchange. Presumably, as suggested by our MD simulations and previous reports[40,41], the Osh4p-sterol interaction relies on numerous other residues. Our results agree with the fact that these mutants are not loss-of function mutants[19,38,42]. Eventually we observed that the lid is crucial for the activity of Osh4p and, moreover, prevents the release of sterol but not PI(4)P into neutral membranes, owing to its versatile dynamic. This mechanism might explain why, when Osh4p transports sterol against its gradient from ER- to Golgi-like membranes the back transport of sterol down its gradient remains slow (**Fig.4**).

The ability to create a lipid gradient by using PI(4)P is likely shared by other ORP/Osh proteins. Recent reports suggest that all members of this family bind PI(4)P[18,43,44] but recognize a second lipid that is not necessary sterol[43,45]. A general and appealing hypothesis is that ORP/Osh proteins use PI(4)P gradients to convey sterol or other lipids from early to late membranes to create various lipid gradients[46]. For such mechanisms to occur, the PIP turn-over should be robust enough. At steady state, PI(4)P levels are low in yeast (80,000 PI(4)P molecules/cell)[24]. This value is however not indicative of the amount of PI(4)P which is hydrolyzed and regenerated over time. Further cellular studies with high temporal and spatial resolution are necessary to define the interplay between PI(4)P metabolism and ORP/Osh-mediated lipid movements.

ACKNOWLEDGMENTS

We thank N. Leroudier and L. D'Esposito for technical help. This work was supported by the CNRS and ANR (2010-1503-01). J.M.F. and B.A. are supported by an ERC Advanced Grant (268888). S.V. was supported by the SNSF (PBELP3_141118).

AUTHORS CONTRIBUTIONS

J.M.F. and B.M performed biochemical and biophysical experiments and data analysis. S.V. carried out molecular dynamic simulation and analysis. B.A. and S.V. assisted with the manuscript. G.D. conceived the project, designed liposome assays, carried out experiments and kinetic modeling, analyzed data and wrote the manuscript

REFERENCES

1. Mesmin, B. & Maxfield, F.R. Intracellular sterol dynamics. *Biochim. Biophys. Acta.* **1791**, 636-645 (2009).
2. Radhakrishnan, A., Goldstein, J.L., McDonald, J.G. & Brown, M.S. Switch-like control of SREBP-2 transport triggered by small changes in ER cholesterol: a delicate balance. *Cell Metab.* **8**, 512-521 (2008).
3. Schneiter, R. et al. Electrospray ionization tandem mass spectrometry (ESI-MS/MS) analysis of the lipid molecular species composition of yeast subcellular membranes reveals acyl chain-based sorting/remodeling of distinct molecular species en route to the plasma membrane. *J. Cell. Biol.* **146**, 741-754 (1999).
4. Andreyev, A.Y. et al. Subcellular organelle lipidomics in TLR-4-activated macrophages. *J. Lipid. Res.* **51**, 2785-2797 (2010).
5. Baumann, N.A. et al. Transport of newly synthesized sterol to the sterol-enriched plasma membrane occurs via nonvesicular equilibration. *Biochemistry* **44**, 5816-5826 (2005).
6. Urbani, L. & Simoni, R.D. Cholesterol and vesicular stomatitis virus G protein take separate routes from the endoplasmic reticulum to the plasma membrane. *J. Biol. Chem.* **265**, 1919-1923 (1990).
7. Lev, S. Non-vesicular lipid transport by lipid-transfer proteins and beyond. *Nat. Rev. Mol. Cell. Biol.* **11**, 739-750 (2010).
8. Prinz, W.A. Lipid trafficking sans vesicles: where, why, how? *Cell* **143**, 870-874 (2010).
9. Raychaudhuri, S. & Prinz, W.A. The diverse functions of oxysterol-binding proteins. *Annu. Rev. Cell. Dev. Biol.* **26**, 157-177 (2010).
10. Alpy, F. & Tomasetto, C. START ships lipids across interorganelle space. *Biochimie* **96**, 85-95 (2014).

11. Sullivan, D.P., Ohvo-Rekila, H., Baumann, N.A., Beh, C.T. & Menon, A.K. Sterol trafficking between the endoplasmic reticulum and plasma membrane in yeast. *Biochem. Soc. Trans.* **34**, 356-358 (2006).
12. Radhakrishnan, A. & McConnell, H.M. Condensed complexes of cholesterol and phospholipids. *Biophys. J.* **77**, 1507-1517 (1999).
13. Ali, M.R., Cheng, K.H. & Huang, J. Assess the nature of cholesterol-lipid interactions through the chemical potential of cholesterol in phosphatidylcholine bilayers. *Proc. Natl. Acad. Sci. U S A* **104**, 5372-5377 (2007).
14. Huang, J. & Feigenson, G.W. A microscopic interaction model of maximum solubility of cholesterol in lipid bilayers. *Biophys. J.* **76**, 2142-2157 (1999).
15. Klemm, R.W. et al. Segregation of sphingolipids and sterols during formation of secretory vesicles at the trans-Golgi network. *J. Cell. Biol.* **185**, 601-612 (2009).
16. Holthuis, J.C., Pomorski, T., Raggers, R.J., Sprong, H. & Van Meer, G. The organizing potential of sphingolipids in intracellular membrane transport. *Physiol. Rev.* **81**, 1689-1723 (2001).
17. de Saint-Jean, M. et al. Osh4p exchanges sterols for phosphatidylinositol 4-phosphate between lipid bilayers. *J. Cell. Biol.* **195**, 965-978 (2011).
18. Mesmin, B. et al. A Four-Step Cycle Driven by PI(4)P Hydrolysis Directs Sterol/PI(4)P Exchange by the ER-Golgi Tether OSBP. *Cell* **155**, 830-843 (2013).
19. Im, Y.J., Raychaudhuri, S., Prinz, W.A. & Hurley, J.H. Structural mechanism for sterol sensing and transport by OSBP-related proteins. *Nature* **437**, 154-158 (2005).
20. Strahl, T. & Thorner, J. Synthesis and function of membrane phosphoinositides in budding yeast, Saccharomyces cerevisiae. *Biochim. Biophys. Acta.* **1771**, 353-404 (2007).
21. Foti, M., Audhya, A. & Emr, S.D. Sac1 lipid phosphatase and Stt4 phosphatidylinositol 4-kinase regulate a pool of phosphatidylinositol 4-phosphate that functions in the control of the actin cytoskeleton and vacuole morphology. *Mol. Biol. Cell.* **12**, 2396-2411 (2001).
22. Manford, A. et al. Crystal structure of the yeast Sac1: implications for its phosphoinositide phosphatase function. *Embo J.* **29**, 1489-1498 (2010).
23. Faulhammer, F. et al. Growth control of Golgi phosphoinositides by reciprocal localization of sac1 lipid phosphatase and pik1 4-kinase. *Traffic* **8**, 1554-1567 (2007).
24. Fairn, G.D., Curwin, A.J., Stefan, C.J. & McMaster, C.R. The oxysterol binding protein Kes1p regulates Golgi apparatus phosphatidylinositol-4-phosphate function. *Proc. Natl. Acad. Sci. U S A* **104**, 15352-15357 (2007).
25. Schaaf, G. et al. Functional anatomy of phospholipid binding and regulation of phosphoinositide homeostasis by proteins of the sec14 superfamily. *Mol. Cell* **29**, 191-206 (2008).
26. Proszynski, T.J. et al. A genome-wide visual screen reveals a role for sphingolipids and ergosterol in cell surface delivery in yeast. *Proc. Natl. Acad. Sci. U S A* **102**, 17981-17986 (2005).
27. Beh, C.T., Cool, L., Phillips, J. & Rine, J. Overlapping functions of the yeast oxysterol-binding protein homologues. *Genetics* **157**, 1117-1140 (2001).
28. Beh, C.T. & Rine, J. A role for yeast oxysterol-binding protein homologs in endocytosis and in the maintenance of intracellular sterol-lipid distribution. *J. Cell. Sci.* **117**, 2983-2996 (2004).

29. Lenoir, M. et al. Structural basis of wedging the Golgi membrane by FAPP pleckstrin homology domains. *EMBO Rep.* **11**, 279-284 (2010).
30. Stefan, C.J. et al. Osh proteins regulate phosphoinositide metabolism at ER-plasma membrane contact sites. *Cell* **144**, 389-401 (2011).
31. Leventis, R. & Silvius, J.R. Use of cyclodextrins to monitor transbilayer movement and differential lipid affinities of cholesterol. *Biophys. J.* **81**, 2257-2267 (2001).
32. West, M., Zurek, N., Hoenger, A. & Voeltz, G.K. A 3D analysis of yeast ER structure reveals how ER domains are organized by membrane curvature. *J. Cell. Biol.* **193**, 333-346 (2011).
33. John, K., Kubelt, J., Muller, P., Wustner, D. & Herrmann, A. Rapid transbilayer movement of the fluorescent sterol dehydroergosterol in lipid membranes. *Biophys. J.* **83**, 1525-1534 (2002).
34. Mesmin, B. et al. STARD4 abundance regulates sterol transport and sensing. *Mol. Biol. Cell.* **22**, 4004-4015 (2011).
35. Hanada, K. et al. Molecular machinery for non-vesicular trafficking of ceramide. *Nature* **426**, 803-809 (2003).
36. Ghaemmaghami, S. et al. Global analysis of protein expression in yeast. *Nature* **425**, 737-741 (2003).
37. Georgiev, A.G. et al. Osh proteins regulate membrane sterol organization but are not required for sterol movement between the ER and PM. *Traffic* **12**, 1341-1355 (2011).
38. Alfaro, G. et al. The sterol-binding protein Kes1/Osh4p is a regulator of polarized exocytosis. *Traffic* **12**, 1521-1536 (2011).
39. Santiago-Tirado, F.H. & Bretscher, A. Membrane-trafficking sorting hubs: cooperation between PI4P and small GTPases at the trans-Golgi network. *Trends Cell. Biol.* **21**, 515-525 (2011).
40. Canagarajah, B.J., Hummer, G., Prinz, W.A. & Hurley, J.H. Dynamics of cholesterol exchange in the oxysterol binding protein family. *J. Mol. Biol.* **378**, 737-748 (2008).
41. Singh, R.P., Brooks, B.R. & Klauda, J.B. Binding and release of cholesterol in the Osh4 protein of yeast. *Proteins* **75**, 468-477 (2009).
42. Mousley, C.J. et al. A sterol-binding protein integrates endosomal lipid metabolism with TOR signaling and nitrogen sensing. *Cell* **148**, 702-715 (2012).
43. Tong, J., Yang, H., Eom, S.H. & Im, Y.J. Structure of Osh3 reveals a conserved mode of phosphoinositide binding in oxysterol-binding proteins. *Structure* **21**, 1203-1213 (2013).
44. Charman, M., Colbourne, T.R., Pietrangelo, A., Kreplak, L. & Ridgway, N.D. Oxysterol-binding protein (OSBP)-related protein 4 (ORP4) is essential for cell proliferation and survival. *J. Biol. Chem.* (2014).
45. Maeda, K. et al. Interactome map uncovers phosphatidylserine transport by oxysterol-binding proteins. *Nature* (2013).
46. Drin, G. Topological Regulation of Lipid Balance in Cells. *Annu. Rev. Biochem.* (2014).

FIGURE LEGENDS

Figure 1. Working model of sterol/PI(4)P transport cycles mediated by Osh4p at the ER/Golgi interface

Figure 2. Coupling of DHE and PI(4)P transport by Osh4p between ER- and Golgi-like liposomes. (a) DHE transport assay. DOPC/DNS-PE/DHE liposomes (92.5/2.5/5 mol/mol, 200 µM total lipids, L_E) were mixed with DOPC liposomes (200 µM lipids, L_G) containing or not 4 mol% PI(4)P at 30°C. After 3 min, Osh4p (200 nM) was added. FRET between DHE and DNS-PE in the L_E liposomes diminishes as DHE is transported to the L_G liposomes. The signal was converted into amount of DHE present in L_E liposome (in µM). The slow decay observed without Osh4p was due to spontaneous DHE transfer. The dashed line corresponds to full equilibration of DHE between liposomes. **(b)** PI(4)P transport assay. DOPC/PI(4)P/Rhod-PE liposomes (94/4/2 mol/mol, 200 µM lipids, L_G) were incubated with NBD-PH_{FAPP} (250 nM). Then DOPC liposomes (200 µM lipids, L_E) containing or not 5 mol% DHE were added. After 3 min, Osh4p (200 nM) was injected. The dequenching of NBD signal mirrors the translocation of NBD-PH_{FAPP} from L_G to L_E liposomes. The dashed line corresponds to the signal of NBD-PH_{FAPP} obtained under conditions mimicking full PI(4)P equilibration between liposomes. **(c)** Plot of initial DHE transport rates versus initial PI(4)P transport rates (mean ± SEM (n = 2)) for Osh4p WT or mutants (200 nM) measured with L_E and L_G liposomes containing 5 mol% DHE and 4 mol% PI(4)P, respectively. Localization of key residues (in stick with nitrogen in blue, and oxygen in red) are shown in a close-up view of the PI(4)P headgroup or sterol binding-pocket. The H-bonds are represented.

Figure 3. PI(4)P hydrolysis by Sac1p on ER-like liposome sustains sterol transport by Osh4p. (a) DOPC/DOGS-NTA-Ni^2/DNS-PE/DHE liposomes (90.5/2/2.5/5 mol/mol, 200 µM total lipids, L_E liposomes) were preincubated or not with Sac1p[1-522]His_6 or an inactive variant (C392S) and mixed with DOPC liposomes (200 µM lipids, L_G liposomes) containing 0 or 4 mol% PI(4)P. After 3min3 min, Osh4p (200 nM) was added and DHE transport was monitored. The experiment with soluble Sac1p (200 nM) was done with L_E liposome devoid of DOGS-NTA-Ni^{2+}. **(b)** The transport of PI(4)P was monitored with L_E liposomes devoid of Sac1p or with L_E liposomes covered by 200 nM Sac1p[1-522]His_6 or Sac1p[1-522]His_6 (C392S). The amount of PI(4)P (solid line) transported by the protein is only indicated for experiments in which no PI(4)P hydrolysis occurs. For experiments with Sac1p, only the F_{Norm} signal is indicated (dashed line). The estimated trace corresponds to the amount of

PI(4)P which is likely transported by Osh4p into L_E liposome when Sac1p is present on L_E liposome and active.

Figure 4. Osh4p uses PI(4)P to create and maintain sterol gradient. (a) *Upper panel*: DHE transport assay. Osh4p (200 nM) is added to DOPC/DOGS-NTA-Ni^{2+}/DNS-PE/DHE liposomes (90.5/2/2.5/5 mol/mol, 200 µM total lipids, L_E liposome) mixed with DOPC liposomes (200 µM total lipids, L_G liposome) containing 0, 5 or 10 mol% DHE, with or without 4 mol% PI(4)P. Alternatively, an equivalent amount of HKM buffer was injected. *Lower panel*: PI(4)P transport assay. DOPC/PI(4)P/Rhod-PE liposomes (96/4/2 mol/mol, 200 µM total lipids, L_G liposome) containing 0, 5 or 10 mol% DHE were incubated with NBD-PH_{FAPP} (250 nM). Next, DOPC/DOGS-NTA-Ni^{2+} liposomes (98/2 mol/mol, 200 µM total lipids, L_E liposome) doped with 5 mol% DHE were added. PI(4)P and DHE were incorporated in the liposome at the expense of DOPC. After 3 min, Osh4p (200 nM) was injected. For experiments with Sac1p (200 or 400 nM) L_E liposomes were premixed on ice for 10 minutes with Sac1p[1-522]His_6. (b) Initial DHE and PI(4)P transport rates as a function of the difference of DHE (ΔDHE) between L_G and L_E liposome. The rates (mean ± SEM (DHE transport assay: n = 3; PI(4)P transport assay, n=4)) were determined from experiments similar to that shown in (a) performed in the absence of Sac1p and with L_G liposome doped with 4 mol% PI(4)P

Figure 5. Acyl-chain saturation in Golgi-like membranes favors sterol transport up its gradient by Osh4p. (a) *Upper panel*: DHE transport assay. DOPC/DOGS-NTA-Ni^{2+}/DNS-PE/DHE liposomes (90.5/2/2.5/5 mol/mol, 200 µM total lipids, L_E liposome) were mixed with DOPC/DHE (90/10 mol/mol), POPC/DHE (90/10) or DOPC/SM/DHE (45/45/10) liposomes (200 µM total lipids, L_G liposome) doped or not with 4 mol% PI(4)P (at the expense of DOPC or POPC). Thereafter, Osh4p (200 nM) or an equivalent volume of HKM buffer was injected. *Lower panel*: PI(4)P transport assay. DOPC/DHE (90/10 mol/mol), POPC/DHE (90/10) or DOPC/SM/DHE (45/45/10) liposomes (200 µM lipids, L_G liposome) containing 2 mol% Rhod-PE and 4 mol% PI(4)P (at the expense of DOPC) were incubated with NBD-PH_{FAPP} (250 nM) and mixed with DOPC/DHE/DOGS-NTA-Ni^{2+} liposomes (97.5/5/2 mol/mol, 200 µM lipids, L_G liposome). After 3 min, Osh4p (200 nM) was added. For experiments with Sac1p, L_E liposomes were premixed on ice for 10 minutes with Sac1p[1-522]His_6. (b) Initial DHE and PI(4)P transport rates as a function of the bulk composition of L_G liposomes. The rates (mean ± SEM (DHE transport assay: n = 3; PI(4)P

transport assay, n=4)) were determined from experiments, as shown in (a), carried out in the absence of Sac1p with L_G liposome doped with 4 mol% PI(4)P.

Figure 6. Effect of lipid packing and curvature of L_E liposomes on sterol/PI(4)P exchange. (a) Intrinsic fluorescence at 340 nm of Osh4p[PI(4)P] (500 nM) upon addition to large liposomes (500 µM total lipids) made of DOPC (blue trace) or POPC (black trace), and containing 0.5 or 5 mol% DHE. A reference signal was measured with DHE-free liposomes. (b) Osh4p[PI(4)P] (500 nM) was added to large POPC of defined radius and doped with 0.5 or 5 mol% (DHE). (c) *Upper panel* : the transport of DHE mediated by Osh4p (200 nM) was measured between POPC/DNS-PE/DHE liposomes (92.5/2.5/5 mol/mol, 200 µM lipids, L_E liposome) of defined radii and large DOPC liposomes (200 µM lipids, L_G liposome) doped with 4 mol% PI(4)P. *Lower panel* : the transport of PI(4)P by Osh4p (200 nM) was measured with NBD-PH_{FAPP} (250 nM) from DOPC/PI(4)P/Rhod-PE liposomes (92.5/2.5/5 mol/mol, 200 µM lipids, L_G liposome) to POPC liposomes (200 µM lipids, L_E liposome) of defined radius doped with 5 mol% DHE. (d) Initial transport rate for DHE and PI(4)P (mean ± SEM (n = 2)) as deduced from the experiment shown in (c) and plotted as a function of the hydrodynamic radius (R_H) of L_E liposomes.

Figure 7. Differential control of ligand release by the N-terminal lid of Osh4p (a) Electrostatic and Van der Waals contribution in the binding of ergosterol or PI(4)P to Osh4p. (b) Dynamic behavior of ergosterol (left) and PI(4)P (right) inside the binding pocket of Osh4p. The time evolution of the lipids is shown during 1 µs of MD simulations with colors going from red (beginning of the MD trajectory) to blue (end of the trajectory). The RMSD of ergosterol or PI(4)P polar head and acyl chains is represented. (c) Contribution to the ligand-protein interaction energy of residues that closely interact with sterol or PI(4)P. (d) Motion of the N-terminal lid (residues 1-29) during 1 µs MD simulation of Osh4p bound to PI(4)P (left) or ergosterol (right). The time evolution of the lid is shown with colors going from red to blue. Lipids are shown in licorice representation. RMSF of residues 1-29 are plotted for the simulation of Osh4p bound to ergosterol (blue) or PI(4)P (orange) in the bottom panel. (e) Osh4p (500 nM) preloaded with PI(4)P was added, in the presence of NBD-PH_{FAPP} (250 nM), to DOPC liposomes containing or not 5 mol% DHE at 30°C. As a control, we incubated empty Osh4p. (f) DNS-Osh4p loaded with DHE (~500 nM) was incubated at 30°C in buffer. At the indicated time, large liposomes (with or without 5 mol% ergosterol) were injected (500

μM final lipid concentration). The release of DHE was followed by measuring the diminution in FRET between DHE and DNS-Osh4p.

METHODS

Protein expression and purification. Full-length Osh4p and Osh4p[30-434] were cloned in pGEX-4T-3 vector to code for GST-fused constructs. The different site-specific mutations in Osh4p (Q96A, Y97F, K109A, H143A/H144A, K336E,…) were obtained by the Quikchange kit (Stratagene). The PH domain (FAPP1[1-100] construct, PH_{FAPP}) of the Phosphoinositol 4-phosphate Adaptor Protein-1 (FAPP1) protein was cloned in a pGEX-4T-3 vector. A linker of 9 residues was inserted by the Quikchange kit between the thrombine cleavage site and the first residue of the PH domain (NGNLSSLSA) to guarantee accessibility to thrombin. The PH_{FAPP} sequence was next mutated to replace two solvent-accessible cysteines by serine (mutation C37S and C94S) and to introduce a cysteine into a membrane-inserting wedge of the domain (T13C). A Sac1p[1-552] fragment was PCR-amplified from a initial plasmid using primers incorporating a Nhe1 and Not1 restriction site and inserted into a pET-21b(+) vector to code for a soluble form of Sac1p tagged with a C-terminal hexahistidine sequence. A single mutation was introduced to obtain a catalytically-dead Sac1p (mutation C392S). All sequences of Osh4p, PH_{FAPP} and Sac1p were checked by DNA sequencing.

GST-Osh4p, GST-Osh4p[30-434] and Sac1p[1-522]His_6 were expressed in *E. coli* at 30°C overnight whereas the GST-PH_{FAPP} was expressed at 37°C for 3 h upon induction with 1 mM IPTG (at O.D.600= 0.6). For GST-tagged proteins, all purification steps were conducted in 50 mM Tris, pH 7.4, 120 mM NaCl, 2 mM DTT. For His_6-tagged proteins a buffer containing 50 mM Tris, pH 7.5, 300 mM NaCl, 20 mM imidazole was used. All buffers were supplemented during the first purification steps with PMSF (1 mM), bestatine (1 μM), pepstatine (10 μM), phosphoramidon (10 μM) and protease inhibitor tablets (Roche). Cells were lysed by a French press and the lysate was centrifuged at 200,000 g for 1 hour.

For GST-fused protein (Osh4p and PH_{FAPP}), the supernatant was applied to Glutathione Sepharose 4B beads. After 3 washing steps, the beads were incubated with thrombin at 4°C overnight to cleave the GST fusion and allow the release of Osh4p or PH_{FAPP}. All constructs contain an N-terminal GS sequence from the thrombin cleavage site. All Osh4p constructs were next purified by gel filtration on a Sephacryl S300 HR XK16-70 column.

For His_6-tagged proteins (Sac1p), the supernatant was mixed with Ni-NTA Agarose beads (Qiagen). After 3 washing steps, proteins were eluted from the beads with buffer containing first 250 mM, then 500 mM imidazole. All Sac1p constructs were subsequently purified by gel filtration on a Sephacryl S300 HR XK16-70 column.

For NBD labeling of PH_{FAPP}, the crude eluate was mixed (after DTT removal by gel filtration on illustra NAP-10 columns (GE Healthcare)) with a 10-fold excess of N,N'-dimethyl-N-(iodoacetyl)-N'-(7-nitrobenz-2-oxa-1,3-diazol-4-yl)ethylenediamine (IANBD-amide, Molecular Probes). After 90 min on ice, the reaction was stopped by adding a 10-fold excess of L-cysteine over the probe. The free probe was removed by gel filtration on a Sephacryl S200 HR XK16-70 column. The labeled protein was analyzed by SDS-PAGE and UV-visible spectroscopy. The gel was directly visualized in a fluorescence imaging system (FUJI LAS-3000 fluorescence imaging system) to detect NBD-labeled PH_{FAPP} excited in near-UV and then stained with Sypro Orange to determine the purity of NBD-PH_{FAPP}. The labeling yield (≈ 100 %) was estimated from the ratio of the optical density (OD) of tyrosine and tryptophan at 280 nm (ε=29,450 $M^{-1}.cm^{-1}$) and NBD at 495 nm (ε=25,000 $M^{-1}.cm^{-1}$ according to the manufacturer). The production and purification of DNS-Osh4p have been described previously[17].

For all purified proteins, the concentration was determined by a Bradford assay, by SDS-PAGE analysis using a BSA standard curve and UV spectrometry.

Lipids. DOPC (1,2-dioleoyl-*sn*-glycero-3-phosphocholine), POPC (1-palmitoyl-2-oleoyl-*sn*-glycero-3-phosphocholine), liver PI (L-α-phosphatidylinositol), brain PI(4)P (L-α-phosphatidylinositol-4-phosphate), DNS-PE (1,2-dioleoyl-*sn*-glycero-3-phosphoethanolamine-N-(5-dimethylamino-1-naphthalenesulfonyl)), NBD-PE (1,2-dioleoyl-*sn*-glycero-3-phosphoethanolamine-N-(7-nitro-2-1,3-benzoxadiazol-4-yl)) , Rhod-PE (1,2-dipalmitoyl-*sn*-glycero-3-phosphoethanolamine-N-(lissamine rhodamine B sulfonyl)) and DOGS-NTA-Ni^{2+} (1,2-dioleoyl-*sn*-glycero-3-[(N-(5-amino-1-carboxypentyl)iminodiacetic acid)succinyl]) and 18:0 SM (N-stearoyl-D-erythro-sphingosylphosphorylcholine) were purchased from Avanti Polar Lipids. Ergosterol and dehydroergosterol (DHE) were from Sigma Aldrich. The concentration of DHE in stock solution in methanol was determined by UV-spectroscopy using an extinction coefficient of 13,000 $M^{-1}.cm^{-1}$. The preparation of radiolabeled [^{32}P]PI(4)P was described previously[17].

Liposomes preparation. Lipids in stock solutions in $CHCl_3$ were mixed at the desired molar ratio and the solvent was removed in a rotary evaporator. For lipid films including PI(4)P or DOGS-NTA-Ni^{2+}, the mix was pre-warmed to 33°C for 5 minutes prior to drying under vacuum. For formulations containing [^{32}P]PI(4)P, the mixture was dried in a hemolysis tube under argon. The films were hydrated in 50 mM Hepes, pH 7.2, 120 mM K-acetate (HK buffer) to obtain a suspension of multilamellar liposomes. Alternatively, to produce liposomes loaded with sucrose, films were hydrated with 50 mM Hepes, pH 7.2, 220 mM sucrose. After five thawing-freezing cycles with liquid nitrogen, the suspensions were extruded through polycarbonate filters of 0.2 µm pore size using a mini-extruder (Avanti Polar Lipids). The extruder was set with a heating/holder block to extrude at 45°C liposomes containing SM. To produce liposomes of defined curvature, the liposomes were extruded sequentially through 0.4, 0.2, 0.1, 0.05 and 0.03 µm (pore size) filters. The liposome hydrodynamic radius (R_H) was estimated by dynamic light scattering in a Dyna Pro instrument. Liposomes were stored at 4°C and in the dark when containing light-sensitive lipids (DHE, DNS-PE, ergosterol, NBD-PE, Rhod-PE) and used within 2 days. .

Fluorimetric activity assays. All fluorimetric activity assays were carried out in a Shimadzu RF 5301-PC fluorimeter. The sample (volume 600 µl) was placed in a cylindrical quartz cell, continuously stirred with a small magnetic bar and thermostated at 30°C. At the indicated time, sample was injected from stock solutions through a guide in the cover of the fluorimeter adapted to Hamilton syringes, such as to not interrupt the fluorescence recording.

DHE transport assay - A suspension (570 µl) of L_G liposomes (200 µM total lipids) was incubated at 30°C under constant stirring in HKM (HK + 1mM $MgCl_2$) buffer. After 1 min, 30 µl of L_E liposomes (200 µM lipid, final concentration) containing 2.5 mol% of DNS-PE and 5 mol% of DHE was added. The volumic concentration of DHE was equal to 10 µM. DHE is quickly equilibrated between the inner and outer leaflet of liposomes ($t_{1/2}$ of transbilayer movement <1 minute[33]) implying that the entire DHE pool is accessible to Osh4p. After 3 min, Osh4p was injected at 200 nM. Lipid transport was followed by measuring the dansyl signal at 525 nm (bandwidth 10 nm) upon DHE excitation at 310 nm (bandwidth 1.5 nm). The amount of DHE (in µM) transferred from L_E to L_G liposome corresponds to $10 * ((F-F_0)/(F_{max}-F_0))$. F_{max} is the signal before Osh4p injection and F_0 is the signal measured with liposomes containing 2.5 mol% DNS-PE but devoid of DHE.

PI(4)P transport assay - A suspension (570 µl) of L_G liposome (200 µM total lipids) containing 2 mol% Rhod-PE and 4 mol% PI(4)P was incubated with 250 nM NBD-PH_{FAPP} at 30°C in HKM buffer under constant stirring. The volume concentration of accessible PI(4)P (in the outer leaflet) is 4 µM. After 1 min, 30 µl of L_E liposome (200 µM total lipids, final concentration) were injected. After additional 3 min, Osh4p (200 nM) was injected. PI(4)P transport was followed by measuring the NBD signal at 530 nm (bandwidth 10 nm) upon excitation at 460 nm (bandwidth 1.5 nm). The NBD signal mirrors the distribution of NBD-PH_{FAPP} between L_E and L_G liposome. In the case of a transport process without PI(4)P hydrolysis, we could directly determine the amount of PI(4)P transported by Osh4p by normalizing the NBD signal. To do so, we measured the NBD signal (F_{eq}) that corresponds to a situation where PI(4)P is fully equilibrated between liposomes. NBD-PH_{FAPP} (250 nM) was mixed with L_E and L_G liposome (200 µM total lipid each) with a size and lipid composition similar to that of the liposomes used in the transport assay, except that each contains initially 2 mol% PI(4)P. Liposome-binding assays indicated that NBD-PH_{FAPP} is completely bound to membrane for a surface-accessible amount of PI(4)P between 2 and 4 µM (**Supplementary Figure 2f**). Consequently, the fraction of PI(4)P on L_E liposome, $PI(4)P_E/PI(4)P_T$, is directly equal to the fraction of PH_{FAPP} on L_E liposome and correspond to $F_{Norm} = 0.5*(F-F_G/F_{eq}-F_G)$ with F_G corresponding to the NBD signal prior to the addition of Osh4p. The amount of PI(4)P (in µM) transferred from L_G to L_E liposome corresponds to $4* F_{Norm}$.

PI(4)P hydrolysis assay - DOPC/PI(4)P/Rhod-PE liposomes (96/2/2 mol/mol, 200 µM total lipids) and DOPC/PI(4)P liposomes (98/2 mol/mol, 200 µM total lipids) were mixed with NBD-PH_{FAPP} (250 nM) at 30°C under constant stirring. At the indicated time, Sac1p[1-522]His_6 or Sac1p[1-522](C392S)His_6 (200 or 400 nM) was injected. The NBD signal was measured at 530 nm (bandwidth 10 nm) upon excitation at 460 nm (bandwidth 1.5 nm). To calculate the amount of PI(4)P hydrolyzed by Sac1p on L_E liposome (x), we considered that the normalized NBD signal $F_{Norm}=0.5*(F-F_G/F_{max}-F_G)$ is equal to $(PI(4)P_E-x)/(PI(4)P_T-x)$ with F_{max} corresponding to the initial signal measured prior to the injection of Sac1p and F_0 is the signal measured with NBD-PH_{FAPP} in the presence of Rhod-PE-containing liposomes only. Considering that $PI(4)P_E=2$ µM and $PI(4)P_T=4$ µM at the beginning of the experiment, x is equal to $(2-4F_{Norm})/(1-F_{Norm})$.

DHE loading assay - The loading of Osh4p with DHE is measured by following the quenching of the intrinsic fluorescence of the protein as described in detail in [17].

DHE extraction assay - The sample (150µl) containing DOPC liposomes (150 µM total lipids) doped with 2.5 mol% of DNS-PE and 2 mol% of DHE was incubated at 30 °C in a small quartz cuvette. Lipid extraction was followed by recording the dansyl signal at 525 nm (bandwidth 10 nm) upon DHE excitation at 310 nm (bandwidth 1.5 nm) before and 5 min after the addition of 3 µM Osh4p or mutants. The signal corresponds to F_{max} and F, respectively; the intensity signal corresponding to the maximal DHE extraction (F_0), was determined with 2mM methyl-β-cyclodextrin. The percentage of DHE extraction is given by $100*(1-((F-F_0)/(F_{max}-F_0))$.

PI(4)P extraction assay. The protocol has been described in detail in [17].

PI(4)P and DHE delivery assays - We prepare Osh4p in complex with PI(4)P and DNS-Osh4p in complex with DHE as described previousl[17]. For PI(4)P delivery, we added Osh4p-PI(4)P to large liposomes (500 µM total lipids) in the presence of 250 nM NBD-PH_{FAPP}. PI(4)P delivery was monitored at 530 nm (bandwidth 10 nm) upon excitation at 460 nm (bandwidth 1.5 nm). For DHE delivery, we added 30 µl of liposomes (stock solution 5 mM, final concentration 500 µM) to DNS-Osh4p-DHE (~500 nM). Sterol delivery was monitored at 510 nm (bandwidth 20 nm) upon excitation at 310 nm (bandwidth 1.5 nm) at 30°C. The recordings were corrected for the light scattering signal and the dilution effect induced by liposome addition

Flotation experiments. The protocol has been described in detail[47]. Briefly, proteins (750 nM) were incubated with NBD-PE containing liposomes (750 µM total lipids) in 150 µl HKM buffer at room temperature for 5 min. The suspension was adjusted to 30% sucrose by mixing 100 µl of a 75% (w/v) sucrose solution in HKM buffer and overlaid with 200 µl HKM containing 25% (w/v) sucrose and 50 µl sucrose-free HKM. The sample was centrifuged at 240,000 g in a swing rotor (TLS 55 Beckmann) for 1 h. The bottom (250 µl), middle (150 µl) and top (100 µl) fractions were collected. The top fractions were analyzed by SDS-PAGE using Sypro-Orange staining and a FUJI LAS-3000 fluorescence imaging system.

Data fitting and kinetic simulations. In order to determine the time evolution of PI(4)P in L_E and L_G liposomes (P_E and P_G, respectively) from the raw NBD signal (F), in transport experiments in the presence or absence of Sac1p, we considered the general function.

$$F = \alpha[PH - P_E] + \beta[PH - P_G] + \chi[PH] \quad (1)$$

where PH corresponds to NBD-PH_{FAPP}, $[PH - P_E]$ and $[PH - P_G]$ are the concentration of the PH domain bound to L_E and L_G liposomes, respectively, *via* its interaction with the polar head of PI(4)P. The parameters α, β and χ correspond to the molar fluorescence of the PH domain bound to L_E liposome, of the quenched NBD–PH_{FAPP} bound to L_G liposomes and of the soluble PH domain, respectively. As $[PH] = PH_0 - [PH - P_E] - [PH - P_G]$, with PH_0 corresponding to the total concentration of PH domain, we have

$$F = (\alpha - \chi)[PH - P_E] + (\beta - \chi)[PH - P_G] + \chi PH_0 \quad (2)$$

If we consider a competition between the PI(4)P pools of L_E and L_G liposomes for recruiting PH_{FAPP},

$$[PH - P_E] = PH_0 \frac{[P_E]}{K_E\left(1+\frac{[P_G]}{K_G}\right)+[P_E]} \quad (3)$$

$$[PH - P_G] = PH_0 \frac{[P_G]}{K_G\left(1+\frac{[P_E]}{K_E}\right)+[P_G]} \quad (4)$$

By combining the equation (2), (3) and (4), we obtain

$$F = (\alpha - \chi)PH_0 \frac{[P_E]}{K_E\left(1+\frac{[P_G]}{K_G}\right)+[P_E]} + (\beta - \chi)PH_0 \frac{[P_G]}{K_G\left(1+\frac{[P_E]}{K_E}\right)+[P_G]} + \chi PH_0 \quad (5)$$

The dissociation constant K_E and K_G are identical and are equal to ~0.25 µM, as estimated from the binding curve of NBD-PH_{FAPP} with DOPC liposomes containing 2 or 4 mol% PI(4)P (data not shown). The total amount of NBD-PH_{FAPP} in the experiment is 0.25 µM. Therefore,

$$F = 0.25((\alpha - \chi)(\frac{[P_E]}{0.25+[P_E]+[P_G]}) + (\beta - \chi)(\frac{[P_G]}{0.25+[P_G]+[P_E]}) + \chi) \quad (6)$$

The χ value was estimated from the fluorescence (F_0) of 0.25 µM soluble NBD-PH_{FAPP} ([PH]=0.25) in buffer ; γ is equal to F_0/0.250. The β value is equal to F_G/0.25 where F_G is the fluorescence of 0.25 µM NBD-PH_{FAPP} bound to L_G liposome ($[PH - P_G]$ =0.25 µM) prior to the injection of Osh4p. The α value was estimated from the fluorescence F_{eq} measured under conditions where the NBD-PH_{FAPP} construct was equally bound to L_E and L_G liposomes (which each contains 2 mol% PI(4)P). Consequently $[PH - P_E] = [PH - P_G]$ = 0.125 µM, and F_{eq}=0.125α + 0.125β meaning that α=(F_{eq}-0.125β)/0.125.

To analyze the experimental data, we considered that the Osh4p-mediated sterol/PI(4)P transport cycle shown in **Figure 1** can be described by the following sequence of reactions:

$$OS \underset{k2}{\overset{k1}{\rightleftarrows}} O_G + S_G$$

$$O_G + P_G \underset{k4}{\overset{k3}{\rightleftarrows}} OP$$

$$OP \underset{k6}{\overset{k5}{\rightleftarrows}} O_E + P_E$$

$$O_E + S_E \underset{k8}{\overset{k7}{\rightleftarrows}} OS$$

$$O_E \underset{k10}{\overset{k9}{\rightleftarrows}} O_G$$

$$P_E \underset{k11}{\longrightarrow} P_E^*$$

O_E and O_G corresponds to Osh4p, in an empty state, bound to ER- and Golgi-like liposomes, respectively; OS and OP corresponds to Osh4p, in solution, bound to sterol and PI(4)P, respectively ; S_E and S_G are the amount (in µM) of DHE in the L_E and L_G liposomes, respectively ; P_E and P_G are the amount of PI(4)P (in µM) in the L_E and L_G liposomes, respectively. P_E^* is the amounts of PI derived from the hydrolysis of PI(4)P by Sac1p on the surface of L_E liposomes. For simplicity the very slow spontaneous DHE transfer between membranes is not taken into account in our model.

The time evolution of the sterol and PI(4)P concentrations in ER- and Golgi-like membranes is determined by integrating a system of ordinary differential equations corresponding to our model whose parameters are adjusted to fit the F function with the raw NBD trace. The initial S_E, S_G, P_E and P_G concentration were set according to the experiment that was analyzed. At time zero, when Osh4p is injected, Osh4p (200nM) is empty and is

considered to equally target L_E and L_G liposome ($O_{E=}O_G$ =100 nM). To reduce the number of adjustable parameters, k_9 and k_{10} values were arbitrary set at 0.5. The value of k_{11} (PI(4)P hydrolysis by 200 nM Sac1p on L_E liposome) was derived from the measure of PI(4)P hydrolysis by Sac1p, assuming a first-order reaction (**Fig. S2d**). For conditions without Sac1p, k_{11} was set to zero. The implementation of the kinetic model, the fitting procedure and the simulations were carried out with the software GEPASI v3.3[48]. For graphical representation, the predicted raw NBD traces (F) were normalized to obtain F_{Norm}.

MD simulations. All simulations are based on the crystal structure of Osh4p bound to ergosterol (PDB ID: 1ZHZ[19] and to PI(4)P (PDB ID: 3SPW)[17]. Missing residues (notably residues 1-12 of the N-terminal lid) were added to the PI(4)P-bound structure using MODELLER9v10[49] The model with the lowest DOPE score [50] was retained. All ionizable side chains, as well as the C- and N-termini were modeled in their default ionization state, with the exception of H143 and H144 residues in the PI(4)P simulations, where the two histidines were modeled as protonated to balance the negative charge of the PI(4)P molecule. The system was immersed in a box of water of approximately 83x76x96 $Å^3$ containing 16350 molecules. The box dimensions are chosen in such a way that the minimum distance between periodic images of the protein is always larger than 25 Å during the simulation. Neutrality of the system at physiological ion concentration (120 mM) was obtained by adding 47 sodium and 37 chloride ions to the aqueous phase. The total number of atoms in our models is about 56000. After insertion of the protein, the system was minimized using a steepest descent algorithm and then heated up to 300K in 1200 ps while keeping positional restraints on crystallographic Cα atoms (Cαs) that were slowly removed in two successive runs of 3 ns at 300K. Positional restraints on crystallographic Cαs were set to 1000 kJ mol-1 nm-2 and 100 kJ mol-1 nm-2, respectively. The all-atom CHARMM27[51] force field was used in combination with the TIP3P [52] model for water. The force field for non standard residue ergosterol was taken from[53] while the force field for PI(4)P was adapted from[54]. Electrostatic interactions were calculated with the Ewald particle mesh method[55] with a real space cutoff of 10 Å. Bonds involving hydrogen atoms were constrained using the LINCS algorithm[56] and the integration time step was set to 2 fs. The system was coupled to a Bussi thermostat[57] and to an isotropic Parrinello-Rahman barostat[57] at a temperature of 300K and a pressure of 1 atm. The MD trajectories described in the text are the following: two MD runs of 1 μs each of Osh4p bound to PI(4)P; one MD run of 1 μs of Osh4 bound to ergosterol.

All data analysis were done using GROMACS[38] utilities and all molecular images were made with Visual Molecular Dynamics (VMD)[39]. All analyses reported are performed over the last 500 ns of the trajectories; for PI(4)P the data are averaged over two independent trajectories.

47. Bigay, J. & Antonny, B. Real-time assays for the assembly-disassembly cycle of COP coats on liposomes of defined size. *Methods Enzymol.* **404**, 95-107 (2005).
48. Mendes, P. GEPASI: a software package for modelling the dynamics, steady states and control of biochemical and other systems. *Comput. Appl. Biosci.* **9**, 563-571 (1993).
49. Sali, A. & Blundell, T.L. Comparative protein modelling by satisfaction of spatial restraints. *J. Mol. Biol.* **234**, 779-815 (1993).
50. Shen, M.Y. & Sali, A. Statistical potential for assessment and prediction of protein structures. *Protein Sci.* **15**, 2507-2524 (2006).
51. Bjelkmar, P., Larsson, P., Cuendet, M. A., Bess, B., and Lindhal, E. . Implementation of the CHARMM force field in GROMACS: analysis of protein stability effect from correction maps, virtual site and water models. *J. Chem. Theory Comput.* **6**, 459-466 (2010).
52. Jorgensen, W.L., Chandrasekhar, J., Madura, J.D., Impey, R.W. & M.L., K. Comparison of simple potential functions for simulating liquid water. *J. Chem. Phys.* **79**, 926-935 (1983).
53. Cournia, Z., Smith, J. & Ullmann, G. A molecular mechanics force field for biologically important sterols. *J. Comput. Chem.* **26**, 1383–1399 (2005).
54. Lupyan, D., Mezei, M., Logothetis, D.E. & Osman, R. A molecular dynamics investigation of lipid bilayer perturbation by PIP2. *Biophys. J.* **98**, 240-247 (2010).
55. Essmann, U. et al. A smooth particle mesh Ewald method. *J. Chem. Phys.* **103**, 8577-8593 (1995).
56. Hess, B., Bekker, H., Berendsen, H.J.C. & Fraaije, J.G.E.M. LINCS: A linear constraint solver for molecular simulations. *J. Comput. Chem.* **18**, 1463-1472 (1997).
57. Parrinello, M. & Rahman, A. Polymorphic transitions in single-crystals - A new molecular-dynamics method. *J. Appl. Phys.* **52** 7182-7190 (1981).
58. Van der Spoel, D. et al. GROMACS: Fast, flexible and free. *J. Comput. Chem.* **26** 1701-1718 (2005).
59. Humphrey, W., Dalke, A. & Schulten, K. VMD: visual molecular dynamics. *J Mol. Graph.* **14**, 33-38, 27-38 (1996).

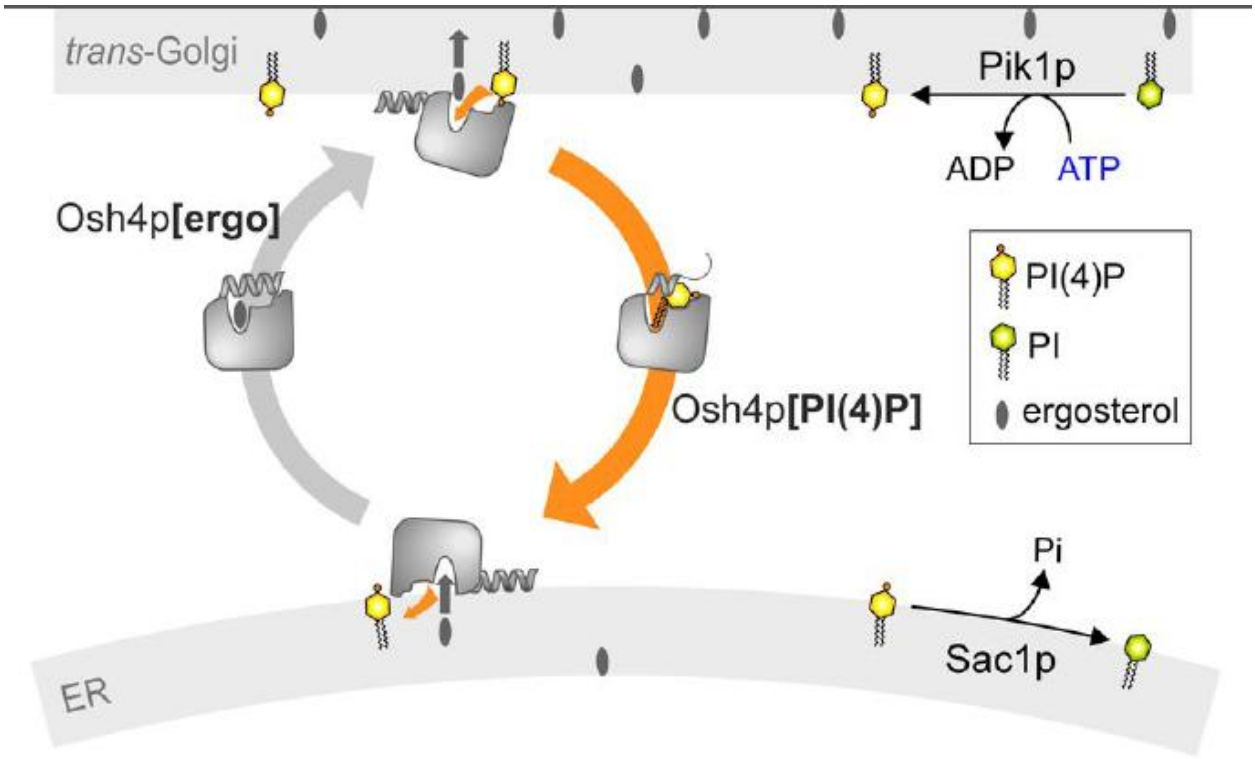
trans-Golgi
Pik1p
ADP
ATP
Osh4p[ergo]
Osh4p[PI(4)P]
PI(4)P
PI
ergosterol
Pi
Sac1p
ER

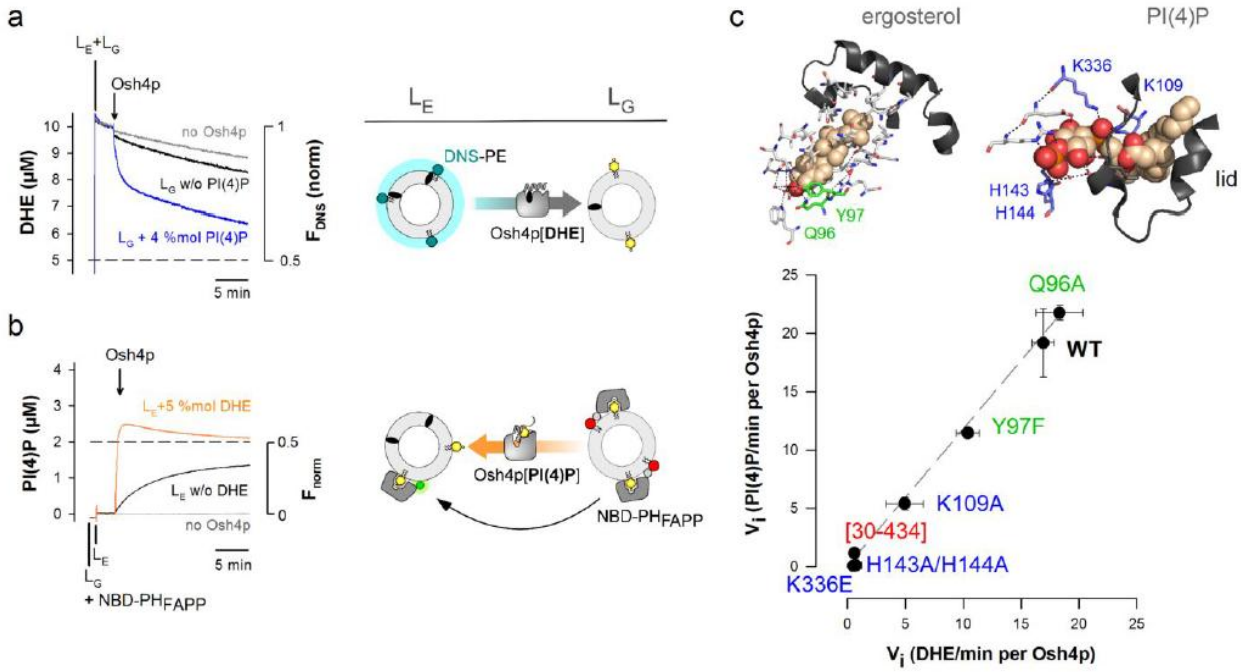
a
b
c
Osh4p
no Osh4p
DHE (μM)
PI(4)P (μM)
5 min
DNS-PE
Osh4p[DHE]
Osh4p[PI(4)P]
NBD-PHFAPP
ergosterol
PI(4)P
K336
K109
H143
H144
lid
Y97
Q96
Q96A
WT
Y97F
K109A
[30-434]
H143A/H144A
K336E
Vi (PI(4)P/min per Osh4p)
Vi (DHE/min per Osh4p)

Figure 2

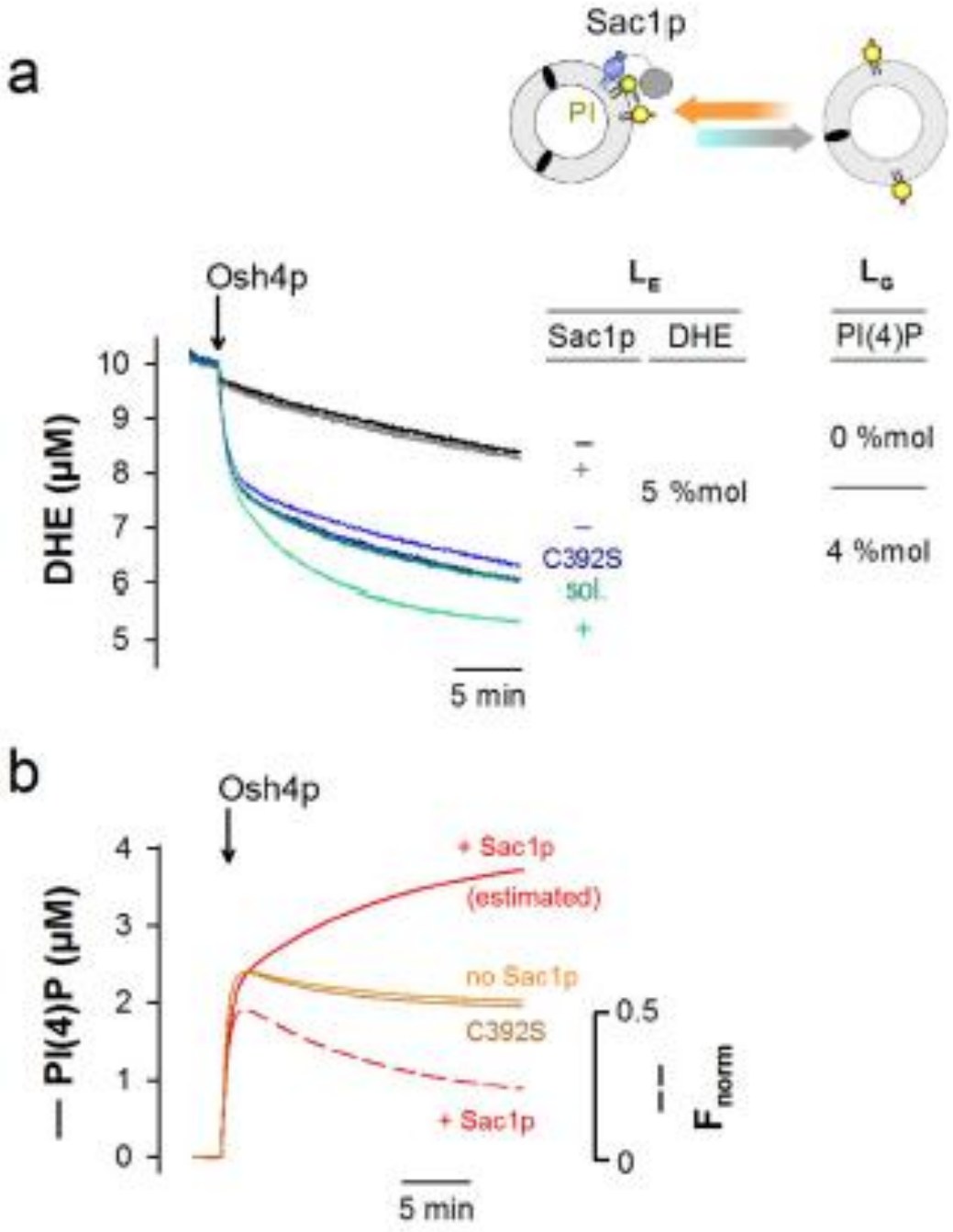
a
Sac1p
PI
Osh4p
L_E
Sac1p
DHE
L_C
PI(4)P
DHE (μM)
10
9
8
7
6
5
–
+
–
+
5 %mol
C392S
sol.
0 %mol
4 %mol
5 min
b
Osh4p
— PI(4)P (μM)
4
3
2
1
0
+ Sac1p
(estimated)
no Sac1p
C392S
+ Sac1p
0.5
0
F_{norm}
5 min

Figure 3

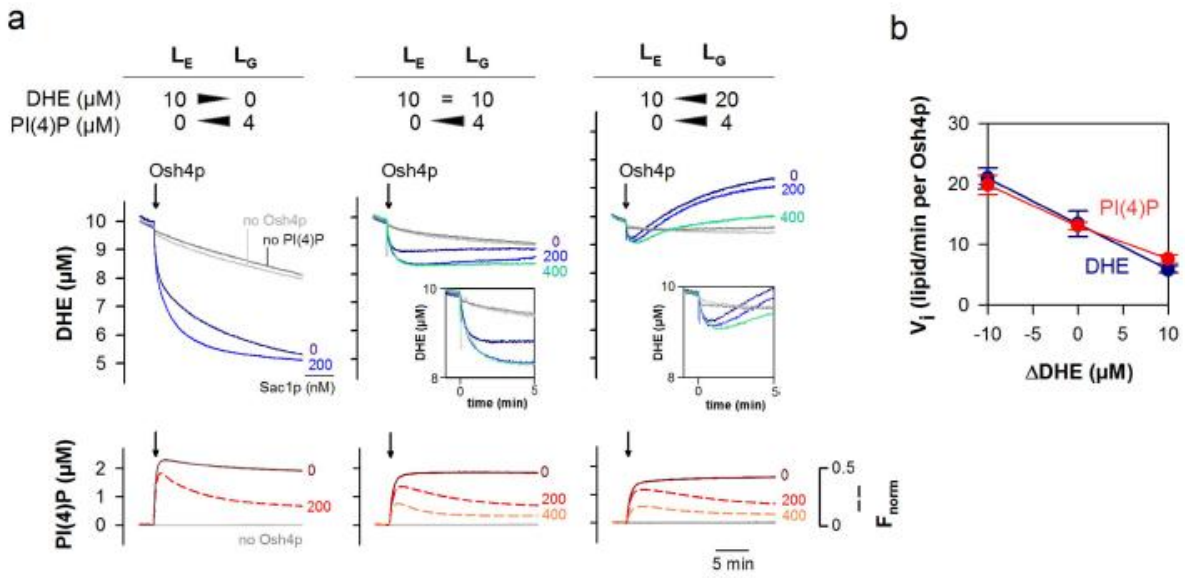
a
b
L_E L_G
DHE (μM) 10 0
PI(4)P (μM) 0 4
10 = 10
0 4
10 20
0 4
Osh4p
no Osh4p
no PI(4)P
DHE (μM)
Sac1p (nM)
0
200
400
time (min)
PI(4)P (μM)
5 min
F_{norm}
V_i (lipid/min per Osh4p)
ΔDHE (μM)
PI(4)P
DHE

Figure 4

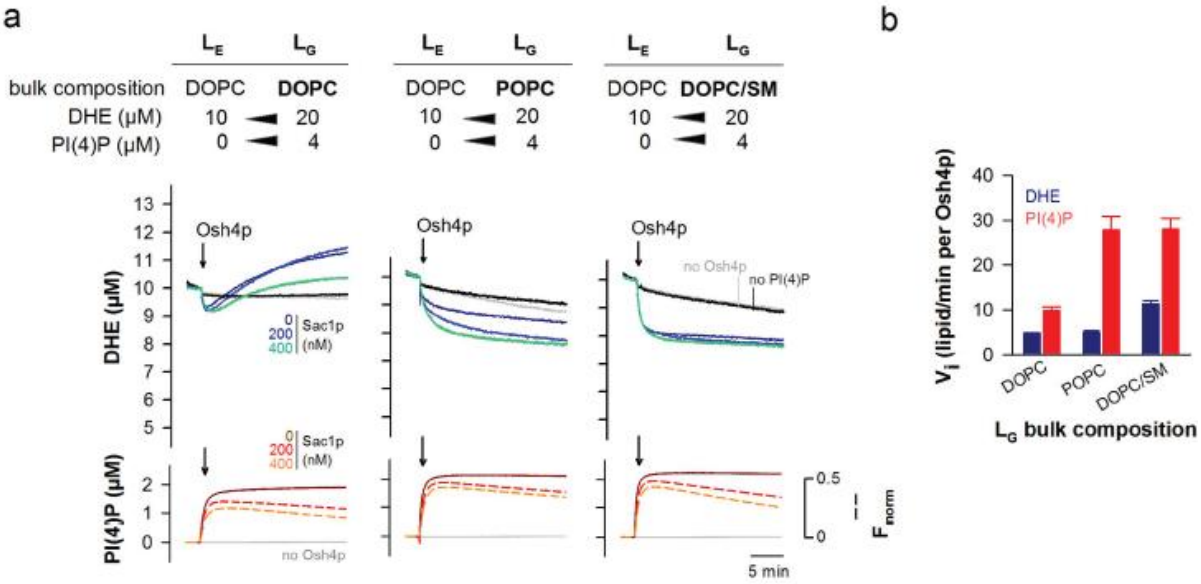
a
b
L_E
L_G
bulk composition
DOPC
DOPC
DOPC
POPC
DOPC
DOPC/SM
DHE (μM)
10
20
10
20
10
20
PI(4)P (μM)
0
4
0
4
0
4
Osh4p
Osh4p
Osh4p
no Osh4p
no PI(4)P
DHE (μM)
PI(4)P (μM)
0
200
400
Sac1p
(nM)
no Osh4p
5 min
F_norm
V_i (lipid/min per Osh4p)
DHE
PI(4)P
DOPC
POPC
DOPC/SM
L_G bulk composition

Figure 5

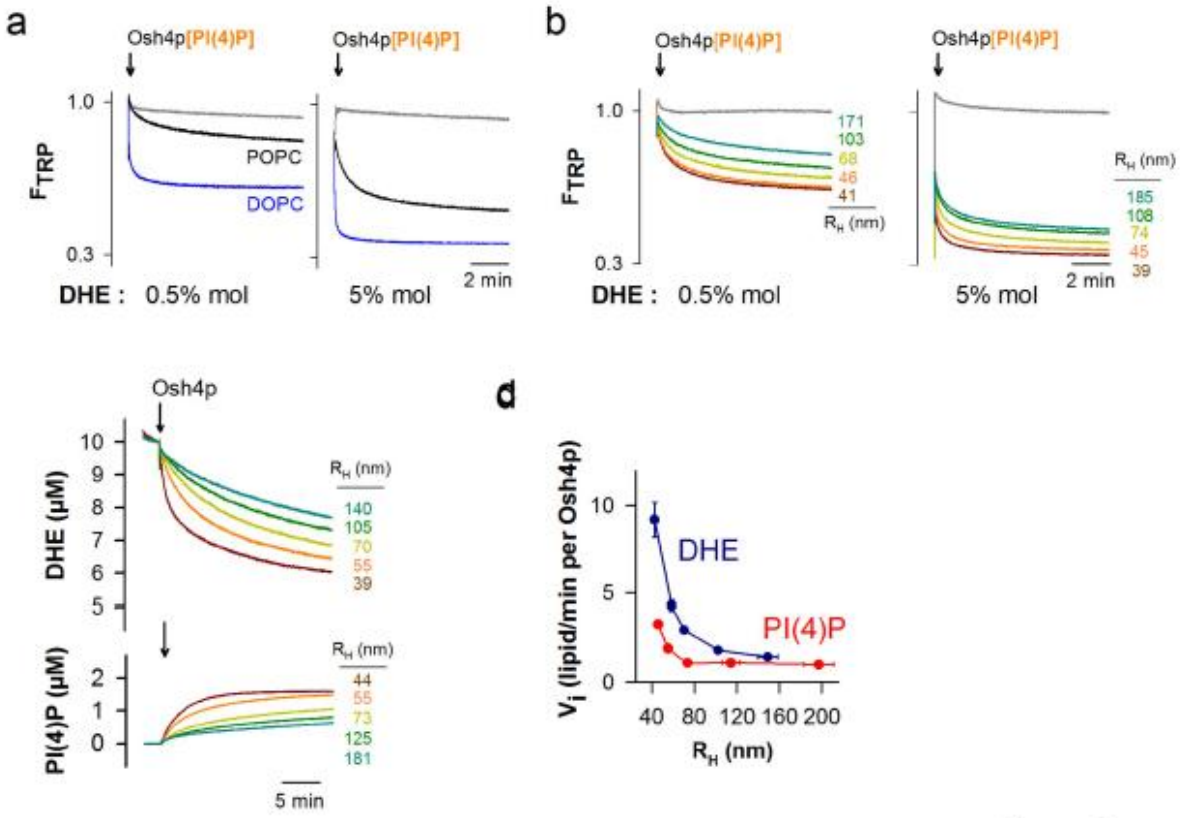
a
Osh4p[PI(4)P]
Osh4p[PI(4)P]
1.0
0.3
FTRP
POPC
DOPC
2 min
DHE : 0.5% mol
5% mol
b
Osh4p[PI(4)P]
Osh4p[PI(4)P]
1.0
0.3
FTRP
171
103
68
46
41
RH (nm)
RH (nm)
185
108
74
45
39
2 min
DHE : 0.5% mol
5% mol
Osh4p
DHE (μM)
10
9
8
7
6
5
RH (nm)
140
105
70
55
39
PI(4)P (μM)
2
1
0
RH (nm)
44
55
73
125
181
5 min
d
Vi (lipid/min per Osh4p)
10
5
0
DHE
PI(4)P
40 80 120 160 200
RH (nm)

Figure 6

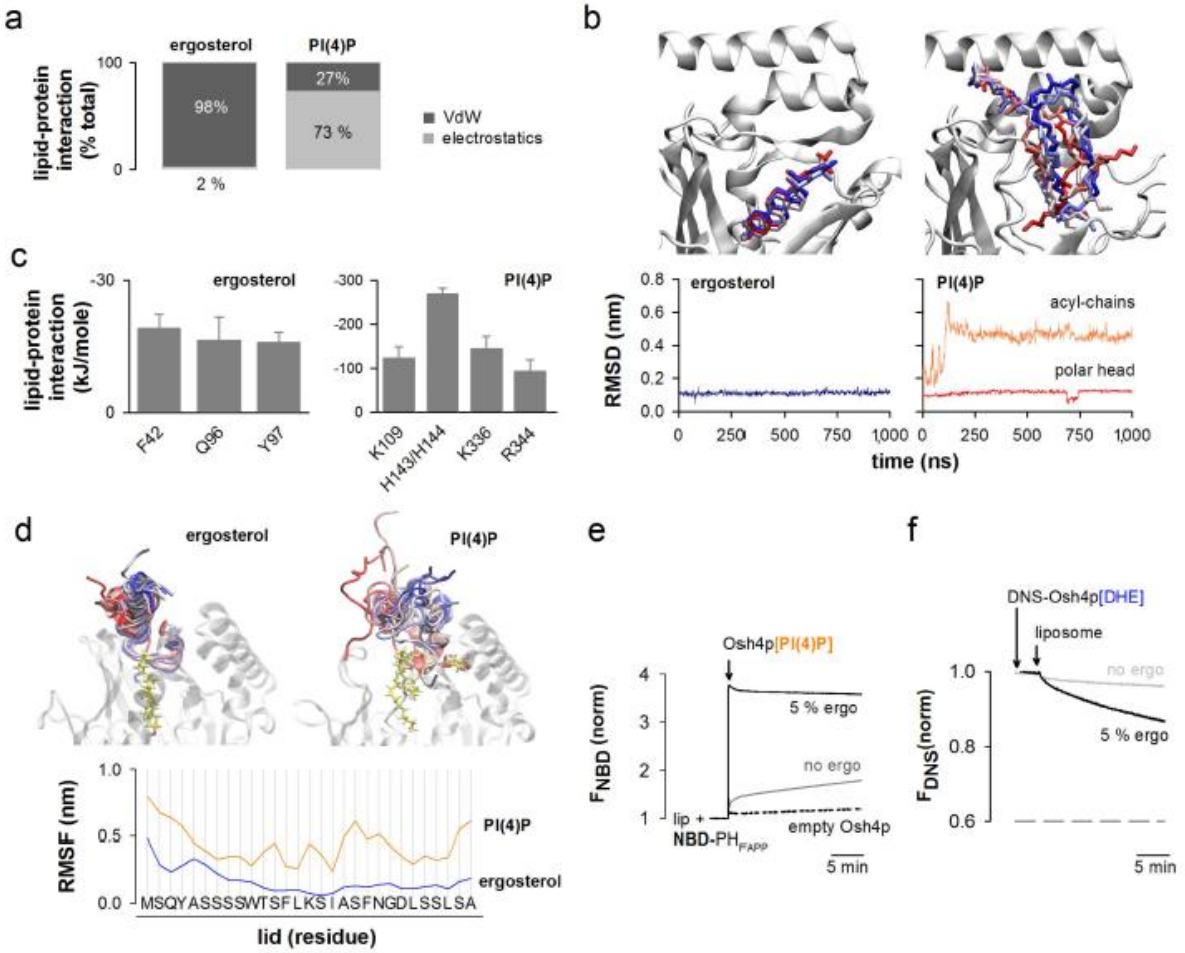
a
ergosterol
PI(4)P
lipid-protein interaction (% total)
100
0
98%
2 %
27%
73 %
VdW
electrostatics
b
ergosterol
PI(4)P
RMSD (nm)
acyl-chains
polar head
time (ns)
c
lipid-protein interaction (kJ/mole)
F42
Q96
Y97
K109
H143/H144
K336
R344
d
RMSF (nm)
MSQYASSSSWTSFLKSIASFNGDLSSLSA
lid (residue)
e
Osh4p[PI(4)P]
5 % ergo
no ergo
empty Osh4p
5 min
f
DNS-Osh4p[DHE]
liposome
no ergo
5 % ergo
5 min

Figure 7

SUPPLEMENTARY RESULTS

A phosphatiylinositol-4-phosphate powered exchange mechanism to create a lipid gradient between membranes. Joachim Moser von Filseck, Stefano Vanni, Bruno Mesmin, Bruno Antonny and Guillaume Drin*

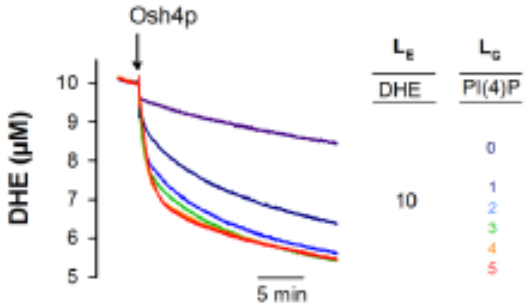

Supplementary Figure 1. The amount of PI(4)P in L_G liposome directly governs the transport of DHE mediated by Osh4p from L_E to L_G liposomes. Osh4p (200 nM) was added to DOPC/DNS-PE/DHE liposomes (92.5/2.5/5 mol/mol, 200 µM total lipids, L_E liposomes) and DOPC liposomes (200 µM total lipids, L_G liposomes) containing 0,1, 2, 3, 4, or 5 mol% PI(4)P. The FRET signal was converted into DHE concentration.

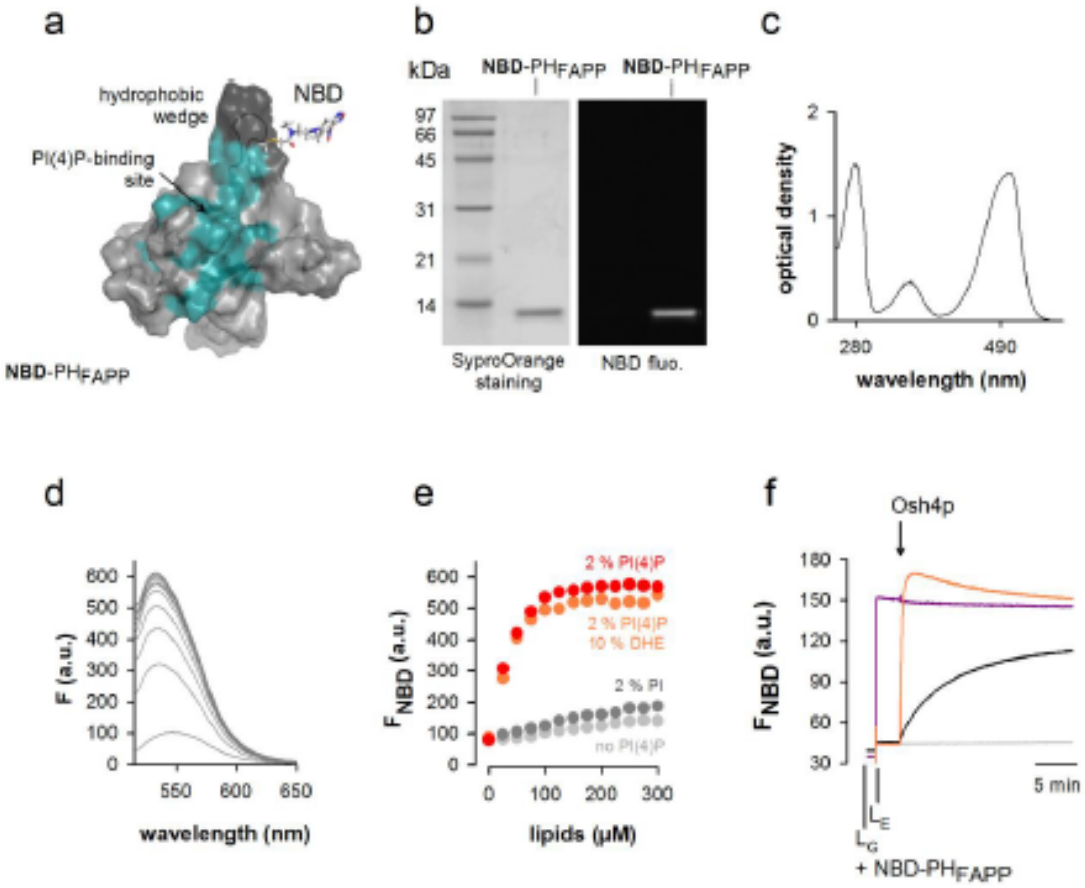

Supplementary Figure 2. Biochemical characterization of the NBD-PH$_{FAPP}$ PI(4)P sensor. (**a**) Tridimensional model of the NBD-labeled PH$_{FAPP}$ based on the NMR structure of the PH domain of the human FAPP1 protein (PDB ID: 2KCJ). The solvent-exposed cysteine C37 is mutated for serine; threonine T13 is replaced by a cystein. An N,N'-dimethyl-N-(thioacetyl)-N'-(7-nitrobenz-2-oxa-1,3-diazol-4-yl)ethylenediamine moiety (in stick, with carbon in grey, nitrogen in blue and oxygen in red), built manually and energetically minimized, is grafted to the thiol function of C13. The hydrophobic wedge (residues 8 to 16), is colored in dark grey and the PI(4)P-binding residues (Lenoir *et al.*, EMBO Rep. 11, 279-284 (2010)) are colored in green. The figure is prepared with PyMOL (http://pymol.org/). (**b**) SDS-PAGE of purified NBD-PH$_{FAPP}$. The gel was directly visualized in a fluorescence imaging system to identify labeled proteins (right picture) and then stained with Sypro Orange to visualize all proteins and molecular weight markers (left picture). (**c**) UV-visible absorption spectrum of NBD-PH$_{FAPP}$. Considering a purity grade of 100% for the protein, the optical density value at 280 nm (Trp) and 495 nm (IANBD) indicated that the PH domain was labeled with the probe in a 1:1 ratio. (**d**) Fluorescence spectrum of NBD-PH$_{FAPP}$ (250 nM) with increasing amount of large DOPC/PI(4)P liposomes (98/2 mol/mol; from 0 to 500 μM total lipids). (**e**) NBD intensity measured at 525 nm as function of total lipids concentration and for different membrane compositions (in mol/mol : DOPC, DOPC/PI(4)P 98/2, DOPC/PI 98/2, or DOPC/DHE/PI(4)P 88/10/2). NBD-PH$_{FAPP}$ only binds to PI(4)P-containing liposomes and this interaction is not impaired when membrane contains large DHE amounts (**f**) To convert the NBD signal in term of quantity of transported PI(4)P, we determined the NBD signal corresponding to a full equilibration of PI(4)P between L_E and L_G liposomes. NBD-PH$_{FAPP}$ (250 nM) was mixed with DOPC/PI(4)P liposomes (98/2 mol/mol, 200μM total lipids) and DOPC/PI(4)P/Rhod-PE liposomes (96 /2//2 mol/mol, 200 μM lipids).

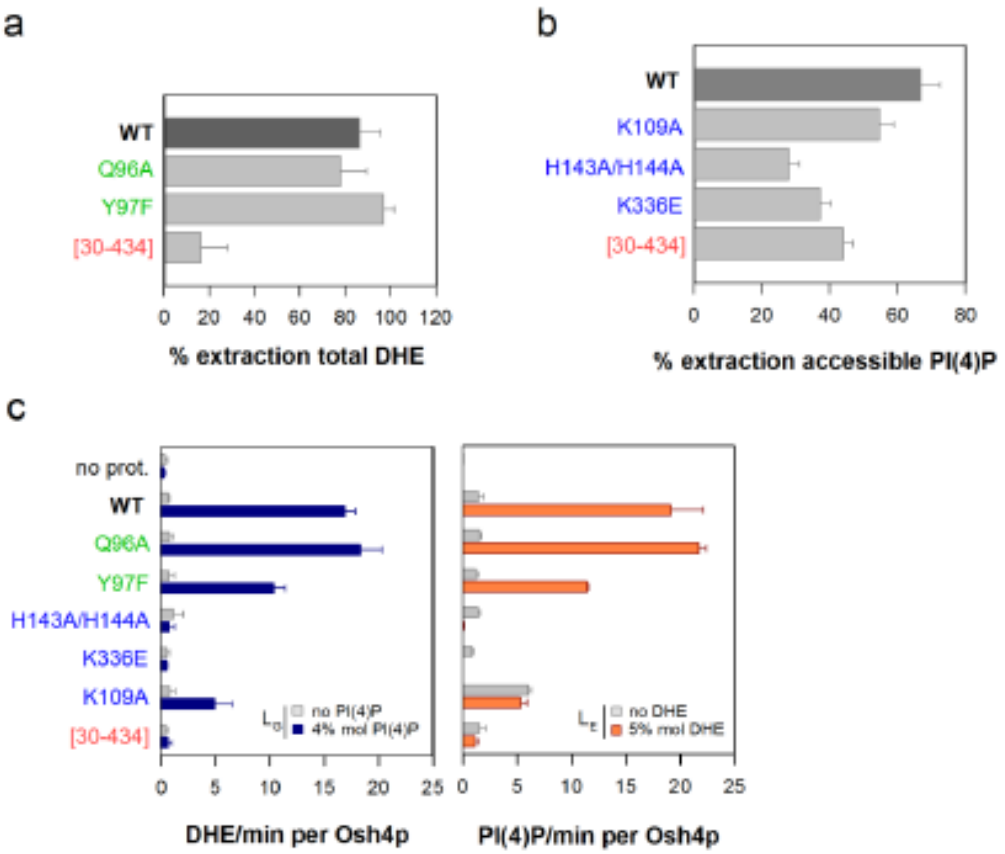

Supplementary Figure 3. Lipid extraction and transport ability of Osh4p mutants. (**a**) DHE extraction assay. DOPC liposomes (150 µM) containing 2.5 mol% DNS-PE and 2 mol% DHE were incubated with Osh4p WT or mutants (3µM) for 5 minutes at room temperature. The amount of extracted DHE was calculated by normalizing the dansyl signal measured in the absence and the presence of protein. (**b**) PI(4)P extraction assay. Sucrose-loaded DOPC liposomes (500 µM lipids), containing 2 mol% PI(4)P and doped with [^{32}P]PI(4)P, were incubated with Osh4p WT or mutants (5 µM) for 20 minutes at room temperature. After centrifugation, radioactivity in the supernatant and in the pellet was counted to calculate the fraction of extracted lipid. Data are represented as mean ± SEM (n=2-3). (**c**) *Left panel* : Osh4p WT or mutants (200 nM) were added to DOPC/DNS-PE/DHE liposomes (92.5/2.5/5 mol/mol, L_E liposomes, 200 µM total lipids,) mixed with DOPC liposome (L_G liposome, 200 µM) doped or not with 4 mol% PI(4)P at 30°C. The horizontal bar, corresponding to the initial transport rates, are indicated for each mutant (grey bars, 0 mol% PI(4)P ; dark blue bars, 4 mol% PI(4)P in L_G liposome). Data are represented as mean ± SEM (n = 2). *Right panel* : PI(4)P transport by Osh4p and mutants (200 nM) were measured with DOPC liposomes (200 µM total lipids, L_E liposome) doped or not with 5 mol% DHE and DOPC/PI(4)P/Rhod-PE liposomes (94/4/2 mol/mol, 200 µM lipids, L_G liposome). The initial transport rates are indicated for each mutant (grey bars, 0 mol% DHE; orange bars, 5 mol% DHE in L_E liposome). Data are represented as mean ± SEM (n = 2).

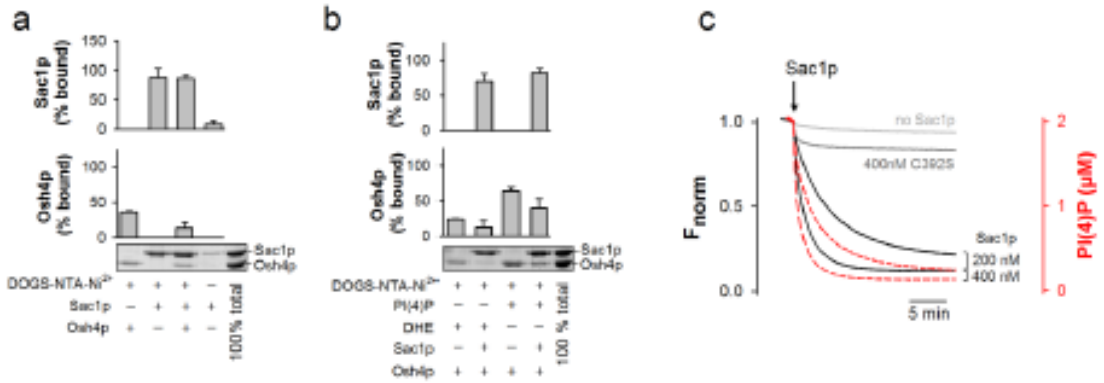

Supplementary Figure 4. Characterization of Sac1p[1-522]His$_6$ bound to liposomes (a) Flotation assays. Osh4p (750 nM), Sac1p[1-522]His$_6$ (750 nM) or both proteins were incubated with DOPC liposomes doped or not with 2 mol% DOGS-NTA-Ni^{2+} (750 µM total lipids). After centrifugation, the liposomes were recovered by centrifugation at the top of a sucrose cushion and analyzed by SDS-PAGE. The amount of protein recovered in the top fraction (lane 1 to 4) was quantified and the fraction of liposome-bound Osh4p and Sac1p, as reported in the upper panels, was determined by using the content of lane 5 (total 100%) as a reference. The error bars show the variation observed between two independent experiments. **(b)** Flotation assays. Osh4p (750 nM) was incubated with or without Sac1p[1-522]His$_6$ in the presence of DOPC liposomes (750 µM total lipids) containing 2 mol% DOGS-NTA-Ni^{2+} and either 5 mol% DHE or 4 mol% PI(4)P. **(c)** Hydrolysis activity of Sac1p attached to L_E liposomes as monitored with the PI(4)P sensor under condition where PI(4)P was equilibrated between L_E and L_G liposomes. Sac1p[1-522]His$_6$ or Sac1p[1-522](C392S)His$_6$ (200 or 400 nM) was incubated with DOPC/PI(4)P/Rhod-PE liposomes (92.5/2/2.5 mol/mol, 200 µM lipids) and DOPC/PI(4)P liposomes (98/2 mol/mol). The amount of hydrolyzed PI(4)P was calculated from the normalized NBD signal (see procedure in the Material and Methods section).

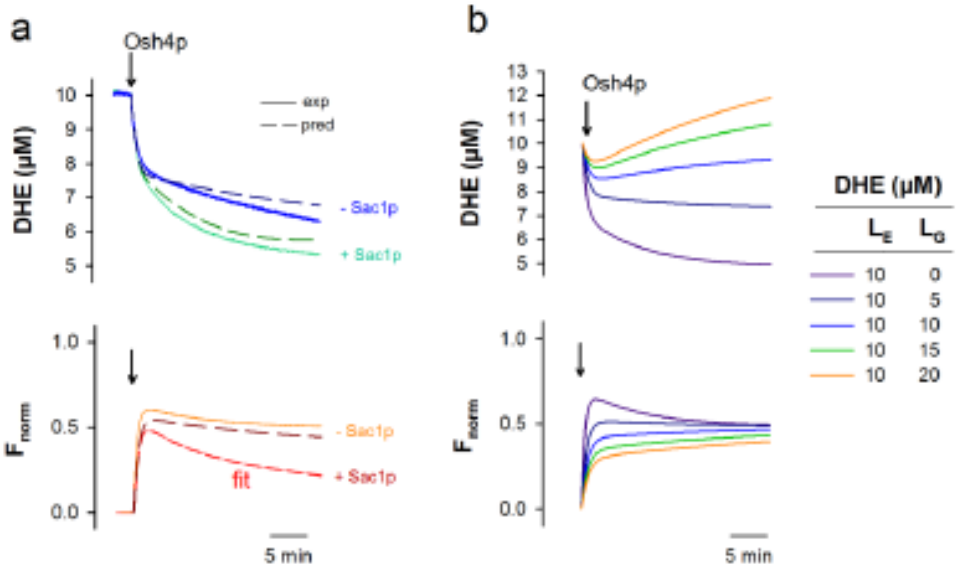

Supplementary Figure 5. Analysis of the kinetic trace of DHE and PI(4)P transport. (a) The kinetic traces of DHE and PI(4)P transport by 200 nM Osh4p in the presence or the absence of 200 nM Sac1p are represented (corresponding to experiments shown in **Fig3.a,b**). The kinetic constants associated with the sterol/PI(4)P exchange cycle model described in the Material and Method were optimized to fit the raw NBD trace measured in the presence of 200 nM Sac1p (dashed red line).The transport of PI(4)P (represented in **Fig.3b**) and DHE (upper panel, dashed dark green trace) were predicted. The lipid transport activity of Osh4p was also simulated for situations where Sac1p is absent (dashed dark red line, lower panel; dashed dark blue line, upper panel). (b) Simulated kinetic traces of Osh4p-mediated DHE/PI(4)P exchange as a function of a pre-existing DHE gradient between L_E and L_G membranes. NBD traces corresponding to several experiments in which Osh4p (200 nM) is added to DOPC/PI(4)P/Rhod-PE liposomes (96/4/2 mol/mol, 200 µM total lipids, L_G liposome) and L_E liposomes containing either 0, 5 or 10 mol% DHE in the presence of NBD-PH_{FAPP} (250 nM) were averaged (n=2-3 for each gradient condition). The three curves, each representing one gradient condition were individually fitted with the kinetic model. The parameters were averaged and adjusted to obtain a general model, which was then used to simulate the transport of PI(4)P (normalized signal F_{Norm}) and DHE for different initial DHE gradient between L_E and L_G liposomes.

Article II

A Four-Step Cycle Driven by PI(4)P Hydrolysis Directs Sterol/PI(4)P Exchange by the ER-Golgi Tether OSBP

Bruno Mesmin, Joëlle Bigay, Joachim Moser von Filseck,
Sandra Lacas-Gervais, Guillaume Drin and Bruno Antonny

"A Four-Step Cycle Driven by PI(4)P Hydrolysis Directs Sterol/PI(4)P Exchange by the ER-Golgi Tether OSBP"

Analyzing the architecture of OSBP, we were able to show that the N-terminal region, containing the PH domain and the FFAT motif are responsible for the targeting to these perinuclear structures that we identified to be ER-Golgi contact sites by thin-section electron microscopy. For the full length protein, this targeting is however controlled by binding of 25-OH (**Article Figure 1**). Using giant unilamellar vesicles, bead-supported bilayers and small liposomes we showed by transmission electron microscopy, fluorescence microscopy and dynamic light scattering that the PH-FFAT tandem efficiently aggregated functionalized bilayers containing VAP-A or Arf1-GTP and PI(4)P, respectively. (**Article Figure 2**) Interestingly, OSBP was capable of tethering artificial membranes in the absence of 25-OH *in vitro*. Trying to link this relocalization to a molecular function, we observed the Golgi PI(4)P level with a tagged version of the PH domain of OSBP, and we found that the levels were significantly decreased when OSBP was overexpressed. This decrease was found to be dependent on 25-OH binding and mutation of residues in OSBP corresponding to residues that are implied in PI(4)P binding in Osh4p, as well as deletion of the ORD. These findings imply that OSBP like Osh4p is capable of extracting and transport PI(4)P from Golgi membranes. Following the movement of DHE we observed that OSBP overexpression prevented retrograde movement of exogenous sterol to lipid droplets. (**Article Figure 3**) Jointly, these results suggested that OSBP transports cholesterol towards Golgi membranes in a PI(4)P-dependent manner.

We therefore assayed the sterol transport activity *in vitro* using the abovementioned FRET-based assay for following DHE transfer between artificial membranes. We observed little transfer by the full length OSBP, but proteolysis with trypsin produced fragments of different lengths that were capable of transporting DHE efficiently between liposomes. The active fragments all comprised the ORD of OSBP, whereas the PH-FFAT-containing fragments had little activity. (**Article Figure 4**) We thus tried to integrate the tethering activity of the PH-FFAT into the transport by the ORD by functionalizing the liposomes: DHE-containing, ER-mimicking liposomes were covered with VAP-A (by interaction of the VAP-A His_6-tag with Ni^{2+}-displaying lipids) and Golgi-mimicking liposomes were decorated with myristoylated

Arf1-GTP. DHE transport by OSBP was activated by both VAP-A and Arf1-GTP, though activation by VAP-A was a prerequisite for Arf1-GTP activation. (**Article Figure 5**)

Intrigued by the question whether PI(4)P could stimulate the transfer of DHE by OSBP in the same manner as for Osh4p, we replaced myristoylated Arf1-GTP by PI(4)P. The observed effect was complex: whereas PI(4)P increased the initial transport velocity of DHE transport by OSBP it became inhibitory after several transport cycles, decreasing the overall transport velocity. Integrating PI(4)P and control PIPs in the DHE-containing liposomes, only PI(4)P competed with DHE for extraction and reduced the DHE transport activity. This indicated a mutually exclusive DHE- and PI(4)P-binding as shown for Osh4p. Importantly, we showed using the NBD-PH_{FAPP} PI(4)P probe that OSBP is able to of extract and transports PI(4)P between artificial membranes. (**Article Figure 6**)

If OSBP transports both DHE and PI(4)P in opposite directions, why is counterexchange slowed after a certain number of exchange cycles? As PI(4)P is delivered to the DHE-containing membranes, it would compete with DHE for extraction by OSBP and thus block the DHE transport. In cells, PI(4)P is hydrolyzed by the ER-resident phosphatase Sac1. Hence we attached Sac1p-His_6 to Ni^{2+}-displaying lipids in addition to VAP-A and hydrolysis of PI(4)P *in cis* on the DHE-containing liposomes actually relieved the competition between the two lipids. To make sure that Sac1p would not act *in trans* on PI(4)P on the Golgi-mimicking liposomes we tested the phosphatase activity in absence of tethering between liposomes and with liposomes tethered by the PH-FFAT tandem that was shown not to transport PI(4)P. Sac1p was not capable of hydrolyzing PI(4)P *in trans*, contradictory to previous findings (Stefan, Manford *et al.* 2011). (**Article Figure 7**)

We have shown how OSBP uses retrograde transport of PI(4)P for anterograde transport of sterols both *in vivo* and *in vitro*. Maintenance of a PI(4)P gradient between membranes is a prerequisite for continuous sterol transport, as demonstrated in presence of the PI(4)P phosphatase Sac1p *in vitro*. Presence of PI(4)P also controls transport by another mechanism: The PH domain's PI(4)P recognition and Arf1-GTP-binding, together with VAP-A-recognition, allows OSBP to target both ER and TGN membranes and thus serve as a tethering factor to create a MCS. This would also explain why blocking OSBP with its high-affinity ligand 25-OH triggers its relocalization on the Golgi, as PI(4)P levels there are increased in absence of OSBP PI(4)P/cholesterol counterexchange. With PI(4)P providing both targeting to membranes and transport activity, kinase and phosphatase activity regulation

would allow regulation of sterol transport towards late membranes.

This could additionally affect transport of other lipids as OSBP regulates the recruitment of CERT and FAPP2 at ER-Golgi junctions. CERT transfers ceramide from the ER to *trans*-Golgi, in which ceramide is converted into SM, whereas FAPP2 is a glucosylceramide transporter at the same site. CERT and FAPP2 share a common domain organization with OSBP, comprising both a PI(4)P-specific PH domain and a FFAT motif. By modulating the Golgi PI(4)P pool, OSBP likely controls the presence of CERT and FAPP2 in ER-Golgi junctions. Such a mechanism would synchronize fluxes of sterol, ceramide and glucosylceramide, and eventually other lipids by controlling Nir2, thereby allowing co-enrichment of several lipids at the *trans*-Golgi, essential for the proper function of the secretory pathway (Drin 2014) (**Figure 44**).

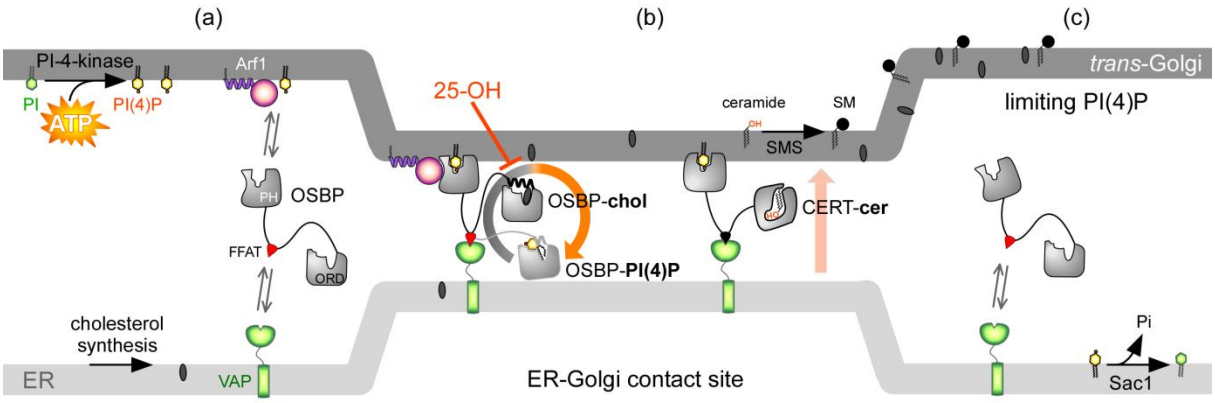

Figure 44. Function of OSBP at ER-Golgi contact sites.

(a) OSBP interacts through its FFAT motif with the ER-resident VAP receptors and, *via* its PH domain, with Arf1 (in the GTP-bound state) and PI(4)P. **(b)** As such, OSBP tethers the ER and the Golgi membrane and operates cycles of cholesterol/PI(4)P exchange, thereby creating a cholesterol gradient. This tethering activity could facilitate the recruitment of CERT by PI(4)P and VAP and allows synchronizing cholesterol and ceramide fluxes, thus guarantying the co-enrichment of sterol and SM in the *trans*-Golgi. **(c)** The consumption of PI(4)P would eventually trigger the disassembly of ER-Golgi contact sites and stop lipid transfer. 25-OH block the transport of sterol and would block the OSBP function, thereby increasing PI(4)P levels at the Golgi surface and a stable recruitment of OSBP in ER-Golgi contact sites. SM: sphingomyelin; SMS: sphingomyelin synthase. See also **Figure 7F**.

Cell

A Four-Step Cycle Driven by PI(4)P Hydrolysis Directs Sterol/PI(4)P Exchange by the ER-Golgi Tether OSBP

Bruno Mesmin,[1,3] Joëlle Bigay,[1,3] Joachim Moser von Filseck,[1] Sandra Lacas-Gervais,[2] Guillaume Drin,[1] and Bruno Antonny[1,*]
[1]Institut de Pharmacologie Moléculaire et Cellulaire, Université Nice Sophia Antipolis and CNRS, 06560 Valbonne, France
[2]Centre Commun de Microscopie Appliquée, Université Nice Sophia Antipolis, Parc Valrose, 06000 Nice, France
[3]These authors contributed equally to this work
*Correspondence: antonny@ipmc.cnrs.fr
http://dx.doi.org/10.1016/j.cell.2013.09.056

SUMMARY

Several proteins at endoplasmic reticulum (ER)-Golgi membrane contact sites contain a PH domain that interacts with the Golgi phosphoinositide PI(4)P, a FFAT motif that interacts with the ER protein VAP-A, and a lipid transfer domain. This architecture suggests the ability to both tether organelles and transport lipids between them. We show that in oxysterol binding protein (OSBP) these two activities are coupled by a four-step cycle. Membrane tethering by the PH domain and the FFAT motif enables sterol transfer by the lipid transfer domain (ORD), followed by back transfer of PI(4)P by the ORD. Finally, PI(4)P is hydrolyzed in *cis* by the ER protein Sac1. The energy provided by PI(4)P hydrolysis drives sterol transfer and allows negative feedback when PI(4)P becomes limiting. Other lipid transfer proteins are tethered by the same mechanism. Thus, OSBP-mediated back transfer of PI(4)P might coordinate the transfer of other lipid species at the ER-Golgi interface.

INTRODUCTION

Membrane contact sites (MCSs) are regions where the membranes of two organelles are closely apposed, typically 10–20 nm apart (Friedman and Voeltz, 2011; Helle et al., 2013; Levine, 2004). In a few cases, such structures are obvious by thin-section electron microscopy (EM) as the two membranes are aligned along significant distances. The best examples are contact sites between the endoplasmic reticulum (ER) and the plasma membrane (PM) in yeast (Manford et al., 2012; West et al., 2011). In most cases, however, more elaborate morphological approaches are required; for example, EM tomography of cryo-fixed preparations identified MCSs between a specialized region of the ER, called *trans* ER, and the *trans* Golgi (Ladinsky et al., 1999).

MCSs are diverse, but a recurrent observation is the involvement of the ER (Friedman and Voeltz, 2011; Helle et al., 2013; Levine, 2004). By making an extensive network, the ER is indeed in the best position to contact other cellular organelles. In addition, because the ER is the main site for lipid synthesis, MCSs suggest ways to supply lipids to a second membrane with limited lipid synthesis ability. This hypothesis is supported by the presence of proteins with lipid exchange activity in many MCSs (Helle et al., 2013; Lev, 2010; Levine, 2004).

MCSs between the ER and the Golgi contain the following lipid transporters: CERT, which transports ceramide (Hanada et al., 2003); FAPP2, which transports glucosylceramide (D'Angelo et al., 2007); Sec14/Nir2, which transports phosphatidylinositol (Litvak et al., 2005); and OSBP, which might transport cholesterol (Perry and Ridgway, 2006). ER-to-Golgi transfer of ceramide and glucosylceramide by CERT and FAPP2 are of key functional importance because they are mandatory for the synthesis of sphingomyelin and glycosphingolipids by enzymes present only in the *trans* Golgi (D'Angelo et al., 2007; Hanada et al., 2003). The function of OSBP is less clear, and it has been proposed that OSBP and related proteins (ORP in mammals, Osh in yeast) either sense or transfer sterols (Beh et al., 2012; Beh and Rine, 2004; Mousley et al., 2012; Raychaudhuri et al., 2006; Wang et al., 2005). Nevertheless, the presence of OSBP in zones where CERT and FAPP2 act is intriguing because coenrichment in sphingolipids and cholesterol is a hallmark of late (*trans* Golgi, endosomes and PM), as opposed to early (ER and *cis* Golgi), compartments. OSBP and other lipid transporters might work in a coordinated manner to control the composition of the *trans* Golgi using the reservoir of lipids present in the ER (Lev, 2010; Peretti et al., 2008).

OSBP, FAPP2, and CERT share a similar domain organization consisting of an N-terminal pleckstrin homology (PH) domain, a central FFAT motif (two phenylalanines in an acidic track), and a C-terminal lipid transport domain (Lev, 2010; Levine, 2004). The PH domain detects two determinants of the *trans* Golgi: the phosphoinositide PI(4)P and the small G protein Arf1-GTP (Godi et al., 2004; Levine and Munro, 2002). On the other hand, the FFAT motif binds specifically the type II ER membrane protein VAP (Furuita et al., 2010; Kaiser et al., 2005; Loewen et al., 2003; Mikitova and Levine, 2012). Thus, OSBP, FAPP2, and CERT are equipped to bridge the ER and the Golgi, although this tethering activity has not been recapitulated in vitro. As for

their C-terminal regions, they are structurally diverse and correspond to domains that can extract specific lipid species; for example, the OSBP-related domain (ORD) in the case of OSBP (Im et al., 2005) or the START domain in the case of CERT (Kudo et al., 2008). Overall, and despite differences between these transporters, their domain organization suggests a similar division of labor between the PH-FFAT tandem, which might bridge the ER and the Golgi, and the C-terminal domain, which conveys specific lipids between the two membranes.

OSBP has recently been identified as the target of several anticancer and antiviral compounds (Arita et al., 2013; Burgett et al., 2011) pointing to its important role in cellular homeostasis. However, how OSBP and its relatives function at membrane interfaces is poorly understood. Here, we use a combination of reconstitutions on artificial membranes and cellular approaches to address the mechanism of membrane tethering and lipid transfer by OSBP, as well as the coupling between these activities. We show that the PH-FFAT region of OSBP bridges membranes containing the ER protein VAP-A to membranes containing PI(4)P or Arf1-GTP. Furthermore, membrane bridging directs sterol transfer by the ORD domain. Surprisingly, however, the ORD domain in turn controls membrane tethering by the PH-FFAT region. This feedback is due to two additional reactions. First, PI(4)P is transported by the ORD domain, which, like the yeast protein Osh4, acts as a sterol/PI(4)P exchanger (de Saint-Jean et al., 2011). Second, PI(4)P, once transported back from the Golgi to the ER, becomes accessible to the PI(4)P phosphatase Sac1, which, in contrast to a previous report (Stefan et al., 2011), preferentially hydrolyzes PI(4)P in *cis* rather than in *trans*. This first complete reconstitution of a lipid transporter at ER-Golgi contact sites suggests a general way to couple a specific lipid transfer reaction with the back transfer and hydrolysis of PI(4)P.

RESULTS

OSBP Contains a Potent Membrane Tethering Region but Is Predominantly Cytosolic

To determine the ability of OSBP to tether the ER to the Golgi, we first compared the localization of full-length OSBP and a construct encompassing the PH domain, the coiled-coil region and the FFAT motif (PH-FFAT; Figure 1A). Both constructs were tagged with mCherry and cotransfected with a GFP version of the ER receptor VAP-A (GFP-VAP-A) in HeLa cells.

Figure 1B and Figure S1A (available online) show that OSBP is predominantly cytosolic, with some faint staining of the ER network, which is marked by GFP-VAP-A. In agreement with previous observations (Ridgway et al., 1992), the addition of the oxysterol 25-OH induced a dramatic shift in the localization of OSBP, which translocated completely to perinuclear structures (Figure S1A). This shift was accompanied by the displacement of VAP-A, which no longer decorated the ER network, but instead concentrated in the same perinuclear regions as OSBP (Figure 1B).

In contrast to OSBP, PH-FFAT was never cytosolic: even in the absence of 25-OH, it localized to perinuclear regions where VAP-A, but not a mutant deficient in FFAT motif binding (KM > DD), concentrated (Figures 1C and S1A). These regions were also positive for the *trans* Golgi marker TGN-46 (Figure S1B), thereby suggestive of ER-Golgi MCSs.

To further characterize the perinuclear regions where VAP-A and the OSBP constructs concentrated, we used thin-section EM. We observed extensive ER/Golgi apposed regions in cells treated with 25-OH and expressing VAP-A and OSBP, as well as in untreated cells expressing VAP-A and PH-FFAT (Figures 1D, S1C, and S1D). In some cases, Golgi cisternae and vesicles were completely enwrapped by the ER and lipid bilayers were systematically paired at an even distance of ~20 nm. Fluorescence recovery after photobleaching (FRAP) indicated that VAP and OSBP or PH-FFAT exchanged very slowly from such zones ($t_{1/2}$ > 5 min) compared to conditions where VAP and the OSBP constructs do not colocalize (Figures 1E and 1F).

We introduced point mutations in PH-FFAT to determine the molecular basis of membrane tethering. The R108L mutation, which prevents the interaction of the PH domain with PI(4)P (Levine and Munro, 2002), shifted the localization of PH-FFAT toward the ER (Figure S1E). Conversely, mutating the FFAT motif shifted the localization of PH-FFAT toward the Golgi (Figure S1E). Intriguingly, when the same mutations were introduced in full-length OSBP, the membrane association of this essentially soluble protein increased: the PH domain mutation promoted OSBP binding to the ER, whereas the FFAT motif mutation promoted OSBP binding to the Golgi (Figure S1F). Therefore, whereas the PH domain and the FFAT motif have additive effects for the localization of PH-FFAT at ER-Golgi MCS, they have a curious subtractive effect in the context of full-length OSBP.

These experiments indicate that the PH-FFAT tandem of OSBP is a very potent bridge to connect ER and Golgi membranes and that it does so by binding VAP-A via its FFAT motif and PI(4)P via its PH domain. However, in the context of full-length OSBP, the availability of the PH-FFAT tandem for membrane tethering is reduced and can be controlled by 25-OH, which targets the ORD.

Reconstitution of Membrane Tethering by the PH-FFAT Region of OSBP

We wished to recapitulate membrane tethering by the PH-FFAT tandem of OSBP in minimal systems. For this, we mixed purified PH-FFAT with two types of artificial liposomes (Figure 2A). Liposomes L_a contained a nickel lipid (DOGS-NiNTA) to which the cytosolic domain of VAP-A was attached through a C-terminal polyhistidine tag; liposomes L_b contained PI(4)P and/or were covered by Arf1-GTP (Figure 2B). As such, L_a and L_b mimicked the ER and the Golgi apparatus, respectively.

We first used dynamic light scattering (DLS) to follow liposome aggregation. Initially, the L_a + L_b mixture showed an apparent radius of ~70 nm. Upon PH-FFAT addition, the radius increased steadily, reaching values in the range of 500 nm within tens of minutes, suggesting massive liposome aggregation (Figure 2C), which was confirmed by negative stained EM (Figure 2D). Control experiments indicated that aggregation required VAP-A on L_a and Arf1-GTP or PI(4)P on L_b. At low tether concentration, the effects of Arf1-GTP and PI(4)P were additive; at high tether concentration, efficient tethering was observed with either Arf1-GTP or PI(4)P (Figure 2C).

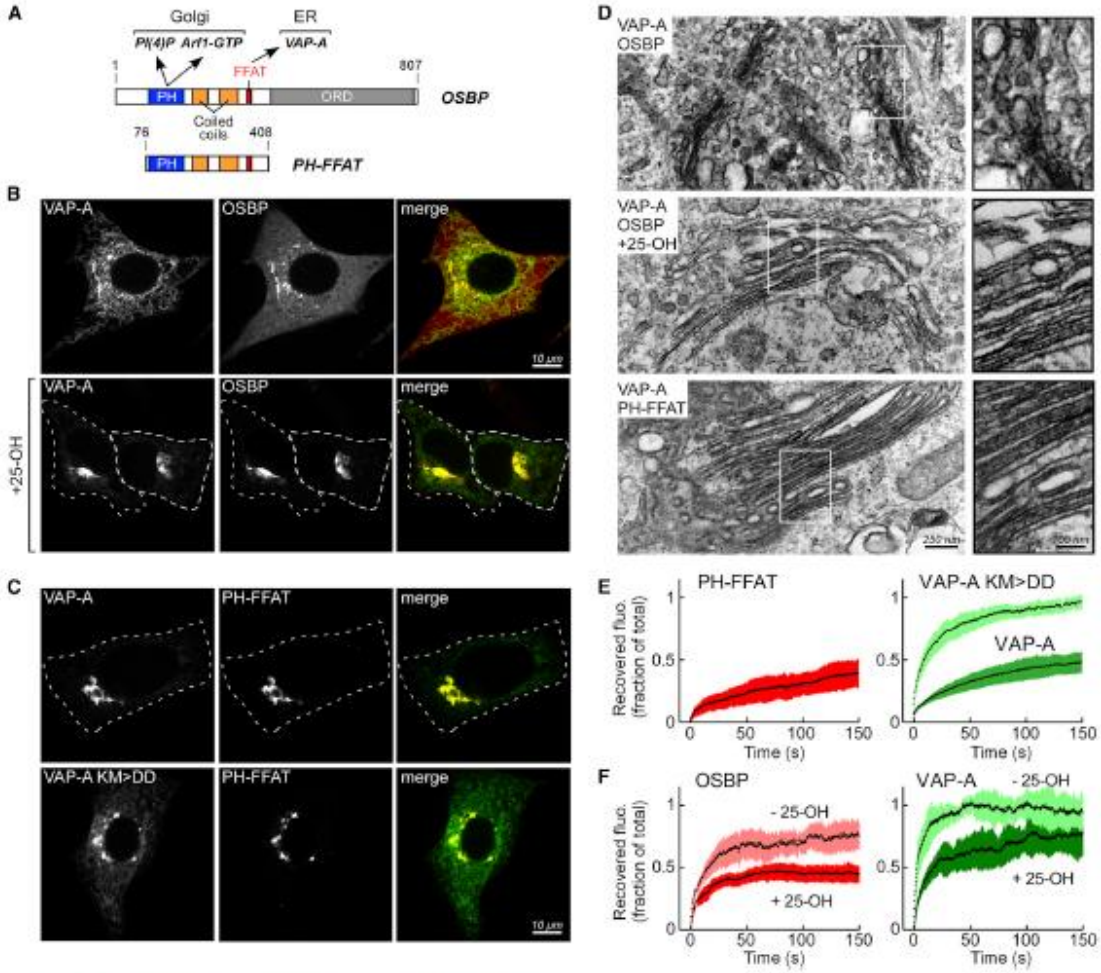

Figure 1. The PH-FFAT Region of OSBP Promotes ER-Golgi Tethering

(A) Domain organization of OSBP and of the PH-FFAT construct.

(B) HeLa cells coexpressing GFP-VAP-A and mCherry-OSBP; VAP-A labels the ER network, whereas OSBP is mostly cytosolic (top). Upon addition of 25-OH (6.5 μM, for 1 hr at 37°C), OSBP translocates to a perinuclear region where VAP-A also concentrates.

(C) HeLa cells expressing GFP-VAP-A and PH-FFAT-mCherry; the latter is enriched in perinuclear structures in which GFP-VAP-A concentrates. The VAP-A mutant deficient in FFAT binding (VAP-A KM > DD) remains spread in the ER network.

(D) Thin-section EM of cells expressing GFP-VAP-A and PH-FFAT-mCherry or mCherry-OSBP. Extended membrane-apposed regions are observed in cells treated by 25-OH and coexpressing VAP-A and OSBP and in cells coexpressing VAP-A and PH-FFAT. Magnifications of ER digitations within Golgi stacks are shown on the right.

(E and F) FRAP analysis of cells coexpressing GFP-VAP and PH-FFAT-mCherry (E) or GFP-VAP and mCherry-OSBP in the presence or in the absence of 25-OH (F). The traces show the mean of at least three experiments. Shaded areas represent SD.

See also Figure S1.

To further analyze PH-FFAT-mediated membrane tethering, we used artificial membranes that can be visualized by light microscopy, namely giant liposomes and bead-supported bilayers, which were labeled with red and green fluorescent lipids, respectively. PH-FFAT promoted the formation of extended contact zones between the giant liposomes, which carried VAP-A, and the bead-supported bilayers, which carried PI(4)P (Figure 2E; Movie S1). Contact zones were also observed when PH-FFAT was added to two populations of bead-supported bilayers with a similar segregation of membrane determinants (Figure 2F).

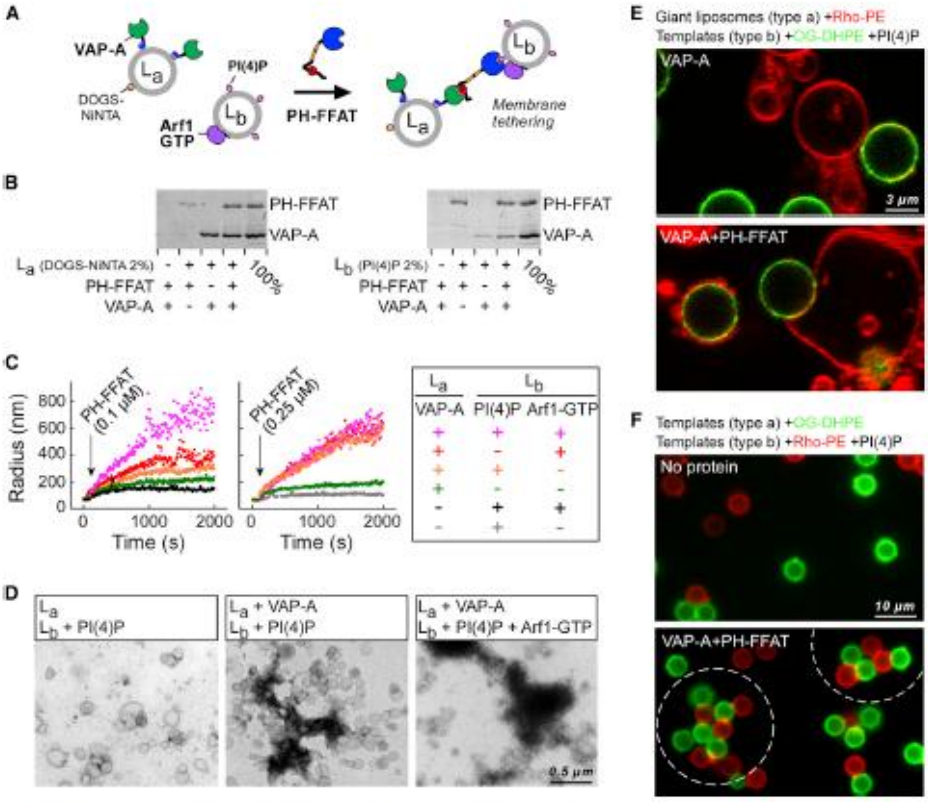

Figure 2. Reconstitution of Membrane Tethering by the PH-FFAT Region of OSBP

(A) Experimental strategy.

(B) Binding of the various constructs to liposomes L_a or L_b.

(C) Aggregation of L_a and L_b liposomes by PH-FFAT as followed by DLS. The determinants present on L_a and L_b are indicated in the table (VAP-A: 0.2 μM; accessible PI(4)P: 0.2 μM; Arf1-GTP: 0.2 μM).

(D) Electron micrographs of liposomes incubated with PH-FFAT as in (C).

(E) Confocal microscopy images of giant liposomes (red) covered with VAP-A through the nickel lipid DOGS-NINTA and mixed with bead-supported lipid bilayers (green) containing 2 mol % PI(4)P and with or without PH-FFAT.

(F) Same as in (E) with two populations of bead-supported bilayers.

See also Figure S2 and Movie S1.

Full-Length OSBP Promotes Membrane Tethering In Vitro Independently of 25-OH

Using the same assays, we compared the tethering activity of purified full-length OSBP to that of PH-FFAT. Given our cellular observations (Figure 1), we expected OSBP to be much less active than PH-FFAT. Surprisingly, OSBP readily promoted the tethering of lipid membranes containing Arf1-GTP and/or PI(4)P to lipid membranes containing VAP-A. In fact, under all conditions tested, OSBP was at least as efficient as PH-FFAT (Figures S2A–S2C). Furthermore, 25-OH, which promotes OSBP-mediated membrane tethering in cells, did not influence the tethering activity of OSBP in these reconstituted systems (Figure S2D). Thus, whereas the tethering activities of PH-FFAT in vivo and in vitro matched well (compare Figures 1C and 2), this was not the case for OSBP, which efficiently connected membranes in vitro (Figure S2), but not in cells, except in the presence of 25-OH (Figure 1B).

OSBP Changes the Cellular Distribution of Sterol and PI(4)P

Despite the lack of observable association of OSBP with organelles, we wondered whether the protein affects the distribution of its two putative lipid ligands: cholesterol and PI(4)P.

To follow the distribution of PI(4)P, we used a GFP fusion of the PH domain of OSBP, which has been shown to be a fair reporter of PI(4)P levels at the Golgi (Levine and Munro, 2002). In control cells, the PI(4)P probe stained the Golgi apparatus and showed minor cytosolic distribution (Figure 3A). In contrast,

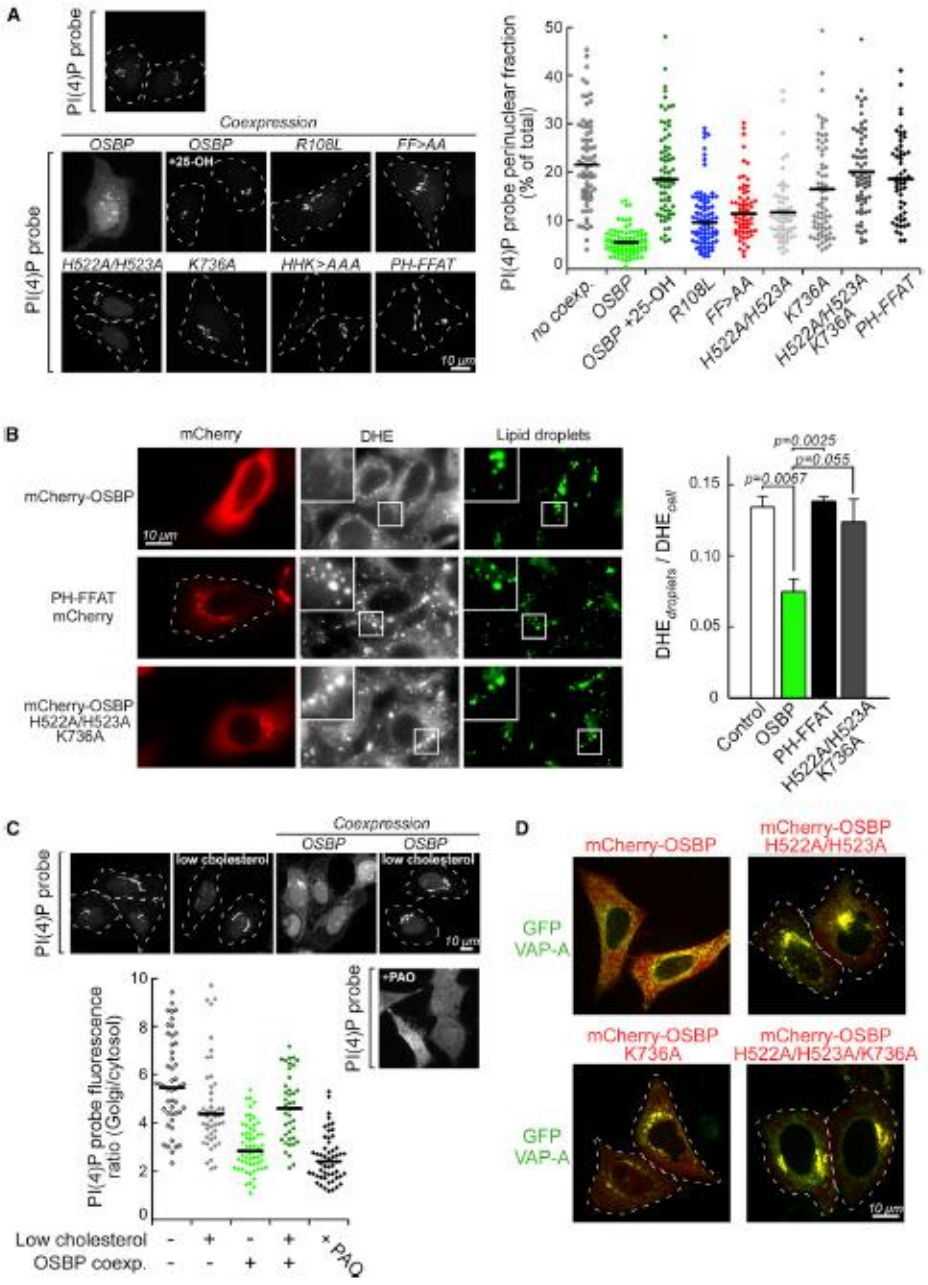

Figure 3. OSBP Affects the Cellular Distribution of Sterol and PI(4)P

(A) HeLa cells were transfected with a PI(4)P probe and various mCherry-OSBP constructs. The plot shows the amount of the PI(4)P probe in the perinuclear region. Measurements were performed on 50–80 cells for each condition using widefield fluorescence microscopy. Horizontal bars represent median values of the samples.

(legend continued on next page)

overexpression of OSBP caused a 3.5-fold drop in the Golgi staining by the probe (Figure 3A), suggesting a large decrease in the amount of PI(4)P in this organelle. Experiments using different forms of OSBP indicated that this decrease required a fully functional protein. First, mutations that compromise the interaction of OSBP with either VAP-A (mutation FF > AA in the FFAT motif) or PI(4)P (mutation R108L in the PH domain) made OSBP less efficient in reducing the PI(4)P level. Second, mutating two histidines and one lysine, which are strictly conserved in the ORD and essential for the extraction of PI(4)P by Osh4p (de Saint-Jean et al., 2011), abolished the drop in PI(4)P (Figures 3A and S3A). PH-FFAT, which lacks the ORD, also did not affect the localization of the PI(4)P probe. Third, 25-OH reversed the effect of OSBP on PI(4)P levels, causing relocalization of the PI(4)P probe to the Golgi (Figure 3A). Taken together these experiments suggest that OSBP controls the turnover of PI(4)P at the Golgi in a manner that involves its PH domain, its FFAT motif and its ORD. This effect requires the protein to not be blocked by 25-OH and involves the same residues that enable Osh4p to extract PI(4)P.

Visualizing cholesterol levels in cells is challenging due to its broad subcellular distribution and the lack of organelle-specific probes for this lipid. As a first step toward assessing the effect of OSBP on sterol trafficking, we pulse-labeled cells with dehydroergosterol (DHE), a naturally fluorescent analog of cholesterol, and chased it with an excess of cholesterol (Figure 3B). DHE can substitute for cholesterol because both have a very similar chemical structure in contrast to artificial fluorescent analogs (Mukherjee et al., 1998). In control cells, the exogenous addition of DHE caused immediate staining of the PM, followed within a few minutes of internal membranes and, after 1–2 hr, of lipid droplets (Figure 3B), indicative of a retrograde route from the PM to the ER, where lipid droplets form. In contrast, overexpression of OSBP, but not of PH-FFAT, prevented DHE incorporation in lipid droplets (Figure 3B). These experiments suggest that OSBP counteracts the retrograde traffic of sterols. However, they do not indicate at which location OSBP prevents this flux.

How can the inhibition of the flux of sterol from PM to lipid droplets be linked to the reduction of the Golgi pool of PI(4)P? The first effect leaves many possibilities for the exact site of OSBP action, whereas the second effect suggests that OSBP works at the ER-Golgi interface. Interestingly, mutations predicted to abolish PI(4)P binding (Figure S3A) prevented OSBP from counteracting the accumulation of DHE in lipid droplets (Figure 3B), suggesting that the two activities of OSBP are coupled.

Cholesterol is esterified and incorporated into lipid droplets when its level at the ER is high. Therefore, we hypothesized that OSBP exports sterol out of the ER at the expense of sterol incorporation into lipid droplets and in a manner that "consumes" PI(4)P at the Golgi. Specifically, OSBP might exchange the two lipids at the ER-Golgi interface. Measuring such an exchange in vivo and in the confined environment of Golgi/ER MCSs was, however, not possible. To determine if OSBP acts on the pool of cholesterol present in the ER, we used an alternative strategy: we lowered the level of cholesterol at the ER using lovastatin. As shown in Figures 3C and S3B, this treatment protected the pool of PI(4)P at the Golgi from being consumed by OSBP, which became trapped at the ER-Golgi interface. We concluded that OSBP controls the balance between sterol at the ER and PI(4)P at the Golgi.

Altogether, the experiments of Figures 3 and S3 suggest that the apparent cytosolic localization of OSBP is deceptive and masks an ephemeral interaction with the ER and the Golgi. In the case of PH-FFAT, we observe stable tethering because this construct acts solely as an ER-Golgi bridge. In contrast, OSBP via its ORD displaces PI(4)P from the Golgi (Figure 3A). Because PI(4)P contributes to the Golgi attachment of OSBP (via the PH domain), its displacement should eventually interfere with membrane tethering. In line with this hypothesis, OSBP mutants predicted to be deficient in PI(4)P transfer not only preserved the Golgi localization of the PI(4)P probe (Figure 3A) but also remained concentrated at ER-Golgi MCSs (Figure 3D). Therefore, OSBP might be controlled by a negative feedback loop whereby membrane tethering promotes sterol/PI(4)P exchange, which in turn impairs membrane tethering.

OSBP Is Autoinhibited for Sterol Transport

As a first step toward testing this feedback model, we assessed the lipid transport activity of OSBP in vitro. OSBP did not accelerate the exchange of the sterol DHE between liposomes that contained no determinants to promote binding of the PH-FFAT region (Figure 4A, black trace). We then submitted OSBP to limited proteolysis and observed a dramatic acceleration of DHE transfer, which paralleled the first steps of OSBP cleavage (Figure 4A, red traces). These results suggest that OSBP is autoinhibited for sterol exchange.

We analyzed the products of the proteolysis using N-terminal sequencing and gel filtration chromatography (Figures 4B, 4C, and S4). This analysis revealed a few major products: (1) a 43 kDa fragment encompassing the PH domain and the FFAT motif, (2) a 35 kDa fragment derived from the previous one but lacking the FFAT motif, (3) various fragments of 30–35 kDa corresponding to the N-terminal part of the ORD, and (4) a 20 kDa fragment corresponding to the remaining region of the ORD. In

(B) Epifluorescence images of HeLa cells pulse-chased with DHE and subsequently incubated for 2 hr at 37°C with 500 μM cholesterol-loaded MCD. Cells were labeled with the lipid-droplet marker LipidTOX green 15 min prior imaging. Note the absence of colocalization between DHE and LipidTOX in the mCherry-OSBP-transfected cells, but not in control cells or in cells transfected with the indicated OSBP mutants. Histogram represent quantification (±SE) of DHE colocalization with the lipid droplets from three independent experiments.

(C) HeLa cells were transfected with a PI(4)P probe and with or without mCherry-OSBP. To lower ER cholesterol, the cells were first incubated overnight in growth medium supplemented with 5% lipoprotein-deprived serum. Thereafter and 2 hr before imaging, 15 μM lovastatin was added to the medium in order to stop cholesterol biosynthesis. Under these conditions, OSBP does not promote disappearance of PI(4)P from the Golgi. Maximal and minimal PI(4)P staining at the Golgi were determined from two control experiments where HeLa cells expressing the PI(4)P probe only were treated or not with phenylarsine oxide (PAO, 10 μM, 5 min) to block PI(4)P biosynthesis. Measurements were performed on 40 to 50 cells for each condition using confocal microscopy.

(D) In contrast to wild-type mCherry-OSBP, the H522A/H523A, K736A, and triple mutants concentrated with VAP-A in the perinuclear region.

See also Figure S3.

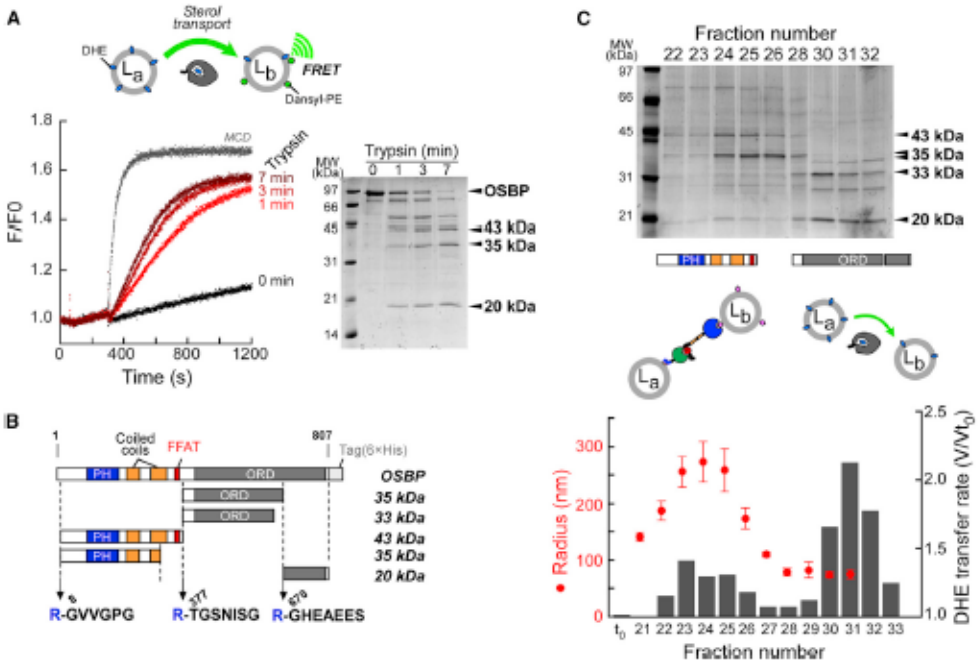

Figure 4. Analysis of Trypsin-Digested OSBP

(A) Time course of DHE transfer between donor and acceptor liposomes (63 μM lipids each) containing 18% DHE and 2.5% Dansyl-PE, respectively. Transfer was initiated by the addition of 1 mM MCD (gray trace), 0.1 μM OSBP (black trace), or the same amount of OSBP after digestion with trypsin for 1, 3, or 7 min at 30°C (light to dark red curves). Trypsin digestion was analyzed by SDS-PAGE.

(B) OSBP fragments generated by trypsin as identified by N-terminal sequencing.

(C) OSBP fragments from a 5 min digestion with trypsin were resolved by size-exclusion chromatography. Fractions were analyzed by SDS-PAGE and tested for DHE transfer (gray bars) and liposome tethering as in Figure 2C (red dots represent mean radius ± polydispersity).

See also Figure S4.

gel filtration chromatography, the first two products eluted at an apparent molecular weight (MW) of about ~80 kDa, suggesting dimerization through coiled-coil regions between the PH domain and the FFAT motif. The ORD fragments (30–35 and 20 kDa) co-eluted at a MW of 50 kDa, suggesting that cleavage of the ORD at position R_{669}-G_{670} does not promote separation of the domain parts. Membrane tethering activity was present in the first gel-filtration peak, whereas DHE exchange activity was present predominantly in the second peak (Figure 4C). This analysis confirms the division of labor in OSBP: the PH-FFAT tandem mediates membrane tethering and the ORD mediates lipid transport.

Sterol Transfer by OSBP Requires VAP-A and Is Facilitated by Arf1-GTP

To determine the mechanism by which OSBP becomes active for sterol transfer, we included various combinations of VAP-A, Arf1-GTP, and PI(4)P on the liposomes used for the DHE assay. The red trace in Figure 5A shows a representative time course of DHE transfer in an experiment where VAP-A was attached to L_a and Arf1-GTP was attached to L_b. Under such conditions, the rate of DHE transfer catalyzed by 10^{-7} M OSBP was very fast and close to that observed with 10^{-3} M methyl-β-cyclodextrin (MCD; Figure 5A, gray trace), indicating that OSBP has a 10,000-fold higher exchange activity than the drug.

Removing VAP-A from L_a abolished OSBP-catalyzed DHE transfer, whereas removing Arf1-GTP from L_b reduced the rate ~3-fold to 5-fold (Figures 5A–5C). Therefore, the interaction of OSBP with VAP-A is mandatory for sterol exchange, whereas the interaction with Arf1-GTP is helpful, but not strictly required. Titration experiments gave a half-stimulatory effect of 300 nM for VAP-A and of 100 nM for Arf1-GTP (Figures 5B and 5C). From the amounts of DHE and OSBP present (11 μM and 100 nM, respectively), we calculated that each cycle of sterol transfer takes about 2–3 s ($k = 0.3–0.5\ s^{-1}$) under optimal conditions (Figures 5B and 5C). 25-OH blocked OSBP-catalyzed transfer of DHE with a K_i of 50 nM (Figure 5D), a value compatible with the reported affinity of 25-OH for OSBP (~10 nM) (Ridgway et al., 1992).

To better characterize the mechanism of OSBP activation, we conducted experiments with soluble forms of VAP-A and Arf1-GTP. VAP-A retained a substantial stimulatory effect

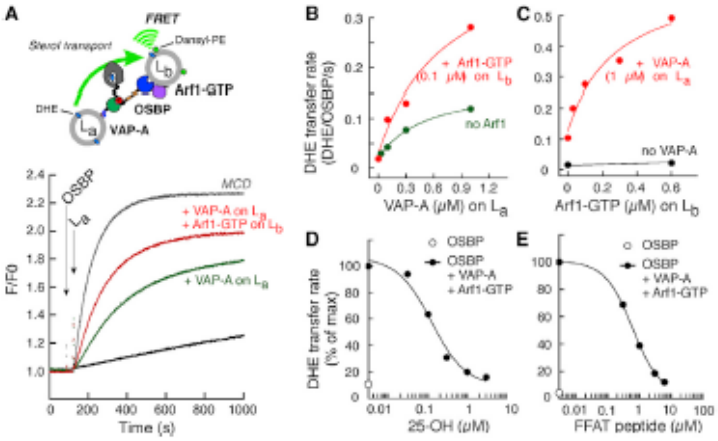

Figure 5. Membrane Tethering Controls the Sterol Transfer Activity of OSBP

(A) DHE transfer assay between liposomes L_a (63 μM lipids) and L_b (63 μM lipids) in the presence of 0.1 μM OSBP or 1 mM MCD. L_a and L_b were supplemented with 1 μM VAP-A and 0.1 μM Arf1-GTP, as indicated.

(B and C) Dose-response curves for the effects of VAP-A (B) or Arf1-GTP (C) on OSBP-mediated DHE transfer as measured in (A).

(D and E) Inhibitory effects of 25-OH (D) or the FFAT peptide (E) on OSBP-mediated DHE transfer. L_a and L_b contained 1 μM VAP and 0.1 μM Arf1-GTP, respectively.

See also Figure S5.

even in the absence of nickel lipids (Figure S5A), whereas soluble Arf1-GTP had no significant effect (Figure S5B). These observations suggest that VAP-A not only acts as a membrane anchor but also affects the conformation of OSBP, whereas Arf1-GTP acts primarily as a membrane anchor. The importance of the VAP-FFAT interaction in OSBP-mediated DHE exchange was underscored by the effect of a peptide corresponding to the FFAT motif, which completely blocked DHE transfer (Ki = 0.82 ± 0.15 μM, Figure 5E). As for the stimulatory effect of Arf1-GTP, it disappeared when the small G protein was attached to L_a instead of L_b (Figure S5B), suggesting that the membrane determinants of OSBP should be present on different liposomes to promote lipid exchange.

Complex Effect of PI(4)P on Sterol Transfer by OSBP

In membrane tethering assays, Arf1-GTP and PI(4)P had interchangeable roles, both promoting liposome aggregation by PH-FFAT (Figure 2C). In contrast, the effects of PI(4)P and Arf1-GTP on DHE transfer by OSBP were very different. In the presence of PI(4)P in L_b, the kinetics of DHE transfer from L_a to L_b displayed a biphasic shape (Figures 6A and S6A). During the first minute, DHE transfer occurred rapidly. Then, it abruptly slowed down. Considering that, under our conditions, the overall transfer of DHE from L_a to L_b requires about 50 cycles of OSBP-mediated DHE transfer, this observation suggests that PI(4)P becomes inhibitory after OSBP has undergone a few cycles (Figure S6B).

To explain these observations we envisaged that, through a mechanism akin to Osh4p (de Saint-Jean et al., 2011), the ORD of OSBP could extract PI(4)P from L_b and transfer it to L_a. As such, PI(4)P should gradually inhibit DHE transfer by two effects: competition with DHE on L_a for OSBP extraction and redirection of the PH domain of OSBP from L_b to L_a. In agreement with the competition hypothesis, PI(4)P strongly and specifically inhibited DHE transfer by trypsin-activated OSBP; i.e., under conditions where the ORD domain is dissociated from the PH-FFAT tandem (Figure 6B).

OSBP Is a PI(4)P Transporter

To directly address the ability of OSBP to transfer PI(4)P, we used a novel assay based on the detection of PI(4)P by a fluorescent PH domain, ^{NBD}PH. When PI(4)P is present in unlabeled liposomes, the fluorescence of membrane-bound ^{NBD}PH is high; when PI(4)P is present in liposomes containing a rhodamine lipid (Rho-PE), FRET occurs between ^{NBD}PH and Rho-PE at the expense of NBD fluorescence. As schematized in Figure 6C, PI(4)P is initially present in L_b, which also contain Rho-PE, resulting in low ^{NBD}PH fluorescence. PI(4)P transfer to L_a, which do not contain Rho-PE, causes an increase in the fluorescence of ^{NBD}PH.

Figure 6C demonstrates that OSBP, but not PH-FFAT, transfers PI(4)P from L_b to L_a and that this transfer is promoted by the presence of VAP-A. Of note, whereas OSBP was initially able to transfer PI(4)P with a rate comparable to that observed for Osh4p, the reaction slowed down significantly after a few rounds. As a result, less PI(4)P was transported compared to the reaction with Osh4p. This observation hints at a possible inhibition of OSBP activity as the PI(4)P transfer reaction proceeds, an effect reminiscent to what we observed for DHE transfer (Figure 6A).

Control of OSBP-Induced Membrane Tethering by the PI(4)P Phosphatase Sac1

We reasoned that OSBP, by being able to transfer PI(4)P in a VAP-A-dependent manner, should, in the context of ER-Golgi MCS, promote the transfer of PI(4)P from the *trans* Golgi, which is rich in this phosphoinositide, to the ER. There, PI(4)P could be hydrolyzed by the integral ER membrane protein Sac1 (Kim et al., 2013). This sequence of events would explain why OSBP reduces the amount of PI(4)P at the Golgi (Figure 3A) and why the combined effects of the PH domain and the FFAT motif are subtractive for the localization of full-length OSBP (Figure S1D): membrane tethering is followed by the transfer and degradation of PI(4)P, leading to membrane detachment of OSBP.

To test this hypothesis, we first used small interfering RNA (siRNA) against Sac1 in cells expressing OSBP and VAP-A. Strikingly, knocking down Sac1 completely shifted the localization of OSBP from an essentially cytosolic distribution to a perinuclear one where VAP-A colocalized (Figure 7A). Thus, in the cell,

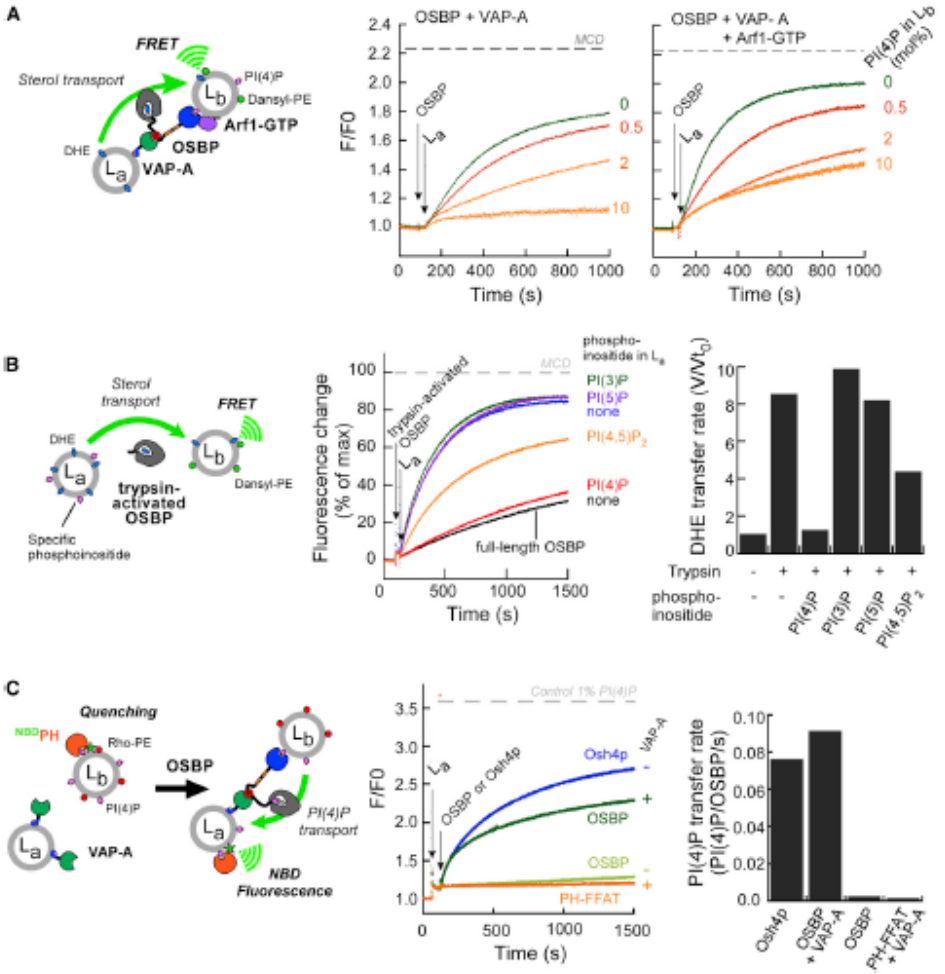

Figure 6. OSBP Transfers PI(4)P between Liposomes

(A) Transfer of DHE between liposomes L_a (63 μM lipids + 1 μM VAP-A) and L_b (63 μM lipids) in the presence of 0.1 μM OSBP. L_b were supplemented (right) or not (left) with 0.1 μM Arf1-GTP and contained increasing amounts of PI(4)P. Dashed line is fluorescence observed after DHE equilibration with 1 mM MCD.

(B) PI(4)P specifically inhibits the sterol transfer activity of trypsin-activated OSBP. DHE transfer was carried out as in Figure 4 except that specific phosphoinositides were incorporated at 2 mol % in liposomes L_a. Rates were normalized to that observed with full-length OSBP (black curve).

(C) Real-time measurement of PI(4)P transfer. ^{NBD}PH (250 nM) was mixed with L_b (300 μM lipids + 2 mol % PI(4)P +2.5 mol % Rho-PE). At t = 60 s, L_a (300 μM lipids ± 1 μM VAP) were added followed by Osh4p, OSBP, or PH-FFAT (all at 100 nM) at t = 120 s. Dashed line represents the signal for full equilibration of PI(4)P between L_a and L_b.

See also Figure S6.

OSBP has the ability to tether ER and Golgi membranes, but Sac1 counteracts this activity.

Next, we addressed the effect of Sac1 on the tethering activity of OSBP in vitro. For this, we mixed L_a and L_b liposomes to imitate the ER/*trans* Golgi interface and monitored liposome aggregation by DLS. Liposomes L_a were coated with both VAP-A and with Sac1 via their C-terminal polyhistidine tags, which replaced the juxtamembrane regions of these ER proteins. L_b contained PI(4)P. Thus, PI(4)P and Sac1 were initially present in different membranes, i.e., in a *trans* orientation. These experiments revealed a marked difference between full-length OSBP and PH-FFAT (Figure 7B): membrane tethering induced by OSBP strongly diminished in the presence of 5 to 10 nM Sac1, whereas membrane tethering induced by PH-FFAT was more resistant, diminishing significantly only at Sac1 concentration above 15 nM.

The experiments shown in Figures 7A and 7B suggest that Sac1 is the missing link for reconciling the in vitro and cellular observations. Adding Sac1 to liposome reconstitutions recapitulated the differences in the tethering activities of OSBP and PH-FFAT that were obvious in cellular experiments (Figures 1B and 1C). Conversely, depleting Sac1 from cells by siRNA rendered OSBP as efficient as PH-FFAT in Golgi-ER tethering, in agreement with our initial liposome reconstitutions where Sac1 was absent (Figures 2 and S2).

Sac1 Preferentially Hydrolyzes PI(4)P in *cis*

In Sac1, the catalytic site is cytosolic and is connected to the transmembrane domain with a putative 17 nm flexible linker. It has been proposed that this feature allows Sac1 to hydrolyze PI(4)P in *trans*, i.e., when PI(4)P is present in an apposed membrane (Stefan et al., 2011). However, we noted that the results of our tethering assay were more consistent with a *cis* activity of Sac1. In this assay, PI(4)P was initially present in *trans* from Sac1, yet Sac1 disrupted more efficiently membrane tethering by OSBP, which should transfer PI(4)P between the liposomes, than by PH-FFAT, which should leave the *trans* segregation unchanged (Figure 7B).

To directly address the optimal orientation of PI(4)P for Sac1-mediated hydrolysis, we monitored phosphate release using a green malachite assay. Again, L_a and L_b liposomes were mixed; the former contained DOGS-NiNTA to bind Sac1 and VAP-A, and the latter contained PI(4)P. PH-FFAT, which stably bridges these liposomes, thereby imposing a *trans* segregation of Sac1 and PI(4)P, did not promote PI(4)P hydrolysis (Figure 7C, gray circles). In contrast, OSBP, which transfers PI(4)P from L_b to L_a, stimulated PI(4)P hydrolysis in a VAP-A-dependent manner (Figure 7D). Control experiment in which PI(4)P was directly included in L_a demonstrated that Sac1 readily hydrolyzed PI(4)P in *cis* (Figure 7C, pink circles).

PI(4)P Hydrolysis by Sac1 Relieves OSBP Blockage

As aforementioned, the gradual inhibitory effect of PI(4)P on OSBP-catalyzed DHE transfer probably arises from PI(4)P backward transfer to the ER-like membrane (liposomes L_a), where it should antagonize DHE extraction. We predicted that Sac1, by hydrolyzing PI(4)P in *cis*, should relieve this inhibition. We thus repeated the DHE transport experiment in the presence of Sac1, which was attached to L_a together with VAP-A. As before, L_a contained DHE, whereas L_b contained PI(4)P. Strikingly, Sac1 had no effect on the initial fast phase of DHE transfer but strongly accelerated the second phase in a concentration-dependent manner (Figure 7E), except when 25-OH was present (Figure S7A). This observation demonstrates that VAP-A, OSBP, and Sac1 act in a sequential manner: VAP-A directs the orientation of OSBP, OSBP exchanges sterol for PI(4)P, and Sac1 specifically hydrolyses PI(4)P when this lipid becomes in *cis*. Another cycle of sterol/PI(4)P exchange can then resume until the pool of PI(4)P left in L_b is consumed.

DISCUSSION

Our work suggests a minimal model for how three proteins—the lipid transporter OSBP, the general ER receptor VAP-A, and the PI(4)P phosphatase Sac1—coordinate their activities to tether membranes, to promote the specific exchange of lipids between them and to make these events self-regulated over time. Our model includes four steps (Figure 7F), each of which we have reconstituted with minimal components: (1) membrane tethering, (2) forward sterol transfer, (3) backward PI(4)P transfer, and (4) PI(4)P hydrolysis. This last reaction makes the cycle irreversible and, when PI(4)P becomes limiting, acts as a timer to stop membrane pairing. In the following paragraphs, we discuss each step separately, and then envisage their coordination.

Step 1: Membrane Tethering

The PH-FFAT tandem of OSBP is an efficient membrane tether. In cells, it caused massive pairing of Golgi membranes with the ER (Figures 1C and 1D). In vitro, it promoted the aggregation of membranes in an asymmetric manner according to specific determinants (Figure 2): on the one hand, VAP-A, which interacts with the FFAT motif (Furuita et al., 2010; Kaiser et al., 2005); on the other hand, PI(4)P or Arf1-GTP, which interact with the PH domain (Godi et al., 2004; Levine and Munro, 2002). The next step will be to determine the structure of the entire PH-FFAT module. The presence of coiled coils between the PH domain and the FFAT motif suggests a dimeric rod-like structure (Figures S7B and S7C). This architecture, which is found in many tethering molecules, combines two advantages: it imposes a tether length and allows multivalent interactions with the membrane (Dumas et al., 2001). The predicted coiled coils of OSBP would give a rod of about 11 nm interrupted by an elbow. When the sizes of the other domains are taken into account, this length is compatible with the distance between tethered membranes observed in cells (~20 nm; Figures 1D and S7C).

Step 2: Sterol Transfer

The ability of OSBP to bind sterols and oxysterols is established (Ridgway et al., 1992). More debated is OSBP's function in sterol transfer. It has been argued that the rate of sterol transfer by Osh/ORP proteins is not fast enough to account for the quick redistribution of cholesterol between organelles (Beh et al., 2012). Using assays with high temporal resolution, we report a maximal turnover rate of 0.5 s^{-1}, i.e., 30 DHE transferred per OSBP and per minute (Figure 5C). This value is much faster than what has been measured in vitro for the transfer of ceramide by CERT, which is unambiguously a ceramide transfer protein (Hanada et al., 2003; Kawano et al., 2006). Therefore, OSBP seems intrinsically adapted to quickly transfer sterols between the ER and the Golgi.

Step 3: PI(4)P Transfer

We previously demonstrated that Osh4p exchanges sterol for PI(4)P between artificial membranes and resolved the structure of Osh4p in complex with PI(4)P (de Saint-Jean et al., 2011). Our experiments indicate that OSBP is also capable of transferring PI(4)P between membranes (Figure 6C). Furthermore, mutating conserved residues that allow Osh4p to extract PI(4)P prevented OSBP from reducing the PI(4)P level at the Golgi (Figure 3A). Thus, the ORD might be a general fold to exchange specific lipids with PI(4)P.

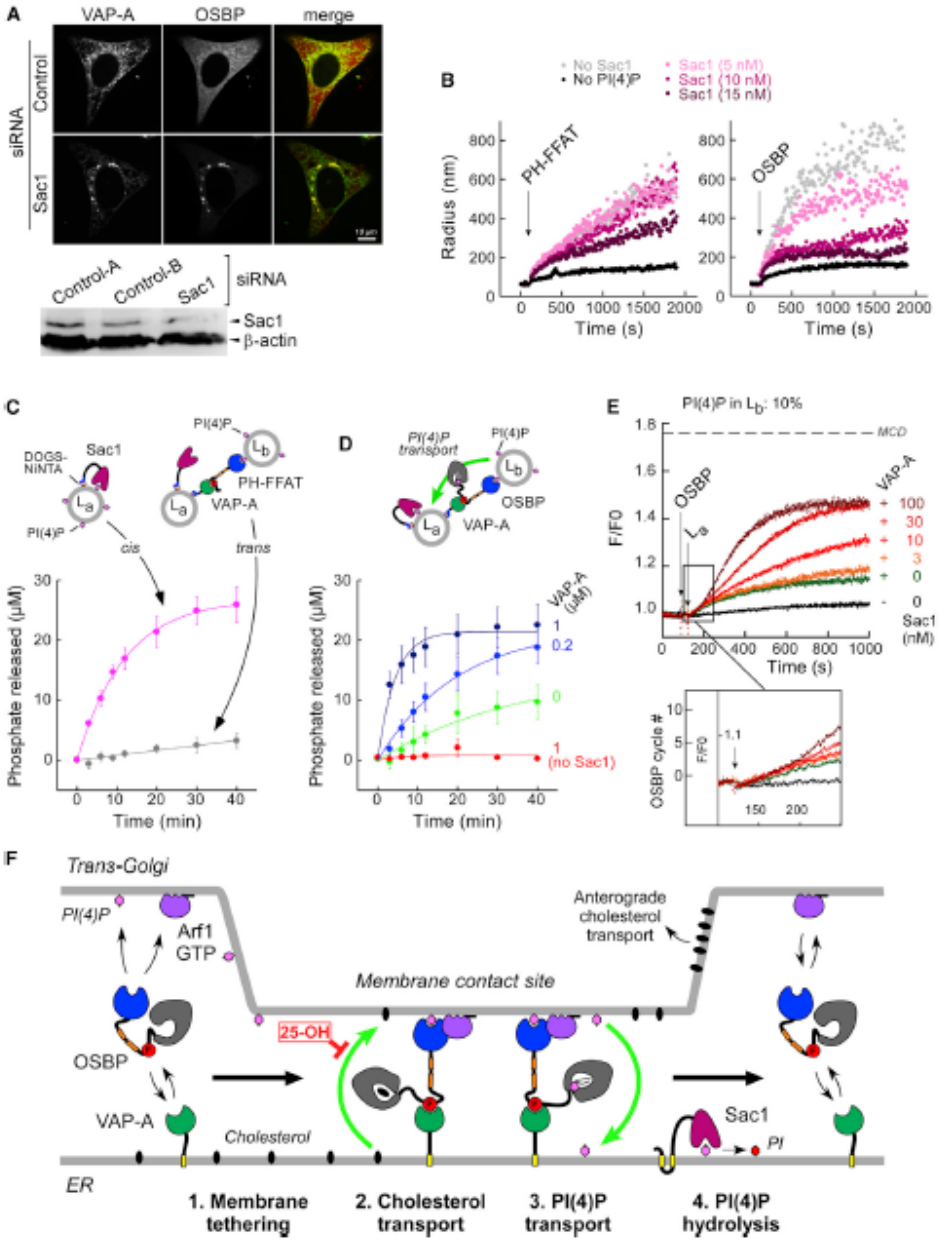

Figure 7. Sac1 Regulates OSBP-Mediated Membrane Tethering and Lipid Exchange

(A) HeLa cells expressing GFP-VAP-A and mCherry-OSBP were transfected with scrambled siRNA (control) or Sac1 siRNA and incubated for 24 hr in growth medium. OSBP and VAP-A moved to perinuclear areas in Sac1-silenced cells.

(B) Liposome tethering assay. The sample contained liposomes L_a (12.5 μM lipids, 2% DOGS-NINTA), L_b (12.5 μM lipids, 2% PI(4)P), 1 μM VAP, and increasing concentrations of Sac1. At t = 100 s, PH-FFAT (0.2 μM, left) or OSBP (0.2 μM, right) was added. Liposome aggregation was followed by DLS. Sac1 drastically reduced liposome tethering induced by OSBP, but not by PH-FFAT.

(legend continued on next page)

Step 4: PI(4)P Hydrolysis

PI(4)P is synthesized by specific PI-4-kinases at the Golgi and the PM, yet its phosphatase, Sac1, is an integral ER membrane protein (Kim et al., 2013). Recently, a mechanism has been proposed to solve this paradox: that Sac1p hydrolyses PI(4)P in *trans* (Stefan et al., 2011). All our results point to the opposite mechanism, whereby Sac1 hydrolyzes PI(4)P *in cis*, i.e., in the same membrane. PH-FFAT, which bridges very efficiently ER to Golgi membranes, thereby positioning Sac1 in *trans* toward PI(4)P, does not affect the cellular distribution of PI(4)P (Figure 3A). Recapitulating the *trans* segregation between Sac1 and PI(4)P using two liposome populations and PH-FFAT as a tether also does not promote PI(4)P hydrolysis (Figure 7C). In contrast, full-length OSBP, which transfers PI(4)P from *trans* to *cis* membrane, allows PI(4)P hydrolysis by Sac1 (Figure 7D). Thus, in the context of ER-Golgi MCSs promoted by OSBP, Sac1 works in *cis*, although we cannot exclude that it acts in *trans* in other circumstances. In yeast, Sac1 deletion causes PI(4)P to redistribute from the Golgi to other membranes, including the ER (Faulhammer et al., 2007; Roy and Levine, 2004), an observation that fits with a sequence of events in which PI(4)P hydrolysis occurs after its transfer from the Golgi to the ER.

Coordination between Membrane Tethering, Lipid Exchange, and PI(4)P Hydrolysis

PI(4)P hydrolysis by Sac1 allows multiple round of sterol transfer by OSBP in the presence of VAP-A (Figure 7E). This result demonstrates that OSBP functions in a cyclic manner by using the metabolic energy of PI(4)P and implies tight coupling between all steps of the cycle.

Conditions for efficient sterol transfer (step 2) parallel conditions for efficient tethering (step 1) (Figures 2C and 5A), suggesting that OSBP simultaneously contacts the ER and the Golgi during at least one step of its cycle. In the confined space between two apposed membranes, the ORD must move within distances ~four times larger than its own size (Figure S7C), implying a fascinating gymnastic. It seems that the PH-FFAT tandem not only restricts the diffusion of the ORD, but also plays an active role. First, the interaction between VAP-A and the FFAT motif is mandatory for lipid transfer by the ORD (Figures 5 and 6C). Second, sequence comparison between ORP/Osh proteins shows that the FFAT motif is localized at fixed distance from the ORD N terminus, which itself acts as a lid to control accessibility to the lipid-binding pocket (Im et al., 2005). Thus, the FFAT-VAP-A interaction is probably critical to unlock the ORD.

When OSBP harbors mutations preventing the ORD from extracting of PI(4)P (Figures 3A and 3D), it can no longer counteract retrograde sterol transport in cells (Figure 3B). Conversely, lowering the amount of cholesterol in the ER prevents OSBP from displacing PI(4)P form the Golgi (Figure 3C). Therefore, forward transport of sterol by OSBP at MCSs seems coupled to backward transport of PI(4)P. Direct demonstration of this coupling will require detecting simultaneously the exchange of these two lipids at MCSs. This task is very challenging in vivo, as it implies following the displacement of lipids within distances of tens of nanometers. In vitro, however, the fact that extended MCSs with a simple geometry can be recapitulated (Figure 2E; Movie S1) suggests possibilities for visualizing lipid movements using fluorescent analogs and probes.

Whereas the causality between membrane tethering (step 1), sterol transfer (step 2), and PI(4)P back-exchange (step 3) could be anticipated given the architecture of OSBP and the similarity between its ORD and Osh4p (Mesmin et al., 2013), the PI(4)P hydrolysis step (step 4) after retrograde transfer of PI(4)P, seems counterintuitive: by transferring PI(4)P to the ER where PI(4)P is hydrolyzed by Sac1, OSBP "shoots itself in the foot," eliminating a determinant that contributes to its own attachment. However, this reasoning is valid when the level of PI(4)P at the Golgi becomes limiting, i.e., when the *trans* Golgi looses its identity. When PI-4-kinases continuously regenerate PI(4)P at the *trans* Golgi, OSBP can cycle many times provided that Sac1 hydrolyses PI(4)P at the ER. For such an unidirectional cycle to function, it is essential that PI(4)P hydrolysis occurs in *cis*; if Sac1 acted in *trans*, it would burn PI(4)P prematurely, i.e., before sterol transfer. The OSBP cycle relies fundamentally on the segregation of VAP-A, Sac1, and PI4-kinases between the ER and the Golgi, which allows PI(4)P hydrolysis at the ER to provide the energy for sterol transfer. Interestingly, similar cycles may occur at other MCS: recent observations indicate that PI-4-kinases contribute to sterol enrichment at the PM where other ORP/Osh proteins act (Nakatsu et al., 2012). Because PI(4)P is present not only at the Golgi but also at the PM, further work is needed to determine the combinations of membrane determinants that direct the specific targeting of OSBP and its relatives to different membranes.

We note that the apparent coupling between various lipid transfer reactions at ER-Golgi MCSs (Peretti et al., 2008; Perry and Ridgway, 2006) can be explained on the basis of the OSBP cycle. FAPP2 and CERT rely on the same membrane determinants as OSBP. By controlling the amount of PI(4)P in the target membrane, OSBP could set the tempo for the delivery of precursors of complex lipids to the *trans* Golgi, thereby insuring that the concentrations of cholesterol and sphingolipids increase in parallel along the ER-Golgi interface.

CONCLUSIONS

The sequence of reactions that we demonstrate for OSBP invites a comparison with ion pumps. Through the use of metabolic

(C and D) Sac1 phosphatase assay. To test the *cis* orientation, Sac1 (50 nM) was added to liposomes L_a containing 2 mol % DOGS-NINTA and 20 mol % PI(4)P. To test the *trans* orientation, Sac1 (50 nM) was added to a mixture of L_a containing 2 mol % DOGS-NINTA and L_b containing 20 mol % PI(4)P. L_a and L_b were bridged with 0.2 μM PH-FFAT (C) or OSBP (D) in the presence of VAP (1 μM). When PI(4)P was initially present in *trans*, PI(4)P hydrolysis occurred in an OSBP- and VAP-A-dependent manner. Data represent average (±SE) from 3 to 6 independent experiments.

(E) Sac1 stimulates DHE transfer. The experimental conditions were the same as in Figure 6A except that increasing amounts of Sac1 were added. L_a contained 1 μM VAP. L_b contained 10% PI(4)P. Sac1 relieves the inhibition caused by PI(4)P after a few rounds of lipid transfer.

(F) Model of the OSBP cycle. For simplicity, only one OSBP monomer is shown.

See also Figure S7.

energy (phosphorylation and dephosphorylation of a catalytic residue), ions pumps cycle up to 100 times/s to maintain an asymmetric distribution of ions across lipid membranes (Palmgren and Nissen, 2011). Functionally, the OSBP cycle seems analogous, except that it helps to maintain an asymmetric distribution of lipids across a hydrophilic barrier using the metabolic energy of phosphoinositides.

EXPERIMENTAL PROCEDURES

Protein expression, purification, limited proteolysis, and gel filtration, as well as cell-culture conditions, transfections, and imaging, are described in the Extended Experimental Procedures.

Liposomes

The default composition of liposomes L_a and L_b was egg PC/brain PS/DOGS-NINTA (93/5/2 mol %) and egg PC/liver PE/brain PS/liver PI (66/19/5/10 mol %), respectively. Depending on the assay, DHE, Dansyl-PE, Rhodamine-PE, Oregon green-DHPE, and/or PI(4)P were included in the lipid composition as indicated. See the Extended Experimental Procedures for additional details.

Liposome Aggregation

Liposome aggregation was followed by DLS on mixtures containing liposomes L_a (25 μM lipids) ± VAP-A (200–250 nM) ± Sac1, and liposomes L_b (25 μM lipids) ± 200 nM Arf1-GTP ± 2 mol % PI(4)P. Aggregation was initiated by the addition of 100–250 nM PH-FFAT or 250 nM OSBP and was followed at 30°C by acquiring one autocorrelation curve every 10 s. Data were analyzed assuming a single Gaussian distribution, thus giving an average radius. See the Extended Experimental Procedures for additional details.

Tethering Assay with Giant Liposomes and Templates

Giant liposomes (type L_a + 2% Rhodamine-PE) were prepared by spontaneous formation. Bead-supported bilayers were prepared by incubating 5 μm silica beads for 30 min with liposomes (type L_b, 200 μM, 2% Oregon green-DHPE). Tethering was initiated by adding the giant liposomes loaded with 250 nM VAP-A to the bead-supported bilayers (5 μM lipids) in the presence of 250 nM PH-FFAT or OSBP. Fluorescence images were acquired with a confocal microscope using a 63× objective. See the Extended Experimental Procedures for details.

DHE Microscopy

DHE imaging was carried out using a Leica DMIRBE microscope equipped with an Andor iXon3 blue-optimized EMCCD camera and Semrock BrightLine fluorescence filters (320/40 nm bandpass filter, 347 nm dichroic beamsplitter, and 390/40 nm bandpass filter). Images were acquired using a 100×/1.3 oil objective. See the Extended Experimental Procedures for additional details.

DHE and PI(4)P Transfer Assays

For DHE transfer, the sample initially contained liposomes L_b (±PI(4)P ± Arf1-GTP) and VAP-A-His, FFAT peptide, or 25-OH as indicated. Liposomes L_a (18% DHE) and OSBP were then added. FRET between DHE and Dansyl was measured at 525 nm (excitation: 310 nm). For PI(4)P transfer, liposomes L_b (2% Rho-PE) were incubated with ^{NBD}PH and with VAP-A as indicated. NBD emission was measured at 510 nm (excitation 460 nm). At the indicated times, liposomes L_a and OSBP were added. See the Extended Experimental Procedures for details.

Sac1 PI(4)P Hydrolysis Assay

Liposomes L_a were incubated with Sac1 and with the indicated amounts of VAP-A and OSBP or PH-FFAT. The reaction was initiated by the addition of liposomes L_b (20% PI(4)P). At the indicated times, an aliquot was withdrawn, mixed with 50 mM NEM, and supplemented with malachite green reagent for phosphate quantification. For the experiment in the *cis* orientation, L_a were supplemented with 20% PI(4)P. See the Extended Experimental Procedures for additional details.

SUPPLEMENTAL INFORMATION

Supplemental Information includes Extended Experimental Procedures, seven figures, and one movie and can be found with this article online at http://dx.doi.org/10.1016/j.cell.2013.09.056.

ACKNOWLEDGMENTS

We thank Céline Thonont, Frédéric Brau, Julie Cazareth, and Nathalie Leroudier for technical assistance; Fabien Alpy, Scott Emr, and Franck Perez for reagents; Alenka Copic for comments on the manuscript; and all members of the laboratory for discussions. This work is supported by the CNRS, the Agence Nationale de la Recherche ("jeune chercheur" ANR-10-JCJC-1503-01 and "Investments for the Future" ANR-11-LABX-0028-01), and by an ERC advanced grant (268888).

Received: April 19, 2013
Revised: July 12, 2013
Accepted: September 23, 2013
Published: November 7, 2013

REFERENCES

Arita, M., Kojima, H., Nagano, T., Okabe, T., Wakita, T., and Shimizu, H. (2013). Oxysterol-binding protein family I is the target of minor enviroxime-like compounds. J. Virol. *87*, 4252–4260.

Beh, C.T., and Rine, J. (2004). A role for yeast oxysterol-binding protein homologs in endocytosis and in the maintenance of intracellular sterol-lipid distribution. J. Cell Sci. *117*, 2983–2996.

Beh, C.T., McMaster, C.R., Kozminski, K.G., and Menon, A.K. (2012). A detour for yeast oxysterol binding proteins. J. Biol. Chem. *287*, 11481–11488.

Burgett, A.W., Poulsen, T.B., Wangkanont, K., Anderson, D.R., Kikuchi, C., Shimada, K., Okubo, S., Fortner, K.C., Mimaki, Y., Kuroda, M., et al. (2011). Natural products reveal cancer cell dependence on oxysterol-binding proteins. Nat. Chem. Biol. *7*, 639–647.

D'Angelo, G., Polishchuk, E., Di Tullio, G., Santoro, M., Di Campli, A., Godi, A., West, G., Bielawski, J., Chuang, C.C., van der Spoel, A.C., et al. (2007). Glycosphingolipid synthesis requires FAPP2 transfer of glucosylceramide. Nature *449*, 62–67.

de Saint-Jean, M., Delfosse, V., Douguet, D., Chicanne, G., Payrastre, B., Bourguet, W., Antonny, B., and Drin, G. (2011). Osh4p exchanges sterols for phosphatidylinositol 4-phosphate between lipid bilayers. J. Cell Biol. *195*, 965–978.

Dumas, J.J., Merithew, E., Sudharshan, E., Rajamani, D., Hayes, S., Lawe, D., Corvera, S., and Lambright, D.G. (2001). Multivalent endosome targeting by homodimeric EEA1. Mol. Cell *8*, 947–958.

Faulhammer, F., Kanjilal-Kolar, S., Knödler, A., Lo, J., Lee, Y., Konrad, G., and Mayinger, P. (2007). Growth control of Golgi phosphoinositides by reciprocal localization of sac1 lipid phosphatase and pik1 4-kinase. Traffic *8*, 1554–1567.

Friedman, J.R., and Voeltz, G.K. (2011). The ER in 3D: a multifunctional dynamic membrane network. Trends Cell Biol. *21*, 709–717.

Furuita, K., Jee, J., Fukada, H., Mishima, M., and Kojima, C. (2010). Electrostatic interaction between oxysterol-binding protein and VAMP-associated protein A revealed by NMR and mutagenesis studies. J. Biol. Chem. *285*, 12961–12970.

Godi, A., Di Campli, A., Konstantakopoulos, A., Di Tullio, G., Alessi, D.R., Kular, G.S., Daniele, T., Marra, P., Lucocq, J.M., and De Matteis, M.A. (2004). FAPPs control Golgi-to-cell-surface membrane traffic by binding to ARF and PtdIns(4)P. Nat. Cell Biol. *6*, 393–404.

Hanada, K., Kumagai, K., Yasuda, S., Miura, Y., Kawano, M., Fukasawa, M., and Nishijima, M. (2003). Molecular machinery for non-vesicular trafficking of ceramide. Nature *426*, 803–809.

Helle, S.C., Kanfer, G., Kolar, K., Lang, A., Michel, A.H., and Kornmann, B. (2013). Organization and function of membrane contact sites. Biochim. Biophys. Acta *1833*, 2526–2541.

Im, Y.J., Raychaudhuri, S., Prinz, W.A., and Hurley, J.H. (2005). Structural mechanism for sterol sensing and transport by OSBP-related proteins. Nature *437*, 154–158.

Kaiser, S.E., Brickner, J.H., Reilein, A.R., Fenn, T.D., Walter, P., and Brunger, A.T. (2005). Structural basis of FFAT motif-mediated ER targeting. Structure *13*, 1035–1045.

Kawano, M., Kumagai, K., Nishijima, M., and Hanada, K. (2006). Efficient trafficking of ceramide from the endoplasmic reticulum to the Golgi apparatus requires a VAMP-associated protein-interacting FFAT motif of CERT. J. Biol. Chem. *281*, 30279–30288.

Kim, Y.J., Hernandez, M.L., and Balla, T. (2013). Inositol lipid regulation of lipid transfer in specialized membrane domains. Trends Cell Biol. *23*, 270–278.

Kudo, N., Kumagai, K., Tomishige, N., Yamaji, T., Wakatsuki, S., Nishijima, M., Hanada, K., and Kato, R. (2008). Structural basis for specific lipid recognition by CERT responsible for nonvesicular trafficking of ceramide. Proc. Natl. Acad. Sci. USA *105*, 488–493.

Ladinsky, M.S., Mastronarde, D.N., McIntosh, J.R., Howell, K.E., and Staehelin, L.A. (1999). Golgi structure in three dimensions: functional insights from the normal rat kidney cell. J. Cell Biol. *144*, 1135–1149.

Lev, S. (2010). Non-vesicular lipid transport by lipid-transfer proteins and beyond. Nat. Rev. Mol. Cell Biol. *11*, 739–750.

Levine, T. (2004). Short-range intracellular trafficking of small molecules across endoplasmic reticulum junctions. Trends Cell Biol. *14*, 483–490.

Levine, T.P., and Munro, S. (2002). Targeting of Golgi-specific pleckstrin homology domains involves both PtdIns 4-kinase-dependent and -independent components. Curr. Biol. *12*, 695–704.

Litvak, V., Dahan, N., Ramachandran, S., Sabanay, H., and Lev, S. (2005). Maintenance of the diacylglycerol level in the Golgi apparatus by the Nir2 protein is critical for Golgi secretory function. Nat. Cell Biol. *7*, 225–234.

Loewen, C.J., Roy, A., and Levine, T.P. (2003). A conserved ER targeting motif in three families of lipid binding proteins and in Opi1p binds VAP. EMBO J. *22*, 2025–2035.

Manford, A.G., Stefan, C.J., Yuan, H.L., Macgurn, J.A., and Emr, S.D. (2012). ER-to-plasma membrane tethering proteins regulate cell signaling and ER morphology. Dev. Cell *23*, 1129–1140.

Mesmin, B., Antonny, B., and Drin, G. (2013). Insights into the mechanisms of sterol transport between organelles. Cell. Mol. Life Sci. *70*, 3405–3421.

Mikitova, V., and Levine, T.P. (2012). Analysis of the key elements of FFAT-like motifs identifies new proteins that potentially bind VAP on the ER, including two AKAPs and FAPP2. PLoS ONE *7*, e30455.

Mousley, C.J., Yuan, P., Gaur, N.A., Trettin, K.D., Nile, A.H., Deminoff, S.J., Dewar, B.J., Wolpert, M., Macdonald, J.M., Herman, P.K., et al. (2012). A sterol-binding protein integrates endosomal lipid metabolism with TOR signaling and nitrogen sensing. Cell *148*, 702–715.

Mukherjee, S., Zha, X., Tabas, I., and Maxfield, F.R. (1998). Cholesterol distribution in living cells: fluorescence imaging using dehydroergosterol as a fluorescent cholesterol analog. Biophys. J. *75*, 1915–1925.

Nakatsu, F., Baskin, J.M., Chung, J., Tanner, L.B., Shui, G., Lee, S.Y., Pirruccello, M., Hao, M., Ingolia, N.T., Wenk, M.R., and De Camilli, P. (2012). PtdIns4P synthesis by PI4KIIIα at the plasma membrane and its impact on plasma membrane identity. J. Cell Biol. *199*, 1003–1016.

Palmgren, M.G., and Nissen, P. (2011). P-type ATPases. Annu. Rev. Biophys. *40*, 243–266.

Peretti, D., Dahan, N., Shimoni, E., Hirschberg, K., and Lev, S. (2008). Coordinated lipid transfer between the endoplasmic reticulum and the Golgi complex requires the VAP proteins and is essential for Golgi-mediated transport. Mol. Biol. Cell *19*, 3871–3884.

Perry, R.J., and Ridgway, N.D. (2006). Oxysterol-binding protein and vesicle-associated membrane protein-associated protein are required for sterol-dependent activation of the ceramide transport protein. Mol. Biol. Cell *17*, 2604–2616.

Raychaudhuri, S., Im, Y.J., Hurley, J.H., and Prinz, W.A. (2006). Nonvesicular sterol movement from plasma membrane to ER requires oxysterol-binding protein-related proteins and phosphoinositides. J. Cell Biol. *173*, 107–119.

Ridgway, N.D., Dawson, P.A., Ho, Y.K., Brown, M.S., and Goldstein, J.L. (1992). Translocation of oxysterol binding protein to Golgi apparatus triggered by ligand binding. J. Cell Biol. *116*, 307–319.

Roy, A., and Levine, T.P. (2004). Multiple pools of phosphatidylinositol 4-phosphate detected using the pleckstrin homology domain of Osh2p. J. Biol. Chem. *279*, 44683–44689.

Stefan, C.J., Manford, A.G., Baird, D., Yamada-Hanff, J., Mao, Y., and Emr, S.D. (2011). Osh proteins regulate phosphoinositide metabolism at ER-plasma membrane contact sites. Cell *144*, 389–401.

Wang, P.Y., Weng, J., and Anderson, R.G. (2005). OSBP is a cholesterol-regulated scaffolding protein in control of ERK 1/2 activation. Science *307*, 1472–1476.

West, M., Zurek, N., Hoenger, A., and Voeltz, G.K. (2011). A 3D analysis of yeast ER structure reveals how ER domains are organized by membrane curvature. J. Cell Biol. *193*, 333–346.

EXTENDED EXPERIMENTAL PROCEDURES

Reagents

Full-length and fragments sequence of human OSBP1 were PCR amplified from the ImaGENES clone IRAUp969H0566D. Methyl-β-cyclodextrin, N-ethylmaleimide (NEM), the oxysterol 25-hydroxycholesterol (25-OH), Phenylarsine Oxide (PAO) and lovastatin were purchased from Sigma-Aldrich. The SYPRO-Orange protein gel stain and the neutral lipid stain LipidTOX green were from Invitrogen. Rabbit anti-Sac1 and anti beta-actin were purchased from Thermo Fisher Scientific and Epitomics, respectively.

OSBP Expression and Purification

Full-length, C-terminal His-tagged OSBP1 was expressed and purified from baculovirus-infected Sf9 cells. DNA was amplified by PCR and cloned into pENTR/D-Topo (Invitrogen), then modified by insertion of a thrombin site sequence in frame at the end of the OSBP sequence. Inserts were verified by sequencing, inserted into linearized BaculoDirect (C-terminal V5 and His tagged) by recombination, and transfected into Sf9 cells. For large-scale expression and purification, Sf9 cells were infected at an MOI of 0.1 for 1 hr at room temperature, suspended in 500–1000 ml of Sf-900 II media with 1.5% FCS and incubated with shaking at 27°C. After 72 hr, cells were collected by centrifugation at 300 × g for 10 min and stored at −20°C. Pellets were resuspended in 1/50 volume of lysis buffer (20 mM Tris pH 7.5, 300 mM NaCl, 20 mM imidazole, EDTA-free protease inhibitors and phosphatases inhibitors) and lysed with Dounce homogenizer. After centrifugation (50 000 × g, 30 min, 4°C) OSBP from the supernatant was adsorbed on an Ni-NTA metal-affinity resin (QIAGEN), submitted to 3 washes with lysis buffer supplemented with 800, 500, and 300 mM NaCl, respectively, and then eluted with 0.25 M imidazole-containing buffer. OSBP fractions were pooled, concentrated on Amicon Ultra (cut-off 30 000 kDa), and then purified on a Superdex 200 HR10/30 column (GE Healthcare). OSBP fractions were pooled, concentrated and then submitted to thrombin cleavage for 1 hr at 25°C to eliminate the C-terminal His tag. The purified protein was stored at −80°C in presence of 10% glycerol.

Expression and Purification of PH-FFAT, FAPP1-PH Domain, VAP-A, and Sac1

PH-FFAT (= OSBP 76-408) was sub-cloned into pGEX-4T3 vector (GE Healthcare) for expression as a GST fusion protein in *E. coli*. FAPP1-PH domain (kindly provided by Franck Perez, Institut Curie) was sub-cloned into pGEX-4T3 and was modified by point mutagenesis (C37S/C94S/T13C/T100S) for specific NBD labeling of C13. A linker insertion (NGNLSSLSA) upstream of the PH sequence allows thrombin cleavage of the GST fusion as well as recovery of the isolated FAPP1-PH domain. Human VAP-A (8-212) and yeast Sac1 (1-522) fragments were sub-cloned into pET-21b for expression as C-terminal His-tag proteins in *E. coli*. In both cases the position of the C-terminal tag corresponds to beginning of the C-ter transmembrane region. As such, the constructs should be positioned on DOGS-NiNTA liposomes in a manner similar to the authentic membrane proteins. GST fusion proteins were purified on glutathione Sepharose beads (GE Healthcare), cleaved by thrombin, and His-tag fusion proteins were purified on Ni-NTA beads (QIAGEN). Myristoylated Arf1 was purified from *E. coli* coexpressing bovine Arf1 and N-myristoyltransferase through ammonium sulfate precipitation, DEAE chromatography, and MonoS chromatography as described (Franco et al., 1995). Purified recombinant proteins were stored with 10% glycerol at −80°C. NBD labeling of FAPP1-PH domain was performed as described (de Saint-Jean et al., 2011).

N-Terminal Sequence Determination

OSBP fragments obtained from 250 μg of purified OSBP after trypsin proteolysis were resolved on a Superose 12 gel filtration column. Fragments separated in two peaks. The protein material from each peak was pooled, concentrated and separated on SDS-PAGE before transfer onto PVDF membrane. Two main fragments of 43 kDa and 35 kDa were obtained from peak 1, whereas three other main fragments of 35 kDa, 33 kDa and 20 kDa were obtained from peak 2. Isolated protein bands were extracted from the membrane and sent for sequencing at the Plate-forme Protéomique de l'Institut de Microbiologie de la Méditerranée (Marseille Protéomique, IBiSA, CNRS).

Cell Culture and Transfection

HeLa cells were grown in DMEM (Invitrogen) supplemented with 10% fetal calf serum (FCS) and antibiotics (Zell Shield, Minerva biolabs). For protein expression, cells were transfected with Lipofectamine 2000 reagent for 18 to 24 hr. OSBP with mCherry at the N terminus was constructed in a pmCherry-C1 vector. The PH-FFAT tandem (OSBP[76-408]) with mCherry at the C terminus was constructed in a pmCherry-N1 vector. Alternatively, PH-FFAT was subcloned in a PTunerC-GFP vector (Clontech Laboratories). Mutants were generated with the QuikChange Lightning site-directed mutagenesis kit (Agilent Technologies). The PI(4)P probe (OSBP PH domain with GFP at the N terminus) was cloned in a pEGFP-C1 vector. VAP-A and VAP-A K94D/M96D (VAP-A KM > DD) with N-terminal GFP were constructed in a pEGFP-C1 vector (gift from Fabien Alpy, Illkirsch). For Sac1 silencing, Sac1 siRNA (Santa Cruz Biotechnology) was transfected in HeLa cells with Lipofectamine 2000 for 24 hr. Control siRNA were purchased from Santa Cruz. For confocal fluorescence microscopy, cells were plated on fibronectin-coated glass coverslips. For wide-field imaging, cells were plated on ibiTreat μ-Slides 8 well (Ibidi).

Live Cell Imaging, FRAP Assay, and Data Acquisition

For live cell imaging and FRAP assay, HeLa cells were maintained at 37°C in growth medium supplemented with 2.5 mM HEPES, or in medium A (NaCl 150 mM, HEPES 20 mM pH 7.55, $CaCl_2$ 1 mM, KCl 5 mM, $MgCl_2$ 1 mM) supplemented with 2 mg/ml glucose in the case of DHE imaging. Confocal fluorescence microscopy and FRAP assays were carried out using a Nikon Eclipse Ti inverted microscope equipped with an UltraVIEW VoX spinning disc imaging system (PerkinElmer) driven by Volocity software. Images were acquired using an 100× oil-immersion objective (Nikon CFI Plan Apochromat 100×/1.4). For FRAP experiments, photobleaching was performed on circular areas of 3.5 μm^2 within cell perinuclear regions. Fluorescence in these areas was then recorded every 0.5 s.

Wide-field microscopy imaging of the PI(4)P probe was carried out using a Plan-FLUAR 100×/1.45 oil objective on a Axiovert 200 M microscope (Zeiss) equipped with a CoolSNAP HQ CCD camera (Roper Scientific). Image acquisition and analysis was performed with MetaMorph software (Molecular Devices). To determine the fraction of the PI(4)P probe in the perinuclear region, images were first background corrected, then two fluorescence intensity thresholds were applied to the images. A low threshold was set to define the total area of the cells, whereas a high threshold was set to identify the bright, PI(4)P probe-labeled, perinuclear regions. The fluorescence intensity ratio obtained from the two threshold values gives PI(4)P probe amounts in the perinuclear region of the cells. Alternatively, imaging of the PI(4)P probe was carried out using confocal microscopy. In this case, the Golgi/cytosol PI(4)P probe fluorescence ratio per cell was determined by dividing the mean fluorescence intensity obtained from three regions of 3 μm^2 within the Golgi area to the mean fluorescence intensity obtained from three regions of 3 μm^2 within the cytosol area.

Wide-field microscopy for DHE imaging was carried out using a Leica DMIRBE microscope equipped with an Andor iXon3 blue-optimized EMCCD camera driven by Solis software (Andor). Cells were incubated with DHE in complex with MCD (1:5 ratio) for one min at 37°C and washed 3 times in medium A. Cells were further incubated in growth medium containing cholesterol in complex with MCD for 2 hr before imaging. DHE was imaged using Semrock BrightLine fluorescence filters (320/40 nm bandpass filter, 347 nm dichroic beamsplitter, and 390/40 nm bandpass filter). Images were acquired using a Leica HCX APO 100×/1.3 oil U-V-I objective.

FFAT Peptide

Peptide synthesis was ordered from Proteogenix (Oberhausbergen, France). The sequence (**W**CSGKGDMSDEDDENEFFDAPEIITM PENLGH) reproduces the FFAT motif sequence of OSBP with an extra N-terminal tryptophan for accurate concentration determination by UV spectroscopy.

Lipids

Egg-PC, brain PS, brain PI(4)P, brain PI(4,5)P2, liver PI, liver PE, Dansyl-PE (1,2-dioleoyl-*sn*-glycero-3-phosphoethanolamine-*N*-(5-dimethylamino-1-naphthalenesulfonyl)), Rhodamine-PE [1,2-dipalmitoyl-*sn*-glycero-3-phosphoethanolamine-*N*-(lissamine rhodamine B sulfonyl)], and DOGS-NiNTA [1,2-dioleoyl-*sn*-glycero-3-[(N-(5-amino-1-carboxypentyl)iminodiacetic acid)succinyl] (nickel salt)] were obtained from Avanti Polar Lipids. PI(3)P (1,2-dioleoyl-*sn*- glycero-3-inositol-3-phosphate) and PI(5)P (1,2-dioleoyl-*sn*-glycero-3- inositol-5-phosphate) were obtained from Echelon. Oregon green 488 DHPE (1,2-Dihexadecanoyl-*sn*-Glycero-3-Phosphoethanolamine) was from Invitrogen. Cholesterol and DHE were from Sigma-Aldrich. The concentration of DHE in the stock solution in methanol was carefully determined by UV spectroscopy.

Liposome Preparation

Lipids in stock solutions in chloroform were mixed at the desired molar ratio, and the solvent was removed in a rotary evaporator. The lipid film was hydrated in 50 mM HEPES pH 7.2 and 120 mM potassium acetate (HK buffer) to give a suspension of large multilamellar liposomes (lipid concentration: 2–5 mM). The suspension was then frozen and thawed five times (using liquid nitrogen and a water bath) and extruded through polycarbonate filters of 0.1-μm pore size using a mini-extruder (Avanti Polar Lipids). Liposomes were stored in the dark and used within 2 days.

In all experiments except those performed with proteolyzed OSBP, liposomes L_a have an ER-like composition: egg PC/ brain PS/ DOGS-NiNTA (93/ 5/ 2 mol %) and are supplemented with 18 mol % DHE in the case of DHE transfer experiment. Liposomes L_b have a Golgi-like composition: egg PC/ liver PE/ brain PS/ liver PI/ Dansyl-PE (63.5/ 19/ 5/ 10/ 2.5 mol %). When indicated, these liposomes were supplemented with PI(4)P at the expense of liver PI.

For experiments with proteolyzed OSBP, both liposomes L_a and L_b have a Golgi-like composition (egg PC/ liver PE/ brain PS/ liver PI/ [65/ 19/ 5/ 10 mol %]) and are supplemented with 18 mol % DHE or 2.5 mol % Dansyl-PE, respectively. When indicated, liposomes La were further supplemented with 2 mol % of specific phosphoinositide at the expense of liver PI.

For PI(4)P transfer assay, liposomes L_a were supplemented with 2 mol % cholesterol and liposomes L_b with 2 mol % PI(4)P and 2 mol % Rhodamine-PE.

OSBP Proteolysis

Purified OSBP was incubated at 30°C under constant agitation, in the presence of either 1 or 2 μg/ml trypsin. The reaction was stopped at the indicated time by addition of 2 mM PMSF. For activity measurements, the fragments obtained from 250 μg purified OSBP were resolved on a Superose 12 column. Each fraction was then tested for DHE transfer and liposome tethering activity.

DHE and PI(4)P Transfer Assays

All fluorescence experiments were performed in a Shimadzu RF-5301-PC spectrofluorometer using a cylindrical quartz cuvette (600 µL) equilibrated at 37°C and equipped with a magnetic bar for continuous stirring. For most DHE transfer assays using full-length OSBP (Figures 5, 6, and 7), the cuvette initially contained Golgi-like liposomes (L_b) with 2.5 mol % Dansyl-PE (63 µM total lipids) in HK buffer supplemented with 1 mM $MgCl_2$ (HKM buffer). When indicated, VAP-A-His, Arf1-GTP, FFAT peptide, or 25-OH were included in the cuvette. At the indicated times, OSBP (0.1 µM) and ER-like liposomes (L_a; 63 µM lipid) containing 18 mol % DHE were sequentially added. The sterol transport activity of OSBP was monitored by FRET between DHE and Dansyl, measured at 525 nm (bandwidth 5 nm) upon excitation at 310 nm (bandwidth 1.5 nm) (John et al., 2002). Concentrated MCD (1 mM) was used to determine the maximal FRET signal due to full sterol equilibration between L_a and L_b liposomes.

For the DHE transfer experiments of Figures 4A and 6B, liposomes L_a and L_b displayed the same Golgi-like composition. L_a also contained 18 mol % DHE and L_b contained 2.5 mol % dansyl-PE.

To analyze the sterol exchange activity of the various Superose 12 fractions, 250 µl of each fraction were mixed with pure DOPC liposomes (450 µM total lipids). DHE transport was initiated by the addition of 50 µM DOPC/DHE/Dansyl-PE (87.5/10/2.5 mol %) liposomes and was followed by measuring the decrease of the FRET signal at 525 nm (bandwidth: 5 nm) upon excitation at 310 nm (bandwidth: 1.5 nm). The signal for maximal DHE transport was determined by addition of 1 mM MCD.

For PI(4)P transfer assay, Golgi-like liposomes with 2% Rho-PE (L_b, 300 µM lipids) were incubated in HKM buffer with 250 nM NBD-FAPP1 PH domain (^{NBD}PH) and with 1 µM VAP-A-His when indicated. PI(4)P transport was followed by measuring the NBD emission signal at 510 nm (bandwidth 10 nm) upon excitation at 460 nm (bandwidth 1.5 nm). At the indicated times, ER-like liposomes (L_a, 300 µM lipid) and 0.1 µM OSBP were sequentially added. Maximal signal corresponding to PI(4)P equilibration between both types of liposomes was determined by mixing control ER-like (A) and Golgi-like (B) liposomes, each containing 1% PI(4)P.

Liposome Binding Assay and Liposome Aggregation Measurements

Flotation assays on sucrose gradient were used to determine protein binding to liposomes, as described previously (Bigay et al., 2005). Liposome aggregation induced by OSBP and PH-FFAT was followed by dynamic light scattering (DLS) using a Dynapro apparatus (Protein Solutions) as described (Drin et al., 2008). The sample in HKM buffer initially contained ER-like liposomes (L_a, 25 µM lipids) loaded or not with VAP-A-His (200-250 nM) and with Sac1-His (when indicated), and Golgi-like liposomes (L_b, 25 µM lipids) supplemented or not with 200 nM Arf1-GTP and with 2 mol % PI(4)P. A first set of 10 autocorrelation curves was acquired to assess the initial size distribution of the liposome suspension. Then tether proteins were added manually (100-250 nM PH-FFAT or 250 nM OSBP), mixed thoroughly and the kinetics of aggregation was followed by acquiring one autocorrelation curve every 10 s (temperature 30°C). The data were analyzed using the algorithm provided by the Dynamics v6.1 software (Protein Solutions). During the aggregation process, the autocorrelation functions were fitted assuming that the size distribution is a Gaussian function, giving a mean radius and the polydispersity.

Tethering Assay with Giant Liposomes and Templates

For membrane tethering observation by light microscopy, giant ER-like liposomes were prepared by spontaneous formation as described (Drin et al., 2008). Briefly, a lipid film containing egg PC/ brain PS/ Rhodamine-PE/ DOGS-NiNTA (91, 5, 2, 2 mol %) was prepared in a 50 ml round flask, sealed under argon, and then hydrated overnight at 37°C in 50 mM HEPES, pH 7.2, 210 mM sucrose. Red clouds formed by giant liposomes in the supernatant were harvested and lipid concentration was estimated by fluorescence. To prepare bead-supported bilayers, we used a protocol derived from that of Pucadyil and Schmid (Pucadyil and Schmid, 2008). Extruded Golgi-like liposomes (200 µM lipids) containing egg PC/ liver PE/ liver PI/ brain PS/ PI(4)P/ Oregon green-DHPE (65, 18, 8, 5, 2, 2 mol %) were incubated with 5×10^8 uniform silica beads of 5 µm (Bangs Laboratories) in HK buffer (100 µl total volume) for 30 min at room temperature under regular vortex. Templates were washed three times by centrifugation in HK buffer (200 × g for 2 min). The lipid concentration of the templates was estimated by fluorescence. Tethering was initiated by mixing at room temperature a small volume of giant liposomes loaded with 250 nM VAP-A-His with templates (5 µM lipids) and with 250 nM PH-FFAT or OSBP as indicated. Fluorescence microscopy was carried out using a Confocal Leica TCS SP5 microscope. Images were acquired using a HCX Plan Apo CS 63×/1.4 objective. Alternatively, templates were imaged using wide-field microscopy.

Electron Microscopy

For transmission electron microscopy analysis, cells expressing GFP-VAP-A and mCherry-OSBP or PH-FFAT-mCherry were sorted using a FACS Aria III cell sorter (BD Biosciences) and plated for 4 hr. Cells were fixed with 1.6% glutaraldehyde in 0.1 M phosphate buffer, rinsed in 0.1 M cacodylate buffer, and postfixed for 1 hr in 1% osmium tetroxide and 1% potassium ferrocyanide in 0.1 M cacodylate buffer to enhance membrane staining. The cells were then rinsed in distilled water, dehydrated in alcohols and lastly embedded in epoxy resin. Contrasted ultrathin sections (70 nm) were analyzed under a JEOL 1400 transmission electron microscope mounted with a Morada Olympus CCD camera. For liposomes negative contrasts, samples were deposited on glow discharge carbon-coated grids and negatively stained with 1% uranyl acetate and then directly observed with the microscope.

Sac1 PI(4)P Hydrolysis Assay

The reactions were carried out in small test tubes in a final volume of 110 µl at room temperature under gentle shaking. L_a liposomes (500 µM, ER-like) were incubated with 50 nM Sac1-His, with the indicated amount of VAP-A-His and with 200 nM OSBP or 200 nM PH-FFAT. The reaction was initiated by the addition of L_b liposomes (500 µM, egg PC/liver PE/brain PS/PI(4)P: 57/18/5/20 mol %). At the indicated times, an aliquot of the mixture was withdrawn and mixed with 50 mM NEM to stop the reaction. Phosphate concentration was determined by a colorimetric assay (absorbance at 650 nm) using malachite green reagent (Pucadyil and Schmid, 2008). For the Sac1 *cis* experiment, ER-like liposomes were supplemented with 20 mol % PI(4)P at the expense of egg PC. In this case, the reaction was initiated by the addition of Sac1.

SUPPLEMENTAL REFERENCES

Bigay, J., Casella, J.F., Drin, G., Mesmin, B., and Antonny, B. (2005). ArfGAP1 responds to membrane curvature through the folding of a lipid packing sensor motif. EMBO J. *24*, 2244–2253.

Creighton, T.E. (1993). Proteins. Structure and Molecular Properties, Second Edition (New York: W. H. Freeman and Company).

Dawson, P.A., Ridgway, N.D., Slaughter, C.A., Brown, M.S., and Goldstein, J.L. (1989). cDNA cloning and expression of oxysterol-binding protein, an oligomer with a potential leucine zipper. J. Biol. Chem. *264*, 16798–16803.

Drin, G., Morello, V., Casella, J.F., Gounon, P., and Antonny, B. (2008). Asymmetric tethering of flat and curved lipid membranes by a golgin. Science *320*, 670–673.

Franco, M., Chardin, P., Chabre, M., and Paris, S. (1995). Myristoylation of ADP-ribosylation factor 1 facilitates nucleotide exchange at physiological Mg^{2+} levels. J. Biol. Chem. *270*, 1337–1341.

John, K., Kubelt, J., Müller, P., Wüstner, D., and Herrmann, A. (2002). Rapid transbilayer movement of the fluorescent sterol dehydroergosterol in lipid membranes. Biophys. J. *83*, 1525–1534.

Kahn, R.A., Randazzo, P., Serafini, T., Weiss, O., Rulka, C., Clark, J., Amherdt, M., Roller, P., Orci, L., and Rothman, J.E. (1992). The amino terminus of ADP-ribosylation factor (ARF) is a critical determinant of ARF activities and is a potent and specific inhibitor of protein transport. J. Biol. Chem. *267*, 13039–13046.

Lupas, A., Van Dyke, M., and Stock, J. (1991). Predicting coiled coils from protein sequences. Science *252*, 1162–1164.

Pucadyil, T.J., and Schmid, S.L. (2008). Real-time visualization of dynamin-catalyzed membrane fission and vesicle release. Cell *135*, 1263–1275.

Tong, J., Yang, H., Yang, H., Eom, S.H., and Im, Y.J. (2013). Structure of Osh3 reveals a conserved mode of phosphoinositide binding in oxysterol-binding proteins. Structure *21*, 1203–1213.

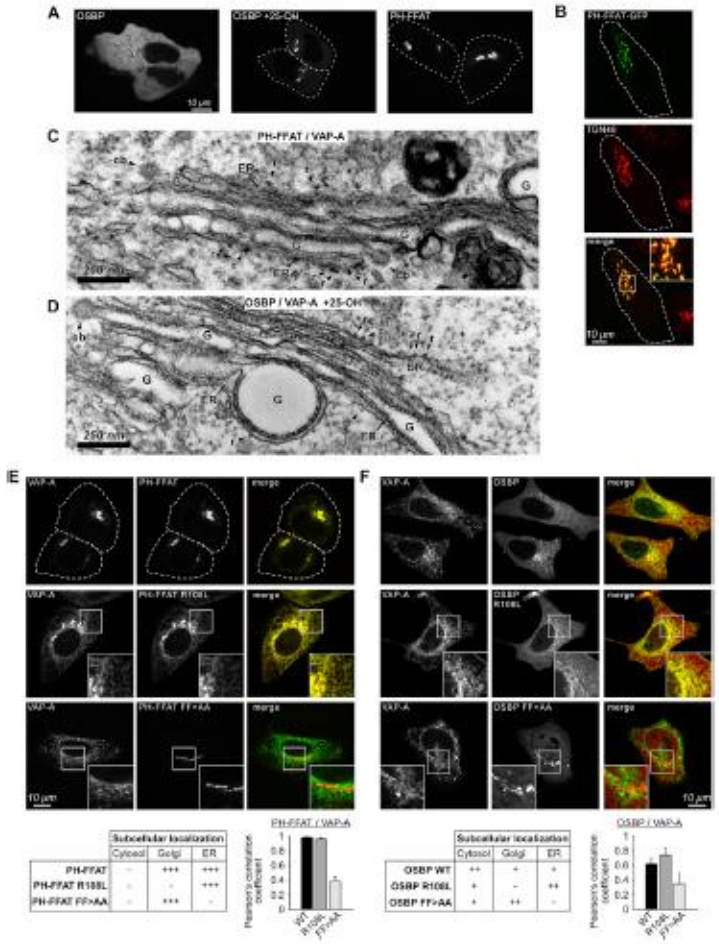

Figure S1. Characterization of the Membrane Contact Sites Induced by OSBP or by its PH-FFAT Region, Related to Figure 1

(A) HeLa cells expressing mCherry-OSBP (treated or not with 25-OH) or PH-FFAT- mCherry. The localization patterns are similar to that observed in cells co-expressing these constructs with VAP-A-GFP (Figures 1B and 1C).

(B) HeLa cells expressing PH-FFAT-GFP were fixed and immuno-labeled with a TGN46 polyclonal antibody (AbD Serotec) and a donkey anti-sheep Alexa-Fluor594-conjugated secondary antibody (Invitrogen).

(C and D) Electron micrographs of membrane apposed regions in HeLa cells expressing VAP-A and PH-FFAT in the absence of 25-OH (C) or expressing VAP-A and OSBP and treated with 25-OH (D). The ER is identified by the presence of bound ribosomes (r) and by a dark lumen, whereas the Golgi apparatus (G) is identified by the presence of coated buds (cb) and by a clear lumen.

(E and F) HeLa cells coexpressing GFP-VAP-A and mutants of PH-FFAT-mCherry (E) or mCherry-OSBP (F). When the PH domain cannot interact with PI(4)P (mutation R108L), OSBP and PH-FFAT are found associated with the ER (middle row). When the FFAT motif cannot interact with VAP-A (mutation FF > AA), OSBP and PH-FFAT are found associated with the Golgi (lower row). Thus, OSBP and PH-FFAT use the same membrane determinants to interact with cellular membranes. However, the presence of a functional PH domain and of a functional FFAT motif leads to the formation of extensive ER-Golgi clusters in the case of PH-FFAT, but not in the case of full-length OSBP, which is more soluble than its mutants. Thus, and as summarized in the tables, PH-FFAT follows an additive rule: functional PH + functional FFAT motif = Golgi + ER localization, whereas OSBP follows a different rule: functional PH + functional FFAT motif = cytosol localization. Histograms represent measurements (±SD) performed on 15–20 cells.

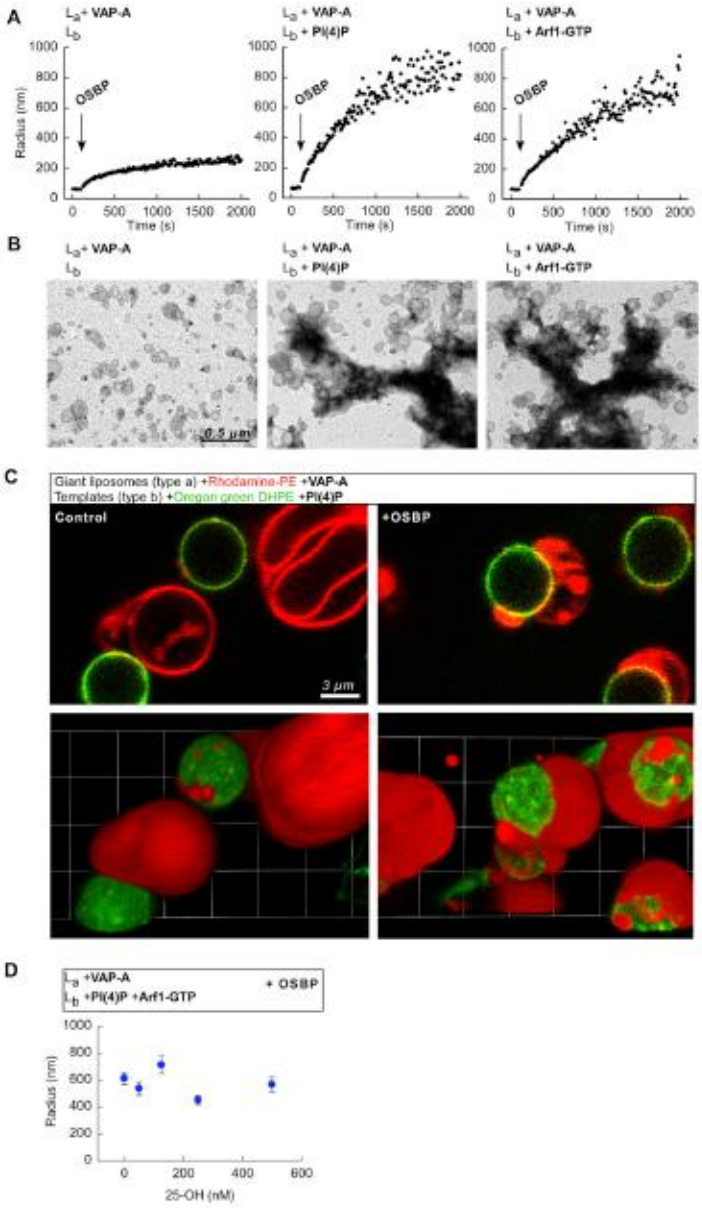

Figure S2. OSBP Is Competent for Membrane Tethering In Vitro, Related to Figure 2

(A–C) Experiments similar to that shown in Figure 2 were performed with full-length OSBP (0.2 μM) instead of PH-FFAT and analyzed by DLS (A), EM (B) and light microscopy (C). (C) shows confocal images (top) and 3D reconstitutions (bottom) of the same fields to highlight the extended contacts between templates and giant liposomes when OSBP is present.

(D) Dynamic light scattering experiments similar to that shown in (A) were performed in the presence of 25-OH. The plot shows the apparent radius (mean ± SD from 15 autocorrelation curves) at t = 2000 s as a function of 25-OH concentration.

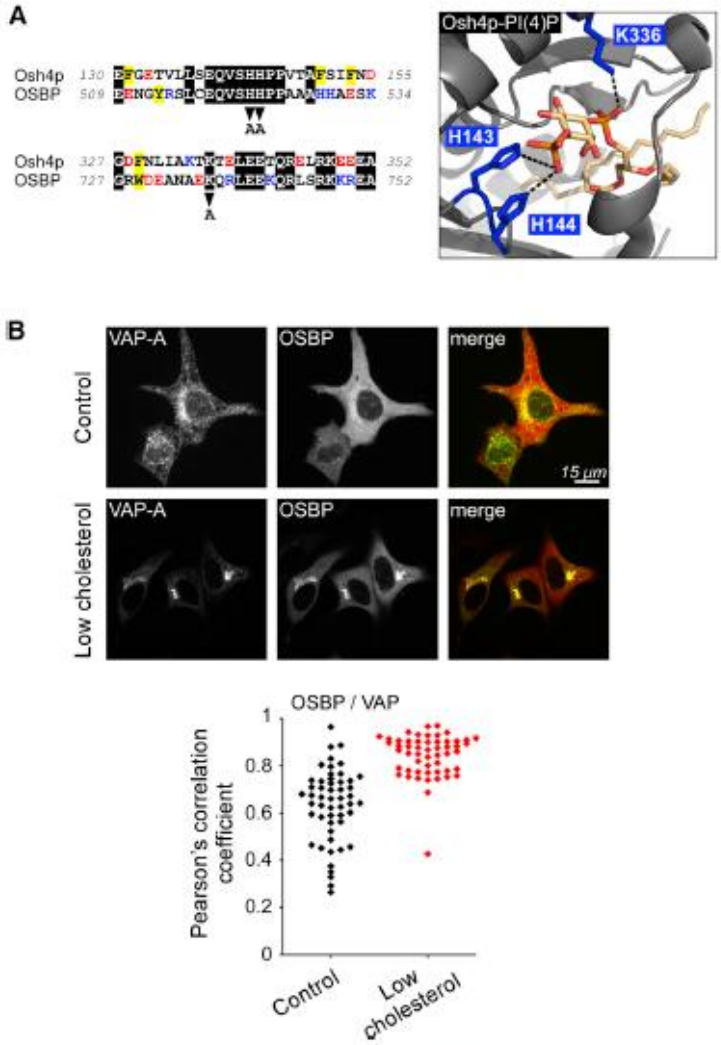

Figure S3. Inhibition of Sterol Biosynthesis at the ER Prevents OSBP from Displacing PI(4)P at the Golgi, Related to Figure 3

(A) Sequence alignment of the ORD of OSBP and of Osh4p and close-up view of the Osh4p-PI(4)P complex (PDB entry: 3SPW). Arrowheads: conserved basic residues involved in PI(4)P interaction and chosen for mutagenesis.

(B) HeLa cells coexpressing GFP-VAP-A and mCherry-OSBP. When sterol biosynthesis is inhibited as in Figure 3C, OSBP and VAP-A concentrate to a perinuclear region.

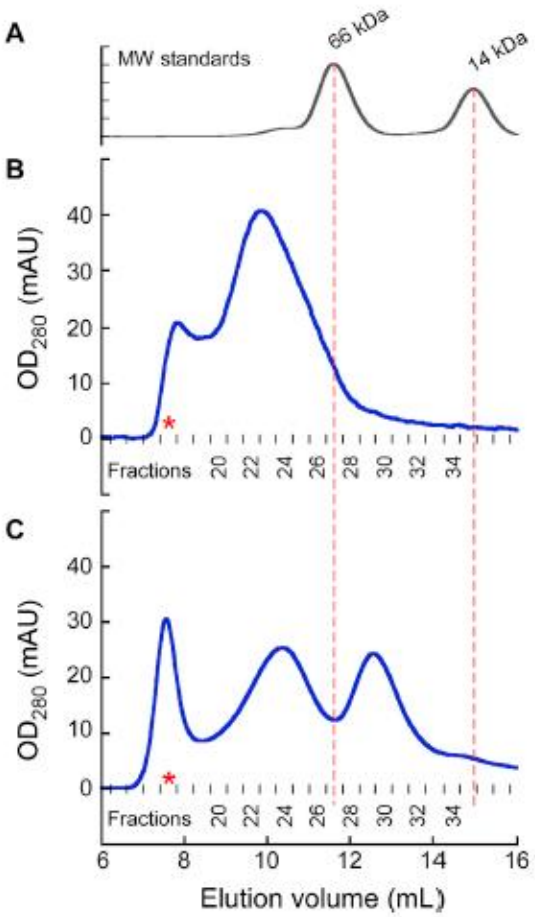

Figure S4. Gel Filtration Analysis of OSBP or Trypsin-Digested OSBP, Related to Figure 4

(A–C) Elution profiles (as monitored by UV absorbance) of molecular weight standards (A), of full-length OSBP (B), and of trypsin-digested OSBP (C) on a Superose 12 column. The profile shown in (C) corresponds to the experiment shown in Figure 4C. The asterisk indicates the excluded volume of the column.

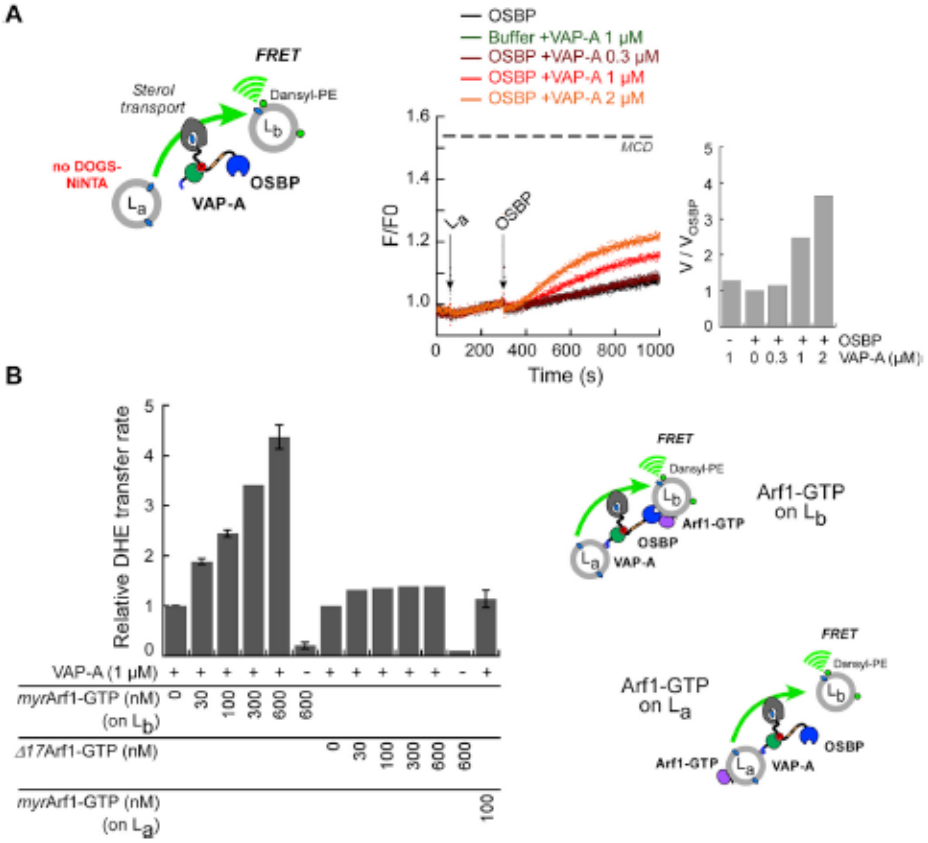

Figure S5. Mechanism of OSBP Activation, Related to Figure 5

(A) Effect of soluble VAP on OSBP-mediated DHE transfer. The experimental conditions were as Figure 4A (liposomes L_a contained no DOGS-Ni-NTA). VAP-A has a significant stimulatory effect on OSBP-mediated DHE transfer despite the lack of membrane attachment.

(B) Arf1-GTP stimulates OSBP only when bound to liposomes L_b. The experimental conditions were as in Figure 5A except that myristoylated Arf1 was attached to liposomes L_a or L_b, or was replaced by [Δ17]Arf1-GTP, a soluble form of active Arf1 (Kahn et al., 1992). The error bars indicate the values of two independent experiments.

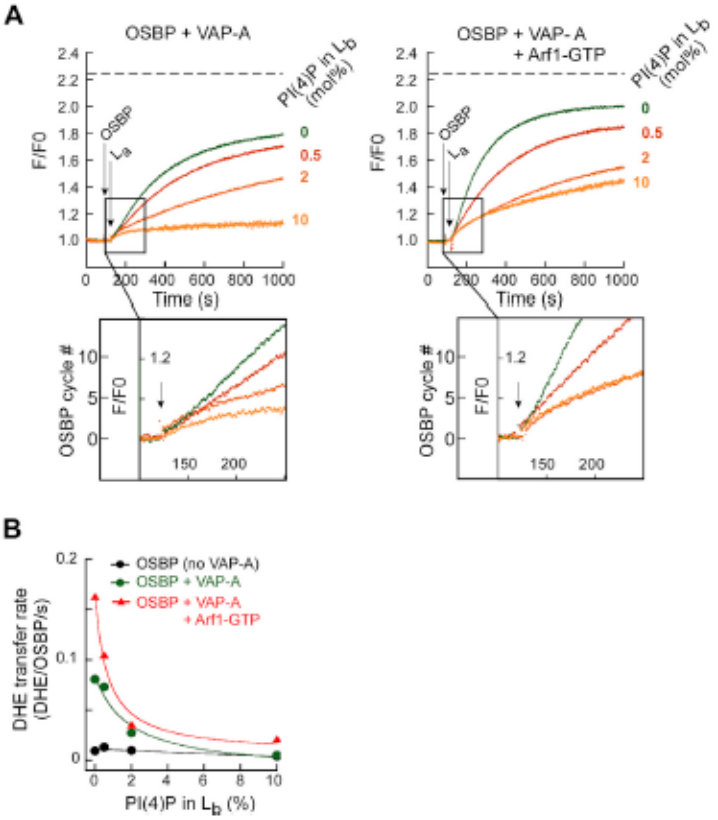

Figure S6. PI(4)P Inhibits OSBP after a Few Rounds of DHE Transfer, Related to Figure 6

(A) The original recordings of Figure 6A are shown again, together with an expanded view of the first minutes of DHE transfer to highlight the biphasic shape of the kinetics. In this expanded view, the FRET signal is converted into a number (#) of OSBP cycles between liposomes L_a and L_b. This number equals $[(F/F_0-1)/(F_{max}/F_0-1] \times [63 \times 0.09 / 0.1]$, where F is the fluorescence level at time t, F_0 is the initial fluorescence level, F_{max} is the final fluorescence level after DHE equilibration between liposomes L_a and L_b (as determined by the addition of MCD, horizontal dashed line), and $[63 \times 0.09 / 0.1]$ is the total number of cycles that OSBP has to undergo in order to equilibrate DHE between L_a and L_b. Indeed, the concentration of OSBP is 0.1 μM and the concentration of DHE that equilibrates between L_a and L_b equals 5.7 μM (= 63 × 0.18 / 2 since L_a and L_b were used at 63 μM and contained 0 and 18 mol % DHE, respectively). This calculation leads to 57 cycles. Overall, PI(4)P clearly inhibits DHE transfer in a dose-dependent manner. However, this inhibitory effect applies only after the first fifty seconds of DHE transfer. Initially, the time courses with or without PI(4)P are roughly parallel, suggesting that OSBP is not inhibited by PI(4)P during the first cycle of DHE transfer.

(B) Quantification of the data shown in A as determined from linear fits of the second phase.

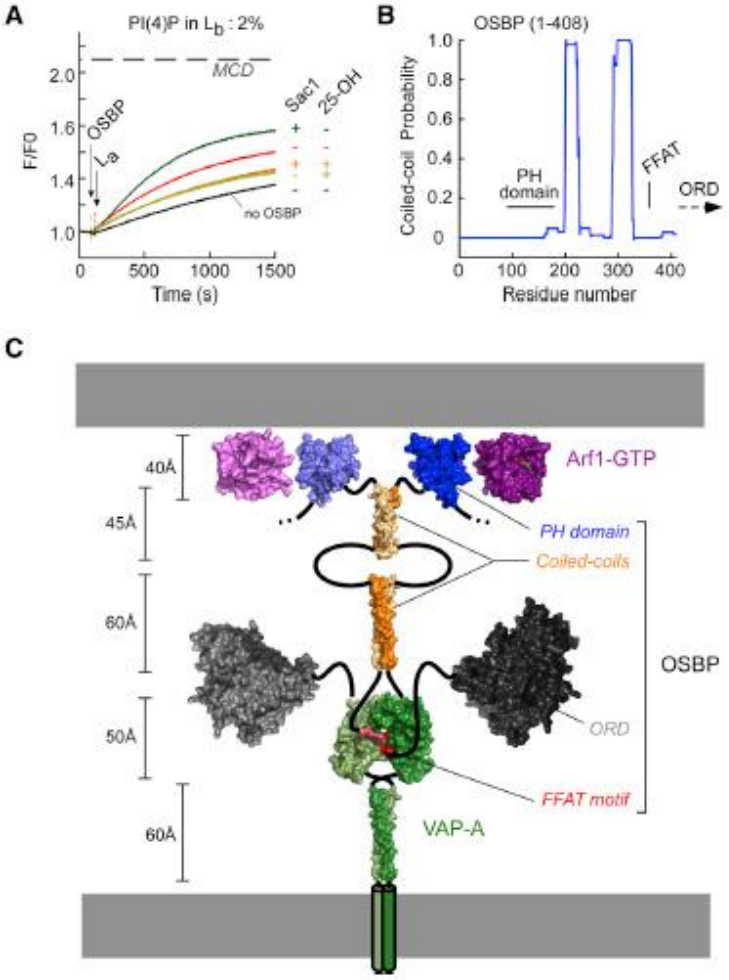

Figure S7. Pharmacological and Structural Aspects of the 4-Step Cycle of OSBP, Related to Figure 7

(A) The four-step cycle of OSBP is inhibited by 25-OH. The experimental conditions were similar to that used in Figure 6A and 7E with the following modifications. Transfer of DHE between liposomes L_a (63 μM lipids + 1 μM VAP-A) and L_b (63 μM lipids, 2 mol % PI(4)P) was measured in the presence of 0.1 μM OSBP. When indicated, 50 nM Sac1 and/or 10 μM 25-OH were added. 25-OH inhibits DHE transfer under these turnover conditions where OSBP exchanges DHE for PI(4)P, which is then hydrolyzed by Sac1. Dashed line: maximal fluorescence observed after DHE equilibration with 1 mM MCD.

(B) Coiled-coil probability in the N-ter sequence of OSBP using a sliding window of 21 aa as determined by COILS (http://www.ch.embnet.org/software/COILS_form.html) (Lupas et al., 1991). Two coiled-coil regions of 30 and 50 aa, respectively, are predicted, although only the first one was identified in early studies on OSBP (Dawson et al., 1989).

(C) Putative domain organization of OSBP at the interface between two membranes. The aim of this model is to show protein domains at scale, thus allowing comparison with the distance between apposed membranes as observed experimentally (~20 nm; see Figure 1D). This model was constructed using the structures of the PH domain of ORP11 (2D9X), the ORD domain of Osh4p (1ZHZ), the soluble region of VAP-A in complex with a FFAT motif (1Z9O), and Arf1-GTP (1O3Y). Coiled-coil regions were modeled according to the structure of tropomyosin (2D3E). This model also suggests questions for the functioning of OSBP at membrane interfaces, including the roles of protein dimerization and of linker regions. Notably, the linker between the FFAT motif and the ORD domain contains ~50 amino acids, which corresponds, in the case of a random amino acid chain, to an end-to-end distance of $(130 \times 50)^{1/2} = 80$ Å (Creighton, 1993). This length seems barely enough to allow the ORD domain flipping between apposed membranes, thus leaving the possibility that, at some point of the lipid exchange cycle, the FFAT motif dissociates from VAP-A. It is interesting to compare this model, in which the membrane are closely apposed, to another model derived from the structural analysis of the individual domains of the OSBP homolog Osh3p. In this case, the distance between the two membranes is proposed to be much larger because the protein does not seem to contain coiled-coil regions but rather extended and unstructured regions (Tong et al., 2013).

PART II:

PHOSPHATIDYLSERINE DISTRIBUTION

Introduction

Phosphatidylserine (PS) is an anionic GPL that serves multiple functions in eukaryotic cells. In budding yeast, PS is a key intermediate for GPL biosynthesis as the role of the Kennedy pathway enzymes is reduced there (Leventis and Grinstein 2010). Its synthesis from CDP-DAG and serine is catalyzed by the PS synthase Pss1p that is localized to the ER: It is particularly enriched at MCSs, such as ER-mitochondria and most importantly ER-PM contact sites (Gaigg, Simbeni *et al.* 1995; Pichler, Gaigg *et al.* 2001). However, PS concentration of the ER is low, whereas it is higher at the PM (van Meer, Voelker *et al.* 2008). Most of the GPLs at the PM have higher saturation levels compared to other compartments of the cell to allow a denser packing of the membrane, and this is also the case for PS (Schneiter, Brugger *et al.* 1999). Of particular importance is that PS displays a pronounced transmembrane asymmetry as it is almost completely excluded from the exoplasmic face of the PM and present at > 50 mol% in its cytosolic leaflet (estimation based on total PS at the PM and its absence (< 10 %) on the exoplasmic face) (Zinser, Sperka-Gottlieb *et al.* 1991; Schneiter, Brugger *et al.* 1999; van Meer, Voelker *et al.* 2008).

Recently, two members of the Osh protein family, Osh6p and Osh7p have been identified as cytosolic PS transporters between cortical ER and the PM in budding yeast, possibly at a MCS. Depletion of Osh6/7p reduced the accumulation of a fluorescent PS probe ($C2_{Lact}$-GFP) on the PM by ≈ 30 % and increased its signal at the ER and vacuoles. The authors showed Osh6p/Osh7p-dependent PS transport between artificial membranes *in vitro*, and targeting of Osh6p to vacuoles lead to increasing PS levels there, in the absence of Osh7p. The reported crystal structure of an Osh6p-PS complex showed an overall fold similar to other Osh3p and Osh4p, with PS acyl chains bound in the slightly deeper lipid-binding pocket. Residues Leu64, Ile67, Leu69, Lys126, Asn129 and Ser183 make specific polar contacts with the carboxyl group of PS. These residues are not conserved in Osh4p, explaining why Osh4p is not capable of efficient PS binding. Based on their findings the authors proposed that Osh6p and Osh7p would transport PS at ER-PM contact sites towards the PM. They also posit that this transport is driven by local, very high ER PS levels due to specific recruitment of the PS synthase Pss1p to ER-PM contact sites (Pichler, Gaigg *et al.* 2001). Locally elevated PS levels in the ER would thus permit transport along a PS concentration gradient towards the PM (Maeda, Anand *et al.* 2013).

Interestingly, another article recently linked PS distribution with PIP metabolism. Total PS levels are reduced despite constant Pss1p expression by deletion of Sac1p. The reduction was found to be independent of the decarboxylation pathway and Kennedy pathway, but dependent on the phosphatase activity of Sac1p. Levels were further decreased by suppression of PIK deletions (PI4K Stt4p and PI3K Vps34p), blocking the syntheses of Sac1p substrates. Deletion of Sac1p lead to depletion of PS in the PM, monitored using a GFP-$C2_{Lact}$ PS probe (Tani and Kuge 2014). Intriguingly, the phenotype is similar to that observed upon deletion of Osh6/7p (Maeda, Anand *et al.* 2013). A last and other intriguing observation is that the deletion of PS synthase Pss1p leads to an accumulation of PI(4)P, particularly the Stt4p-derived PM PI(4)P pool (Zhong, Hsu *et al.* 2012).

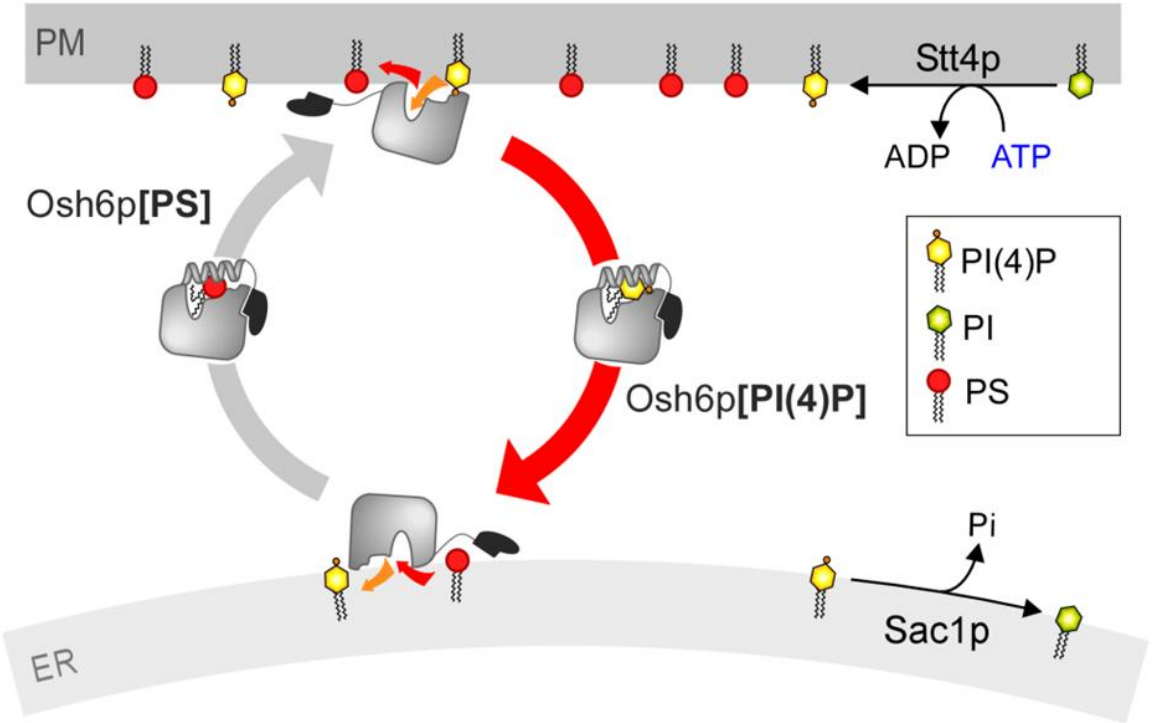

Figure 45. Our hypothesis on the function of Osh6p in yeast

See main text for description.

Based on these findings, initial data we obtained on Osh6p/Osh7p and our previous work on Osh4p, we currently aim to demonstrate that PI(4)P metabolism provides the energy for Osh6/7p-dependent non-vesicular PS traffic. The PM PI4K Stt4p would produce a pool of PI(4)P that is exchanged for PS by Osh6p/7p, which in turn would exchange PI(4)P for newly synthesized PS at the ER. Phosphatase activity of Sac1p in the ER would sustain the PI(4)P gradient between the ER and the PM, allowing continuous transport of PS by Osh6p/7p (**Figure 45)**. As proposed for sterol, this mechanism could beautifully explain how the accumulation of PS in the PM is driven. This study would also explain better why PS is mostly found in the lumen side of the ER membrane and mostly in the cytosolic side of the PM (Fairn, Schieber *et al.* 2011): As a cytosolic carrier, Osh6p/Osh7p extracts newly synthesized PS from the cytosolic side of the ER and delivers PS exclusively in the cytoplasmic face of the PM. This mechanism might particularly explain how the transversal asymmetry of PS is inverted from the ER to the PM.

Results

A brief overview of our efforts studying the Osh proteins

We started with the project to demonstrate that all Osh proteins are sterol/PI(4)P exchangers and we end up with the idea that Osh proteins (and also ORPs) are proteins that use a PI(4)P-exchange mechanism to convey various lipids in cells to create lipid gradient between the ER and late membranes. Some of our findings and anticipations on the Osh proteins have been published during this project by our competitors; nevertheless they will be described here in chronological order as to confirm the similarity between our data and the published data and to demonstrate the reasoning of our approach.

Osh3p-ORD, Osh6p and Osh7p do not bind or transport sterol, unlike Osh4p and Osh5p

Based on the findings on sterol- and PI(4)P-binding by Osh4p (Im, Raychaudhuri *et al.* 2005; de Saint-Jean, Delfosse *et al.* 2011), we were curious to find whether other Osh proteins also had the capacities to bind these lipids in a mutually exclusive manner and to

exchange them between membranes. Because the short Osh proteins (Osh5p, Osh6p, Osh7p) were easily purified from bacterial overexpression, they were the first to be tested in PI(4)P and DHE extraction assays. After a preliminary paper about the crystallization procedure of the ORD and PH domain of Osh3p by Tong *et al.* and of their protein purification protocol, we were able to optimize a protocol to obtain the Osh3p-ORD (residues 632-996) (Tong, Yang *et al.* 2012). Comparing Osh3p-ORD, Osh4p, Osh5p, Osh6p and Osh7p revealed that only Osh4p and Osh5p were capable of extracting sterol from artificial membranes, as well as of transporting DHE, and for both proteins DHE transport was accelerated by counterexchange with PI(4)P. The two proteins showed comparable affinities, which was not surprising as they display a very high sequence similarity (**Figure 46**).

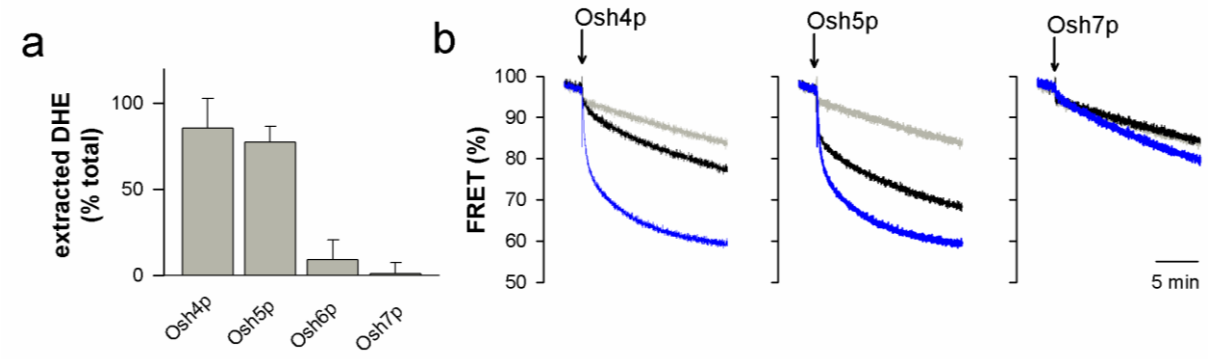

Figure 46. Osh6p and Osh7p do neither extract nor transport DHE

(a) DHE extraction (2 mol%) from 150 µM liposomes was quantified by measuring the decrease in FRET between DHE and DNS-PE (2.5 mol%) 5 min after the addition of 3 µM Osh protein. Data were normalized in comparison to extraction of 10 mM M-β-CD. **(b)** DHE transport was measured between 100 µM liposomes containing 10 mol% DHE and 2.5 mol% DNS-PE and 900 µM liposomes containing (blue curves) or not (black curves) 2 mol% PI(4)P after addition of 100 nM Osh protein. Buffer control is shown in grey. Osh6p displayed transport kinetics very similar to Osh7p (data not shown).

Osh6p and Osh7p were found to transport of DHE very slowly, corroborating previous results based on a radioactive cholesterol transport assay (Schulz, Choi *et al.* 2009). Importantly, we were able to indicate for the first time that these proteins were unable to extract sterol from liposomes, suggesting that they do not recognize this type of molecule. Interestingly, we also note that the very slow transport activity of Osh6p and Osh7p was blocked completely by the presence of PI(4)P in the system. Similar results were found for Osh3p-ORD (data not shown). Jointly, these results suggested that these proteins were unable to recognize sterol, are not sterol/PI(4)P exchanger but can extract PI(4)P (**Figure 46**).

PI(4)P-binding is a conserved feature of Osh proteins

At this point we made some attempts to analyze the structural aspects of Osh proteins: We compared the sequences of Osh4-7p and sequence conservation levels, finding that the residues interacting with PI(4)P in the crystal structure of Osh4p are highly conserved between Osh proteins. The residues implied in PI(4)P recognition form the core of the ORP/Osh protein fingerprint motif EQVSHHPP that is strictly conserved in ORP/Osh proteins from yeast to human (**Figure 30**, **Figure 32**, **Figure 47a**). Importantly, we built an homology model of Osh7p based on the crystal structure of Osh4p-PI(4)P and identified a steric hindrance that would exclude sterol from the lipid-binding pocket, results that anticipated those reported later by Maeda *et al.* in the crystal structure of Osh6p-PS (Maeda, Anand *et al.* 2013). These structural features of Osh lipid binding lead us to study the binding of PI(4)P in Osh proteins (**Figure 47a**).

We therefore sought different ways of proving PI(4)P extraction, and finally opted for the NBD-PH_{FAPP} PI(4)P probe we developed to test Osh3p-ORD, Osh5p, Osh6p and Osh7p. Using this fluorescent tool, we found that all of the tested Osh proteins are capable of extracting PI(4)P, but that this extraction was inhibited by ergosterol only for Osh4p and Osh5p, whereas Osh3-ORD (data not shown), Osh6p and Osh7p extracted PI(4)P to the same extent from membranes whether they contained ergosterol or not. All Osh proteins transported PI(4)P between liposomes, yet at a slower rate compared to Osh4p, except for Osh5p. Activation of PI(4)P transport by sterol was only observed for Osh4p and Osh5p (**Figure 47b,c**).

These results were important because they suggested that all the Osh proteins tested extract PI(4)P but that only some of them efficiently bind to sterol. In other words, the common function of the ORP/Osh proteins would not be binding to and extracting sterol as initially thought (Beh, Cool *et al.* 2001) but to bind to and extract PI(4)P. Few months later, Im and co-workers published the structure of the Osh3p-ORD in complex with one PI(4)P molecule confirming the ability of another Osh protein to bind and extract PI(4)P, thus revealing the conserved binding mode of PI(4)P between Osh3p and Osh4p (Tong, Yang *et al.* 2013). Moreover, they demonstrate with Trp-based assays we had developed for Osh4p (de Saint-Jean, Delfosse *et al.* 2011) that Osh3p-ORD does not extract DHE. Structural analysis indicated that a steric hindrance in the lipid-binding pocket prevents Osh3p from binding

sterol (Tong, Yang *et al.* 2013). Thus, they provided the first demonstration that the common function of ORP/Osh proteins is not to bind sterol but likely to interact with and extract PI(4)P molecules.

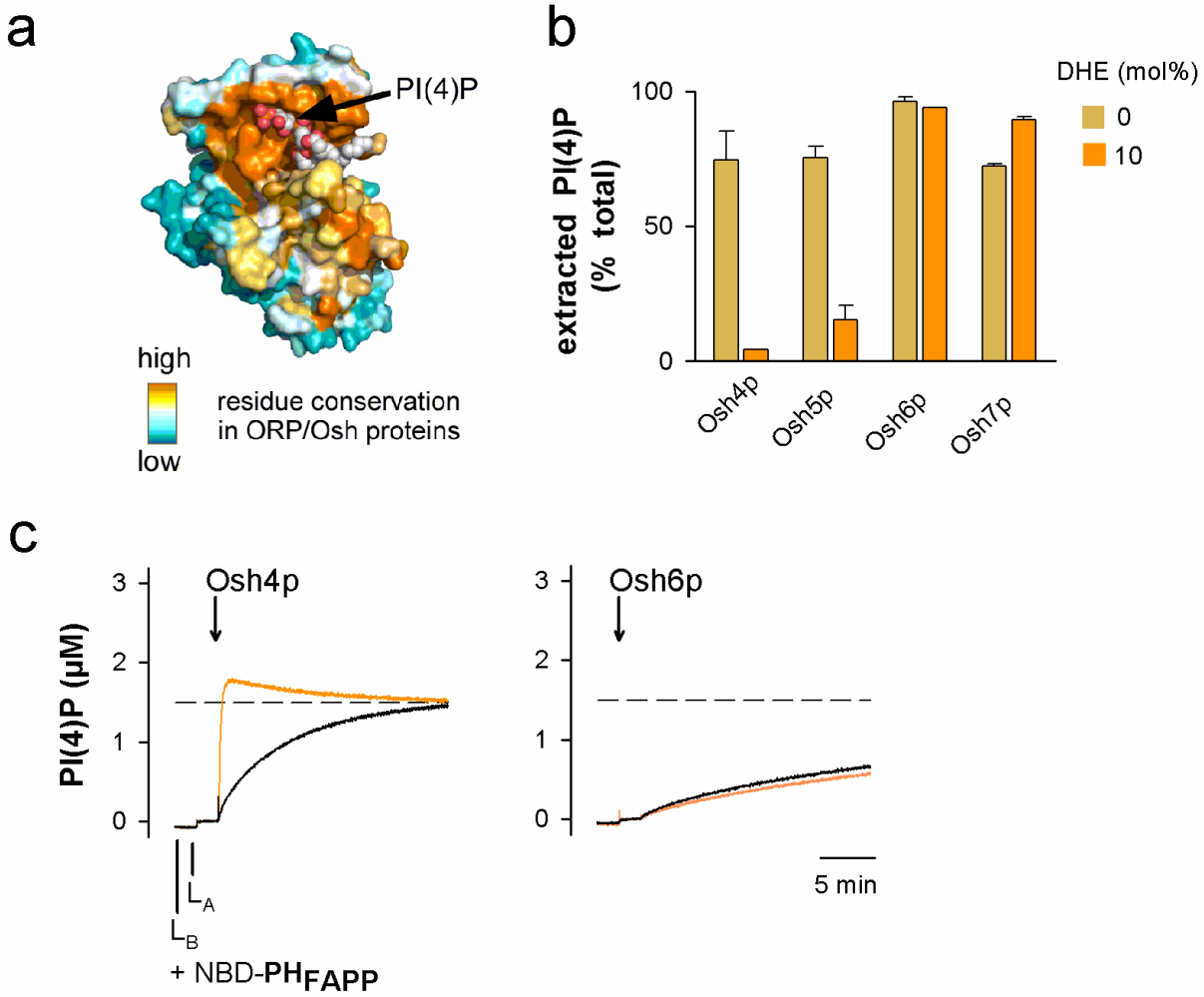

Figure 47. PI(4)P extraction and competition with ergosterol.

(a) Residues that mediate the interaction between Osh4p and PI(4)P are strictly conserved in the other ORP/Osh proteins. **(b)** DOPC liposomes (300 µM) containing PI(4)P and doped or not with 10 mol% DHE were incubated with Osh protein (3 µM) at 30°C in the presence of NBD-PH_{FAPP} (250 nM). The signal was normalized to estimate the amount of PI(4)P that is extracted by using the signal measured with similar liposomes but devoid of PI(4)P as a reference. The values are mean ± S.E.M. of three independent experiments. **(c)** PI(4)P transport assay. DOPC/PI(4)P/Rhod-PE liposomes (96/2/2 mol/mol, 300 µM lipids, L_B) were incubated with NBD-PH_{FAPP} (250 nM). Then DOPC liposomes (300 µM lipids, L_A) containing or not 5 mol% DHE were added. After 3 min, Osh6p or Osh4p (500 nM) was injected. The dashed line corresponds to full equilibration of PI(4)P between liposomes. Osh5p has an activity similar to that Osh4p whereas Osh7p has an activity similar to that of Osh6p.

Identification of novel lipid ligands for Osh proteins

In an interesting comment on the crystal structures of Osh3p, Levine and Menon raised a question we had been asking ourselves for quite some time then: If Osh4p binds PI(4)P and sterol, and Osh3p binds PI(4)P by the same mode, but not sterols, what is then the sterol-equivalent for Osh3p (Levine and Menon 2013)?

Our first strategy for the identification of an alternative ligand for Osh6p was to co-crystallize Osh6p empty or with PI(4)P and solve its three-dimensional structure. This could allow us to define how PI(4)P is bound to Osh6p but also to use docking tools with the empty Osh6p to identify potential ligands. The GST-tagged Osh6p was purified on an affinity column (glutathione sepharose beads) and the GST was cleaved by thrombin. Next the protein was incubated with DOPC liposomes doped with 10 mol% PI(4)P and loaded with 220 mM Sucrose, 50 mM K-Acetate, pH=7.2. The sample after incubation undergoes an ultracentrifugation to pellet the liposomes and to recover the supernatant which contain the soluble Osh6p, loaded with PI(4)P. The complex was next purified to homogeneity by size exclusion chromatography. The details of the crystal structure solved by Vanessa Delfosse at the CBS, Montpellier, will be described below.

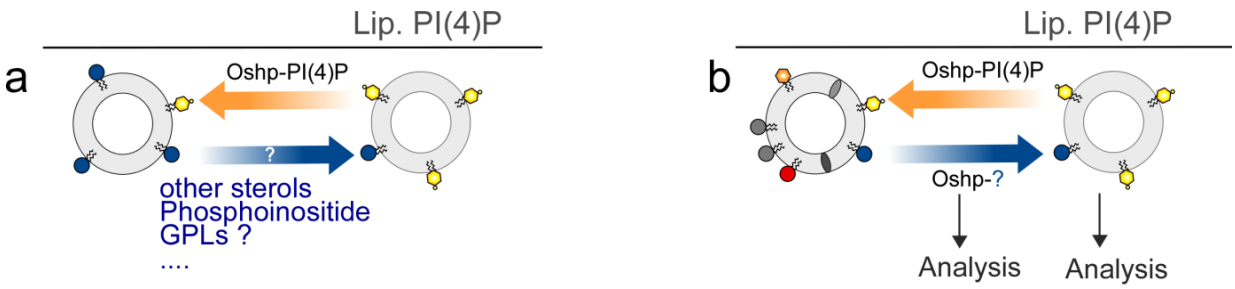

Figure 48. Screening strategies to identify a second lipid ligand for Osh proteins.

(a) One possible strategy would have been to use the transport assay based on the NBD-PH_{FAPP} to see whether Osh6p or Osh7p transport PI(4)P between two populations of liposomes more efficiently in the presence of a second lipid ligand (other than ergosterol, in blue). For this, we would have produced large set of DOPC liposomes incorporating each a few amount of one particular lipid species (marked) to see if the proteins transport PI(4)p faster. **(b)** Another strategy was to see whether Osh6p or Osh7p transports more efficiently PI(4)P into liposomes incorporating yeast total lipid extract and to analyze which lipid is bound to the Osh proteins (by TLC, mass spectrometry, electrophoretic mobility shift assay) and/or which lipid is removed from liposome that contains TYE.

At the same time, as an alternative for identifying unknown interaction partners we tried to use a total membrane extract of yeast cells (Yeast Total Extract, YTE, Avanti Polar Lipids). We wanted to see whether incorporation of YTE *in trans* of PI(4)P would accelerate

transport of the latter *in vitro*. In order words, in a PI(4)P transport assay, one population of liposome contains PI(4)P, the second populations contain or nor YTE. If in this latter case, an acceleration of PI(4)P was seen, this could indicate that YTE contains a lipids that is efficiently counterexchanged with PI(4)P. (**Figure 48b**) We found significant activation of PI(4)P transport by Osh4p, which was not surprising as ergosterol is the most abundant lipid species in yeast and thus in YTE (Ejsing, Sampaio *et al.* 2009). The transport of PI(4)P by Osh6p was increased, but only when higher amounts of YTE were incorporated in liposomes (> 10 mol%) (data not shown).

We also tried to look at the loading of Osh protein by electrophoretic mobility shift assay on native PAGE. We used Osh4p as a control and found that it displayed varying migration distances on Native-PAGE depending on its loading and the nature of the loaded ligand. We also tried to see differences in migration with Osh6p and could detect them for Osh6p incubated with PI(4)P, but not for the YTE (data not shown). We thus wanted to identify the lipid species that accelerated the PI(4)P transport by thin layer chromatography (TLC), but our efforts were anticipated by the abovementioned publication of the crystal structure of Osh6p in complex with PS by the Gavin group (Maeda, Anand *et al.* 2013). Based on their results demonstrating the ability of Osh6p and Osh7p to transport PS, we modified our scope towards the identification of a PS/PI(4)P exchange activity for these proteins.

Molecular characterization of the lipid transport activity of Osh6p

Structural basis of the PI(4)P recognition by Osh6p

As we had previously shown that Osh6p and Osh7p are capable of binding PI(4)P we aimed to determine whether the binding mode for PI(4)P is the same as for Osh4p. We restricted our efforts to Osh6p due to the very high sequence homology between Osh6p and Osh7p. The group of William Bourguet at the CBS, Montpellier, were able to solve the crystal structure of the Osh6p-PI(4)P complex at a 2.55 Å resolution (PBD entry 4PH7). The electron density of the ligand matched perfectly well with a C18:0-C20:4 PI(4)P, the major species found in the porcine brain PI(4)P (Avanti Polar Lipids) we used to obtain the Osh6p-PI(4)P complex. The overall structure of Osh6p-PI(4)P displays a fold similar to Osh6p-PS (PDB entry: 4B2Z) (Maeda, Anand *et al.* 2013) (**Figure 49b**) with a hydrophobic lipid-binding tunnel

defined by an incomplete β-barrel (residues 133-317), completed by a C-terminal region (residues 318-435) and flanked by a N-terminal domain (70-128) (**Figure 49a**). With an RMSD of 0.363 Å for *403* residues, the structure of the PI(4)P and PS-bound form of Osh6p are very similar (**Table 1**).

	Osh6p/PI4P (*pdb id 4PH7*)
Data collection	
Space group	$P\,2_12_12_1$
Cell dimensions	
a, *b*, *c* (Å)	114.11, 122.26, 141.49
α, β, γ (°)	90.00, 90.00, 90.00
Resolution (Å)	48.56 – 2.55 (2.69 – 2.55)*
R_{sym}	0.106 (0.496)
$I / \sigma I$	15.65 (4.95)
Completeness (%)	100.00 (100.00)
Redundancy	8.2 (8.1)
Refinement	
Resolution (Å)	47.29 – 2.60
No. reflections	30,180
R_{work} / R_{free}	0.188 / 0.237
No. atoms	
protein	12,697
ligand	260
water	543
B-factors	
protein	33.9
ligand	32.5
water	32.7
R.m.s. deviations	
Bond lengths (Å)	0.003
Bond angles (°)	0.727

*Values in parentheses are for the highest-resolution shell.

Table 1. Data collection and refinement statistics.

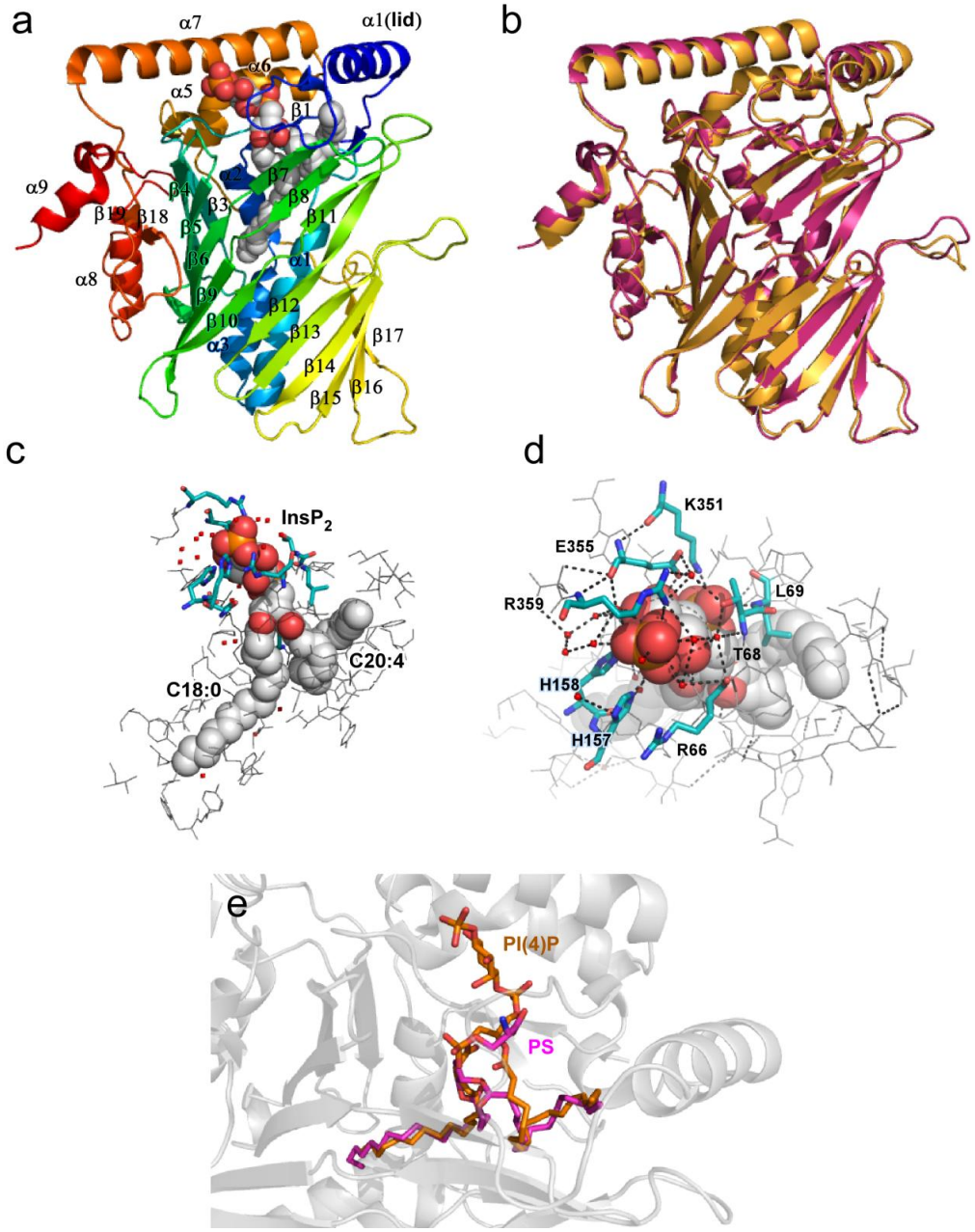

Figure 49. Structure of Osh6p in complex with PI(4)P

(a) Overall structure. The short lid region is shown in blue (residues 35-69), the N-terminal domain in blue-green (70-128), the β-barrel in green (133-317) and the C-terminal domain in red-orange (318-435). PI(4)P is represented as sticks with carbon atoms colored in grey, oxygen atoms in red and phosphorus in orange. **(b)** Structure superposition of Osh6p in complex with brain PI(4)P (in orange, PDB entry: 4PH7) or PS (in purple; PDB entry: 4B2Z). **(c)** Conformation of the PI(4)P molecule bound to Osh6p. The position of the two acyl chains and the polar head of the lipid ($InsP_2$) are indicated. Water molecule are represented **(d)** Close-up view of the PI(4)P binding site. PI(4)P is shown in black with oxygen atoms colored in red and phosphorus atoms in orange. Water molecules contacting PI(4)P and the protein are displayed (red dot). The key residues involved in the recognition of the PI(4)P polar head are in stick, with carbon atom in cyan, oxygen atoms in red and nitrogen atom in blue. H-bonds are represented by black dashed line. **(e)** Superposition of PI(4)P (colored in orange) and DOPS (colored in purple) molecules in Osh6p. The backbone of the protein is shown in light-grey.

The lid segment (residues 35-69) adopts a similar conformation to shield the PS or PI(4)P molecule. The *sn*-1 oleate (C18:0) chain of PI(4)P is inserted deep in the hydrophobic ligand binding pocket whereas the *sn*-2 arachidonate (C20:4) chain is twisted towards the lid (**Figure 49c**). The 4-phosphate group of PI(4)P makes direct hydrogen-bonds with the side-chains of H157, H158 (β4-β5) and R359 (α7) and water-mediated interaction with the side-chain of R359, the main chain oxygen atom of R66 (lid) and E355 (α7). The 1-phosphate group joining the inositol ring and the glycerol moiety makes direct contact with K126 (β2), K351 (α7) and the backbone amide of L69 in the lid (**Figure 49d**) and a water-mediated interaction with the backbone amide of N129. Finally, the hydroxyl groups of the inositol ring are engaged in direct or water-mediated hydrogen bonds with the main chain oxygen atoms of R66, T68 (lid) and N129 (loop connecting β2 and β3) and with the side chain of E355 (α7).

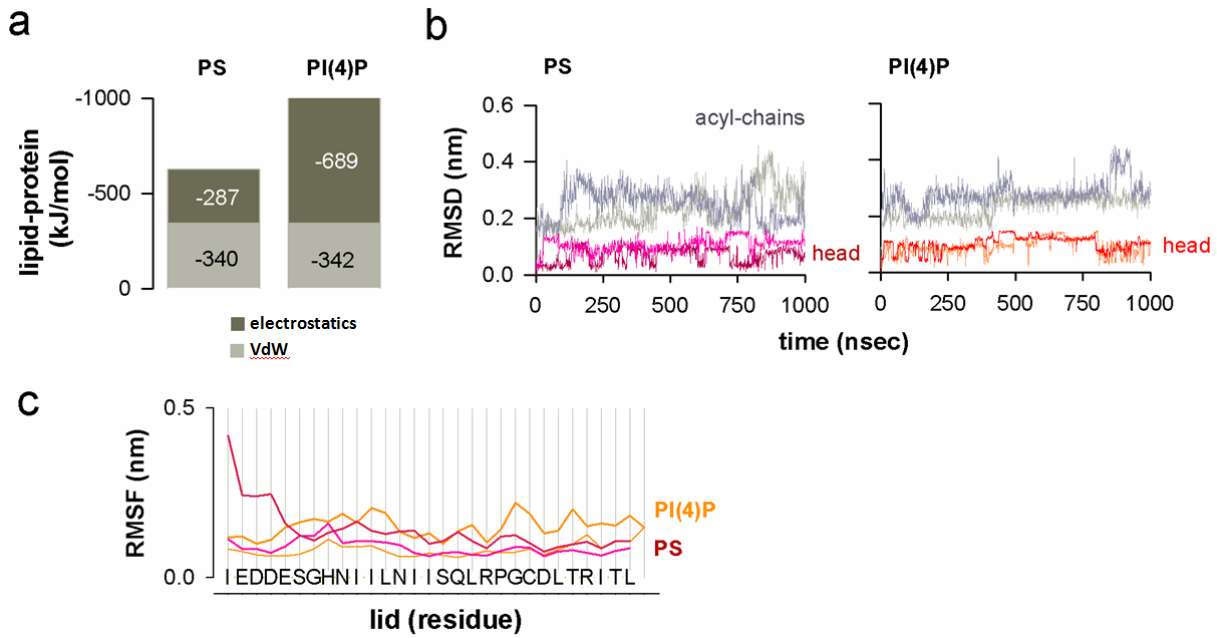

Figure 50. MD simulations of Osh6p in complex with PS or PI(4)P.

(a) Electrostatic and van der Waals contribution in the binding of PS or PI(4)P to Osh4p. **(b)** Dynamic behavior of PS (left) and PI(4)P (right) inside the binding pocket of Osh4p. The RMSD of two independent trajectories of PS or PI(4)P polar head and acyl chains are represented. **(c)** RMSF of residues 39-69, indicative of the motion of the ORD lid during 1 μs MD simulation of Osh6p bound to PS or PI(4)P, determined for each case from two independent trajectories.

Not only the headgroups of PI(4)P and PS interact with different residues, but also the glycerol backbones of PI(4)P and PS that are chemically identical in both ligands. We were therefore interested in the dynamics of the two ligands in their binding site and performed molecular dynamics simulation of the two ligands bound to Osh6p (Experiments performed by Stefano Vanni). Two important facts must be noted: First, both ligands display similar

restricted mobility inside the binding pocket: The lid remains tightly closed and the heads are tightly bound, whereas the acyl chains are more mobile. However, the binding energy of PI(4)P is significantly higher than for PS, mainly due to increased electrostatic interactions between the polar head and the Osh6p protein. (**Figure 50**)

We furthermore compared the PI(4)P-binding mode by Osh4p (PBD entry 3SPW) and Osh6p. Intriguingly, PI(4)P binding energy to Osh6p is higher for both Coulomb and van der Waals-interactions. Mobility of the protein lid and the lipid acyl chains are increased in Osh4p compared to Osh6p. Overall, these data suggest that the stability of PI(4)P is higher when this lipid is bound to Osh6p than bound to Osh4p. (**Figure 51**)

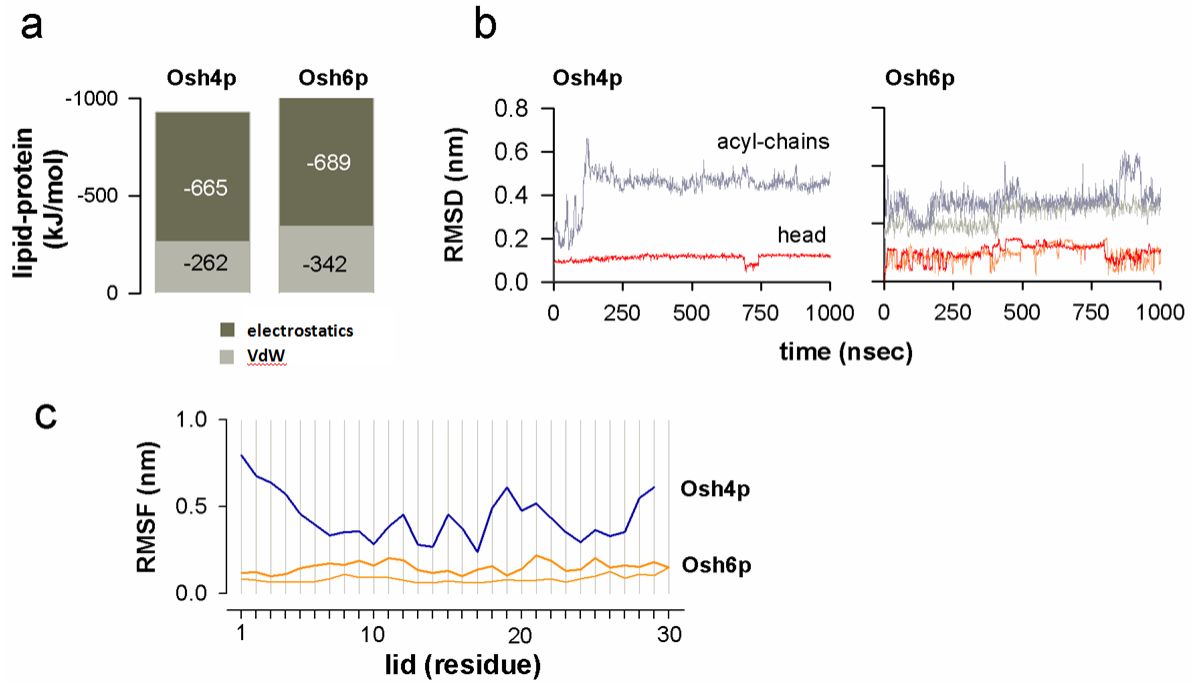

Figure 51. Comparison between the dynamic behavior of PI(4)P in Osh4p and Osh6p.

(a) Electrostatic and Van der Waals contribution in the binding of PI(4)P to Osh4p and Osh6p. **(b)** Dynamic behavior of PI(4)P inside the binding pocket of Osh4p (left, one trajectory) or Osh6p (right, two independent trajectories). The RMSD of PI(4)P polar head and acyl chains is represented. **(c)** RMSF of residues that constitute the lid of Osh4p ORD (one trajectory) or Osh6p ORD (two trajectories) during 1 µs MD simulation.

PS competes with saturated PI(4)P for binding Osh6p.

In a first step toward demonstrating that Osh6p exchange PS with PI(4)P, we examined the ability of sterol or PS to compete with PI(4)P for binding Osh6p. As expected, the presence of an excess (10 mol%) of DHE in liposomes prevents Osh4p but not Osh6p

from extracting PI(4)P. (**Figure 52a**) Surprisingly, the presence of 10 mol% of dioleyl-phosphatidylserine (DOPS) had also no clear inhibitory effect on the extraction of PI(4)P by Osh6p. (**Figure 52a**) Thus, whereas DHE prevents the extraction of PI(4)P by Osh4p, DOPS fails to efficiently compete with PI(4)P for occupying Osh6p.

It is noteworthy that budding yeast does not synthesize polyunsaturated fatty acids such as found in the PI(4)P we used for our experiments. We therefore prepared liposome containing saturated PI(4)P, namely di-C16:0 PI(4)P that is chemically closer to the PI(4)P species found in yeast. Control experiments with Osh4p showed that 10 mol% DOPS has a mild inhibitory effect on its ability to extract di-C16:0 PI(4)P (**Figure 52**). Contrastingly, the extraction of di-C16:0 PI(4)P by Osh6p was half-inhibited by 5 mol% of DOPS and almost fully abolished by 10 mol% DOPS. Jointly, these data suggested that saturated PI(4)P was more prone to be substituted by PS. Di-C16:0 PI(4)P is structurally closer to the PI(4)P species found in yeast, and we pursued further experiments mainly with the fully saturated PI(4)P.

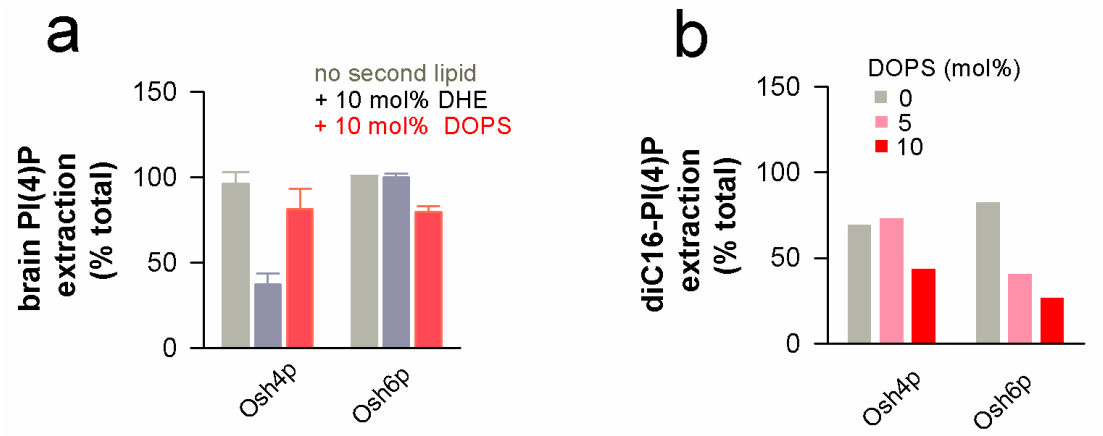

Figure 52. PI(4)P extraction assay.

(a) DOPC liposomes (300 µM) containing 4% brain PI(4)P and doped or not with 10% mol of a second lipid ligand (DOPS or DHE) were mixed with Osh4p or Osh6p (3 µM) at 30 °C in the presence of NBD-PH_{FAPP} (250 nM). The NBD spectrum was recorded from 505 to 650 nm (λ_{ex}=490 nm) before and after the addition of Osh proteins. Each value is a mean ± SEM of three independent experiments. **(b)** DOPC liposomes (300 µM) containing di-C16:0 PI(4)P and increasing amount of DOPS (0, 5 or 10 mol%) were incubated with Osh4p or Osh6p (3 µM) at 30 °C in the presence of NBD-PH_{FAPP} (250 nM). The signal was normalized to estimate the amount of PI(4)P that is extracted by using the signal measured with similar liposomes but devoid of PI(4)P as a reference.

Osh6p exchanges PI(4)P for PS between two distinct membranes.

We then examined whether Osh6p exchanged PS with PI(4)P between two distinct membranes. In order to follow the transport of PS we have developed a tool to detect PS movement quantitatively in real-time. This tool is based on the discoidin-like C2 domain of lactadherin that had previously been used as GST-fusion for PS sensing *in vivo* (Yeung, Gilbert *et al.* 2008; Fairn, Schieber *et al.* 2011). Probe design and characterization is detailed in the Materials and Methods section: Recognition of phosphatidyl-L-serine with NBD-C2Lact. Ultimately we developed a fluorescence-based lipid transfer assay for PS with the NBD-$C2_{Lact}$ probe similar to the assay used for PI(4)P transport with the NBD-PH_{FAPP} probe.

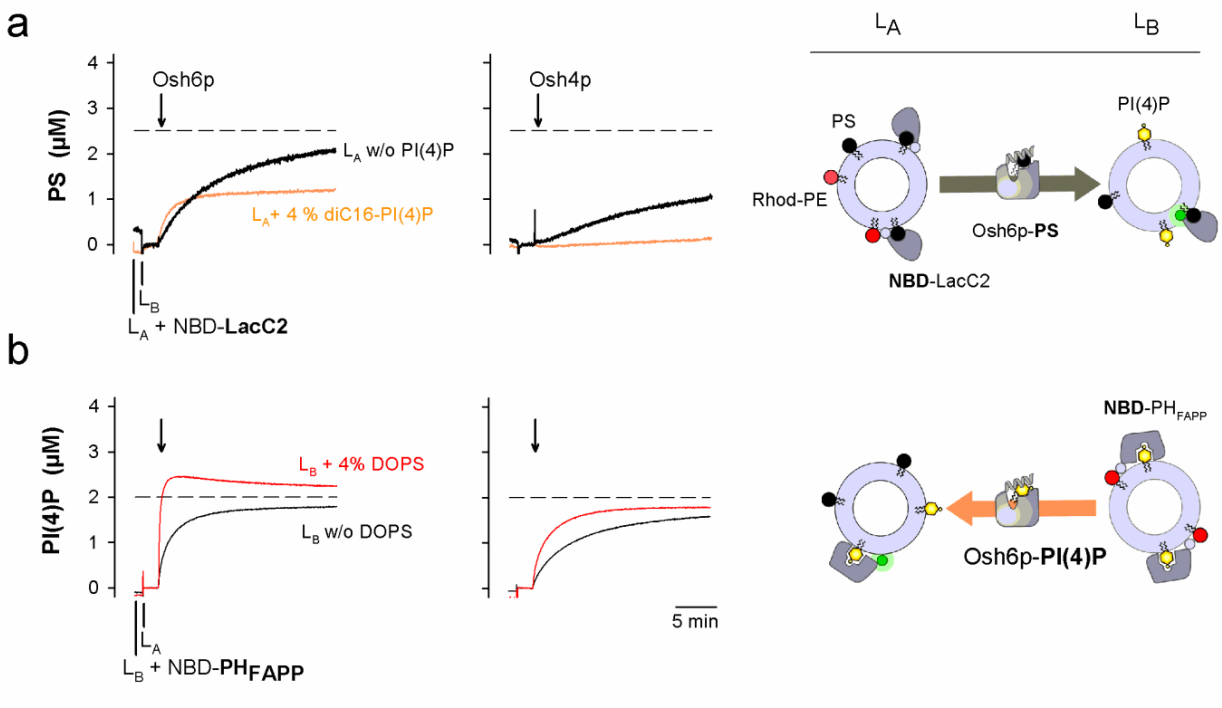

Figure 53. Transport of PS and PI(4)P between liposomes by Osh6p.

(a) PS transport assay. DOPC/DOPS/Rhod-PE liposomes (93/5/2 mol/mol, 200 µM total lipids, L_A) were mixed with NBD-$C2_{Lact}$ (250 nM) at 30°C. After one minute, DOPC liposomes (200 µM lipids, L_B) containing or not 4 mol% di-C16:0 PI(4)P were added. After 2 min, Osh6p or Osh4p (200 nM) was injected. The NBD signal increases since PS is transported to the L_B liposomes and the NBD-$C2_{Lact}$ translocates from L_A to L_B liposomes. The signal was converted into amount of PS present in L_B liposome (in µM). The dashed line corresponds to a condition where DOPS is fully equilibrated between liposomes. **(b) PI(4)P transport assay**. DOPC/PI(4)P/Rhod-PE liposomes (94/4/2 mol/mol, 200 µM lipids, L_B) were incubated with NBD-PH_{FAPP} (250 nM). Then DOPC liposomes (200 µM lipids, L_A) containing or not 5 mol% DOPS were added. After 2 min, Osh6p or Osh4p (200 nM) was injected. The dashed line corresponds to full equilibration of PI(4)P between liposomes.

Briefly, NBD-$C2_{Lact}$ (250 nM) was mixed with liposome L_A containing both 5 mol% PS and 2 mol% Rhod-PE and liposome L_B solely made of DOPC. The fluorescence of NBD-$C2_{Lact}$ was quenched due to a FRET process with Rhod-PE as the construct binds to PS-containing liposomes. Adding Osh6p (200 nM) caused a dequenching of the NBD signal, mirroring the transport of PS from liposome L_A to L_B and the translocation of NBD-$C2_{Lact}$ (**Figure 53a**). We determined the amount of PS transported by Osh6p by normalizing the NBD signal. To do so, we measured the NBD signal (F_{eq}) that corresponds to a situation where DOPS was fully equilibrated between liposomes, i.e. with L_A and L_B liposomes each containing 2.5 mol% PS. The initial transport rate was 1.2 PS/min *per* Osh6p. In comparison, Osh4p had a very slow initial PS transport rate (0.09 PS/min). In the presence of di-C16:0 PI(4)P, the rate of PS transport by Osh6p increased 3.5-fold (3.8 PS/min) whereas it was completely inhibited in the case of Osh4p.

We also measured the transport of PI(4)P in the reverse direction from liposome L_B containing 4 mol% PI(4)P to liposome L_A doped or not with 5 mol% DOPS. In the absence of DOPS, Osh6p transported PI(4)P with an initial velocity of 13.6 ± 2 PI(4)P/min (n=2). In the presence of DOPS, the rate (64 ± 5 PI(4)P/min (n=2)) was almost five-time higher (**Figure 53b**) and PI(4)P was equilibrated between liposomes within one minute. With Osh4p, a slight acceleration of the PI(4)P transport rate was seen (from 3 to 12 PI(4)P/min) but is not related to a counterexchange process, as PS transport was abolished. Jointly, our assays indicated that Osh6p transports more efficiently lipids when PS and PI(4)P are initially present in distinct membranes, suggesting that Osh6p can act as PS/PI(4)P exchanger.

PS and PI(4)P transport experiments were repeated by substituting di-C16:0 PI(4)P with brain PI(4)P. The transport of DOPS from L_A to L_B liposome (1.41 molecules/min *per* Osh6p) did not increase when liposomes L_B contained brain PI(4)P. The transport of brain PI(4)P in the absence of PS was very slow (0.27 PI(4)P/min per Osh6p) and was ten-time faster when L_A liposome contained DOPS (3 ± 0.25 PI(4)P/min (n=2)) but remained dramatically slower than in similar experiments done with di-C16:0 PI(4)P.

It is important to mention that Osh4p transports di-C16:0 PI(4)P and C18:0-C20:4 PI(4)P with the same efficiency (2.45 and 1.9 PI(4)P/min, respectively, data not shown) and also exchanges these two PI(4)P species with DHE at the same speed (23.91 and 22.2 PI(4)P/min, respectively).

Discussion

Our data, together with previous findings, shows that Osh6p transports PS *in vitro* (Maeda, Anand *et al.* 2013). In conditions where PS and PI(4)P are in distinct membranes, the transport of both lipids is stimulated. However, unlike for sterol transport by counterexchange with PI(4)P for Osh4p, the transport rates are not identical for PI(4)P and PS, indicating a lesser extent of coupling between the two transport kinetics In addition, PS transport by Osh6p is blocked after a certain number of exchange cycles (**Figure 53a**), eventually by competition between PI(4)P and PS for Osh6p-binding.

We suggest that Osh6p has a higher affinity for PI(4)P than for PS. As we have structural data of the protein bound to PS or PI(4)P, it is possible to provide quantitative evidence of that. MD simulation indicate that the interaction energy between Osh6p and a molecule of PI(4)P is higher than between Osh6p and PS. This is mainly due to the fact that the polar head of PI(4)P makes numerous and specific electrostatic interaction with charged residues of Osh6p that the polar head of PS do not. It appears to us that the presence of PI(4)P in the ER might inhibit the ability of Osh6p to extract PS from the ER and to convey it to the PM. This might explain why yeast lacking Sac1p presents a defect in PS distribution, with PS accumulating in the ER membrane (Tani and Kuge 2014).

We also observed for OSBP that the transport of sterol is blocked after a few rounds of sterol/PI(4)P exchange as PI(4)P accumulates in the ER-like liposomes and competes with sterol for occupying the lipid-binding site of the OSBP ORD. This blockage could be overcome by removing PI(4)P through hydrolysis by its phosphatase Sac1p (Mesmin, Bigay *et al.* 2013). In a near future, we will carry out PS/PI(4)P exchange experiments with ER-like liposome decorated by Sac1p and containing PS to test whether the transport of PS to Golgi-like liposomes (doped with saturated PI(4)P) is rapid and sustained over time. Likewise, in collaboration with Alenka Copic, IJM, Paris, we will examine in yeast how PI(4)P regulates the PS transport ability of Osh6p, notably by examining whether an Osh6p mutant, deficient in binding PI(4)P, still transports PS in an unregulated manner in the absence of Sac1p.

It will furthermore be interesting to see whether Osh6p can use the metabolic energy of PIPs like Osh4p to transport PS against a concentration gradient. We are able to purify an active fragment of PI4KIIα. An interesting idea would be to anchor Sac1p and this PI4KIIα-fragment to ER- and Golgi-like liposomes, respectively, in order to generate from PI,

contained in Golgi-like membrane, in the presence of ATP, a PI(4)P gradient between these two liposome populations' membranes, which will be self-maintained by the two enzymes for several minutes. In this model system, we will test the ability of Osh6p to create a PS gradient by PS/PI(4)P exchange.

Intriguingly, in eukaryotic cells, PS at the PM has a higher saturation level than at the ER (Schneiter, Brugger *et al.* 1999). We have observed an important effect of acyl chain saturation on the transport of PI(4)P by Osh6p. It would be interesting to see whether acyl chain saturation also affects transport of PS by this LTP. Owing to its acyl chain specific PS transport Osh6p could participate in the accumulation of saturated PS at the PM, and thus in the formation of a saturation gradient at the ER/PM interface.

To sum up, we aim to fully demonstrate that Osh6p uses PI(4)P to participate in the accumulation of PS at the PM. Further characterization of the effect of kinetic coupling, PI(4)P hydrolysis and PS saturation levels on the transport of PS by Osh6p is therefore required. This work will allow us to propose a general model: ORP/Osh proteins use PI(4)P gradients to convey sterol or other lipid species for creating, in turn, various other lipid gradients in eukaryotic cells.

CONCLUSION

A major feature of eukaryotic cells is their uneven lipid distribution. Organellar membranes have different lipid compositions to ensure their functionality. Accumulation of certain lipid species in organelles at the expense of other ones leads to lipid concentration gradients within the cells. Such gradient are particularly pronounced for sterols, sphingolipids and PS that are enriched at the TGN and PM but are ,paradoxically, scarce at the ER where they are synthesized; these lipids thus need to be transported from the ER to other organellar membranes (van Meer, Voelker *et al.* 2008). Vesicular trafficking exchanges large amounts of lipid material between organelles, but does not appear to be the major route for the transfer of sterol and PS. More generally, lipid homeostasis does not seem to solely depend on vesicular trafficking. It is rather and widely assumed that non-vesicular lipid transfer mechanisms exist to maintain lipid homeostasis in cells, guaranteed by LTPs (Lev 2010).

Proteins from the ORP/Osh family are among the proteins that could mediate non-vesicular lipid traffic. Some of them have been initially found to bind and transport sterols between membranes. Three years ago, our group has identified that one ORP/Osh protein, the yeast Osh4p, has a striking feature and a unique ability among all the other LTPs: the capacity to extract and transport a very singular lipid of the Golgi, PI(4)P, and to exchange this lipid with sterol (de Saint-Jean, Delfosse *et al.* 2011). These findings allow proposing a new model to explain how sterol is transported in a vectorial manner from the ER to late membranes. One goal of my thesis was to detail in a very accurate manner the biochemical properties of Osh4p. I established to which extent Osh4p is capable of intimately coupling transport of both its ligands in opposite directions. Moreover, we established that the rapid sterol/PI(4)P counterexchange allows transport of sterol against its concentration gradient. In addition we showed that the lipid saturation gradient, as found at the ER/Golgi interface facilitates sterol transport by Osh4p, but cannot bypass the requirement for PI(4)P. Maintenance of the PI(4)P gradient by PI(4)P hydrolysis sustains sterol transport. These findings show that Osh4p has the intrinsic ability to use the energy of a PI(4)P gradient controlled by PI4K and PI(4)P phosphatase that exist at the ER/late membrane to create and maintain in turn a sterol gradient between these compartments. This is the first demonstration that a lipid transport protein can create *de novo* a lipid gradient between two distinct membranes.

We next tested whether other Osh proteins can bind sterols and/or PI(4)P and showed that not all of them bind sterols, but that the majority of Osh proteins (all of the tested) are capable of binding PI(4)P. The high conservation of the residues interacting with PI(4)P among ORP/Osh proteins in addition to recent findings (Tong, Yang *et al.* 2013) implies that this is also the case for the ORP/Osh proteins we did not test. Osh6p has been shown to extract PS from membrane and transport it *in vitro* and *in vivo* (Maeda, Anand *et al.* 2013). In collaboration with the Bourguet's lab we have solved the crystal structure of the Osh6p/PI(4)P complex, showing mutually exclusive binding of PS and PI(4)P as observed for sterol and PI(4)P in Osh4p. Our preliminary experiments suggest that Osh6p ensures a vectorial transport of PS, driven by PI(4)P in a manner similar to Osh4p, i.e. Osh6p likely function as a PS/PI(4)P counterexchanger. Further aspects of this mechanism need to be elucidated, such as the effect of PI(4)P gradient maintenance, the transport of PS against a concentration gradient and the effect of lipid saturation on transport activity. Determination for the role of this mechanism in transport activity *in vivo* is currently ongoing.

Connecting sterol transport by the Osh proteins to PIP metabolism can also explain certain findings linking Osh deletions to other PIP-dependent processes, such as *post*-Golgi secretion (Alfaro, Johansen *et al.* 2011), PS translocase activity by Drs2p (Muthusamy, Raychaudhuri *et al.* 2009) or sphingolipids biosynthesis (LeBlanc, Fairn *et al.* 2013). Numerous data suggest that Osh4p counteracts two enzymes Sec14p and Pik1p, responsible for producing the Golgi PI(4)P pool that is mandatory for vesicle genesis but also regulates Drs2p, likewise involved in this process by creating curvature. The sterol/PI(4)P exchange model that we propose for Osh4p might well explain these findings as PI(4)P is exploited by this protein to convey sterol. In certain conditions, this resource becomes rare (as in Sec14p-deficient yeast) and its exploitation by Osh4p blocks vesicle formation. It is however not clear whether the use of a common lipid, PI(4)P, by lipid transport and the genesis of *post*-Golgi vesicles is a proof of a necessary synchronization between these two processes.

The link between Osh proteins and PI(4)P might also explain observations about the common essential function of this class of proteins: Deletion of all Osh proteins is lethal, but any single Osh protein (except Osh1p) restores viability (Beh, Cool *et al.* 2001). Which is the master switch for Osh-related viability in yeast? All Osh proteins capable of restoring viability of a yeast strain deprived of Osh proteins are found in the region between the TGN and the PM (only Osh1p localizes to the NVJ). One hypothesis is that Osh proteins with the exception

of Osh1p play a major role in the remodeling of the *trans*-Golgi, as proposed for Osh4p, and of *pos*t-Gogi traffic vesicles *en route* to the PM. The use of PI(4)P might allow Osh protein to remodel the lipid composition of these compartments by supplying sterol and PS in exchange with PI(4)P. Such membrane remodeling processes, as they depend on PI(4)P, would be intimately linked with a second event in the life of secretory vesicles: docking with the PM. Recently, PI(4)P extraction by Osh4p has been shown to be required in *post*-Golgi secretion (Ling, Hayano *et al.* 2014). An appealing idea is that the disappearance of PI(4)P from secretory vesicles is a consequence of an exchange process mediated by Osh protein and thus signals a full remodeling of the lipid composition of these vesicles. The absence of PI(4)P could then also act as an "on" signal for docking processes at a stage when the secretory vesicles have a lipid composition similar or close to that of the PM, with a high density of PS and sterol. Such a hypothesis might well explain why in ΔOsh-strains sterols are wrongfully distributed to internal membranes at the expense of the PM (Beh, Cool *et al.* 2001) and why docking processes are blocked (Beh and Rine 2004).

Another important result has been to establish that the sterol/PI(4)P counterexchange is conserved from yeast to human by demonstrating the PI(4)P-dependent cholesterol transport of OSBP. In addition, OSBP uses PI(4)P not only for cholesterol counterexchange but also for tethering of ER and Golgi membranes to form a MCS. Cholesterol/PI(4)P counterexchange and PIP metabolism hence also influence OSBP's tethering activity. Availability of PI(4)P on the Golgi would hence control recruitment of OSBP, and its tethering activity would facilitate the recruitment of other LTPs such as CERT, Nir2 and possibly FAPP2. Recruitment of CERT could be mutually beneficial, as SM, synthesized from the CERT cargo ceramide, has a positive effect on sterol transport as shown for Osh4p; CERT recruitment could thus favor sterol transport by OSBP. These findings are resumed in **Figure 54**. Recent findings demonstrating that ORP9L also extracts cholesterol and PI(4)P and is capable of transporting each ligand (Liu and Ridgway 2014) further endorse our hypothesis of PI(4)P-binding as common feature of ORP/Osh proteins.

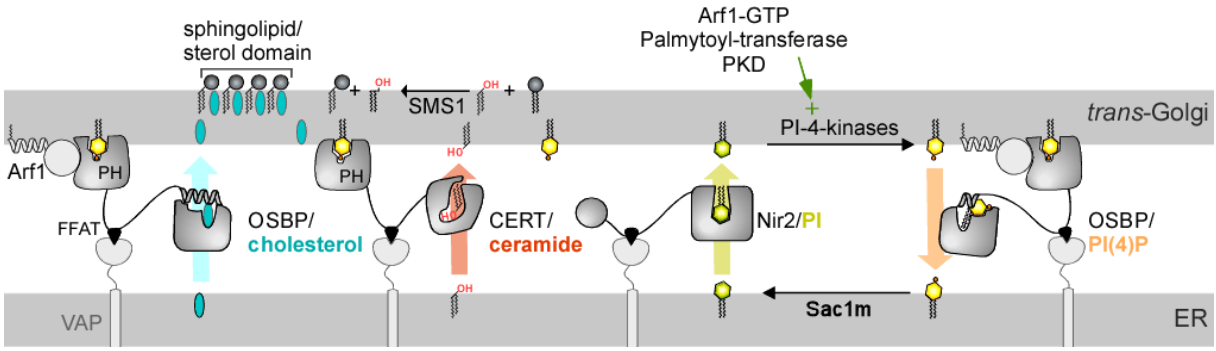

Figure 54. Interplay of LTPs at the ER-Golgi contact site

OSBP and CERT both bind ER and Golgi membranes simultaneously in a PI(4)P-dependent manner, allowing transport of cholesterol by OSBP and ceramide by CERT. Ceramide is metabolized on the lumenal face of the Golgi into SM, and formation of condensed sphingolipid/cholesterol complexes favors cholesterol transport. Retrograde PI(4)P transport by OSBP and anterograde PI transport by Nir2, coupled to PI4K and PI(4)P phosphatases allows to provide energy for the cholesterol transport of OSBP and control life-time of MCSs through PI(4)P degradation. Illustration from (Drin 2014).

There are now general interesting questions. First, what other ligands can be transported by the ORP/Osh protein family? For example, one interesting aim would be to provide an explanation for findings on Osh3p in its requirement for Opi3p PEMT activity at ER-PM MCSs (Tavassoli, Chao *et al.* 2013). Sac1p hydrolyzes the PM Stt4p-derived PI(4)P pool in a Osh3p-dependent manner (Stefan, Manford *et al.* 2011). Rather than tethering ER and PM to allow *in trans*-hydrolysis by Sac1p (Stefan, Manford *et al.* 2011), Osh3p could transport PE or PME, the substrates of Opi3p towards the enzyme by PI(4)P counterexchange. We aim also to define, on the basis of our preliminary results on Osh6p, whether or not ORP/Osh proteins create not only lipid concentration gradients, depending on the polar headgroup, but also lipid saturation gradients, by selecting lipid with a specific degree of acyl chain saturation between cellular regions. How does PI(4)P-mediated membrane tethering by ORP/Osh proteins affect transport by other proteins at MCSs? How is the regulator, PI(4)P, regulated in response to ORP/Osh proteins activity?

Coupling transport of one lipid ligand to the back-transport of PI(4)P also couples it to chemical energy in the form of ATP: In cell, a PI(4)P gradient is maintained by the activity of ATP-consuming PI4K and PI(4)P phosphatases. The intimate kinetic coupling of sterol transfer to PI(4)P provides directionality to transport and PI(4)P metabolism provides energy required to build up a sterol concentration gradient. Though chemical activity gradients favor transport of sterol by Osh4p, it cannot account for the directionality and rapidity of its transport. STARD4 has been proposed to rapidly equilibrate cholesterol between organellar

membranes along concentration gradients *in vivo* without specific targeting (Mesmin, Pipalia *et al.* 2011). It would be interesting to assess whether or not such a sterol transporter is capable of creating sterol gradients along a steep chemical activity gradient at rates compatible with the cellular time scale.

However, one of our favorite hypotheses is that the principle of lipid counterexchange is a general feature of LTP activity (Drin 2014). Sec14p and Sfh1p both bind two lipid ligands in a mutually exclusive manner and transport them between membranes, although kinetic coupling by counterexchange has not been observed yet (Gnamusch, Kalaus *et al.* 1992). Also, the Sec14-like human α-tocopherol (vitamin E) transport protein transports α-tocopherol. Recent findings by Kono *et al.* revealed that it recognizes a second lipid ligand, $PI(4,5)P_2$, and the extraction and stoichiometric, mutually exclusive binding of both ligands is a prerequisite for α-TTP function. In fact, α-TTP exchanges its two ligands by replacing one with the other between endosomes and the PM (**Figure 55**) (Min, Kovall *et al.* 2003; Kono, Ohto *et al.* 2013).

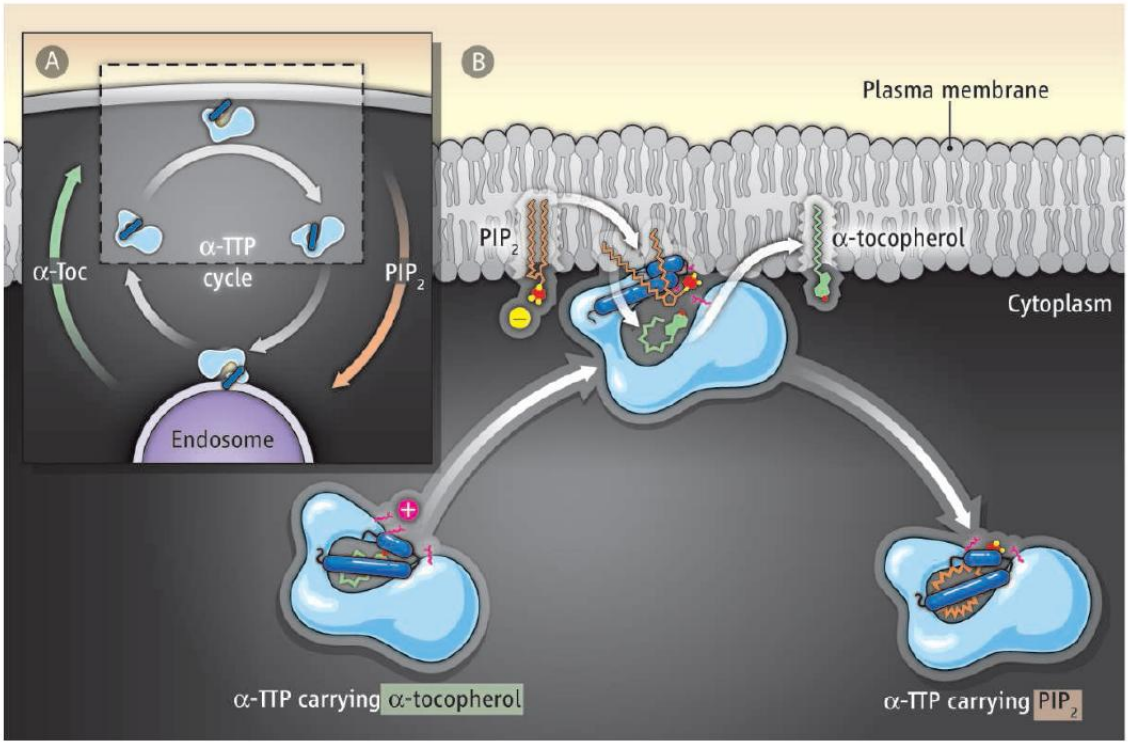

Figure 55. Lipid counterexchange as general feature of LTPs?

Proposed counterexchange mechanism for $PI(4,5)P_2$ and α-tocopherol by α-TTP. (Kono, Ohto *et al.* 2013) Illustration from (Mesmin and Antonny 2013).

A large number of the abovementioned issues and challenges are well known to biologists, yet in a different context: Membraneous ion pumps transport ions across membranes, such as the Na^+K^+-ATPase, a Na^+K^+ antiporter (Jorgensen 1982). Even though the challenge is the opposite (transporting polar cargo across an apolar territory for ion channels *versus* transporting apolar cargo across a polar territory for LTPs), many features are shared between these two. Transport must be specific to prevent perturbation of intra- and extracellular ion concentration and lipid homeostasis, respectively. The transport cannot simply follow the concentration gradient but needs directionality to create membrane potential and lipid asymmetry, respectively. Counterexchange is a frequent mechanism for ion homeostasis, and it may also be for lipid transport. Additionally, proteins are required for transport as they can have domains for interacting with both polar and apolar cargo and environment, respectively. And finally, both processes require chemical energy in the form of ATP that is converted into physical activity: Whereas ATP-consuming protein phosphorylation provides energy for protein pump activity, PI4K-mediated PI phosphorylation could provide it for LTP activity.

APPENDIX

Supplementary article

Building lipid 'PIPelines' throughout the cell by ORP/Osh proteins

Joachim Moser von Filseck, Bruno Mesmin, Joëlle Bigay, Bruno Antonny and Guillaume Drin

Biochemical Society TRANSACTIONS
Biochemical Society Transactions www.biochemsoctrans.org

Building lipid 'PIPelines' throughout the cell by ORP/Osh proteins

Joachim Moser von Filseck*, Bruno Mesmin*, Joëlle Bigay*, Bruno Antonny* and Guillaume Drin*[1]
*Institut de Pharmacologie Moléculaire et Cellulaire, Université de Nice Sophia-Antipolis and CNRS, 660 route des lucioles, 06560 Valbonne, France

Abstract

In eukaryotic cells, a sterol gradient exists between the early and late regions of the secretory pathway. This gradient seems to rely on non-vesicular transport mechanisms mediated by specialized carriers. The oxysterol-binding protein-related protein (ORP)/oxysterol-binding homology (Osh) family has been assumed initially to exclusively include proteins acting as sterol sensors/transporters and many efforts have been made to determine their mode of action. Our recent studies have demonstrated that some ORP/Osh proteins are not mere sterol transporters, but sterol/phosphatidylinositol 4-phosphate [PI(4)P] exchangers. They exploit the PI(4)P gradient at the endoplasmic reticulum (ER)/Golgi interface, or at membrane-contact sites between these compartments, to actively create a sterol gradient. Other recent reports have suggested that all ORP/Osh proteins bind PI(4)P and recognize a second lipid that is not necessary sterol. We have thus proposed that ORP/Osh proteins use PI(4)P gradients between organelles to convey various lipid species.

Introduction

Membranes define the limits and internal architecture of eukaryotic cells. Multiple lipid species belonging to three major classes (glycerophospholipids, sphingolipids and sterols) constitute the bilayer structure of organelle membranes. These lipids are distributed unevenly between the early [endoplasmic reticulum (ER), *cis*-Golgi] and late regions [*trans*-Golgi, plasma membrane (PM)] of the secretory pathway, such as to define the identity and properties of these compartments. Notably, sterol is scarce in the ER (<5 mol% of lipids) [1] and, contrastingly, represents up to 40 mol% of lipids in the *trans*-Golgi and the PM [2,3]. This accumulation of sterol in late membranes is key for cell function. Owing to its rigid structure, sterol reduces the flexibility of neighbouring lipids at the PM and guarantees its impermeability [4]. Because sterol is synthesized in the ER, mechanisms must exist to mediate the transfer of sterol from this organelle to other compartments.

Early studies from Simoni's group suggested that sterol is transferred rapidly (half-time of ~10 min) from the ER to PM mostly along non-vesicular routes in an energy-dependent manner [5,6]. Likewise, ER to PM transfer of ergosterol, the major sterol in yeast, takes place along non-vesicular routes [7]. Because sterol is hardly soluble in the cytosol, it needs specialized lipid-transfer proteins (LTPs) to be transferred between these compartments. Large efforts have been made at identifying these cytosolic LTPs and how they operate to create a sterol gradient. The best candidates belong to the oxysterol-binding protein-related protein (ORP)/oxysterol-binding homology (Osh) family [8] and, additionally in higher eukaryotes, to the StART [StAR (steroidogenic acute regulatory protein)-related lipid transfer] family [9]. In terms of mechanism, a first model posits that LTPs randomly equilibrate sterol between compartments by bidirectional shuttling [7]. The accumulation of sterol in the *trans*-Golgi membrane and the PM would be driven solely by its higher affinity for saturated glycerophospholipids and sphingolipids, which are highly abundant in these membranes [10]. Our recent studies on ORP/Osh proteins suggest an alternative model: LTPs would actively transport sterol in a vectorial manner throughout the cells by using the phosphatidylinositol 4-phosphate [PI(4)P] metabolic energy, thereby building sterol gradients.

The ORP/Osh family

ORP/Osh proteins constitute an evolutionarily conserved family in eukaryotes whose founding member is OSBP (oxysterol-binding protein). OSBP, identified in the 1980s, integrates a C-terminal domain specific for oxysterol [11] and cholesterol [12]. By definition, all other ORP/Osh proteins have an OSBP-related domain (ORD), the hallmark of which is the EQVSHHPP sequence motif [13]. Mammals, including humans, express 16 ORPs, whereas *Saccharomyces cerevisiae* encodes seven Osh proteins. ORP/Osh proteins are classified into subgroups on the basis of the sequence homology of their ORD. Most of them integrate additional domains, which target organelles and/or possibly translate a binding to sterol into specific functions [8].

Key words: lipid gradient, lipid-transfer protein, oxysterol-binding protein-related protein (ORP)/oxysterol-binding homology (Osh) family protein, phosphatidylinositol 4-phosphate, sterol

Abbreviations: CERT, ceramide-transfer protein; ER, endoplasmic reticulum; FFAT, two phenylalanine residues in an acidic tract; LTP, lipid-transfer protein; MCS, membrane-contact site; ORD, OSBP-related domain; ORP, oxysterol-binding protein-related protein; ORPTL, long ORPT; OSBP, oxysterol-binding protein; Osh, oxysterol-binding homology; PH, pleckstrin homology; PI, phosphatidylinositol; PI(4)P, phosphatidylinositol 4-phosphate; PM, plasma membrane; RILP, Rab-interacting lysosomal protein; SM, sphingomyelin; StART, StAR (steroidogenic acute regulatory protein)-related lipid transfer; VAP, VAMP (vesicle-associated membrane protein)-associated protein.

[1]To whom correspondence should be addressed (email drin@ipmc.cnrs.fr).

Biochem. Soc. Trans. (2014) 42, 1465–1470; doi:10.1042/BST20140143

Initial studies were mainly based on the hypothesis that ORP/Osh proteins mediated sterol transfer. Yeast was a valuable model to address this issue because, besides the Osh proteins, no other putative LTPs for sterol were described. Pioneering observations suggested that all Osh proteins were involved in intracellular sterol distribution [14]. The resolution of the crystal structure of Osh4p, which consists only of an ORD [15], empty or bound to ergosterol, suggested scenarios on how they might operate. The ORD fold is a 19-strand β-barrel that defines a cavity for a sterol molecule and is closed by a molecular lid. The ability of the lid to adopt two different conformations depending on the state of Osh4p (empty or sterol-bound) suggested how the protein might target donor and acceptor organelles for operating transport cycles [15]. However, the idea that Osh proteins act as sterol transporters was challenged rapidly. *In vitro* assays indicate that Osh4p transports sterol between artificial lipid vesicles, but at low velocity [16], and that a majority of Osh are unable to transfer sterol [17]. Moreover, there was no conclusive evidence that Osh proteins transfer sterol along specific directions between organelles [14,17]. Finally, it was proposed that Osh proteins are not essential for sterol movement in yeast [18].

Building a sterol gradient by using a PI(4)P gradient

Enigmatic data have been obtained on Osh4p. It recognizes sterol, but it also down-regulates cellular PI(4)P levels and the availability of this lipid on Golgi surface [19]. PI(4)P is a phosphoinositide that mostly labels the *trans*-Golgi and the PM and is mandatory for the recruitment of multiple effectors at the surface of these compartments. In yeast, the phosphoinositide 4-kinase Pik1p produces the Golgi PI(4)P pool [20]. Osh4p counteracts Pik1p and Sec14p [19], a phosphatidylinositol (PI)/phosphatidylcholine exchanger that teams with Pik1p to yield PI(4)P [21]. Osh4p also acts as a regulator of exocytosis [19,22], which relies on the PI(4)P-dependent formation of post-Golgi transport vesicles. Eventually, Osh4p and other Osh proteins were proposed to exert signalling functions by directly down-regulating PI(4)P [23]. Interestingly, an Osh4p mutant defective in binding sterol is not a loss-of-function mutant and acts as a major inhibitor of the TORC1 (target of rapamycin complex 1) signalling pathway [24]. Together, these observations indicate that Osh4p could have other cellular functions than transporting sterol. Nevertheless, several results suggest that Osh4p regulates specifically the level and transversal distribution of sterol in the *trans*-Golgi membrane and the PM [14,18,25].

We have tested with novel biochemical approaches whether Osh4p has a built-in ability to transfer sterol in a vectorial manner between membranes. Unexpectedly, we have found that Osh4p binds ergosterol and PI(4)P in a mutually exclusive manner. The structure of Osh4p in complex with PI(4)P indicates that the sterol-binding pocket accommodates the PI(4)P acyl chains. Charged residues defining an adjacent pocket specifically select the PI(4)P headgroup. Strikingly, we have observed that Osh4p could quickly transfer sterol and PI(4)P along opposed directions between distinct membranes by counterexchange [26]. We have thus proposed that Osh4p might build a sterol gradient at the ER–Golgi interface by using PI(4)P as a driving force.

Although PI(4)P is present at the cytosolic surface of the Golgi and the PM, it is absent from the ER, implying that a PI(4)P gradient exists between these distant cellular regions. Sac1p, the major PI(4)P phosphatase in yeast [27], resides at the ER and ensures the maintenance of this gradient by hydrolysing PI(4)P into PI [28]. We have proposed that Osh4p might extract sterol from the ER and then release it by exchanging it for PI(4)P at the Golgi and transport PI(4)P from the Golgi to the ER. The production of PI(4)P at the Golgi surface by Pik1p and its consumption at the ER by Sac1p would sustain sterol/PI(4)P transport cycles and allow accumulation of sterol in late membranes at the expense of the ER (Figure 1). Interestingly, this model might explain the dependency of non-vesicular sterol-transfer routes on energy, as the production of PI(4)P needs ATP. Using refined sterol and PI(4)P transport assays, we have gathered new data to demonstrate that Osh4p, by consuming a PI(4)P gradient, establishes a sterol gradient between distant membranes within seconds (J. Moser von Filseck, S. Vani, B. Mesmin, B. Antonny and G. Drin, unpublished work).

Novel insights on OSBP and sterol transport at membrane-contact sites

Membrane-contact sites (MCSs) are specialized zones in which the ER membrane is apposed closely to the membrane of a second organelle (10–20 nm apart) and are considered essential hubs for the non-vesicular transport of lipids [29]. In higher eukaryotes, MCSs between the ER and the *trans*-Golgi are remarkable because they host various LTPs, including OSBP, CERT (ceramide-transfer protein) and Nir2, which play key roles for the remodelling of the Golgi membrane [30–32]. OSBP has an N-terminal PH (pleckstrin homology) domain recruited on the Golgi surface by both PI(4)P and the small G-protein Arf1 [33] and an FFAT (two phenylalanine residues in an acidic track) motif that binds VAP-A [VAMP (vesicle-associated membrane protein)-associated protein A], an ER-resident receptor [34]. It has been hypothesized that OSBP, owing to this architecture, could create ER–Golgi junctions to reduce the distance between these organelles and efficiently transport sterol [35]. Recently, we have established how OSBP combines the ability to tether membranes and to transport lipids in ER–Golgi junctions [36]. First, OSBP, via its PH domain and FFAT motif, bridges the ER with the *trans*-Golgi. Next, membrane tethering enables sterol transfer by the ORD from the ER to the Golgi membrane. The transport of sterol is coupled with back delivery of PI(4)P from the *trans*-Golgi to the ER. Finally, PI(4)P, once transferred, is hydrolysed into PI by Sac1 (Figure 2). OSBP transfers up to

Figure 1 | Sterol/PI(4)P exchange by Osh4p at ER-Golgi interfaces

Ergosterol is synthesized at the ER. Osh4p transports ergosterol from the ER to the *trans*-Golgi and PI(4)P in a backward direction. ATP-dependent phosphorylation of PI into PI(4)P by Pik1p and hydrolysis of PI(4)P by Sac1p allow multiple sterol/PI(4)P transport cycles by Osh4p. The maintenance of the PI(4)P gradient allows in turn the vectorial transport of sterol and, thereby, the creation and maintenance of a sterol gradient.

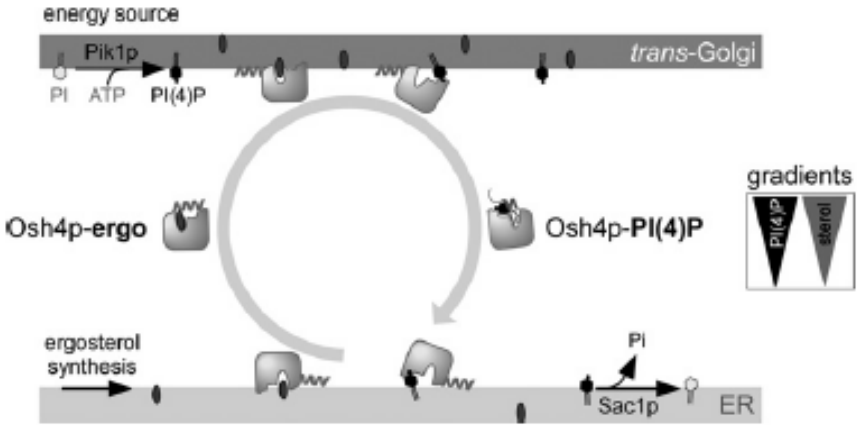

Figure 2 | Function of OSBP at ER-Golgi contact sites

(**a**) OSBP interacts through its FFAT motif with the ER-resident VAP receptors and, via its PH domain, with Arf1 (in the GTP-bound state) and PI(4)P. (**b**) As such, OSBP tethers the ER and the Golgi membrane and operates cycles of cholesterol/PI(4)P exchange, thereby creating a cholesterol gradient. This tethering activity could facilitate the recruitment of CERT by PI(4)P and VAP and allows synchronizing cholesterol and ceramide fluxes, thus guaranteeing the co-enrichment of sterol and sphingomyelin in the *trans*-Golgi. (**c**) The consumption of PI(4)P would eventually trigger the disassembly of ER-Golgi contact sites and stop lipid transfer. SMS, sphingomyelin synthase.

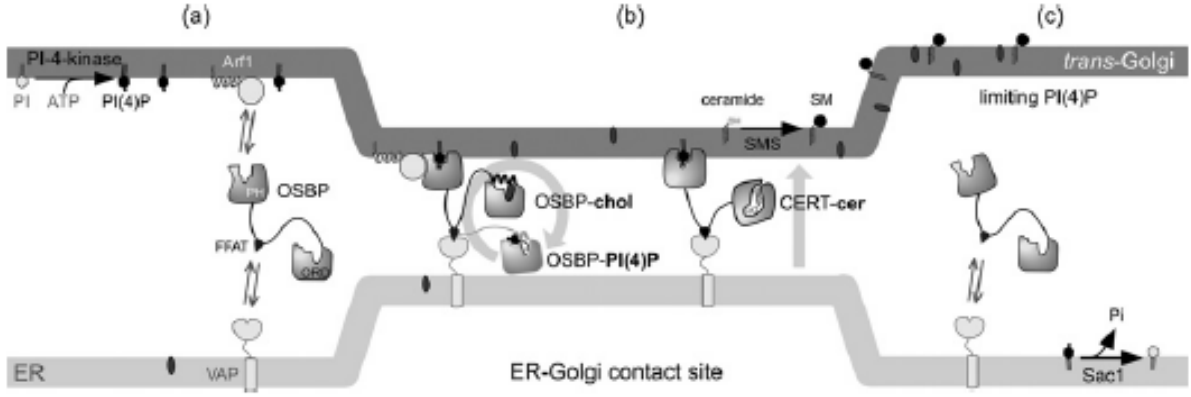

30 sterols per min between connected membranes [36], and its natural abundance in U2OS cells corresponds to 4×10^5 copies/cell (B. Mesmin, unpublished work). Considering that only approximately half of the OSBP copies populate ER–Golgi junctions, up to 6×10^6 cholesterol molecules could be delivered to the *trans*-Golgi every minute. In a typical cell (10 μm in diameter), the PM is estimated to contain $\sim 3 \times 10^8$ cholesterol molecules [37]. Thus the sole activity of OSBP might ensure within 1 h the complete renewal of the sterol PM pool, if there is continuous delivery of lipids from the *trans*-Golgi to the PM by secretory vesicles occurs.

Importantly, we have also found that the consumption of PI(4)P by OSBP not only provides the energy to drive sterol transfer, but also governs the ability of OSBP to create/populate ER–Golgi junctions, because the binding of OSBP to the Golgi surface depends on the Golgi PI(4)P pool. This might explain additionally how OSBP regulates the recruitment of CERT at ER–Golgi junctions [38]. CERT transfers ceramide from the ER to the *trans*-Golgi, in which

ceramide is converted into sphingomyelin (SM) [31]. Instead of having an ORD, CERT displays a StART domain to specifically bind ceramide, but it has the same domain organization as OSBP, with a PI(4)P-specific PH domain and a FFAT motif. By modulating the PI(4)P Golgi pool, OSBP probably controls the presence of CERT in ER–Golgi junctions. Such a mechanism would synchronize fluxes of sterol and ceramide, and possibly of other lipids by controlling Nir2, thereby allowing co-enrichment of several lipids at the *trans*-Golgi, essential for the proper function of the secretory pathway [39].

Redefining the function of ORP/Osh proteins

A new vision for the functioning of ORP/Osh family is currently emerging. We have suggested that binding of PI(4)P is a common function of the ORP/Osh family because PI(4)P is recognized by the histidine pair of the EQVSHHPP motif and by other residues that are conserved strictly [26,40]. Since then, several Osh/ORPs have been described to interact with PI(4)P [36,41,42]. Interestingly, cellular observations have suggested that all Osh proteins in yeast are capable of extracting PI(4)P. Silencing the seven Osh proteins blocks the docking of exocytotic vesicles with the PM [22], a process known to require the disappearance of PI(4)P from the surface of these vesicles [43]. Moreover, a structural analysis shows that the Osh3p ORD extracts PI(4)P, but not sterol [41]. A recent report demonstrates that subtle structural variations in the ORD confer distinct lipid specificity to ORP/Osh proteins. Osh6p has been found to co-crystallize with phosphatidylserine, to have no affinity for sterols and to convey phosphatidylserine from the ER to the PM [44]. Thus ORP/Osh proteins probably share the ability to bind PI(4)P, but recognize a second lipid that is not necessary sterol. An appealing hypothesis is that the general function of ORP/Osh proteins is to exchange PI(4)P with either sterol or a non-sterol ligand between organelles.

From these findings, we can envisage that several ORP/Osh proteins, for which the ability to bind sterol is validated [45], use PI(4)P. Interestingly, some of them work between the endosomal compartment, which is essential for sterol homoeostasis as it mediates the import of exogenous sterol in higher eukaryotes and the ER. It has been shown that ORP1L (long ORP1) in the Rab7-RILP (Rab-interacting lysosomal protein)–ORP1L complex [46] acts as a cholesterol-sensing switch that regulates the attachment of late endosomes/lysosomes to the ER network or to microtubule tracks through dynein recruitment by controlling RILP–homotypic fusion and protein sorting (HOPS)–p150^{Glued} interactions [47]. It remains unclear, however, whether ORP1L is capable of transporting sterol at ER–endosome junctions. Interestingly, Hammond et al. [48] have identified recently new PI(4)P pools, notably in Rab7-positive late endosomes/lysosomes. An attractive idea is that certain ORP/Osh proteins exploit different PI(4)P pools as a driving force for transporting sterol at the ER–endosome interface.

Structural data obtained on Osh proteins [41,44], notably Osh3p, suggest that certain ORP/Osh proteins exchange PI(4)P with a non-sterol lipid between organelles. Osh3p, which displays an OSBP-like architecture, targets the PM PI(4)P pool and interacts with the Scs2p/Scs22p VAP receptor to occupy ER–PM junctions [23]. It has been suggested that, in such junctions, the catalytic domain of Sac1p, which is connected by a long flexible linker to its ER membrane-spanning domain, reaches the PM [23] and that Osh3p activates Sac1p to promote the degradation *in trans* of the PM PI(4)P pool. However, because it is unclear what would be the function of this down-regulation of PI(4)P [49], we have proposed alternatively that Osh3p exploits a PI(4)P gradient sustained over time by Sac1p, acting *in cis*, to supply the PM with a non-sterol ligand.

Conclusions

We have proposed that ORP/Osh proteins take advantage of inter-organelle PI(4)P gradients to actively convey, across long distance or within MCSs, various lipids species from the ER to the Golgi, the PM and endosomes. For most of these proteins, their ability to bind and exchange PI(4)P with a second ligand and the nature of this ligand remain to be determined. In addition, cellular studies will be necessary to define whether the turnover of PI(4)P in cells is fast enough to guarantee such ORP/Osh-mediated transport mechanisms. Interestingly, it has been reported recently that α-TTP (α-tocopherol-transfer protein), a member of the Sec14 superfamily, supplies the PM with the liposoluble vitamin E by exchanging it with phosphatidylinositol 4,5-bisphosphate/phosphatidylinositol 3,4-bisphosphate [50]. Therefore our model for the functioning of ORP/Osh proteins might be valid for other unrelated LTP proteins.

Funding

This work was supported by the Centre National de la Recherche Scientifique (CNRS) and the Agence Nationale de la Recherche (ANR) [grant number 2010-1503-01]. J.M.v.F., B.M and B.A. are supported by the European Research Council (ERC) program [advanced grant number 268888].

References

1 Radhakrishnan, A., Goldstein, J.L., McDonald, J.G. and Brown, M.S. (2008) Switch-like control of SREBP-2 transport triggered by small changes in ER cholesterol: a delicate balance. Cell Metab. **8**, 512–521 CrossRef PubMed

2 Schneiter, R., Brugger, B., Sandhoff, R., Zellnig, G., Leber, A., Lampl, M., Athenstaedt, K., Hrastnik, C., Eder, S., Daum, G. et al. (1999) Electrospray ionization tandem mass spectrometry (ESI-MS/MS) analysis of the lipid molecular species composition of yeast subcellular membranes reveals acyl chain-based sorting/remodeling of distinct molecular species en route to the plasma membrane. J. Cell Biol. **146**, 741–754 CrossRef PubMed

3 Andreyev, A.Y., Fahy, E., Guan, Z., Kelly, S., Li, X., McDonald, J.G., Milne, S., Myers, D., Park, H., Ryan, A. et al. (2010) Subcellular organelle lipidomics in TLR-4-activated macrophages. J. Lipid Res. **51**, 2785–2797 CrossRef PubMed

4 Mesmin, B. and Maxfield, F.R. (2009) Intracellular sterol dynamics. Biochim. Biophys. Acta **1791**, 636–645 CrossRef PubMed

5 DeGrella, R.F. and Simoni, R.D. (1982) Intracellular transport of cholesterol to the plasma membrane. J. Biol. Chem. **257**, 14256–14262 PubMed

6 Urbani, L. and Simoni, R.D. (1990) Cholesterol and vesicular stomatitis virus G protein take separate routes from the endoplasmic reticulum to the plasma membrane. J. Biol. Chem. **265**, 1919–1923 PubMed

7 Baumann, N.A., Sullivan, D.P., Ohvo-Rekila, H., Simonot, C., Pottekat, A., Klaassen, Z., Beh, C.T. and Menon, A.K. (2005) Transport of newly synthesized sterol to the sterol-enriched plasma membrane occurs via nonvesicular equilibration. Biochemistry **44**, 5816–5826 CrossRef PubMed

8 Raychaudhuri, S. and Prinz, W.A. (2010) The diverse functions of oxysterol-binding proteins. Annu. Rev. Cell Dev. Biol. **26**, 157–177 CrossRef PubMed

9 Alpy, F. and Tomasetto, C. (2014) START ships lipids across interorganelle space. Biochimie **96**, 85–95 CrossRef PubMed

10 Lange, Y. and Steck, T.L. (2008) Cholesterol homeostasis and the escape tendency (activity) of plasma membrane cholesterol. Prog. Lipid Res. **47**, 319–332 CrossRef PubMed

11 Ridgway, N.D., Dawson, P.A., Ho, Y.K., Brown, M.S. and Goldstein, J.L. (1992) Translocation of oxysterol binding protein to Golgi apparatus triggered by ligand binding. J. Cell Biol. **116**, 307–319 CrossRef PubMed

12 Ngo, M. and Ridgway, N.D. (2009) Oxysterol binding protein-related protein 9 (ORP9) is a cholesterol transfer protein that regulates Golgi structure and function. Mol. Biol. Cell **20**, 1388–1399 CrossRef PubMed

13 Lehto, M., Laitinen, S., Chinetti, G., Johansson, M., Ehnholm, C., Staels, B., Ikonen, E. and Olkkonen, V.M. (2001) The OSBP-related protein family in humans. J. Lipid Res. **42**, 1203–1213 PubMed

14 Beh, C.T. and Rine, J. (2004) A role for yeast oxysterol-binding protein homologs in endocytosis and in the maintenance of intracellular sterol-lipid distribution. J. Cell Biol. **117**, 2983–2996

15 Im, Y.J., Raychaudhuri, S., Prinz, W.A. and Hurley, J.H. (2005) Structural mechanism for sterol sensing and transport by OSBP-related proteins. Nature **437**, 154–158 CrossRef PubMed

16 Raychaudhuri, S., Im, Y.J., Hurley, J.H. and Prinz, W.A. (2006) Nonvesicular sterol movement from plasma membrane to ER requires oxysterol-binding protein-related proteins and phosphoinositides. J. Cell Biol. **173**, 107–119 CrossRef PubMed

17 Schulz, T.A., Choi, M.G., Raychaudhuri, S., Mears, J.A., Ghirlando, R., Hinshaw, J.E. and Prinz, W.A. (2009) Lipid-regulated sterol transfer between closely apposed membranes by oxysterol-binding protein homologues. J. Cell Biol. **187**, 889–903 CrossRef PubMed

18 Georgiev, A.G., Sullivan, D.P., Kersting, M.C., Dittman, J.S., Beh, C.T. and Menon, A.K. (2011) Osh proteins regulate membrane sterol organization but are not required for sterol movement between the ER and PM. Traffic **12**, 1341–1355 CrossRef PubMed

19 Fairn, G.D., Curwin, A.J., Stefan, C.J. and McMaster, C.R. (2007) The oxysterol binding protein Kes1p regulates Golgi apparatus phosphatidylinositol-4-phosphate function. Proc. Natl. Acad. Sci. U.S.A. **104**, 15352–15357 CrossRef PubMed

20 Strahl, T. and Thorner, J. (2007) Synthesis and function of membrane phosphoinositides in budding yeast, *Saccharomyces cerevisiae*. Biochim. Biophys. Acta **1771**, 353–404 CrossRef PubMed

21 Schaaf, G., Ortlund, E.A., Tyeryar, K.R., Mousley, C.J., Ile, K.E., Garrett, T.A., Ren, J., Woolls, M.J., Raetz, C.R., Redinbo, M.R. and Bankaitis, V.A. (2008) Functional anatomy of phospholipid binding and regulation of phosphoinositide homeostasis by proteins of the sec14 superfamily. Mol. Cell **29**, 191–206 CrossRef PubMed

22 Alfaro, G., Johansen, J., Dighe, S.A., Duamel, G., Kozminski, K.G. and Beh, C.T. (2011) The sterol-binding protein Kes1/Osh4p is a regulator of polarized exocytosis. Traffic **12**, 1521–1536 CrossRef PubMed

23 Stefan, C.J., Manford, A.G., Baird, D., Yamada-Hanff, J., Mao, Y. and Emr, S.D. (2011) Osh proteins regulate phosphoinositide metabolism at ER-plasma membrane contact sites. Cell **144**, 389–401 CrossRef PubMed

24 Mousley, C.J., Yuan, P., Gaur, N.A., Trettin, K.D., Nile, A.H., Deminoff, S.J., Dewar, B.J., Wolpert, M., Macdonald, J.M., Herman, P.K. et al. (2012) A sterol-binding protein integrates endosomal lipid metabolism with TOR signaling and nitrogen sensing. Cell **148**, 702–715 CrossRef PubMed

25 Proszynski, T.J., Klemm, R.W., Gravert, M., Hsu, P.P., Gloor, Y., Wagner, J., Kozak, K., Grabner, H., Walzer, K., Bagnat, M. et al. (2005) A genome-wide visual screen reveals a role for sphingolipids and ergosterol in cell surface delivery in yeast. Proc. Natl. Acad. Sci. U.S.A. **102**, 17981–17986 CrossRef PubMed

26 de Saint-Jean, M., Delfosse, V., Douguet, D., Chicanne, G., Payrastre, B., Bourguet, W., Antonny, B. and Drin, G. (2011) Osh4p exchanges sterols for phosphatidylinositol 4-phosphate between lipid bilayers. J. Cell Biol. **195**, 965–978 CrossRef PubMed

27 Foti, M., Audhya, A. and Emr, S.D. (2001) Sac1 lipid phosphatase and Stt4 phosphatidylinositol 4-kinase regulate a pool of phosphatidylinositol 4-phosphate that functions in the control of the actin cytoskeleton and vacuole morphology. Mol. Biol. Cell **12**, 2396–2411 CrossRef PubMed

28 Faulhammer, F., Kanjilal-Kolar, S., Knodler, A., Lo, J., Lee, Y., Konrad, G. and Mayinger, P. (2007) Growth control of Golgi phosphoinositides by reciprocal localization of sac1 lipid phosphatase and pik1 4-kinase. Traffic **8**, 1554–1567 CrossRef PubMed

29 Helle, S.C., Kanfer, G., Kolar, K., Lang, A., Michel, A.H. and Kornmann, B. (2013) Organization and function of membrane contact sites. Biochim. Biophys. Acta **1833**, 2526–2541 CrossRef PubMed

30 Storey, M.K., Byers, D.M., Cook, H.W. and Ridgway, N.D. (1998) Cholesterol regulates oxysterol binding protein (OSBP) phosphorylation and Golgi localization in Chinese hamster ovary cells: correlation with stimulation of sphingomyelin synthesis by 25-hydroxycholesterol. Biochem. J. **336**, 247–256 PubMed

31 Hanada, K., Kumagai, K., Yasuda, S., Miura, Y., Kawano, M., Fukasawa, M. and Nishijima, M. (2003) Molecular machinery for non-vesicular trafficking of ceramide. Nature **426**, 803–809 CrossRef PubMed

32 Peretti, D., Dahan, N., Shimoni, E., Hirschberg, K. and Lev, S. (2008) Coordinated lipid transfer between the endoplasmic reticulum and the Golgi complex requires the VAP proteins and is essential for Golgi-mediated transport. Mol. Biol. Cell **19**, 3871–3884 CrossRef PubMed

33 Levine, T.P. and Munro, S. (2002) Targeting of Golgi-specific pleckstrin homology domains involves both PtdIns 4-kinase-dependent and -independent components. Curr. Biol. **12**, 695–704 CrossRef PubMed

34 Loewen, C.J., Roy, A. and Levine, T.P. (2003) A conserved ER targeting motif in three families of lipid binding proteins and in Opi1p binds VAP. EMBO J. **22**, 2025–2035 CrossRef PubMed

35 Levine, T. (2004) Short-range intracellular trafficking of small molecules across endoplasmic reticulum junctions. Trends Cell Biol. **14**, 483–490 CrossRef PubMed

36 Mesmin, B., Bigay, J., Moser von Filseck, J., Lacas-Gervais, S., Drin, G. and Antonny, B. (2013) A four-step cycle driven by PI(4)P hydrolysis directs sterol/PI(4)P exchange by the ER-Golgi tether OSBP. Cell **155**, 830–843 CrossRef PubMed

37 Maxfield, F.R. and Mondal, M. (2006) Sterol and lipid trafficking in mammalian cells. Biochem. Soc. Trans. **34**, 335–339 CrossRef PubMed

38 Perry, R.J. and Ridgway, N.D. (2006) Oxysterol-binding protein and vesicle-associated membrane protein-associated protein are required for sterol-dependent activation of the ceramide transport protein. Mol. Biol. Cell **17**, 2604–2616 CrossRef PubMed

39 Drin, G. (2014) Topological regulation of lipid balance in cells. Annu. Rev. Biochem. **83**, 51–77 CrossRef PubMed

40 Mesmin, B., Antonny, B. and Drin, G. (2013) Insights into the mechanisms of sterol transport between organelles. Cell. Mol. Life Sci. **70**, 3405–3421 CrossRef PubMed

41 Tong, J., Yang, H., Eom, S.H. and Im, Y.J. (2013) Structure of Osh3 reveals a conserved mode of phosphoinositide binding in oxysterol-binding proteins. Structure **21**, 1203–1213 CrossRef PubMed

42 Charman, M., Colbourne, T.R., Pietrangelo, A., Kreplak, L. and Ridgway, N.D. (2014) Oxysterol-binding protein (OSBP)-related protein 4 (ORP4) is essential for cell proliferation and survival. J. Biol. Chem. **289**, 15705–15717 CrossRef PubMed

43 Mizuno-Yamasaki, E., Medkova, M., Coleman, J. and Novick, P. (2010) Phosphatidylinositol 4-phosphate controls both membrane recruitment and a regulatory switch of the Rab GEF Sec2p. Dev. Cell **18**, 828–840 CrossRef PubMed

44 Maeda, K., Anand, K., Chiapparino, A., Kumar, A., Poletto, M., Kaksonen, M. and Gavin, A.C. (2013) Interactome map uncovers phosphatidylserine transport by oxysterol-binding proteins. Nature **501**, 257–261 CrossRef PubMed

45 Olkkonen, V.M. (2013) OSBP-related proteins: liganding by glycerophospholipids opens new insight into their function. Molecules **18**, 13666–13679 CrossRef PubMed

46 Rocha, N., Kuijl, C., van der Kant, R., Janssen, L., Houben, D., Janssen, H., Zwart, W. and Neefjes, J. (2009) Cholesterol sensor ORP1L contacts the ER protein VAP to control Rab7–RILP–p150^{Glued} and late endosome positioning. J. Cell Biol. **185**, 1209–1225 CrossRef PubMed
47 van der Kant, R., Fish, A., Janssen, L., Janssen, H., Krom, S., Ho, N., Brummelkamp, T., Carette, J., Rocha, N. and Neefjes, J. (2013) Late endosomal transport and tethering are coupled processes controlled by RILP and the cholesterol sensor ORP1L. J. Cell Biol. **126**, 3462–3474
48 Hammond, G.R., Machner, M.P. and Balla, T. (2014) A novel probe for phosphatidylinositol 4-phosphate reveals multiple pools beyond the Golgi. J. Cell Biol. **205**, 113–126 CrossRef PubMed
49 Stefan, C.J., Manford, A.G. and Emr, S.D. (2013) ER–PM connections: sites of information transfer and inter-organelle communication. Curr. Opin. Cell Biol. **25**, 434–442 CrossRef PubMed
50 Kono, N., Ohto, U., Hiramatsu, T., Urabe, M., Uchida, Y., Satow, Y. and Arai, H. (2013) Impaired α-TTP–PIPs interaction underlies familial vitamin E deficiency. Science **340**, 1106–1110 CrossRef PubMed

Received 15 May 2014
doi:10.1042/BST20140143

BIBLIOGRAPHY

Albers, J. J., S. Vuletic, *et al.* (2012). "Role of plasma phospholipid transfer protein in lipid and lipoprotein metabolism." Biochim Biophys Acta **1821**(3): 345-57.

Alfaro, G., J. Johansen, *et al.* (2011). "The sterol-binding protein Kes1/Osh4p is a regulator of polarized exocytosis." Traffic **12**(11): 1521-36.

Alpy, F., F. Legueux, *et al.* (2009). "[START domain-containing proteins: a review of their role in lipid transport and exchange]." Med Sci (Paris) **25**(2): 181-91.

Alpy, F., A. Rousseau, *et al.* (2013). "STARD3 or STARD3NL and VAP form a novel molecular tether between late endosomes and the ER." J Cell Sci **126**(Pt 23): 5500-12.

Alpy, F. and C. Tomasetto (2014). "START ships lipids across interorganelle space." Biochimie **96**: 85-95.

Alpy, F., C. Wendling, *et al.* (2002). "MENTHO, a MLN64 homologue devoid of the START domain." J Biol Chem **277**(52): 50780-7.

Anniss, A. M., J. Apostolopoulos, *et al.* (2002). "An oxysterol-binding protein family identified in the mouse." DNA Cell Biol **21**(8): 571-80.

Audhya, A. and S. D. Emr (2002). "Stt4 PI 4-kinase localizes to the plasma membrane and functions in the Pkc1-mediated MAP kinase cascade." Dev Cell **2**(5): 593-605.

Audhya, A., M. Foti, *et al.* (2000). "Distinct roles for the yeast phosphatidylinositol 4-kinases, Stt4p and Pik1p, in secretion, cell growth, and organelle membrane dynamics." Mol Biol Cell **11**(8): 2673-89.

Baird, D., C. Stefan, *et al.* (2008). "Assembly of the PtdIns 4-kinase Stt4 complex at the plasma membrane requires Ypp1 and Efr3." J Cell Biol **183**(6): 1061-74.

Baldridge, R. D. and T. R. Graham (2012). "Identification of residues defining phospholipid flippase substrate specificity of type IV P-type ATPases." Proc Natl Acad Sci U S A **109**(6): E290-8.

Baldridge, R. D. and T. R. Graham (2013). "Two-gate mechanism for phospholipid selection and transport by type IV P-type ATPases." Proc Natl Acad Sci U S A **110**(5): E358-67.

Bankaitis, V. A., K. E. Ile, *et al.* (2012). "Thoughts on Sec14-like nanoreactors and phosphoinositide signaling." Adv Biol Regul **52**(1): 115-21.

Bankaitis, V. A., D. E. Malehorn, *et al.* (1989). "The Saccharomyces cerevisiae SEC14 gene encodes a cytosolic factor that is required for transport of secretory proteins from the yeast Golgi complex." J Cell Biol **108**(4): 1271-81.

Bankaitis, V. A., C. J. Mousley, *et al.* (2010). "The Sec14 superfamily and mechanisms for crosstalk between lipid metabolism and lipid signaling." Trends Biochem Sci **35**(3): 150-60.

Baumann, N. A., D. P. Sullivan, *et al.* (2005). "Transport of newly synthesized sterol to the sterol-enriched plasma membrane occurs via nonvesicular equilibration." Biochemistry **44**(15): 5816-26.

Beh, C. T., L. Cool, *et al.* (2001). "Overlapping functions of the yeast oxysterol-binding protein homologues." Genetics **157**(3): 1117-40.

Beh, C. T., C. R. McMaster, *et al.* (2012). "A detour for yeast oxysterol binding proteins." J Biol Chem **287**(14): 11481-8.

Beh, C. T. and J. Rine (2004). "A role for yeast oxysterol-binding protein homologs in

endocytosis and in the maintenance of intracellular sterol-lipid distribution." J Cell Sci **117**(Pt 14): 2983-96.

Behnia, R. and S. Munro (2005). "Organelle identity and the signposts for membrane traffic." Nature **438**(7068): 597-604.

Bigay, J. and B. Antonny (2005). "Real-time assays for the assembly-disassembly cycle of COP coats on liposomes of defined size." Methods Enzymol **404**: 95-107.

Bigay, J. and B. Antonny (2012). "Curvature, lipid packing, and electrostatics of membrane organelles: defining cellular territories in determining specificity." Dev Cell **23**(5): 886-95.

Billcliff, P. G. and M. Lowe (2014). "Inositol lipid phosphatases in membrane trafficking and human disease." Biochem J **461**(2): 159-75.

Bonifacino, J. S. and B. S. Glick (2004). "The mechanisms of vesicle budding and fusion." Cell **116**(2): 153-66.

Bratton, D. L., V. A. Fadok*, et al.* (1997). "Appearance of phosphatidylserine on apoptotic cells requires calcium-mediated nonspecific flip-flop and is enhanced by loss of the aminophospholipid translocase." J Biol Chem **272**(42): 26159-65.

Brice, S. E., C. W. Alford*, et al.* (2009). "Modulation of sphingolipid metabolism by the phosphatidylinositol-4-phosphate phosphatase Sac1p through regulation of phosphatidylinositol in Saccharomyces cerevisiae." J Biol Chem **284**(12): 7588-96.

Brown, M. S. and J. L. Goldstein (2009). "Cholesterol feedback: from Schoenheimer's bottle to Scap's MELADL." J Lipid Res **50 Suppl**: S15-27.

Brugger, B., R. Sandhoff*, et al.* (2000). "Evidence for segregation of sphingomyelin and cholesterol during formation of COPI-coated vesicles." J Cell Biol **151**(3): 507-18.

Cai, Y., Y. Deng*, et al.* (2014). "Sac1-Vps74 structure reveals a mechanism to terminate phosphoinositide signaling in the Golgi apparatus." J Cell Biol **206**(4): 485-91.

Collins, B. M., A. J. McCoy*, et al.* (2002). "Molecular architecture and functional model of the endocytic AP2 complex." Cell **109**(4): 523-35.

Comte, J., B. Maisterrena*, et al.* (1976). "Lipid composition and protein profiles of outer and inner membranes from pig heart mitochondria. Comparison with microsomes." Biochim Biophys Acta **419**(2): 271-84.

Contreras, F. X., A. M. Ernst*, et al.* (2012). "Molecular recognition of a single sphingolipid species by a protein's transmembrane domain." Nature **481**(7382): 525-9.

D'Angelo, G., E. Polishchuk*, et al.* (2007). "Glycosphingolipid synthesis requires FAPP2 transfer of glucosylceramide." Nature **449**(7158): 62-7.

Daleke, D. L. (2003). "Regulation of transbilayer plasma membrane phospholipid asymmetry." J Lipid Res **44**(2): 233-42.

Daum, G., N. D. Lees*, et al.* (1998). "Biochemistry, cell biology and molecular biology of lipids of Saccharomyces cerevisiae." Yeast **14**(16): 1471-510.

de Saint-Jean, M., V. Delfosse*, et al.* (2011). "Osh4p exchanges sterols for phosphatidylinositol 4-phosphate between lipid bilayers." J Cell Biol **195**(6): 965-78.

DeGrella, R. F. and R. D. Simoni (1982). "Intracellular transport of cholesterol to the plasma membrane." J Biol Chem **257**(23): 14256-62.

Del Campo, C. M., A. K. Mishra*, et al.* (2014). "Structural basis for PI(4)P-specific membrane recruitment of the Legionella pneumophila effector DrrA/SidM." Structure **22**(3): 397-408.

Devaux, P. F., A. Herrmann*, et al.* (2008). "How lipid flippases can modulate membrane structure." Biochim Biophys Acta **1778**(7-8): 1591-600.

Diaz-Rohrer, B., K. R. Levental*, et al.* (2014). "Rafting through traffic: Membrane domains in cellular logistics." Biochim Biophys Acta **1838**(12): 3003-3013.

Dickson, R. C. and R. L. Lester (1999). "Metabolism and selected functions of sphingolipids in the yeast Saccharomyces cerevisiae." Biochim Biophys Acta **1438**(3): 305-21.

Drin, G. (2014). "Topological regulation of lipid balance in cells." Annu Rev Biochem **83**: 51-77.

Drin, G., J. F. Casella*, et al.* (2007). "A general amphipathic alpha-helical motif for sensing membrane curvature." Nat Struct Mol Biol **14**(2): 138-46.

Du, X., J. Kumar*, et al.* (2011). "A role for oxysterol-binding protein-related protein 5 in endosomal cholesterol trafficking." J Cell Biol **192**(1): 121-35.

Duran, J. M., F. Campelo*, et al.* (2012). "Sphingomyelin organization is required for vesicle biogenesis at the Golgi complex." EMBO J **31**(24): 4535-46.

Ejsing, C. S., J. L. Sampaio*, et al.* (2009). "Global analysis of the yeast lipidome by quantitative shotgun mass spectrometry." Proc Natl Acad Sci U S A **106**(7): 2136-41.

Elbaz-Alon, Y., E. Rosenfeld-Gur*, et al.* (2014). "A dynamic interface between vacuoles and mitochondria in yeast." Dev Cell **30**(1): 95-102.

Faini, M., R. Beck*, et al.* (2013). "Vesicle coats: structure, function, and general principles of assembly." Trends Cell Biol **23**(6): 279-88.

Fairn, G. D., A. J. Curwin*, et al.* (2007). "The oxysterol binding protein Kes1p regulates Golgi apparatus phosphatidylinositol-4-phosphate function." Proc Natl Acad Sci U S A **104**(39): 15352-7.

Fairn, G. D., M. Hermansson*, et al.* (2011). "Phosphatidylserine is polarized and required for proper Cdc42 localization and for development of cell polarity." Nat Cell Biol **13**(12): 1424-30.

Fairn, G. D. and C. R. McMaster (2005). "Identification and assessment of the role of a nominal phospholipid binding region of ORP1S (oxysterol-binding-protein-related protein 1 short) in the regulation of vesicular transport." Biochem J **387**(Pt 3): 889-96.

Fairn, G. D., N. L. Schieber*, et al.* (2011). "High-resolution mapping reveals topologically distinct cellular pools of phosphatidylserine." J Cell Biol **194**(2): 257-75.

Fang, M., B. G. Kearns*, et al.* (1996). "Kes1p shares homology with human oxysterol binding protein and participates in a novel regulatory pathway for yeast Golgi-derived transport vesicle biogenesis." EMBO J **15**(23): 6447-59.

Faulhammer, F., S. Kanjilal-Kolar*, et al.* (2007). "Growth control of Golgi phosphoinositides by reciprocal localization of sac1 lipid phosphatase and pik1 4-kinase." Traffic **8**(11): 1554-67.

Funato, K. and H. Riezman (2001). "Vesicular and nonvesicular transport of ceramide from ER to the Golgi apparatus in yeast." J Cell Biol **155**(6): 949-59.

Funato, K., B. Vallee*, et al.* (2002). "Biosynthesis and trafficking of sphingolipids in the yeast Saccharomyces cerevisiae." Biochemistry **41**(51): 15105-14.

Gaigg, B., R. Simbeni*, et al.* (1995). "Characterization of a microsomal subfraction associated with mitochondria of the yeast, Saccharomyces cerevisiae. Involvement in synthesis and import of phospholipids into mitochondria." Biochim Biophys Acta **1234**(2): 214-20.

Georgiev, A. G., J. Johansen*, et al.* (2013). "Arv1 regulates PM and ER membrane structure and homeostasis but is dispensable for intracellular sterol transport." Traffic **14**(8): 912-21.

Georgiev, A. G., D. P. Sullivan*, et al.* (2011). "Osh proteins regulate membrane sterol organization but are not required for sterol movement between the ER and PM."

Traffic **12**(10): 1341-55.
Gibellini, F. and T. K. Smith (2010). "The Kennedy pathway--De novo synthesis of phosphatidylethanolamine and phosphatidylcholine." IUBMB Life **62**(6): 414-28.
Giordano, F., Y. Saheki*, et al.* (2013). "PI(4,5)P(2)-dependent and Ca(2+)-regulated ER-PM interactions mediated by the extended synaptotagmins." Cell **153**(7): 1494-509.
Gnamusch, E., C. Kalaus*, et al.* (1992). "Transport of phospholipids between subcellular membranes of wild-type yeast cells and of the phosphatidylinositol transfer protein-deficient strain Saccharomyces cerevisiae sec 14." Biochim Biophys Acta **1111**(1): 120-6.
Godi, A., A. Di Campli*, et al.* (2004). "FAPPs control Golgi-to-cell-surface membrane traffic by binding to ARF and PtdIns(4)P." Nat Cell Biol **6**(5): 393-404.
Goto, A., X. Liu*, et al.* (2012). "Multisite phosphorylation of oxysterol-binding protein regulates sterol binding and activation of sphingomyelin synthesis." Mol Biol Cell **23**(18): 3624-35.
Hama, H., E. A. Schnieders*, et al.* (1999). "Direct involvement of phosphatidylinositol 4-phosphate in secretion in the yeast Saccharomyces cerevisiae." J Biol Chem **274**(48): 34294-300.
Hammond, G. R., M. P. Machner*, et al.* (2014). "A novel probe for phosphatidylinositol 4-phosphate reveals multiple pools beyond the Golgi." J Cell Biol **205**(1): 113-26.
Han, G. S., A. Audhya*, et al.* (2002). "The Saccharomyces cerevisiae LSB6 gene encodes phosphatidylinositol 4-kinase activity." J Biol Chem **277**(49): 47709-18.
Hanada, K., K. Kumagai*, et al.* (2003). "Molecular machinery for non-vesicular trafficking of ceramide." Nature **426**(6968): 803-9.
Hankins, H. M., R. D. Baldridge*, et al.* (2014). "Role of flippases, scramblases, and transfer proteins in phosphatidylserine subcellular distribution." Traffic.
He, J., J. L. Scott*, et al.* (2011). "Molecular basis of phosphatidylinositol 4-phosphate and ARF1 GTPase recognition by the FAPP1 pleckstrin homology (PH) domain." J Biol Chem **286**(21): 18650-7.
Helle, S. C., G. Kanfer*, et al.* (2013). "Organization and function of membrane contact sites." Biochim Biophys Acta **1833**(11): 2526-41.
Henkart, M., D. M. Landis*, et al.* (1976). "Similarity of junctions between plasma membranes and endoplasmic reticulum in muscle and neurons." J Cell Biol **70**(2 pt 1): 338-47.
Henneberry, A. L. and S. L. Sturley (2005). "Sterol homeostasis in the budding yeast, Saccharomyces cerevisiae." Semin Cell Dev Biol **16**(2): 155-61.
Henry, S. A., S. D. Kohlwein*, et al.* (2012). "Metabolism and regulation of glycerolipids in the yeast Saccharomyces cerevisiae." Genetics **190**(2): 317-49.
Holthuis, J. C. and T. P. Levine (2005). "Lipid traffic: floppy drives and a superhighway." Nat Rev Mol Cell Biol **6**(3): 209-20.
Holthuis, J. C. and A. K. Menon (2014). "Lipid landscapes and pipelines in membrane homeostasis." Nature **510**(7503): 48-57.
Honscher, C., M. Mari*, et al.* (2014). "Cellular metabolism regulates contact sites between vacuoles and mitochondria." Dev Cell **30**(1): 86-94.
Honscher, C. and C. Ungermann (2014). "A close-up view of membrane contact sites between the endoplasmic reticulum and the endolysosomal system: from yeast to man." Crit Rev Biochem Mol Biol **49**(3): 262-8.
Hubber, A., K. Arasaki*, et al.* (2014). "The machinery at endoplasmic reticulum-plasma membrane contact sites contributes to spatial regulation of multiple Legionella

effector proteins." PLoS Pathog **10**(7): e1004222.
Hynynen, R., S. Laitinen*, et al.* (2005). "Overexpression of OSBP-related protein 2 (ORP2) induces changes in cellular cholesterol metabolism and enhances endocytosis." Biochem J **390**(Pt 1): 273-83.
Hynynen, R., M. Suchanek*, et al.* (2009). "OSBP-related protein 2 is a sterol receptor on lipid droplets that regulates the metabolism of neutral lipids." J Lipid Res **50**(7): 1305-15.
Ikonen, E. (2008). "Cellular cholesterol trafficking and compartmentalization." Nat Rev Mol Cell Biol **9**(2): 125-38.
Ikonen, E. and M. Holtta-Vuori (2004). "Cellular pathology of Niemann-Pick type C disease." Semin Cell Dev Biol **15**(4): 445-54.
Im, Y. J., S. Raychaudhuri*, et al.* (2005). "Structural mechanism for sterol sensing and transport by OSBP-related proteins." Nature **437**(7055): 154-8.
Infante, R. E., M. L. Wang*, et al.* (2008). "NPC2 facilitates bidirectional transfer of cholesterol between NPC1 and lipid bilayers, a step in cholesterol egress from lysosomes." Proc Natl Acad Sci U S A **105**(40): 15287-92.
Jacquier, N. and R. Schneiter (2012). "Mechanisms of sterol uptake and transport in yeast." J Steroid Biochem Mol Biol **129**(1-2): 70-8.
Jacquot, A., C. Montigny*, et al.* (2012). "Phosphatidylserine stimulation of Drs2p.Cdc50p lipid translocase dephosphorylation is controlled by phosphatidylinositol-4-phosphate." J Biol Chem **287**(16): 13249-61.
Jiang, B., J. L. Brown*, et al.* (1994). "A new family of yeast genes implicated in ergosterol synthesis is related to the human oxysterol binding protein." Yeast **10**(3): 341-53.
Johansen, J., V. Ramanathan*, et al.* (2012). "Vesicle trafficking from a lipid perspective: Lipid regulation of exocytosis in Saccharomyces cerevisiae." Cell Logist **2**(3): 151-160.
Johansson, M., V. Bocher*, et al.* (2003). "The two variants of oxysterol binding protein-related protein-1 display different tissue expression patterns, have different intracellular localization, and are functionally distinct." Mol Biol Cell **14**(3): 903-15.
Johansson, M., M. Lehto*, et al.* (2005). "The oxysterol-binding protein homologue ORP1L interacts with Rab7 and alters functional properties of late endocytic compartments." Mol Biol Cell **16**(12): 5480-92.
Jorgensen, P. L. (1982). "Mechanism of the Na+, K+ pump. Protein structure and conformations of the pure (Na+ +K+)-ATPase." Biochim Biophys Acta **694**(1): 27-68.
Jovic, M., M. J. Kean*, et al.* (2014). "Endosomal sorting of VAMP3 is regulated by PI4K2A." J Cell Sci **127**(Pt 17): 3745-56.
Kaplan, M. R. and R. D. Simoni (1985). "Intracellular transport of phosphatidylcholine to the plasma membrane." J Cell Biol **101**(2): 441-5.
Kay, J. G., M. Koivusalo*, et al.* (2012). "Phosphatidylserine dynamics in cellular membranes." Mol Biol Cell **23**(11): 2198-212.
Kienzle, C. and J. von Blume (2014). "Secretory cargo sorting at the trans-Golgi network." Trends Cell Biol **24**(10): 584-593.
Kim, S., A. Kedan*, et al.* (2013). "The phosphatidylinositol-transfer protein Nir2 binds phosphatidic acid and positively regulates phosphoinositide signalling." EMBO Rep **14**(10): 891-9.
Kim, Y. J., M. L. Guzman-Hernandez*, et al.* (2011). "A highly dynamic ER-derived phosphatidylinositol-synthesizing organelle supplies phosphoinositides to cellular membranes." Dev Cell **21**(5): 813-24.
Klemm, R. W., C. S. Ejsing*, et al.* (2009). "Segregation of sphingolipids and sterols during

formation of secretory vesicles at the trans-Golgi network." J Cell Biol **185**(4): 601-12.
Kono, N., U. Ohto*, et al.* (2013). "Impaired alpha-TTP-PIPs interaction underlies familial vitamin E deficiency." Science **340**(6136): 1106-10.
Konrad, G., T. Schlecker*, et al.* (2002). "Retention of the yeast Sac1p phosphatase in the endoplasmic reticulum causes distinct changes in cellular phosphoinositide levels and stimulates microsomal ATP transport." J Biol Chem **277**(12): 10547-54.
Kopec, K. O., V. Alva*, et al.* (2010). "Homology of SMP domains to the TULIP superfamily of lipid-binding proteins provides a structural basis for lipid exchange between ER and mitochondria." Bioinformatics **26**(16): 1927-31.
Kornmann, B., E. Currie*, et al.* (2009). "An ER-mitochondria tethering complex revealed by a synthetic biology screen." Science **325**(5939): 477-81.
Kozminski, K. G., G. Alfaro*, et al.* (2006). "Homologues of oxysterol-binding proteins affect Cdc42p- and Rho1p-mediated cell polarization in Saccharomyces cerevisiae." Traffic **7**(9): 1224-42.
Kudo, N., K. Kumagai*, et al.* (2008). "Structural basis for specific lipid recognition by CERT responsible for nonvesicular trafficking of ceramide." Proc Natl Acad Sci U S A **105**(2): 488-93.
Kumagai, K., M. Kawano-Kawada*, et al.* (2014). "Phosphoregulation of the ceramide transport protein CERT at serine 315 in the interaction with VAMP-associated protein (VAP) for inter-organelle trafficking of ceramide in mammalian cells." J Biol Chem **289**(15): 10748-60.
Kumagai, K., M. Kawano*, et al.* (2007). "Interorganelle trafficking of ceramide is regulated by phosphorylation-dependent cooperativity between the PH and START domains of CERT." J Biol Chem **282**(24): 17758-66.
Kvam, E. and D. S. Goldfarb (2004). "Nvj1p is the outer-nuclear-membrane receptor for oxysterol-binding protein homolog Osh1p in Saccharomyces cerevisiae." J Cell Sci **117**(Pt 21): 4959-68.
Kwon, H. J., L. Abi-Mosleh*, et al.* (2009). "Structure of N-terminal domain of NPC1 reveals distinct subdomains for binding and transfer of cholesterol." Cell **137**(7): 1213-24.
LeBlanc, M. A., G. D. Fairn*, et al.* (2013). "The yeast oxysterol binding protein Kes1 maintains sphingolipid levels." PLoS One **8**(4): e60485.
LeBlanc, M. A. and C. R. McMaster (2010). "Lipid binding requirements for oxysterol-binding protein Kes1 inhibition of autophagy and endosome-trans-Golgi trafficking pathways." J Biol Chem **285**(44): 33875-84.
Lee, I. and W. Hong (2006). "Diverse membrane-associated proteins contain a novel SMP domain." FASEB J **20**(2): 202-6.
Lehto, M., S. Laitinen*, et al.* (2001). "The OSBP-related protein family in humans." J Lipid Res **42**(8): 1203-13.
Lemmon, M. A. (2008). "Membrane recognition by phospholipid-binding domains." Nat Rev Mol Cell Biol **9**(2): 99-111.
Lenoir, M., U. Coskun*, et al.* (2010). "Structural basis of wedging the Golgi membrane by FAPP pleckstrin homology domains." EMBO Rep **11**(4): 279-84.
Lenoir, M. and M. Overduin (2013). "PtdIns(4)P signalling and recognition systems." Adv Exp Med Biol **991**: 59-83.
Lev, S. (2010). "Non-vesicular lipid transport by lipid-transfer proteins and beyond." Nat Rev Mol Cell Biol **11**(10): 739-50.
Leventis, P. A. and S. Grinstein (2010). "The distribution and function of phosphatidylserine in

cellular membranes." Annu Rev Biophys **39**: 407-27.
Levine, T. P. and A. K. Menon (2013). "A protein pair with PIPs inside." Structure **21**(7): 1070-1.
Levine, T. P. and S. Munro (2001). "Dual targeting of Osh1p, a yeast homologue of oxysterol-binding protein, to both the Golgi and the nucleus-vacuole junction." Mol Biol Cell **12**(6): 1633-44.
Levine, T. P. and S. Munro (2002). "Targeting of Golgi-specific pleckstrin homology domains involves both PtdIns 4-kinase-dependent and -independent components." Curr Biol **12**(9): 695-704.
Li, X., M. P. Rivas*, et al.* (2002). "Analysis of oxysterol binding protein homologue Kes1p function in regulation of Sec14p-dependent protein transport from the yeast Golgi complex." J Cell Biol **157**(1): 63-77.
Ling, Y., S. Hayano*, et al.* (2014). "Osh4p is needed to reduce the level of phosphatidylinositol-4-phosphate on secretory vesicles as they mature." Mol Biol Cell.
Litvak, V., N. Dahan*, et al.* (2005). "Maintenance of the diacylglycerol level in the Golgi apparatus by the Nir2 protein is critical for Golgi secretory function." Nat Cell Biol **7**(3): 225-34.
Liu, X. and N. D. Ridgway (2014). "Characterization of the Sterol and Phosphatidylinositol 4-Phosphate Binding Properties of Golgi-Associated OSBP-Related Protein 9 (ORP9)." PLoS One **9**(9): e108368.
Liu, Y., M. Boukhelifa*, et al.* (2008). "The Sac1 phosphoinositide phosphatase regulates Golgi membrane morphology and mitotic spindle organization in mammals." Mol Biol Cell **19**(7): 3080-96.
Liu, Y., R. A. Kahn*, et al.* (2014). "Interaction of Fapp1 with Arf1 and PI4P at a membrane surface: an example of coincidence detection." Structure **22**(3): 421-30.
Maeda, K., K. Anand*, et al.* (2013). "Interactome map uncovers phosphatidylserine transport by oxysterol-binding proteins." Nature **501**(7466): 257-61.
Manford, A., T. Xia*, et al.* (2010). "Crystal structure of the yeast Sac1: implications for its phosphoinositide phosphatase function." EMBO J **29**(9): 1489-98.
Manford, A. G., C. J. Stefan*, et al.* (2012). "ER-to-plasma membrane tethering proteins regulate cell signaling and ER morphology." Dev Cell **23**(6): 1129-40.
Massey, J. B. (2006). "Membrane and protein interactions of oxysterols." Curr Opin Lipidol **17**(3): 296-301.
Mayinger, P. (2012). "Phosphoinositides and vesicular membrane traffic." Biochim Biophys Acta **1821**(8): 1104-13.
McGee, T. P., H. B. Skinner*, et al.* (1994). "A phosphatidylinositol transfer protein controls the phosphatidylcholine content of yeast Golgi membranes." J Cell Biol **124**(3): 273-87.
Mesmin, B. and B. Antonny (2013). "Cell biology. Vitamin currency in a lipid exchange market." Science **340**(6136): 1051-2.
Mesmin, B., B. Antonny*, et al.* (2013). "Insights into the mechanisms of sterol transport between organelles." Cell Mol Life Sci **70**(18): 3405-21.
Mesmin, B., J. Bigay*, et al.* (2013). "A four-step cycle driven by PI(4)P hydrolysis directs sterol/PI(4)P exchange by the ER-Golgi tether OSBP." Cell **155**(4): 830-43.
Mesmin, B. and F. R. Maxfield (2009). "Intracellular sterol dynamics." Biochim Biophys Acta **1791**(7): 636-45.
Mesmin, B., N. H. Pipalia*, et al.* (2011). "STARD4 abundance regulates sterol transport and sensing." Mol Biol Cell **22**(21): 4004-15.
Metz, R. J. and N. S. Radin (1982). "Purification and properties of a cerebroside transfer

protein." J Biol Chem **257**(21): 12901-7.
Mikitova, V. and T. P. Levine (2012). "Analysis of the key elements of FFAT-like motifs identifies new proteins that potentially bind VAP on the ER, including two AKAPs and FAPP2." PLoS One **7**(1): e30455.
Min, K. C., R. A. Kovall*, et al.* (2003). "Crystal structure of human alpha-tocopherol transfer protein bound to its ligand: implications for ataxia with vitamin E deficiency." Proc Natl Acad Sci U S A **100**(25): 14713-8.
Mioka, T., K. Fujimura-Kamada*, et al.* (2014). "Asymmetric distribution of phosphatidylserine is generated in the absence of phospholipid flippases in Saccharomyces cerevisiae." Microbiologyopen.
Mizuno-Yamasaki, E., M. Medkova*, et al.* (2010). "Phosphatidylinositol 4-phosphate controls both membrane recruitment and a regulatory switch of the Rab GEF Sec2p." Dev Cell **18**(5): 828-40.
Munro, S. (2003). "Lipid rafts: elusive or illusive?" Cell **115**(4): 377-88.
Muthusamy, B. P., S. Raychaudhuri*, et al.* (2009). "Control of protein and sterol trafficking by antagonistic activities of a type IV P-type ATPase and oxysterol binding protein homologue." Mol Biol Cell **20**(12): 2920-31.
Natarajan, P., K. Liu*, et al.* (2009). "Regulation of a Golgi flippase by phosphoinositides and an ArfGEF." Nat Cell Biol **11**(12): 1421-6.
Neefjes, J. and R. van der Kant (2014). "Stuck in traffic: an emerging theme in diseases of the nervous system." Trends Neurosci **37**(2): 66-76.
Nes, W. D. (2011). "Biosynthesis of cholesterol and other sterols." Chem Rev **111**(10): 6423-51.
Ngo, M. and N. D. Ridgway (2009). "Oxysterol binding protein-related Protein 9 (ORP9) is a cholesterol transfer protein that regulates Golgi structure and function." Mol Biol Cell **20**(5): 1388-99.
Nguyen, T. T., A. Lewandowska*, et al.* (2012). "Gem1 and ERMES do not directly affect phosphatidylserine transport from ER to mitochondria or mitochondrial inheritance." Traffic **13**(6): 880-90.
Novick, P., C. Field*, et al.* (1980). "Identification of 23 complementation groups required for post-translational events in the yeast secretory pathway." Cell **21**(1): 205-15.
Nylund, M., M. A. Kjellberg*, et al.* (2006). "Molecular features of phospholipids that affect glycolipid transfer protein-mediated galactosylceramide transfer between vesicles." Biochim Biophys Acta **1758**(6): 807-12.
Odorizzi, G., M. Babst*, et al.* (2000). "Phosphoinositide signaling and the regulation of membrane trafficking in yeast." Trends Biochem Sci **25**(5): 229-35.
Olkkonen, V. M. and S. Li (2013). "Oxysterol-binding proteins: sterol and phosphoinositide sensors coordinating transport, signaling and metabolism." Prog Lipid Res **52**(4): 529-38.
Olsen, B. N., P. H. Schlesinger*, et al.* (2009). "Perturbations of membrane structure by cholesterol and cholesterol derivatives are determined by sterol orientation." J Am Chem Soc **131**(13): 4854-65.
Peretti, D., N. Dahan*, et al.* (2008). "Coordinated lipid transfer between the endoplasmic reticulum and the Golgi complex requires the VAP proteins and is essential for Golgi-mediated transport." Mol Biol Cell **19**(9): 3871-84.
Perry, R. J. and N. D. Ridgway (2006). "Oxysterol-binding protein and vesicle-associated membrane protein-associated protein are required for sterol-dependent activation of

the ceramide transport protein." Mol Biol Cell **17**(6): 2604-16.
Pichler, H., B. Gaigg*, et al.* (2001). "A subfraction of the yeast endoplasmic reticulum associates with the plasma membrane and has a high capacity to synthesize lipids." Eur J Biochem **268**(8): 2351-61.
Pirillo, A., G. D. Norata*, et al.* (2013). "High-density lipoprotein subfractions--what the clinicians need to know." Cardiology **124**(2): 116-25.
Raychaudhuri, S., Y. J. Im*, et al.* (2006). "Nonvesicular sterol movement from plasma membrane to ER requires oxysterol-binding protein-related proteins and phosphoinositides." J Cell Biol **173**(1): 107-19.
Raychaudhuri, S., B. P. Young*, et al.* (2012). "Regulation of lipid metabolism: a tale of two yeasts." Curr Opin Cell Biol **24**(4): 502-8.
Ren, J., C. Pei-Chen Lin*, et al.* (2014). "A phosphatidylinositol transfer protein integrates phosphoinositide signaling with lipid droplet metabolism to regulate a developmental program of nutrient stress-induced membrane biogenesis." Mol Biol Cell **25**(5): 712-27.
Ridgway, N. D., P. A. Dawson*, et al.* (1992). "Translocation of oxysterol binding protein to Golgi apparatus triggered by ligand binding." J Cell Biol **116**(2): 307-19.
Rocha, N., C. Kuijl*, et al.* (2009). "Cholesterol sensor ORP1L contacts the ER protein VAP to control Rab7-RILP-p150 Glued and late endosome positioning." J Cell Biol **185**(7): 1209-25.
Romanowski, M. J., R. E. Soccio*, et al.* (2002). "Crystal structure of the Mus musculus cholesterol-regulated START protein 4 (StarD4) containing a StAR-related lipid transfer domain." Proc Natl Acad Sci U S A **99**(10): 6949-54.
Roy, A. and T. P. Levine (2004). "Multiple pools of phosphatidylinositol 4-phosphate detected using the pleckstrin homology domain of Osh2p." J Biol Chem **279**(43): 44683-9.
Schauder, C. M., X. Wu*, et al.* (2014). "Structure of a lipid-bound extended synaptotagmin indicates a role in lipid transfer." Nature **510**(7506): 552-5.
Schmalix, W. A. and W. Bandlow (1994). "SWH1 from yeast encodes a candidate nuclear factor containing ankyrin repeats and showing homology to mammalian oxysterol-binding protein." Biochim Biophys Acta **1219**(1): 205-10.
Schneiter, R. (1999). "Brave little yeast, please guide us to thebes: sphingolipid function in S. cerevisiae." Bioessays **21**(12): 1004-10.
Schneiter, R., B. Brugger*, et al.* (1999). "Electrospray ionization tandem mass spectrometry (ESI-MS/MS) analysis of the lipid molecular species composition of yeast subcellular membranes reveals acyl chain-based sorting/remodeling of distinct molecular species en route to the plasma membrane." J Cell Biol **146**(4): 741-54.
Schulz, T. A., M. G. Choi*, et al.* (2009). "Lipid-regulated sterol transfer between closely apposed membranes by oxysterol-binding protein homologues." J Cell Biol **187**(6): 889-903.
Shao, C., V. A. Novakovic*, et al.* (2008). "Crystal structure of lactadherin C2 domain at 1.7A resolution with mutational and computational analyses of its membrane-binding motif." J Biol Chem **283**(11): 7230-41.
Shelton, S. N., B. Barylko*, et al.* (2003). "Saccharomyces cerevisiae contains a Type II phosphoinositide 4-kinase." Biochem J **371**(Pt 2): 533-40.
Simanshu, D. K., R. K. Kamlekar*, et al.* (2013). "Non-vesicular trafficking by a ceramide-1-phosphate transfer protein regulates eicosanoids." Nature **500**(7463): 463-7.
Singh, R. P., B. R. Brooks*, et al.* (2009). "Binding and release of cholesterol in the Osh4 protein

of yeast." Proteins **75**(2): 468-77.
Stefan, C. J., A. G. Manford*, et al.* (2011). "Osh proteins regulate phosphoinositide metabolism at ER-plasma membrane contact sites." Cell **144**(3): 389-401.
Stefan, C. J., A. G. Manford*, et al.* (2013). "ER-PM connections: sites of information transfer and inter-organelle communication." Curr Opin Cell Biol **25**(4): 434-42.
Stone, S. J. and J. E. Vance (2000). "Phosphatidylserine synthase-1 and -2 are localized to mitochondria-associated membranes." J Biol Chem **275**(44): 34534-40.
Suchanek, M., R. Hynynen*, et al.* (2007). "The mammalian oxysterol-binding protein-related proteins (ORPs) bind 25-hydroxycholesterol in an evolutionarily conserved pocket." Biochem J **405**(3): 473-80.
Sullivan, D. P., H. Ohvo-Rekila*, et al.* (2006). "Sterol trafficking between the endoplasmic reticulum and plasma membrane in yeast." Biochem Soc Trans **34**(Pt 3): 356-8.
Tahirovic, S., M. Schorr*, et al.* (2005). "Regulation of intracellular phosphatidylinositol-4-phosphate by the Sac1 lipid phosphatase." Traffic **6**(2): 116-30.
Takeda, M., K. Yamagami*, et al.* (2014). "Role of phosphatidylserine in phospholipid flippase-mediated vesicle transport in Saccharomyces cerevisiae." Eukaryot Cell **13**(3): 363-75.
Tamura, Y., H. Sesaki*, et al.* (2014). "Phospholipid transport via mitochondria." Traffic **15**(9): 933-45.
Tan, J. and J. A. Brill (2014). "Cinderella story: PI4P goes from precursor to key signaling molecule." Crit Rev Biochem Mol Biol **49**(1): 33-58.
Tani, M. and O. Kuge (2014). "Involvement of Sac1 phosphoinositide phosphatase in the metabolism of phosphatidylserine in the yeast Saccharomyces cerevisiae." Yeast **31**(4): 145-58.
Tatsuta, T., M. Scharwey*, et al.* (2014). "Mitochondrial lipid trafficking." Trends Cell Biol **24**(1): 44-52.
Tavassoli, S., J. T. Chao*, et al.* (2013). "Plasma membrane--endoplasmic reticulum contact sites regulate phosphatidylcholine synthesis." EMBO Rep **14**(5): 434-40.
Taylor, F. R. and A. A. Kandutsch (1985). "Oxysterol binding protein." Chem Phys Lipids **38**(1-2): 187-94.
Tidhar, R. and A. H. Futerman (2013). "The complexity of sphingolipid biosynthesis in the endoplasmic reticulum." Biochim Biophys Acta **1833**(11): 2511-8.
Tong, J., H. Yang*, et al.* (2013). "Structure of Osh3 reveals a conserved mode of phosphoinositide binding in oxysterol-binding proteins." Structure **21**(7): 1203-13.
Tong, J., H. Yang*, et al.* (2012). "Crystallization and preliminary X-ray crystallographic analysis of the oxysterol-binding protein Osh3 from Saccharomyces cerevisiae." Acta Crystallogr Sect F Struct Biol Cryst Commun **68**(Pt 12): 1498-502.
Toulmay, A. and W. A. Prinz (2012). "A conserved membrane-binding domain targets proteins to organelle contact sites." J Cell Sci **125**(Pt 1): 49-58.
Toulmay, A. and W. A. Prinz (2013). "Direct imaging reveals stable, micrometer-scale lipid domains that segregate proteins in live cells." J Cell Biol **202**(1): 35-44.
Tsujishita, Y. and J. H. Hurley (2000). "Structure and lipid transport mechanism of a StAR-related domain." Nat Struct Biol **7**(5): 408-14.
Tuuf, J. and P. Mattjus (2014). "Membranes and mammalian glycolipid transferring proteins." Chem Phys Lipids **178**: 27-37.
Vamparys, L., R. Gautier*, et al.* (2013). "Conical lipids in flat bilayers induce packing defects similar to that induced by positive curvature." Biophys J **104**(3): 585-93.
van Amerongen, A., R. A. Demel*, et al.* (1989). "Transfer of cholesterol and oxysterol

derivatives by the nonspecific lipid transfer protein (sterol carrier protein 2): a study on its mode of action." Biochim Biophys Acta **1004**(1): 36-43.

van der Kant, R., A. Fish*, et al.* (2013). "Late endosomal transport and tethering are coupled processes controlled by RILP and the cholesterol sensor ORP1L." J Cell Sci **126**(Pt 15): 3462-74.

van der Kant, R., I. Zondervan*, et al.* (2013). "Cholesterol-binding molecules MLN64 and ORP1L mark distinct late endosomes with transporters ABCA3 and NPC1." J Lipid Res **54**(8): 2153-65.

van Meer, G., D. R. Voelker*, et al.* (2008). "Membrane lipids: where they are and how they behave." Nat Rev Mol Cell Biol **9**(2): 112-24.

Vance, J. E., E. J. Aasman*, et al.* (1991). "Brefeldin A does not inhibit the movement of phosphatidylethanolamine from its sites for synthesis to the cell surface." J Biol Chem **266**(13): 8241-7.

Vance, J. E. and R. Steenbergen (2005). "Metabolism and functions of phosphatidylserine." Prog Lipid Res **44**(4): 207-34.

Wang, J., H. Q. Sun*, et al.* (2007). "PI4P promotes the recruitment of the GGA adaptor proteins to the trans-Golgi network and regulates their recognition of the ubiquitin sorting signal." Mol Biol Cell **18**(7): 2646-55.

Wang, M. L., M. Motamed*, et al.* (2010). "Identification of surface residues on Niemann-Pick C2 essential for hydrophobic handoff of cholesterol to NPC1 in lysosomes." Cell Metab **12**(2): 166-73.

Wang, P., W. Duan*, et al.* (2005). "Molecular characterization of Osh6p, an oxysterol binding protein homolog in the yeast Saccharomyces cerevisiae." FEBS J **272**(18): 4703-15.

Wang, P., Y. Zhang*, et al.* (2005). "AAA ATPases regulate membrane association of yeast oxysterol binding proteins and sterol metabolism." EMBO J **24**(17): 2989-99.

Wang, P. Y., J. Weng*, et al.* (2005). "OSBP is a cholesterol-regulated scaffolding protein in control of ERK 1/2 activation." Science **307**(5714): 1472-6.

Wilcox, L. J., D. A. Balderes*, et al.* (2002). "Transcriptional profiling identifies two members of the ATP-binding cassette transporter superfamily required for sterol uptake in yeast." J Biol Chem **277**(36): 32466-72.

Wood, C. S., C. S. Hung*, et al.* (2012). "Local control of phosphatidylinositol 4-phosphate signaling in the Golgi apparatus by Vps74 and Sac1 phosphoinositide phosphatase." Mol Biol Cell **23**(13): 2527-36.

Wu, W. I., S. Routt*, et al.* (2000). "A new gene involved in the transport-dependent metabolism of phosphatidylserine, PSTB2/PDR17, shares sequence similarity with the gene encoding the phosphatidylinositol/phosphatidylcholine transfer protein, SEC14." J Biol Chem **275**(19): 14446-56.

Wu, X., R. J. Chi*, et al.* (2014). "Structural insights into assembly and regulation of the plasma membrane phosphatidylinositol 4-kinase complex." Dev Cell **28**(1): 19-29.

Xie, Z., M. Fang*, et al.* (2001). "Evidence for an intrinsic toxicity of phosphatidylcholine to Sec14p-dependent protein transport from the yeast Golgi complex." Mol Biol Cell **12**(4): 1117-29.

Xu, P., R. D. Baldridge*, et al.* (2013). "Phosphatidylserine flipping enhances membrane curvature and negative charge required for vesicular transport." J Cell Biol **202**(6): 875-86.

Xu, Z., W. Farver*, et al.* (2008). "Regulation of sterol transport between membranes and NPC2." Biochemistry **47**(42): 11134-43.

Ye, H., B. Li*, et al.* (2013). "NMR solution structure of C2 domain of MFG-E8 and insights into its molecular recognition with phosphatidylserine." Biochim Biophys Acta **1828**(3): 1083-93.

Yeung, T., G. E. Gilbert*, et al.* (2008). "Membrane phosphatidylserine regulates surface charge and protein localization." Science **319**(5860): 210-3.

Zhang, M., P. Liu*, et al.* (2002). "MLN64 mediates mobilization of lysosomal cholesterol to steroidogenic mitochondria." J Biol Chem **277**(36): 33300-10.

Zhong, S., F. Hsu*, et al.* (2012). "Allosteric activation of the phosphoinositide phosphatase Sac1 by anionic phospholipids." Biochemistry **51**(15): 3170-7.

Zhou, Y., G. Wohlfahrt*, et al.* (2014). "A vertebrate model for the study of lipid binding/transfer protein function: conservation of OSBP-related proteins between zebrafish and human." Biochem Biophys Res Commun **446**(3): 675-80.

Zinser, E., C. D. Sperka-Gottlieb*, et al.* (1991). "Phospholipid synthesis and lipid composition of subcellular membranes in the unicellular eukaryote Saccharomyces cerevisiae." J Bacteriol **173**(6): 2026-34.